THE ROLE OF 14-3-3 PROTEINS IN REGULATING THE DYNAMIC ACTIVITY AND COMPARTMENTALIZATION OF CYTOKERATIN INTERMEDIATE FILAMENTS

by

RICHARD MARIANI

A Dissertation submitted to the

Graduate School-Newark

Rutgers, The State University of New Jersey

In partial fulfillment of the requirements

for the degree of

Doctor of Philosophy

Graduate Program in Biological sciences

written under the direction of

Gregory F. Weber, Ph.D.

And approved by

_____

_____

_____

_____

_____

Newark, New Jersey

October 2019

ABSTRACT OF THE DISSERTATION

THE ROLE OF 14-3-3 PROTEINS IN REGULATING THE DYNAMIC ACTIVITY AND COMPARTMENTALIZATION OF CYTOKERATIN INTERMEDIATE FILAMENTS

Dissertation Director:

Gregory F. Weber, Ph.D.

.

Intermediate filament cytoskeletal networks simultaneously support mechanical integrity and influence signal transduction pathways. Marked remodeling of the keratin intermediate filament network accompanies collective cellular morphogenetic movements that occur during early embryonic development in the frog *Xenopus laevis.* While this reorganization of keratin is initiated by force transduction on cell-cell contacts mediated by C-cadherin, the mechanism by which keratin filament reorganization occurs remains poorly understood. In this work we demonstrate that 14-3-3 proteins regulate keratin reorganization dynamics in embryonic mesendoderm cells from *Xenopus* gastrula. 14-3-3 co-localizes with keratin filaments near cell-cell junctions in migrating mesendoderm. Co-immunoprecipitation, mass spectrometry and bioinformatic analyses indicate 14-3-3 is associated with Keratin 19 in the whole embryo and, more specifically, mesendoderm tissue. Inhibition of 14-3-3 results in both the decreased exchange of keratin subunits into filaments and blocks keratin filament recruitment toward cell-cell contacts. Synthetically coupling 14-3-3 to Keratin 19 through a unique fusion construct conversely induces the localization of this keratin population to the

region of cell-cell contacts. Taken together, these findings indicate that 14-3-3 acts on keratin intermediate filaments and is involved in their reorganization to sites of cell adhesion.

ACKNOWLEDGEMENTS

I would first like to thank Dr. Gregory F. Weber who has been an outstanding mentor, inspirational scientist, and a wonderful person. His support and guidance have been invaluable throughout the entirety of my studies at Rutgers, and I have greatly benefitted from his uncommon creativity and intelligence. I am honored to have worked alongside him and have many fond memories of his insights, scientific curiosity, and unmatched eye for phenotypes. I consider myself extremely fortunate to have both developed an exciting project with Greg and to have gained his as a friend.

I am also very fortunate to have had Dr. Nan Gao, Dr. Edward Bonder, and Dr. Gary Gorbsky as members of my thesis committee. I admire each of these individuals and have greatly enjoyed all of the scientific discourse that we have shared. Both Nan and Ed have helped me extensively during my education while developing my thesis. It is not an overstatement to say that they were essential to helping me complete my work at Rutgers. In addition, when Gary agreed to join the committee, I was ecstatic to have attracted the interest of a such an outstanding and accomplished scientist. I am proud to have defended my thesis in the company of these great individuals whom I continue to look up to.

Many of my seniors at Rutgers were amazing peers and friends, helping me to get started and supporting me through the hurdles. Pavan, Israel, Khoosheh, Soumya, Chaitali, Dominick, Manpreet, Hyosung, and Ming are all incredible individuals that have watched out for me and personally guided me. I am thankful

for the kindness that they have shown me and the scientific lessons that they have imparted.

I have been lucky to have been a member of a fantastic lab with many wonderful scientists, including Shalaka, Abid, Rucha, and Huri. Shalaka's friendship helped me to endure some of the most difficult phases of my time at Rutgers. Abid's energy and brilliance have been inspirational, and both Rucha and Huri have enriched my growth as a scientist through our shared lab experiences.

The community at Rutgers has been fantastic. All of the Gao lab, including Ivor, Sayantani, Juan, Iyshwarya, Sheila, Xiao, and Victoria have gifted me with many of my most cherished memories at Rutgers. I am constantly impressed by their scientific ethic, and their humor is second to none. Put succinctly, these people are a riot. The same can be said for Brian, Justin, and Henri, who have each shown me kindness and friendship. There were many long hours where Ivor was the last man standing to keep me sane, times that I will always remember. Both Juan and Brian were great company as we worked into the evening of no moon nights.

I would be remiss to not mention my gratitude for all the assistance from the Biology Department Office including Shandel, Neermala, and Sheronda. In addition, both Dr. Jessica Ware and Dr. Claus Holzapfel have been very helpful during the course of my journey at Rutgers.

Even before I began my studies toward the Ph.D., I was exceptionally fortunate to have Dr. Alan Kluger as my first mentor. Alan was the first scientist

who by example inspired me to pursue research and still remains as one of the people I constantly seek to emulate. He was present for me as unyielding support during my most difficult times, and I have him to thank for the opportunity at Rutgers.

Dr. Henry H. Ruiz, whom I have known since the early days of his research endeavors, has been one of my most valued scientific peers and friends. Henry was one of the first to express that he believed in my potential and to guide me directly. Both his enthusiasm and conviction inspired me and the lessons he taught me became invaluable as I was developing my thesis.

I am beyond thankful for the friendship, guidance, and kindness of Dr. Ann Cali, who is without a doubt one of the finest scientists on the planet and an amazing person. The impression that she has left upon me and vigor with which she approaches her life is one of my greatest ongoing sources of inspiration. I cannot express in words how wonderful Ann has been to me.

My Aunt Ann Murray was one of the greatest sources of encouragement for pursuing and completing doctoral work. At a time where my life compass was not lending me obvious direction, Aunt Ann was the person who stepped in and helped me to find my footing again. I feel very grateful for having had the opportunity to share my career growth with her and my Aunt Mary Jo, even chancing upon a meeting in Dublin recently that meant the world to me.

Someone who I will never forget and wish to express my gratitude for is Jonelle Bernardo, a person without equal in my life whom I think about daily. She

has a stake in every part of my personal journey and all of my accomplishments, as I would not be the person I am today without having met Jonelle. I am eternally thankful for having been able to share in a part of her life and that of her family.

I have been lucky to have a group of friends whom I would not trade for the world. Jake, Sergey, Richard, and Adam have enriched my life in innumerable ways. Above all, I owe so much to Shane, Granlore, and Darson. Each of them have so much drive that they inspire me daily. They are the definition of friends who become family. I am grateful to be able to share my accomplishments with them and to forge forward toward even greater ones.

Likewise, I would like to thank Tim for the innumerable ways in which he has enriched my life. He has a resolve unlike any other, and the conviction with which he approaches everything he does is something that I constantly seek to emulate. Even among many other sources of support, he has truly been like a right hand to me.

During my time at Rutgers, Megan Wilson has been my strongest pillar of guidance, kindness, and generosity. She has truly gone out of her way to not only help me to succeed, but to help me keep my purpose and sense of self vibrant all the while. Her dedication, spirit, and genuine warmth are of inestimable value to me. So much of my progress is owed to her willingness to always guide me through, without reservation. I cannot thank Megan enough.

My family comes first and last. My father, Gerald, and my siblings James, Katharine, and Christine as well as her own growing family are the finest folks that

anyone could ever hope to have. They believed in me from the very beginning, and that means everything. I am most proud to be able to share my accomplishments with them. Lastly, I would like to dedicate this thesis and all of my endeavors during the Ph.D. to my mother, Thérèse Murray Mariani, whom I can wholeheartedly say is the reason for all of it.

PREFACE

In undertaking the study of ‘mechanism’, the functional events that produce an outcome, scientists are tasked with discovering and detailing a series of coordinated phenomena. Using strategies such as deductive research methods or design implementation, investigators are able to identify and study the component parts of a mechanism. Furthermore, they can identify how such parts behave intrinsically and in cooperation with one another to initiate a series of events, or a process. The goal is to gain reliable and valid evidence that allows us to as precisely as possible determine how, put simply, something ‘works’.

‘Simple’, however, is neither an asset to the biological scientist nor an apt description of the living environment that she/he endeavors to understand. Despite our inclinations to outline processes in a procedural and straightforward way, living environments influence and are simultaneously influenced by them.

In the cell, component parts are molecules that range from chemical elements to polypeptides. Events in a process originate from their interactions. For any given set of such interactions, some of the simplest aspects include the temporal and spatial. Obtaining evidence, and thus knowledge, of sequential molecular interactions and governing principles allows expectations to be developed and predictions to be made. If investigation and discovery ended here, however, it would neglect the most vital context of any biological mechanism; its place within and impact upon the living world where it exists.

These statements are not simply descriptive perspective or philosophy. Rather, they are a summary of critical awareness that is essential to the study of cell and molecular biology. Take, for example, the term ‘living environment’. If accepted at face value with regard to cell biology, it can be understood broadly as the complex environment in an organism that allows it to survive. Prior to pursuing additional complexity and considering what determines ‘life’, a step back is required. Does acknowledgment of a ‘complex environment’ constitute enough awareness for a biological scientist that is developing and testing a hypothesis about a mechanism? Could further thought be spared here?

The critical awareness is that the ‘living environment’ is component parts. Should our knowledge of all the parts be complete, we would conceptually be able to understand all processes and how they influence one another. Without complete knowledge, we must remain aware of the delicate balance between the properties we discover about these parts, or molecules, and the influence of myriad others. When this influence includes the ability to modify said properties, maintaining this awareness is the most important prerequisite for anyone putting forth an interpretation or conclusion. Ultimately, we each employ a reductionist method and approach. It befalls each of us, then, to appreciate our findings within a wider scope, despite the urge to conclusively and narrowly determine and decide.

TABLE OF CONTENTS

Page

LIST OF ILLUSTRATIONS

Figure **Page**

LIST OF APPENDICES

Appendix **Page**

CHAPTER 1

BACKGROUND AND INTRODUCTION

Characterization of intermediate filaments

A wide viewpoint is certainly required to fully appreciate the intermediate filaments (IFs), a class of molecular filamentous cytoskeleton that is subject to constant re-appreciation in terms of its principle functionality along with its potentially broader roles. Since the first characterization of “intermediate-sized filaments” in myotubes, myoblasts, chondrocytes, and fibroblasts (Ishikawa et al. 1968), our understanding of IF proteins in terms of intrinsic assembly properties, roles in cell biology, and organismal importance is constantly undergoing revision (Kim and Coulombe 2007; Helfand et al. 2003; Herrmann et al. 2009). Early evidence detailing IF tissue distribution and biochemical properties led researchers to propose roles for IF networks including maintenance of cell shape, organization of organelles and the nucleus, and mechanical integration of cellular structures (Steinert and Parry 1985; Lazarides 1980). Continued investigation revealed the roles of IF cytoskeleton to be much wider in scope. Functional roles for IFs have been demonstrated in the context of development (Klymkowsky et al. 1992; Torpey et al. 1992; Sonavane et al. 2017), cellular signaling (Liao and Omary 1996; Margolis et al. 2006; Kim et al. 2006), and mechanical transduction (Helmke et al. 2000; Ridge et al. 2005; Weber et al. 2012), to name a few research areas. It is important to our understanding of IF networks and continually emerging evidence to appreciate that although these cable-like macromolecules may appear simple enough in its structure, their capacity for potential functional roles is anything otherwise.

The apparent contradiction between the structural simplicity of IFs and their varied pool of roles is echoed by the size and diversity of the family of IF proteins. All IF proteins host a shared secondary structure including non-helical N and C terminal regions that flank an α-helical rod region (Geisler and Weber 1982a; Herrmann et al. 2009). It is curious that these highly structurally conserved molecules amount to at least 65 separate conserved genes in humans and other mammals, with some analyses reporting numbers in the excess of 70 (Hesse et al. 2001; Herrmann et al. 2003; Kim and Coulombe 2007). Moreover, these genes have been organized into a larger family of sequence homology classes that besides providing several useful IF distinctions assists in highlighting critical differences in conservation of expression (Hesse et al. 2001). Examples of expression conservation include specificity of cytokeratin expression in epithelia, vimentin in mesenchymal cells, desmin in muscle cells, glial fibrillary associated protein (GFAP) in glial cells, and neurofilament types in neurons (Kim and Coulombe 2007). This conserved cellular restriction of IF proteins despite a strongly shared similarity in structure suggests that IFs may have cell-type specific functions that cannot be easily predicted by structural analysis alone (Herrmann et al. 2003).

Intermediate filament evolutionary insights

When considering the range of functions that IFs may have it is important to recognize that the large amount of IF genes and diversity of filament proteins notwithstanding, cytoplasmic IFs are not necessary for life. IFs are completely absent from plants and yeast, and only nuclear IFs known as lamins are found in

drosophila (Hermann et al. 2003). Although IF networks are not a requirement for eukaryotic lifeforms it is plausible that they were evolutionarily selected for because they conferred significant advantages. Though invertebrate metazoans lack the IFs expressed in chordate eukaryotes, they express IF-like proteins that share distinct similarities with nuclear lamin IFs (Erber et al. 1998). IF-like proteins have been found in yeast, bacteria, and arthropods (Mayordomo and Sanz 2002; Ausmees et al. 2003; Mencarelli et al. 2011). There is a strong likelihood that some of these IF-like proteins are ancestral forms that upon modification allowed for IF diversification into the many subtypes discovered in the mammal (Gerace et al. 1986; Erber et al. 1989; Peter and Stick 2015; Preisner et al. 2018). Some selection criteria may potentially include the need for greater mechanical resistance and more complex cellular signaling mechanisms in chordate eukaryotes compared to more ancestral metazoans, owing to greater tissue diversity.

Intermediate filaments comprise a diverse family of cytoskeleton

Discoveries to date have uncovered a large number of intermediate filament protein types that share sequence conservation and even more marked structural conservation (Geisler and Weber 1981; Geisler, Plessman, and Weber 1982; Crewther et al. 1983). In order to document and describe this diversity in a useful way, an IF family classification system has been created using sequence homology comparisons to divide IF types into specific subgroups (Kim and Coulombe 2007).

The IF family is comprised of Type I filaments through Type 6 (Orphan/Other) filaments. The first four subgroups as well as the orphan group

include ‘cytoplasmic’ filament proteins found within cells. The type I and type II subgroups are exclusive to keratins, type I keratins representing those that are more charge acidic and type II representing the more charge basic relative to each other when compared via two dimensional gel electrophoresis (Hanukoglu and Fuchs 1982; Hanukoglu and Fuchs 1983; Sun et al. 1985). Keratins account for the majority of IF proteins discovered, constituting large and complex subgroups that are subject to ongoing discovery (Hesse et al. 2001; Schweizer et al. 2006). Several key differences divide keratins from the larger IF family. The type I and type II keratins are obligate heteropolymers in filament formation, in contrast to the majority of IFs (Steinert 1990; Hatzfeld and Weber 1990a). The individual keratin genes are clustered within chromosomal loci, with type I keratins located on chromosome 17 and type II keratins located on chromosome 12 in the human (Hesse et al. 2001). Additionally, the type I and type II groups include hair keratins that represent distinct molecules from the cytoplasmic keratins found in epithelial cells (Schweizer et al. 2006). In *Xenopus* species, *tropicalis* demonstrates clustering of type I keratins on chromosome 10 and type II keratins on chromosome 2, while *laevis* hosts both an ‘L’ and ‘S’ subgenome that includes type I keratins on chromosome 9_10 and type II keratins on chromosome 2 for each subgenome (Suzuki et al. 2007).

Type III intermediate filaments represent a broader subgroup due to expression patterns that encompass a wider range of tissues. IF proteins in this subgroup include vimentin, desmin, and glial fibrillary acidic protein (GFAP), which despite their closely shared structure, often appear in different cell types (Kim and

Coulombe 2007). While the type I and II IFs are restricted to epithelia, type III IFs are mainly found in mesenchymal cells (vimentin), muscle cells (desmin), and astrocytes (GFAP) (Franke et al. 1978; Lazarides et al. 1982: Reeves et al. 1989). The type III IF subgroup also includes peripherin and synemin, two IF proteins that show sequence similarities to other type III IFs and a more restricted expression profile (Portier et al. 1983; Granger et al. 1982). Though the type III IF proteins are capable of forming homopolymers, these IFs have also been found to create heteropolymers. In particular, vimentin has been shown to dimerize with GFAP, desmin, and nestin IFs, demonstrating a degree of flexibility and complexity in type III IF cellular network formation (Fedoroff et al. 1983; Wang et al. 1984; Quinlan and Franke 1982; Steinert 1999).

The major intermediate filaments of the type IV subgroup are the neurofilaments, named neurofilament light (NF-L), medium (NF-M), and heavy (NF-H) based on their mass in kDa relative to one another (Hoffman and Lasek 1975; Geisler et al. 1985; Levy et al. 1987; Lees et al. 1988). Filaments comprised of these proteins show strong structural similarity to those of the previous subgroups, with a deviant feature of a C-terminal tail that extends 90 degrees outward relative to the filament body when incorporated into the mature neurofilament (Hirokawa et al. 1984; Hisanaga and Hirokawa 1988). Neurofilaments also demonstrate capability to homodimerize as well as heterodimerize. NF-L exhibits the ability to solely form networks in the absence of NF-M and NF-H *in vitro* (Heins et al. 1993; Lee et al. 1993). In contrast, NF-M and NF-H proteins require a NF-L partner to dimerize and form filaments that are

exclusive from one another (Hisanaga and Hirokawa 1988; Balin and Lee 1991; Lee et al. 1993). While this IF protein triad demonstrates variability in formation of filaments, each neurofilament is found abundantly in neurons (Hoffmann and Lasek 1975). Other than the neurofilaments, the type IV IF subgroup includes nestin and α-internexin in nervous tissue, as well as syncolin in muscle (Lendahl et al. 1990; Fliegner et al. 1990; Feick et al. 1991).

The type V intermediate filaments are the nuclear lamins that are products of the Lamin A gene and Lamin B genes (Aebi et al. 1986; Gerace et al. 1986). Lamin A gene transcripts are translated into Lamins A and C, which demonstrate high sequence similarity, while the Lamin B genes produce several Lamin B isoforms (McKeon et al. 1986; Fisher et al. 1986).These IF proteins form filaments that are restricted to the nuclear compartment of cells where they associate with nuclear membranes and chromatin (Aebi et al. 1986). Lamin IFs show conservation of primary and secondary structure in the α-helical domain when compared to cytoplasmic IFs, particularly type III IFs (McKeon et al. 1986; Fisher et al. 1986). All lamins assemble into coil-coiled dimers, and although heteropolymers such as Lamin A/C form in vitro, lamin IFs form homopolymers in-vivo (Heitlinger et al. 1991; Kolb et al. 2011). As a network in the nucleus, lamins form a characteristic meshwork of orthogonally interposed IFs (Aebi et al. 1986). Though this structure appears highly ordered, each lamin protein is thought to form a separate network, a feature that may be important for regulation of nuclear structure during both mitosis and interphase (Gerace and Blobel 1980; Lammerding et al. 2004; Goldberg et al. 2008; Ferrera et al. 2014).

The final current IF subgroup is referred to as orphan or other and includes the lens specific IF proteins Filensin and Phakinin (Merdes et al. 1991; Merdes et al. 1993; Chang and Goldman 2004). These IF proteins harbor partial sequence homology with IF family proteins in regard to the α-helical rod region, with Phakinin demonstrating stronger resemblance to typical IF peptides (Gounari et al. 1993; Merdes et al. 1993). Filensin, which forms a 10-nm filament heteropolymer with Phakinin, is shown to associate with lens cell membranes and compartmentalize to the periphery of these cells (Merdes et al. 1991; Merdes et al. 1993).

Structure of intermediate filament proteins

Efforts to deduce the structure of intermediate filament proteins date back to pioneer work that established the chemical basis for formation of α-helical structures in peptides (Pauling et al. 1951). Subsequent work predicted that α-helical keratin intermediate filament polypeptides conformed to a coiled-coil molecular structure (Crick 1952; Crick 1953). Early speculations that predicted a triple stranded coiled-coil intermediate filament structure were revised to that of a double stranded coiled-coil upon deriving the first complete sequence of an IF protein (Steinert et al. 1980; Geisler and Weber 1982). Crystal structures ultimately confirmed that two intermediate filament protein α-helices indeed form a coiled-coil polypeptide (Herrmann et al. 2000; Strelkov et al. 2001; Strelkov et al. 2002).

A combination of biochemical proteolysis experiments and sequence analysis revealed that individual IF proteins share a common three-domain structure: a sequence variable amino-terminal ‘head’ and carboxy-terminal ‘tail’ region each flank the central and strongly conserved α-helical ‘rod’ segment

(Geisler et al. 1982; Geisler and Weber 1982; Hanukoglu and Fuchs 1983; Steinert et al. 1983). A wealth of research since has elucidated consensus regions across this central IF rod segment, denoted as the coiled-coil domains 1A, 1B, 2A, and 2B (Herrmann et al. 2009). These α-helical sequences are joined by linker L1, L12, and L2 regions that demonstrate greater sequence variability and primarily non-helical character (Parry 2005). The length of the 1A, 2A, and 2B regions is strictly conserved among IFs at 35, 19, and 115 residues, respectively (Parry 2005; Herrmann et al. 2009). Coil 1B is 101 residues in length in all IFs other than lamins, where it is 42 residues longer (Fisher et al. 1986; McKeon et al. 1986).

The α-helical regions of the IF rod are comprised of a repeating heptad sequence in the order ‘abcdefg’, where the residues at the ‘a’ and ‘d’ position are hydrophobic residues (Parry 1982; Parry 2005). These residues show the highest degree of conservation among IFs, with the mainly charged residues at the ‘e’ and ‘g’ positions demonstrating the second highest conservation. Comparatively, the ‘b’, ‘c’, and ‘f’ positions show the most residue variety (Conway and Parry 1988). This repeating heptad sequence results in α-helical secondary structure mediated by intermolecular interactions that promotes coiled-coil tertiary structure through intramolecular interactions (Lupas 1996; Burkhard et al. 2001). The resulting coiled-coil dimer of IF α-helices positions the hydrophobic residues into the core of the dimer and the majority of the charged and polar residues toward the outer surface (Conway and Parry 1988; Shoeman and Traub 1993).

In contrast to the strong conservation of the IF central rod, the head and tail domains demonstrate marked sequence variability across IF proteins (Herrmann

et al. 2009). The functional significance of these regions has not been well characterized and appears to be different across IF family subgroups and proteins (Parry 2005). These domains have been a subject of interest due to the higher proportion of residues that are subject to post-translational modification in IF heads and tails relative to the rod domain (Omary et al. 2006; Snider and Omary 2014). Such modifications create the potential for changes in regulation of filament formation; among these, one such established mechanism includes phosphorylation and/or dephosphorylation of serine and threonine residues (Omary et al. 2006, Snider and Omary 2014).

Assembly of intermediate filaments

Intermediate filament assembly is distinct from assembly of other cytoskeletal macromolecules in that it does not require hydrolysis of nucleotides to form the IF polymer (Herrmann et al. 2009). In contrast to actin filaments and microtubules, intermediate filaments are non-polar polymers composed of fibrous subunits that exhibit marked insolubility in nonionic detergent buffers (Herrmann et al. 2004; Omary et al. 2006). Purified IF proteins simply require buffers of physiological pH and ionic strength to assemble into filaments *in vitro* (Herrmann et al. 2004).

The initial step of polymer assembly for all intermediate filaments is the formation of the coiled-coil dimer, the only filament precursor that demonstrates N to C terminal polarity (Quinlan et al. 1986; Coulombe and Fuchs 1990). These dimers interact laterally, adopting an anti-parallel and staggered position with respect to one another to form tetramers that are approximately 60 nm in length

(Geisler et al. 1992; Steinert and Parry 1993). *In vitro* tetramers and other higher-order filament precursors laterally associate within the first second of IF polymerization, forming wider unit length filaments (ULFs) of approximately 16 μm via processes that have yet to be completely described (Herrmann et al. 1996; Herrmann et al. 1999). These ULFs are predicted to contain 32 polypeptides, a deduction based on mass-per-length measurements of scanning transmission electron microscopy images (Herrmann et al. 1996; Herrmann and Aebi 1998). Within the following seconds and up to the first minute, ULFs longitudinally associate to form filaments with a length of up to 300 nm (Herrmann et al. 1996). After the first minute and through the first hour the filaments begin to demonstrate a radial compaction, decreasing in width to form much longer filaments that are 10nm in diameter (Hermann et al. 1996; Herrmann and Aebi 1998).

Particular domains within IFs have been shown to be crucial for filament assembly, including the closely conserved residues at the most N-terminal and C-terminal positions of the IF rod (Hatzfeld and Weber 1992; Goldman et al. 1996; Strelkov et al. 2001; Chernyatina et al. 2012). In addition, portions of the head domain are thought to be important for lateral interaction and tetramer stabilization (Steinert and Parry 1993; Traub et al. 1992; Herrmann et al 1992; Chernyatina et al. 2012). While the head regions appear to be necessary for IF assembly (Hatzfeld and Burba 1994; Herrmann et al. 1996; Herrmann et al. 2004), the requirement for the tail varies. The tail regions for some IFs are dispensible in regard to filament assembly, while others require it for the compaction of radial diameter that occurs

during filament maturation (Hatzfeld and Weber 1990; Nakamura et al. 1993; Herrmann et al. 1996).

While the sequential characterization of the IF assembly process by Herrmann and colleagues directly describes that of vimentin and desmin IFs, several important distinctions have been demonstrated for other IFs. The type I and type II keratin heteropolymers demonstrate rapid assembly processes that require protein concentrations to be heavily restricted in order to detect tetramers (Coulombe and Fuchs 1990). When the protein concentrations are increased, the formation of ULFs and elongation into filaments proceeds with such speed that it is difficult to determine whether these steps occur in sequence or can occur simultaneously for keratins (Herrmann et al. 2004). The type V nuclear lamins appear to elongate longitudinally *in vitro* after dimer formation into protofilaments, further assembling laterally into filaments for some time and then appearing as a paracrystalline aggregate (Aebi et al. 1986; Herrmann and Aebi 2004). Such differences in assembly mechanisms *in vitro* highlight a diversity that is an important consideration when examining *in vivo* IF networks.

Mechanical aspects of IF proteins

Early investigations of the mechanical nature of coiled-coil intermediate filaments focused largely on non-cytoplasmic α-helical keratins in wool fibers. These landmark studies demonstrated a striking property of these keratin filaments: they are highly malleable when stretched, undergoing a complete change in secondary structure to that of a β-pleated sheet morphology before deforming past the point of polymer destruction (Astbury and Woods 1933; Bendit

1960; Kreplak et al. 2004). The heavily conserved secondary and tertiary structure of coil-coiled intermediate filaments described previously allows this inherent mechanical resistance to be shared across the diverse IF family (Dowling et al. 1986; Hanukoglu and Fuchs 1983; Geisler and Weber 1982; Steinert et al. 1983).

Several characteristics of IF proteins contribute to their ability to withstand strains. IFs demonstrate an elastic and bendable nature due to their persistence length, which endows them with inherent flexibility (Schopferer et al. 2009; Lichtenstern et al. 2012). The 'buckling' behavior of filaments in cytoplasmic IF networks is a direct observation of the flexibility of IF polymers in the cellular environment (Nolting et al. 2014). The IF polymer is thought to endure pulling forces via the ability of the IF protein rod to transition from α-helix to β-sheet and the ability of the laterally associated subunits of the polymer to slide and change position with respect to one another (Guzman et al. 2006; Kreplak et al. 2008). Cytoplasmic intermediate filaments allow extension by force beyond 200% of their original length in some IF types, demonstrating outstanding strain tolerance (Kreplak et al. 2005).

Intermediate filaments are also endowed with a favorable attribute with regard to strain resistance in that they are known to form extended networks rather than acting as individual polymers. While this facet of IF allows the contribution of multiple filaments when resisting an applied force, IF networks exhibit another key quality when stretched: the network responds to applied forces by stiffening that resists subsequent deformation (Janmey et al. 1991). This increase in the hardness of the network results in a reduction in the degree of deformation that

occurs due to applied force. One mechanism for strain buffering is thought to be crosslinking between the charged and polar residues on the hydrophilic surface of coiled-coil α-helices mediated by divalent cations (Lin et al. 2010a). In addition, the IF tail domain has been demonstrated to be a requirement in some IF proteins for stiffening after application of strain (Bar et al. 2010; Lin et al. 2010b; Pawelzyk et al. 2014).

The properties of stretch resistance intrinsic to intermediate filaments are clearly conferred to and are beneficial for cells. IF networks have been experimentally shown to control cellular stiffness, both broadly for the cell and within intracellular compartments (Seltmann et al. 2013). Cells depleted of IF networks show greater size deformation in response to stretching forces compared to IF expressing cells (Seltmann et al. 2013; Ramms et al. 2013). In addition, IF networks are thought to have a crucial role in determining cell shape, as introduction of a non-native IF network is sufficient to alter the cell morphology (Mendez et al. 2010). This kind of cellular shape determination may be influenced by differences in the mechanical properties across filament networks, allowing IF expression profiles to contribute to establishing distinct mechanical identities for different cell types (Schopferer et al. 2009). Such differences may have considerable ramifications for cells specialized to mitigate direct physical forces, to endure fluid forces, or to interpret and manage forces during migratory events.

The earliest cytoplasmic IFs in eukaryotes: cytokeratin properties and expression patterns

The keratins of the type I and type II IF subgroups stand out from other IF proteins because of their nature as obligate heteropolymers and great diversity compared to any other intermediate filament. The large number of keratin genes and individual keratin molecules has necessitated a separate nomenclature that numerically orders genes (KRT#) and proteins (K#) (Schweizer et al. 2006). Keratins that are known to be functionally expressed include type I and type II epithelial and hair keratins, which are 54 in number. Cytokeratins are the cellular keratin intermediate filaments that are present in various types of epithelia; these comprise 17 type I ‘acidic’ cytokeratins and 20 type II ‘basic’ keratins in the human (Schweizer et al. 2006).

Epithelial keratins are found within a number of tissues in the adult human. Keratin IFs are expressed throughout the layers of the epidermis (Moll et al. 1982) populating keratinocyte epithelial cells throughout basal, spinous, granular, and cornified epithelium (Moll et al. 1982; Sun et al. 1985; Toivola et al. 2005). Type I acidic keratins in this tissue include K9, K10, K14, K15, K16, K17, and K19; type II basic keratins include K1, K2, K5, and K6. Outside of epidermal tissue, keratins are expressed most widely in tissues that contain simple epithelial cells. These include the columnar epithelia of the villi in the small intestine, outer covering liver hepatocyte epithelial cells, and the epithelia of the inner lining of the lung. Type I acidic keratins in these tissues include K18, K19, and K20; type II basic keratins include K7 and K8 (Toivola et al. 2005).

Keratins are expressed during very early stages of embryonic development, including pre-fertilization oocytes in the amphibian *Xenopus laevis*. The type I Keratin 18 and basic Keratin 8 that are detected in many mature simple epithelial cells are the first IFs to be expressed, demonstrating distribution in cells near the embryonic surface. Mouse embryos express K8 and K18 as early as the eight-cell stage, and cytokeratins remain present as the primary cytoplasmic IFs prior to cell differentiation stages (Oshima et al. 1983). K8 and K18 are followed by expression of basic K7 and acidic K19 (Brulet et al. 1980; Paulin et al. 1980) Expression of keratins can be detected in the context of embryonic development as early as pre-fertilization, as the *Xenopus* oocyte demonstrates localization of cytokeratins throughout and particularly at the cortex (Franz et al. 1983; Wylie et al. 1985; Klymkowsky et al. 1987). Early stage embryos form keratin networks that span from the surface superficial to the deep cellular layers. Inhibition of these keratins results in a failure of the embryos to complete gastrulation, demonstrating that they are necessary for the embryo to develop beyond this stage (Torpey et al. 1992; Klymkowsky et al. 1992; Heasman et al. 1992).

Cytokeratins in the context of the cell

Cytoplasmic keratins form filamentous networks throughout cells that appear to be dense and widespread, casting the impression that this cytoskeleton favors total size over specific organization. Closer examination elucidates that while cytokeratins span several cellular locales, these filamentous networks exhibit specific organization in distinct subcellular compartments. As first proposed by Lazarides, keratin networks are perhaps most easily recognized in the cytoplasm

proper, where these filaments are broadly thought of as integrators of cellular space (Lazarides 1980). Indeed, keratins do connect different compartments of the cell- specifically, the widespread keratin IFs throughout the cytoplasm connect to keratins in other compartments that demonstrate organization appropriate for their function. In columnar epithelial cells, where cellular spaces and their relationship to keratins are well-defined, these compartments include cellular interfaces with adhesions and the area proximal to the nucleus (Moll et al. 1982). Both the organization of keratin networks at these locations and the relationship of keratin filaments with molecular structures in these compartments provide broad clues about their major functions in the cell.

Epithelial cellular adhesion interfaces include two major compartments: the cell-cell adhesion and the cell-matrix adhesion. The specific component of the cell-cell adhesion in columnar epithelia that is associated with keratin is known as the desmosome (Culkins and Setzer 2007; Franke et al. 2009). Cells of the developing mouse embryo establish their initial keratin networks proximal to forming desmosomal complexes (Jackson et al. 1980; Magin et al. 1998). These rivet-like, protein dense connection points at the lateral contact between columnar cells are comprised of desmocolin and desmoglein cadherin-like transmembrane proteins that bind one another extracellularly to initiate the desmosomal contact (Koch et al. 1990; Koch et al. 1991). The intracellular domains of these molecules bind a series of proteins that then form a plaque- namely plakophilin, plakoglobin, and desmoplakin (Hatzfeld et al. 1994; Mertens et al. 1996; Gorbsky et al. 1985; Schmidt et al. 1999; Franke et al. 1989; Green et al. 1990). Desmoplakin is capable

of binding keratin filaments in these cells, allowing the keratins to associate with and weave through the protein plaque (Kelly 1966; Franke et al. 1981; Green et al. 1990; Green et al. 1992). The keratin IF network that forms at desmosomes in each of the joined cells allows the adhesion to withstand strains exerted by pulling and pushing forces, thereby fortifying the junction (Stappenbeck and Green 1992; Bornslaeger et al. 1996; Acehan et al. 2008).

Columnar epithelia maintains a well-defined basal surface that interacts with the extracellular matrix protein network known as the basal lamina (Sonnenberg et al. 1991; Hogervorst et al. 1993). Keratin IFs are associated with this cell-matrix compartment through a specific adhesion complex known as the hemidesmosome. The hemidesmosome is comprised of transmembrane integrin molecules that have affinity for specific molecules in the extracellular matrix (Hogervorst et al. 1993). The intracellular domains of these molecules are targets for plectin proteins that also have affinity for keratin IFs (Wiche et al. 1993; Geerts et al. 1999). In addition, the hemidesmosome also includes the matrix-binding collagen type XVII transmembrane proteins that associate with BP230, another keratin-binding molecule (Guo et al. 1995). In similar arrangement to that demonstrated at cell-cell adhesion desmosomes, the keratin network at the hemidesmosome laterally associates with the plectin and BP230 (Svitkina et al. 1996; Hopkinson and Jones 2000). The association of the keratin network at the cell-matrix hemidesmosome also confers buffering against mechanical strains that are transduced at this interface (Bar et al. 2014).

The specific keratin linkages with plaque proteins of adhesion complexes at the cell-cell and cell-matrix interface provide the benefit of both concise localized roles and broad function because of the integrated nature of IFs: the keratin networks are connected (Morgan et al. 2011; Lombardi et al. 2011). Keratins form an extended network throughout the cell that extends to a completely different IF compartment called the ‘peri-nuclear cage’ (Windoffer et al. 2004; Morgan et al. 2011). This keratin network is formed around the periphery of the nucleus and exhibits a ‘woven’ or ‘basket-like’ filament morphology (Windoffer et al. 2004; Kolsch et al. 2010). The strikingly different appearance of keratins at the nuclear compartment compared to those of adhesions demonstrates an advantageous property of IF networks. The filaments are capable of establishing distinct functional arrangements within an interconnected network. These connections likely allow for integration of cellular space in an active way; mechanical changes at one location can have ramifications for all connected locations, allowing cells the opportunity to respond (Lombardi et al. 2011; Conway et al. 2013).

The concept of cellular change is a vital consideration for intermediate filament cytoskeleton, as the IF network must be capable of enough variability to be able to respond and properly mitigate forces. Though the previous examples provide an overview of various keratin functions in the cell, IF arrangements are not restricted to those described. Cellular IF networks including keratins demonstrate ongoing assembly and remodeling, characterized by both motile fibrils and the continual movement of pre-filament subunits (Windoffer et al. 2004; Kolsch et al. 2010; Moch et al. 2019). In addition, other cell and tissue types employ

keratin networks in subcellular contexts that differ from that of highly polarized columnar epithelium. Embryonic germ layer cells demonstrate not only differences in interactions between keratin networks and molecules of the cell-cell adhesion, but also remarkably different IF protein and filament distribution and activity at the cell-matrix interface (Weber et al. 2012). An appreciation of the variety of cellular contexts for keratin networks as well as the potential for these networks to influence this variety is therefore important to understanding the role of IF network reorganization in the cell.

Functional roles of keratins

Expression of keratins in the earliest stage embryos implies an important role for these IFs in development. Global knockout of K8 in the mouse was originally demonstrated to result in embryonic lethality for nearly all embryos by embryonic day 12.5, but the proportion of embryonic death was shown to differ across mice of different genetic lineages (Baribault et al. 1993; Baribault et al. 1994). The majority of mice that survive demonstrate abnormalities in the colon after birth that include hyperplasia and inflammation (Baribault et al. 1994). It is unclear whether these differences in viability after K8 loss are related to compensation by other keratins, but some insight may be garnered from the effect of global K18 and K19 knockout. While loss of K18 and K19 results in no overt phenotypes in the context of individual knockouts of these keratins, double K18 and K19 knockout has a marked effect on embryos (Magin et al. 1998; Tamai et al. 2000; Hesse et al. 2000). K18-/- K19-/- mouse embryos demonstrate an inability to form any keratin IF networks and do no survive beyond day 10 (Hesse et al.

2000). The lethality that arises from loss of both acidic keratins in the early embryo is a consequence of abnormalities in trophoblast cells that normally express keratin networks. Depletion of the keratin network results in mechanical deficiency of the trophoblasts and failure of placental tissue function, demonstrated by the presence of bleeding within the embryos (Hesse et al. 2000). This tissue defect is shared by double knockout of K8 and K19 in mouse embryos that despite exhibiting K7 and K18 containing filaments also demonstrate embryonic bleeding (Tamai et al. 2000).

Although the prominent effects of these keratin knockout strategies first appeared to illuminate a functional role for the IFs in tissues that are not a part of the embryo proper, continued investigation of knockouts provided other insights into properties and roles of keratins in developing organisms. While the structural properties of keratin IFs and networks confer utility in strain resistance, it is important to recognize that keratins are not functionally limited to mechanical roles in the cell. Knockout of K8 has been shown to disrupt apical protein localization and expression in the epithelia of the small intestine and hepatocytes, demonstrating a role for keratin IFs in the compartmental polarization that is a hallmark of epithelial cell types (Ameen et al. 2001; Satoh et al. 1999). Other than K8 deletion, aberrant protein localization has also been shown to result from expression of mutant K18 and knockdown of K19, affecting a number of molecules that are involved in junctional assembly, ion transport, and cellular signaling in both the cytoplasmic and membrane proximal compartments (Salas et al. 1997; Hanada et al. 2005). In addition, knockout of both K8 and K18 has an effect on hepatocyte

cellular signaling. K8-/- and K18-/- resulted in a proportion of hepatocytes becoming larger and multinucleated concomitant with a change in the distribution of an adapter protein involved in multiple signaling pathways, 14-3-3 (Toivola et al. 2001). Changes in the ability of keratin IFs to bind 14-3-3 has ramifications for several cellular processes in different cell types, now characterized in regard to multiple acidic keratins and intermediate filaments types broadly.

The orientation of keratin IF networks in cells is another aspect that provides insight into the variety of roles this cytoskeleton is positioned to perform in the living environment. A key feature of keratin networks, their widespread nature in the cytoplasm, allows these structures the ability to influence the position of organelles in the cell. These networks may perform a cellular organization role in regard to organelles, illustrated by changes in the cytoplasmic architecture after keratin mutation or deletion. Most notably, loss of K8 in hepatocytes results in mitochondrial mislocalization, size decrease, changes in mitochondrial protein expression, decreased ATP, and changes in cytochrome c signaling (Tao et al. 2009). Such changes may account for the predisposition to liver disease that has been linked to abnormal simple epithelial keratins (Ku et al. 1997; Ku et al. 2001; Zhong et al. 2009). Additionally, deletion of K19 in myoblasts has been shown to result in abnormal mitochondrial distribution (Stone et al. 2007). K18 mutation has also been demonstrated to result in an aberrant localization of the Golgi apparatus that is readily apparent in cultured hepatocytes, a finding that has yet to be completely interrogated but nonetheless links keratin networks to a broader role in subcellular organization (Kumemura et al. 2004).

Some of the most directly essential roles for keratin filaments are mechanical functions that have been revealed by mutation and deletion of the keratin IFs expressed within the epidermis. Genetic mutations that result in point mutations in the sequence of both K5 and K14, which form a heteropolymer in epidermal cells, are the direct cause of a disorder known as epidermolysis bullosa simplex (EBS) (Pearson 1962; Letai et al. 1993). Individuals with EBS suffer from severe blistering of the skin, a symptom that is both phenocopied and extended in K5-/- and K14-/- mice (Chan et al. 1994; Peters et al. 2001). This deficiency perturbs the mechanical strength of the epidermis, resulting in widespread basal layer cell lysis and death after birth for all mice with K5 deleted and the majority of those with K14 deleted (Chan et al. 1994; Peters et al. 2001). The requirement for K5 and K14 to establish an epidermis with the ability to resist forces and ultimately promote the survival of the organism demonstrates that the strain mitigation these keratins provide is essential. Keratin networks harboring EBS mutations have been shown to fracture into aberrant aggregates at the cell periphery, highlighting the drastic loss of filament network properties necessary to withstand and buffer against strains (Pekny and Lane 2007).

Other than EBS, dysfunction of keratins results in a variety of diseases. The majority of these diseases result in abnormalities of the skin that present with either specific symptoms or with specific localization, owing to the expression patterns of keratins. Other than diseases of the skin, keratin mutations are known to result in abnormality of the epithelia of the oral cavity as well as the corneal epithelium of the lens in the eye (Terrinoni et al. 2001; Nishida et al. 1997). While mutations of

keratins expressed in simple epithelia do not result in acquirement of developmental diseases, they predispose the organism to major diseases of the liver (Ku et al. 1997; Ku et al. 2001; Zhong et al. 2009). Keratin abnormalities may not be the cause of cancers, but they appear to be markers of tumors and consequences of these diseases. A variety of cancer types have been linked to changes in keratin expression as well as modification of keratins, highlighting intermediate filaments as potential contributors to oncogenesis or cellular invasion (Karantza 2011).

Molecular modification of keratin intermediate filaments

The characteristics of intermediate filament proteins and networks described thus far facilitate polymer assembly based on inter and intra molecular interactions that are independent of other molecules. Though the apparent autonomy of this process presents an advantage in regard to network formation, it raises a critical question – how can the establishment of such networks be regulated in the cell, where cytoplasmic IFs demonstrate a variety of distinct subcellular organizations, protein interactions, and even disassembly mechanisms? The need for the cell to modify and regulate these networks is especially apparent when considering the varied functions of IF networks, as these filaments must be capable of conducting several different roles simultaneously.

The most strongly established mechanism that is known to mediate heterogeneity and functional change in regard to IF networks is post-translational modification (PTM) of IF proteins. Intermediate filament PTMs that are well described involve covalent linkages of chemical groups to residues that are mainly

grouped within the head and tail domains of IF proteins (Omary et al. 2006). These are the IF regions that show the most sequence variety across IF family subgroups as well as within particular groupings, such as the type I and type II keratins (Geisler and Weber 1982; Hanukoglu and Fuchs 1983; Steinert et al. 1983). Modification of IF residues has been shown to affect filament properties, inducing network alterations that have been shown to have consequences for a multitude of cellular processes.

Extensive support exists to demonstrate that PTM of IFs via reversible phosphorylation at serine/threonine residues in the filament head and tail domains results in distinct changes that have ramifications for cells. Foremost among these is an increase in solubility following phosphorylation, a characteristic of IF subunits such as dimers and tetramers that is reduced in extended filaments (Omary et al. 2006). Solubility increases are thought to be important for general dynamic activity of intermediate filament networks, as these changes provide opportunity for restructuring of otherwise stable IFs (Ridge et al. 2005; Woll et al. 2007; Busch et al. 2012). Known restructuring events include dynamic exchange of IF proteins, a process which allows soluble IF subunits to be incorporated laterally along the length of filaments (Sivaramakrishnan et al. 2009). Phosphorylation may also induce changes in IF networks outside of dynamic exchange of precursors by decreasing the stability of intramolecular interactions, promoting disassembly of IFs. Hyperphosphorylation has been demonstrated to result in aggregation of filament proteins, likely due to abnormal configurations and disruption of IF protein interaction mechanisms (Kasahara et al. 1993; Toivola et al. 1997; Strnad et al.

2001). This variety in phosphorylation-induced IF changes illustrates that the aspects of the affected residues, the number of affected residues, and the configuration of the affected IF protein are all components of the vital context required to understand the significance of any IF phosphorylation event in terms of cellular processes.

Site-specific phosphorylation of keratins has been associated with a number of IF network properties, cellular events, and disease mechanisms. During mitosis, which involves a dramatic restructuring of cytoplasmic IF networks, keratin IFs demonstrate phosphorylation of distinct sites that are thought to mediate network disassembly (Toivola et al. 2002). K8 is rapidly phosphorylated at serine 73 during hepatocyte cellular stress, resulting in a marked restructuring of the network (Ku and Omary 2006). K8/K18 filaments in these cells are thought to function as ‘sinks’ for phosphorylation, restricting kinase activation of apoptosis promoting proteins (Ku and Omary 2006). Indeed, K8 Ser53 and K18 Ser73 mutation induces hepatocyte apoptosis during cellular stress (Ku et al. 1998; Ku and Omary 2006). Keratin networks reorganize during migration, and phosphorylation of K8 Ser431 has been shown to increase migration in pancreatic and gastric cancer cells (Busch et al. 2012). In contrast, mutation of this site in oral carcinoma cells also increased migration, demonstrating functional differences in phosphorylation across cell types (Alam et al. 2011). Phosphorylation of particular keratin sites has been shown to be restricted to different cell types in the same tissue and even spatially separated networks in the same cell, highlighting the

context specificity of these PTMs (Ku et al. 2002; Zhou et al. 2006; Fois et al. 2013).

IF modulation by phosphorylation raises an important consideration; are observed changes solely the result of the presence or absence of a phosphate, or alternatively due to secondary molecular interactions that require phosphorylation to enable interaction? A subset of changes in IF networks due to phosphorylation are mediated through interaction with 14-3-3 proteins, a family of molecular adaptors that bind specific sequence motifs that contain a phosphorylated serine or threonine. 14-3-3 proteins are known to interact with several intermediate filament proteins including keratins and to modulate their activity, enabling IF networks to influence signaling pathways that control cell cycle events and cellular growth (Margolis et al. 2006; Kim et al. 2006). Keratins have been shown to modulate such processes by preventing 14-3-3 proteins from engaging in other interactions that are required as critical steps in signaling pathways (Margolis et al. 2006; Kim et al. 2006). In addition, 14-3-3 has been shown to regulate keratins directly, enhancing dynamic activity of keratin filaments and functioning as requirement for network reorganization after fluid shear stress (Sivaramakrishnan et al. 2006).

Though phosphorylation comprises the most extensively examined keratin regulation by PTMs, these IFs are subject to other modifications that have functional consequences for the network. Keratin IFs are also subject to acetylation, sumolyation, ubiquitlyation, glycosylation, and transamidation modifications (Snider and Omary 2014). Similar to phosphorylation, solubility

changes have been observed due to acetylation and sumolyation of lysines in K8 (Snider et al. 2011). These modifications are different in that they target residues in the rod domain rather than the head or tail domains, and in the case of sumolyation demonstrate bi-functionality; monosumolyation promotes IF solubility, and hypersumolyation confers insolubility (Snider et al. 2011). While keratin modification by sumolyation occurs infrequently outside of abnormal contexts, K8 mutants that promote liver disease have been shown to subject to these modifications (Snider et al. 2011).

Ubiquitylation, glycosylation, and transamidation modifications alter filament aspects outside of solubility. Ubiquitin modification serves as a key modification for IF degradation in both general turnover and in response to IF abnormality, with aggregates of mutated IFs containing ubiquitylation modifications (Ku and Omary 2000; Loffek et al. 2010). O-linked glycosylation of K18 is required to facilitate an interaction between AKT1 and K8, allowing AKT1 to become phosphorylated and function as a regulator of cell survival mechanisms (Ku et al. 2010). Transamidation modifications are found in the K8/K18 hepatocyte ‘Mallory-Denk bodies’ characteristic of liver disease and thought to facilitate crosslinking of keratins to these aggregates (Strnad et al. 2007). Although these IF modifications may not be as prevalent as phosphorylation, the fact that the presence or absence of phosphorylation can modulate these PTMs illustrates their relevance to IF function (Ku and Omary 2000).

Dynamic activity of keratin intermediate filament networks

The changing environment of the cell necessitates a dual nature for cytoplasmic IFs: while these filaments must be stable enough to resist forces when needed, the networks must also be able to adjust and restructure. The ability to reorganize refers to several changes for keratin networks, encompassing large-scale disassembly that occurs during phases of mitosis as well as compartmentalized changes in IF network density at adhesion complexes. In order to efficiently provide distinct functions in an environment defined by malleability, keratin networks must be subject to characteristics and processes in the cellular environment that facilitate regular and frequent remodeling.

Intermediate filaments across subgroups host qualities that allow the polymers within an IF network to be subject to augmentation. Mature elongated filaments incorporate injected IF protein subunits into the cytoplasmic IF network, demonstrating an ongoing mechanism of filament modification that is called ‘dynamic exchange’ (Okabe et al. 1993). Studies that have employed photobleaching of fluorescently tagged IFs along with those that have utilized fluorescent photoconvertible IFs have shown that IF protein subunits are constantly added to filaments throughout networks, even in a ‘steady-state’ cell that is not undergoing an obvious dramatic reorganization of the IF network (Vikstrom et al. 1992; Colakoglu and Brown 2009; Noding et al. 2014).

Moreover, evidence strongly suggests there is exchange of proteins among filaments of the same network rather than just continual addition of *de novo* translated or introduced precursors. In particular, keratin networks composed of

K8 and K18 demonstrate compartmental exchange of IF proteins where the central peri-nuclear network donates IF proteins to the connected peripheral keratin network (Kolsch et al. 2010). These cellular keratin networks assemble even when translation is blocked by cyclohexamide. This evidence demonstrates that IF networks employ mechanisms that allow disassembly of filaments into precursors that are then incorporated into other filaments (Kolsch et al. 2010). The incorporation of precursors in dynamic exchange is dose dependant, providing evidence that cellular environments maintain a balance between soluble filament precursors and insoluble filaments. The existence of these two filament populations that can each draw from and contribute to one another provide IF networks the ability to dynamically rearrange, maintaining an ongoing capacity to respond to and contribute to a variety of cellular changes. Dynamic exchange within keratin networks has been shown to occur in some of the earliest stages of mouse embryos, highlighting the relevance of these processes in tissues and the context of development (Schwarz et al. 2015).

The mechanism of IF protein exchange that occurs in mature polymers across the cellular IF network does not orchestrate dynamic filament activity in isolation. Rather, keratin IF networks are subject to a cycle of turnover that allows for continual IF assembly and network rearrangement. Living cells demonstrate a cyclical process of keratin turnover that starts with nucleation of soluble subunits into larger pre-filament structures (Windoffer et al. 2004). These ‘particles’, named for their appearance in fluorescent confocal light microscopy, could potentially be related to ULFs characterized during stop-fix electron microscopy assembly

assays (Herrmann et al. 1996; Windoffer et al. 2004). Though their exact composition is unknown, their activity has been the subject of many recent investigations. Keratin particles have been demonstrated to translocate inward from the cell periphery, utilizing either microtubules or actin filaments depending on the cell (Prahlad et al. 1998; Helfand et al. 2002; Kolsch et al. 2009). Though the motion has been shown to be mainly retrograde, it is not exclusively uni-directional (Hookway et al. 2015). This suggests that keratin particles either traffic on cytoskeletal arrays that project in several directions and/or that particles can associate with either retrograde or anterograde directed motors (Helfand et al. 2002; Hookway et al. 2015).

During the retrograde translocation of the keratin particles, these precursors have been shown to interact and extend into structures called ‘squiggles’ (Yoon et al. 2001). This process is thought to be end-to-end annealing that occurs on the move, as squiggles continue to associate with other precursors (Prahlad et al. 1998; Yoon et al. 2001). Once the inward moving pre-filaments arrive proximal to the dense central peri-nuclear IF network, they are subject to one of two fates: these filaments either incorporate into the filament network, or disassemble and diffuse beyond the point of detection by light microscopy (Kolsch et al. 2010). In this way, the process is thought to contribute to both continual filament formation and dynamic activity by maintaining the soluble keratin fraction (Kolsch et al. 2010; Windoffer et al. 2011). Though this cycle of keratin turnover has been shown to occur within a variety of epithelial and non-epithelial cell types in the manner described above, this process may provide insights for cells in a variety of contexts

that remain to be explored (Windoffer et al. 2004). How this sequence of events manifests in cells that are establishing contacts, enduring mechanical stressors, or migrating as groups may inform how these broad keratin dynamics are adapted in specific situations.

Dynamic activity of keratin networks not only refers to changes that can occur in the structure of the network, but also to an increased variety in cellular application that may be mediated by interactions with particular structures. As previously described, keratin precursors exhibit ‘nucleation’ at sites proximal to the cell periphery (Windoffer et al. 2006). Evidence exists to suggest that focal adhesion complexes influence keratin assembly, indicating a compartmental and complex specific influence on keratin dynamics (Windoffer et al. 2006; Leube et al. 2015). In addition, the relationship between focal adhesions and keratins places these adhesions in position to interact with the keratin network at large. Keratin network association with desmosomes allows both the IF network and the adhesion complex to influence each other, reflecting interplay between IF and adhesion dynamics (Kroger et al. 2013; Loschke et al. 2016; Moch et al. 2019). The ability of adhesion dynamics to affect IF dynamics and vice versa is reflected by keratin modulation of adhesion complexes that these filaments have not been classically associated with (Leonard et al. 2008; Weber et al. 2012).

Perhaps the most prominent outside influence that contributes to dynamic activity of keratin networks and IF networks in general is crosstalk with other cytoskeletal systems (Yoon et al. 2001; Kolsch et al. 2009). Although it is not clear whether keratins associate with actin motor proteins, transport of IF proteins

requires an intact actin network (Kolsch et al. 2009). Actin and keratin filaments have been shown to form complexes that contain 14-3-3 proteins in invasive carcinoma cells (Boudreau et al. 2013) Perturbation of both the cellular IF network and the cytoskeletal crosslinker plectin result in marked changes in actin filament organization, highlighting the interconnected relationship of actin cytoskeleton and keratin network dynamics (Moch et al. 2016; Sonavane et al. 2017). Disruption of either actin or microtubules can result in collapse of keratin networks, echoing the interconnected nature of these cytoskeletal systems (Woll et al. 2005)

Keratin dynamics in developing *Xenopus laevis* embryos

The dynamic activity of keratin cytoskeleton has a clear importance in the gastrula of *Xenopus laevis* embryos, where simple epithelial keratins comprise the sole IF network of the mesodermal and endodermal cells (Franz et al. 1983; Wylie et al. 1985; Klymkowsky et al. 1987; Weber et al. 2012). These keratins, which are homologous to mammalian K8, K18, and K19, are both maternally derived as well as translated zygotically, originating from a gene cluster that resembles the organization found in the human (Suzuki et al. 2017). During gastrulation, a mixed population of mesoderm and endoderm engage in a coordinated collective migration that comprises an essential cellular movement (Weber et al. 2012). In concert with coordinated cellular movements in proximal tissues that include convergent extension and epiboly, the collective migration of this ‘mesendoderm’ contributes to establishment of the embryonic germ layers as well as the body axis of the embryo (Davidson et al. 2002; Longo et al. 2004; Keller et al. 2000). These migratory movements are critical for cellular differentiation events and tissue

specification that occurs in later developmental stages. Failure of these migratory movements can have consequences ranging from tissue abnormalities to embryonic death (Klymkowsky et al. 1992; Weber et al. 2012).

As the cytoplasmic IFs of the early embryo, keratins have a critical structural role. Depletion of the sole basic K8 by injection of morpholino oligonucleotides that are antisense to its transcripts causes the embryo to ‘exogastrulate’ and perish (Weber et al. 2012). Exogastrulation is a result of extravasation of cells that normally involute during the migratory movements of gastrula. While this dysfunction is drastic, it can be triggered by multiple origins and therefore is not easily interpretable in terms of a specific defect. Nonetheless, the clear requirement for K8 in development highlights the importance of the keratin network at this stage, as the acidic K18 and K19 IFs cannot form heteropolymers or networks without this basic keratin.

The critical role of the cytoplasmic keratin network becomes apparent when investigating the properties of these IFs in the cells of *Xenopus* gastrula. Keratin networks in migratory mesendoderm cells demonstrate compartmental specific organization that is characteristic of cytoplasmic IF networks: precursors at the cell-matrix periphery, a widespread cytoplasmic network, a peri-nuclear network, and a population of filaments that are localized to the cell-cell contact (Weber et al. 2012). Investigation of this typical IF network revealed a standout and novel role for keratin IFs in these cells. Application of mechanical force on these cells was shown to rapidly recruit significant densities of keratin IFs to the site of force transduction, a network reorganization that resulted in cellular protrusion formation

and migration in the opposite direction of the pulling force (Weber et al. 2012). Importantly, this force transduction and recruitment was demonstrated to be necessary for the uni-directional migration of the collectively migrating mesendoderm population (Weber et al. 2012). Cells of dorsal marginal zone tissue explants that recapitulate mesendoderm migration *ex vivo* lose the ability to migrate directionally upon disassembly of cadherin adhesions via withdrawal of calcium. These findings provided evidence of an exciting novel role for keratin dynamics in the determination of cell migration.

The dynamic recruitment of the keratin network as a consequence of force transduction and concomitant induction of migratory polarity affords several insights about intermediate filaments. Rather than through desmocolin or desmoglien of keratin associated desmosomes, cell-cell adhesion is mediated by C-cadherin in these cells (Heasman et al. 1994). Plakoglobin associates with this complex and has an affect on keratin recruitment but is not required for it to occur (Weber et al. 2012). Cadherin complexes are typically associated with actin cytoskeleton, demonstrating plasticity in regard to the types of adhesions that keratin networks can link to (Franke et al. 2009). The speed and extent to which keratins are reorganized to these junctions implies that the keratin IF dynamics must be regulated in order to efficiently respond to such stimuli, raising important questions about the molecules and processes that are involved in such dramatic rearrangements.

Characterization of 14-3-3 proteins

Since their discovery just over 50 years ago, 14-3-3 proteins have been revealed to be key modulators of a large spectrum of cellular processes. The 14-3-3 molecules were first identified in 1967 in bovine brain samples and were named for the manner in which they were detected; these proteins eluted in the 14th fraction after DEAE cellulose chromatography and migrated to position 3.3 via starch gel electrophoresis (Moore and Perez 1967). The function of these molecules remained largely unexplored until 20 years later, when 14-3-3 proteins were identified as a requirement for activation of tryptophan 5-monooxygenase and tyrosine 3-monooxygenase by calcium/calmodulin dependant kinase II (Ichimura et al. 1987). Numerous subsequent studies have provided solid evidence for the role of these molecules in regulation of a great variety of proteins, describing an interactome comprised of a startling >200 targets of 14-3-3 proteins (Pozuelo Rubio et al. 2004; Jin et al. 2004).

Evidence of direct binding and modulation of a large variety of proteins by 14-3-3 has demonstrated their importance across cellular signaling pathways and biological processes. In particular, 14-3-3 binds to proteins involved in neurotransmitter synthesis, cell cycle progression, apoptosis, cell growth, development, cell adhesion, protein turnover, nutrient sensing, transport of vesicles, cancer progression, autophaphy, chromatin arrangement, and transcription (Sluchanko and Gusev 2017). This list is by no means exhaustive, as new functions for 14-3-3 proteins continue to be revealed. Moreover, 14-3-3 proteins are remarkably conserved and nearly ubiquitously present in eukaryotes.

Regulatory roles for 14-3-3 homologs and isoforms alike have been characterized in yeast, drosophila, several plant species, amphibians, and mammalian species (Darling et al. 2005).

14-3-3 protein structure

14-3-3 proteins in the mammal constitute multiple isoforms that were assigned greek letters based on their separation pattern via reversed-phase high performance liquid chromatography (Ichimura et al. 1988). Seven isoforms are the products of separate genes typically on separate chromosomes in the mammal, namely beta (β), gamma (γ), epsilon (ε), zeta (ζ), eta (η), tau/theta (τ/θ), and sigma (σ), with σ being characterized later in T-cells and epithelial cells (Ichimura et al. 1988; Leffers et al. 1993; Tommerup and Leffers 1996; Aitken 2002). In addition to these gene derived isoforms, there are two described 14-3-3 variants that are phosphorylated forms of β and ζ, named alpha (α) and delta (δ), respectively (Aitken et al. 1995). 14-3-3 proteins demonstrate expression in a wide range of tissues, with only the phosphorylated forms appearing to be constricted to the brain (Celis et al. 1990; Aitken 2011). There is marked conservation amounting to approximately 70% across the isoforms, and their individual sequence lengths appear to dictate their migration during gel electrophoresis (Wang et al. 1996). The majority of the isoforms have a molecular size that is at or close to 27kDa with ε representing the largest isoform at 30 kDa. When antibody immunolabeled after transfer from SDS-PAGE, these size differences result in the detection of 14-3-3 proteins as a band cluster or multiple bands depending on the percentage of polyacrylamide in the gel (Ichimura et al. 1988).

The sequence conservation of 14-3-3 proteins translates into a structural conformation that is closely shared among the isoforms. Each 14-3-3 protein comprises a monomer that is composed of nine anti-parallel α-helices that result in a cup-like or ‘u’-like three-dimensional shape (Liu et al. 1995). The residues of the cup/u-shaped recess constitute an amphipathic ligand-binding channel that interacts with residue motifs in target proteins (Xiao et al. 1995; Zhang et al. 1997; Wang et al. 1998). Upon dimer formation, the channel becomes 35 angstroms broad and wide as well as 20 angstroms deep, containing two binding grooves that are arranged anti-parallel to one another (Xiao et al. 1995; Liu et al. 1995). While the residues within the channel are absolutely conserved, there is a high degree of variability within the N-terminal as well as the C-terminal residues of each monomer (Rittinger et al. 1999).

The N-terminal regions have been shown to mediate the dimerization of 14-3-3 proteins, containing the residues that establish the interface between the monomers and the floor of the channel (Liu et al. 1995; Jones et al. 1995). This sequence variability determines the extent to which a given 14-3-3 isoform can form heterodimers or homodimers. The selectivity in potential dimer combinations appears to be mediated by the number of salt bridges that can be formed between a pair of monomers. Isoforms such as ε preferentially form heterodimers that include multiple salt bridges instead of a homodimer stabilized by a single salt bridge (Yang et al. 2006). In contrast, 14-3-3 σ preferentially forms homodimers that are interconnected by three salt bridges (Wilker et al. 2005; Verdoodt et al. 2006). Variety in potential dimer combinations may likely may provide 14-3-3

proteins with functional versatility in regard to interaction with target proteins. Indeed, 14-3-3 ζ has been demonstrated to form a number of heterodimer types (Verdoodt et al. 2006). Variability in the N-terminal residues of 14-3-3 proteins thus confers a degree of flexibility in dimer formation that may have functional ramifications as a result of the expression profile of 14-3-3 molecules in a cell type or tissue (Jones et al. 1995; Benzinger et al. 2005; Verdoodt et al. 2006).

Though several combinations of dimers are made possible due to sequence variability, this facet of 14-3-3 proteins would likely have reduced importance if the monomers in the dimer did not possess some differences that impact function. Substrate specificity for monomers is thought to be influenced by the C-terminal tail, the other part of 14-3-3 sequence that shows large variability across isoforms (Truong et al. 2002; Obsilova et al. 2004; Silhan et al. 2004). Although the structural conformation for this portion of the 14-3-3 dimer has yet to be resolved, there is some evidence to suggest that the C-terminal disordered tail can function as an autoinhibitory domain (Truong et al. 2002; Shen et al. 2003). Deletion of the C-terminal tail has been shown to result in higher affinity 14-3-3 binding of targets relative to that of wildtype 14-3-3 (Truong et al. 2002). Differences in the C-terminal domain across 14-3-3 monomers could potentially confer specificity for subsets of molecules within the large pool of 14-3-3 targets, allowing both discrete and varied functions for particular dimer combinations. However, since *in vitro* 14-3-3 binding assays have shown that multiple targets bind different isoforms equally well, it remains to be seen whether potential inhibition via the C-terminal region only

affects non-specific sequences or requires *in vivo* modification of 14-3-3 proteins (Muslin et al. 1996; Rittinger et al. 1999; Wang et al. 1999; Obsilova et al. 2004).

Molecular basis of 14-3-3 binding

Much of what we know about the relationship between 14-3-3 sequence, structure, and mechanism of target binding is a result of binding assays and solved ligand-bound crystal structures that have utilized well characterized peptides (Yaffe et al. 1997; Petosa et al. 1998; Rittinger et al. 1999). Pioneer work by Muslin and colleagues employed a small peptide consensus to the sequence flanking and including Serine 259 of Raf1, a residue that must be phosphorylated for 14-3-3 proteins to bind Raf1 (Muslin et al. 1996). Study of the interaction between this Raf1 peptide and 14-3-3 revealed a binding motif for targets of 14-3-3 proteins, RSxpSxP, where the phosphorylation of the middle serine residue is required for the interaction (Muslin et al. 1996). This finding was further informed by Yaffe and colleagues through utilization of a degenerate peptide library in order to characterize the optimal residues of 14-3-3 binding motifs (Yaffe et al. 1997). Two 14-3-3 binding motifs were established: a ‘mode I’ motif defined as R-[S/Ar]-[+]-pS-[L/E/A/M]-P and a ‘mode II’ motif defined as R-X-[Y/F]-[+]-pS-[L/E/A/M]-P where ‘+’ denotes a basic residue, ‘Ar’ denotes an aromatic residue, and X denotes any residue (Yaffe et al. 1997; Rittinger et al. 1999). Since several molecules had been described to bind 14-3-3 through mode I motifs, including Raf, BAD, and Cdc25c, and mode 2 peptide binding had been demonstrated, these early discoveries were critical for elucidating mechanisms through which 14-3-3 targets

other molecules (Muslin et al. 1996; Zha et al. 1996; Peng et al. 1997; Yaffe et al. 1997).

Continued study of the mechanism of interaction between 14-3-3 and target proteins have revealed a much greater variety in binding mechanisms than first proposed. A large body of discoveries have collectively demonstrated that the residues proximal to the phosphorylated serine or threonine at the center of 14-3-3 motifs are subject to variability. While not entirely revised, the aforementioned mode I and mode II motifs are commonly simplified to R-X-X-pS/pT- X-P and R-X-[Y/F]-X-pS/pT-X-P, respectively (Johnson et al. 2010). While this mode I sequence is an appropriate description of the majority of known 14-3-3 motifs, the arginine at the -3 position is not absolute and approximately half of described motifs do not contain a proline residue at the +2 position (Johnson et al. 2010). 14-3-3 proteins also bind relatively rarer 'mode III' C-terminal ending pS/pT-(X_{1-2})-COOH sequences in proteins such as arylalkylamine N-acetyltransferase and plant H+-ATPase (Ganguly 2005; Ottmann 2007). Plant proteins have been shown bind 14-3-3 mainly through a L-X-(R/K)-S-X-(pS/pT)-X-P motif (Johnson et al. 2010). In addition, binding sites that do not match any of these described motifs also exist, such as the R-P-V-S-S-A-A-pS-V-Y site including serine 33 in human Keratin 18 (Ku et al. 1998). The variability evidenced with the discovery of more 14-3-3 sites should not be interpreted as a lack of specificity in target sequences; rather, the diversity likely allows for different affinity among targets and potentially reflects evolution of different protein mechanisms for binding with 14-3-3 proteins.

Among the rarer interactions, some examples of 14-3-3 binding non-phosphorylated sequences exist. The ExoS viral protein inserts into the 14-3-3 binding groove via hydrophobic interactions with the residues of the groove roof (Masters et al. 1999). In a manner that more closely represents phosphorylated targets, the phage library derived ‘R18’ peptide contains a WLDLE sequence where the aspartic and glutamic acid residues interact with 14-3-3 residues that typically associate with the pS/pT of a target motif and the leucines interact with hydrophobic roof of the groove (Petosa et al. 1998). Thus, ExoS demonstrates binding that is nonpolar in nature while R18 utilizes amphipathic interactions to bind 14-3-3. Though few 14-3-3 interactions with non-phosphorylated sequences have been reported, the contrasting manner through which these two molecules bind 14-3-3 demonstrates that context of the residue interactions are critical to understanding binding. This is apparent in attempted ‘phosphomimetic’ single residue substitutions of aspartic acid or glutamic acid for the pS/pT residue in 14-3-3 motifs, as these substitutions largely fail to preserve binding to 14-3-3 proteins (Johnson et al. 2010).

Although the evidence from co-crystal structures of 14-3-3 proteins and bound ligands is likely unable to completely describe the molecular basis of 14-3-3 interaction, this information provides valuable knowledge of ways that 14-3-3 can engage targets. Analysis of a 14-3-3 ζ bound mode I peptide derived from polyoma middle-tumor antigen demonstrates that the phosphorylated serine in its sequence is engaged with a series of mostly basic resides within the 14-3-3 amphipathic groove (Yaffe et al. 1997). These pS interacting residues include lysine 49 and

arginine 56 of 14-3-3 helix 3/C as well as arginine 127 and tyrosine 128 of helix 5/E. In the case of the middle-tumor peptide, the phosphate forms salt bridges with K49, R56, and R127, while a hydrogen bond facilitates interaction between the peptide phosphate and Y128 (Yaffe et al. 1997). These 14-3-3 residues were shown to be essential for binding the mode I Raf1 peptide via charge reversal mutations including K49E and R56E (Zhang et al. 1997).

Several residues that are not directly engaged in interactions with the target pS/pT are nonetheless involved in substrate binding. These are residues of the largely hydrophobic roof of the 14-3-3 binding groove comprised of helices 7/G and 9/I, including leucines at position 172, 216, 220, and 227 along with a valine at position 176 (Rittinger et al. 1999). When these residues are charge reversed via mutation to aspartic acid, only L216D and L227D result in reduced rather than abrogated peptide binding (Wang et al. 1998). Structural analysis predicts that V176 and L227 residues interact with residues in the -2 position along with a tyrosine at position 179 and a tryptophan at position 228; these are predicted to involve side chain interactions (Rittinger et al. 1999). Likewise, asparagines at positions 173 and 224 along with a lysine at position 120 are predicted to form hydrogen bonds with the peptide backbone of the residues just before and after the pS/pT of the motif, promoting a straightened conformation for the peptide (Rittinger et al. 1999). Each of these residues are absolutely conserved in 14-3-3 proteins across a number of species (Rittinger et al. 1999; Yaffe 2002), demonstrating that while individual interactions may mechanistically vary between

14-3-3 targets, the variety of molecular strategies for binding them likely arise from these critical components of the sequence.

14-3-3 binding induces a variety of functional changes

The mechanisms of 14-3-3 binding are important to understand in order to appreciate how 14-3-3 can interact with a plethora of substrates, but ultimately the emerging question is ‘how does 14-3-3 binding impact the function of its target?’ Our understanding of 14-3-3 protein functions in the cellular environment has identified them as regulatory proteins: These proteins act on other targets via binding, most of these interactions requiring phosphorylation, and modulate their activity. The effect that 14-3-3 binding exerts on any given substrate is a result of characteristics of both the 14-3-3 dimer and the particular sites within the target protein. An interesting facet of 14-3-3 proteins evidenced through study of co-crystal structures is that binding of targets induces relatively little change in the structure of the 14-3-3 dimer (Yaffe et al. 1997; Rittinger et al. 1999; Obsil et al. 2001; Ottmann et al. 2007). This structural rigidity is thought to allow 14-3-3 proteins to function as a platform on which conformational change can occur in bound molecules (Yaffe 2002). Such a mechanism can hypothetically promote a large variety of changes depending on the features of bound targets.

Known binding interactions and resultant changes in the activity of molecules have led to the identification of a number of ways that 14-3-3 proteins regulate other molecules. One such method involves the direct change of protein structure induced by 14-3-3 binding. A well-characterized and outstanding example that illustrates this activity involves H^+-ATPase proteins of plant plasma

membranes, which as dimers exhibit an auto-inhibitory positioning of part of the C-terminal region of each monomer (Ottmann et al. 2007). Phosphorylation of these regions allows 14-3-3 proteins to bind, resulting in a conformational change where the auto-inhibitory region extends away from the dimer. In addition, each monomer of the H^+-ATPase dimer is bound by a single 14-3-3 dimer, leaving one of the 14-3-3 binding grooves free to associate with other H^+-ATPase subunits (Ottmann et al. 2007). This results in formation of a hexamer stabilized by three 14-3-3 proteins, placing 14-3-3 in control of both the activation and oligomerization of this protein via conformational modification (Ottmann et al. 2007).

While this 14-3-3 single motif binding and induction of conformational change is likely the mechanism of regulation for a number of 14-3-3 substrates, 14-3-3 proteins can also induce change by binding multiple sites. The catalytic enzyme Serotonin N-acetyltransferase (AANAT), involved in synthesis of melatonin precursor protein, has been shown to require binding of two phosphorylated sites in order to be bound and activated by 14-3-3 (Obsil et al. 2001; Ganguly et al. 2005). Co-crystal structure of the nearly full-length AANAT molecule bound to 14-3-3 ζ revealed that this interaction results in a conformational change of the AANAT binding groove, resulting in an increase in affinity with its substrate (Obsil et al. 2001). Evidence of binding mediated structural change and activation via dual site binding provides support for a ‘gatekeeper and anvil’ hypothesis proposed by Yaffe (Yaffe 2002). The ‘gatekeeper’ site is thought to be a higher affinity 14-3-3 site that once phosphorylated promotes 14-3-3 binding to a relatively lower affinity site within the same molecule. The rigidity of 14-3-3 allows

it to function as an ‘anvil’ upon which substrates are structurally modified and exhibit changes in activity. AANAT fits this description closely with a mode I 14-3-3 site including pT31, but no recognizable 14-3-3 binding motif around pS205. Only when both sites are phosphorylated does 14-3-3 binding result in the highest binding affinity between AANAT and its target (Ganguly et al. 2005).

Structural analysis of 14-3-3 proteins bound to substrates is required to determine whether the interaction results in a change in shape of the target molecule. Since this extensive level of study has only been applied to a subset of 14-3-3 interactions, it is difficult to conclude if/how many described interactions affect the conformation of 14-3-3 targets. Nonetheless, biochemical strategies to study regions of 14-3-3 binding and a variety of approaches to demonstrate changes in the activity of 14-3-3 targets have identified a number of regulatory activities of 14-3-3 proteins.

Perhaps the simplest activity regulation conferred by 14-3-3 binding is activation or inactivation of target protein’s activity. 14-3-3 binding has been shown to increase activity of tyrosine and tryptophan hydroxylases, and conversely to inhibit the activity of nitrate reductase (Moorhead et al. 1996). In a standout example of this kind of regulation, 14-3-3 binding has been shown to both inhibit the kinase activity of Raf1 and activate this molecule depending on which sites within Raf1 have been phosphorylated (Roy et al. 1998; Dumaz et al. 2003). Target binding by 14-3-3 has also been shown to promote interaction between molecules, and conversely to occlude molecules from associating with one another. Raf1 is activated by forming a complex with Ras that 14-3-3 has been shown to both

promote (Roy et al. 1998) and disrupt (Dumaz et al. 2003). In addition, 14-3-3 has been shown to promote a complex between c-Bcl and Raf1, kinases that do not demonstrate intrinsic ability to bind one another (Braselmann and McCormick 1995). Similarly, 14-3-3 proteins have been shown to mediate formation of a complex that includes kinesin and dynein motors in order to orient mitotic spindles (Lu and Prehoda 2013). In contrast, phosphorylated pro-apoptotic Bcl-2 protein BAD is bound by 14-3-3 and prevented from dimerization with other Bcl-2 proteins, preventing induction of apoptosis (Zha et al. 1996). 14-3-3 interaction also inhibits transcription factor FOXO3, and disruption of this interaction leads to constitutively active FOXO3. In the context of this binding, 14-3-3 also demonstrates another modulatory activity: it prevents dephosphorylation of FOXO3 (Dobson et al. 2011).

Another regulatory activity induced by binding of 14-3-3 proteins is change in the localization of a target protein. A frequently observed role for 14-3-3 binding in determination of protein localization involves prevention of target protein import into the nucleus, often via obstructing the target's nuclear localization signal. Molecules that are sequestered and retained in the cytoplasm in this manner include Cdc25 phosphatase, transcription factor EB, and transcriptional regulator YAP (Margolis et al. 2006; Roczniak-Ferguson et al. 2012; Basu et al. 2003). This often allows 14-3-3 to act as a negative regulator of processes, here preventing cell cycle progression, autophagy induction, and transcription of genes involved in proliferation, respectively (Margolis et al. 2006; Roczniak-Ferguson et al. 2012; Basu et al. 2003). Reports of 14-3-3 mediated protein transport to specific subcellular spaces are comparably less frequent, but such changes in localization

may be mediated through the ability of 14-3-3 to bind kinesin (Ichimura et al. 2002). 14-3-3 has been shown to regulate transport of plakoglobin by functioning as an adapter to a kinesin motor, a process that has been shown to be important for proper desmosomal junction assembly (Sehgal et al. 2014; Vishal et al. 2018). In addition, 14-3-3 has been shown to be important for regulating junctional localization of plakophilin proteins and tight junction proteins (Roberts et al. 2013; Amaya et al. 2019).

14-3-3 roles in developing *Xenopus laevis* embryos

The large interactome of 14-3-3 enables these proteins to influence major organismal processes, such as those observed during embryonic development. A strong literature consisting of studies in yeast have characterized the role of 14-3-3 homolog proteins in regulation of Cdc25 phosphatase as a critical feature of cell cycle checkpoint establishment during mitosis (Zeng and Piwnica-Worms 1999). In drosophila, complete knockout of one of the two expressed 14-3-3 proteins results in embryonic death (Li et al. 1997). Studies in drosophila identified 14-3-3 proteins as a critical activator of Raf1 in eye development, as well as subcellular organizers of par proteins in embryonic axis specification (Kockel et al. 1997; Chang and Rubin 1997). In the mammal 14-3-3 proteins are likewise involved in regulation of Raf1 signaling and of cell division cycle proteins, and a large body of research has investigated the role of 14-3-3 in neuronal cell differentiation and migration (Pozuelo Rubio et al. 2004; Cornell and Toyo-oka 2017). A significant portion of what we understand about these proteins in embryonic development has

been elucidated by studies in the amphibian *Xenopus laevis,* both in regard to the function of 14-3-3 proteins at large and individual isoforms specifically.

Roles for 14-3-3 proteins in *Xenopus* development have been described as early as in the oocyte, major examples including regulatory roles for Raf1 signaling, Cdc25 phosphatase in cell cycle, and par protein localization during gastrulation (Xing et al. 1997; Duckworth et al. 2002; Margolis et al. 2003; Kusakabe and Nishida 2004). In addition, utilization of a broad approach to widely inhibit 14-3-3 isoforms demonstrated important roles in tissue specification and formation in *Xenopus* embryos (Wu and Muslin 2002). Given that 14-3-3 proteins constitute approximately 40 μg/ml within pre-fertilization oocytes, microinjection of as much as 40 ng of RNA encoding an epitope tagged high-affinity 14-3-3 binding peptide (‘GST-R18’) was employed to inhibit both maternally and zygotically derived 14-3-3 (Wang et al. 1999; Wu and Muslin 2002). Inhibition of 14-3-3 proteins resulted in abnormal phenotypes including failure of blastopore closure, embryo bending and size truncation, and abnormal establishment of skeletal muscle. Interestingly, this degree of inhibition resulted in decreased RNA levels for mesodermal markers Xbra, Xwnt8, and XmyoD when GST-R18 was expressed in presumptive ventral lateral mesoderm. Prevention of mesoderm formation was further evidenced by failure of fibroblast growth factor to induce differentiation of animal cap ectoderm to mesoderm when these cells were 14-3-3 inhibited. The effect appeared to be specific to mesoderm, as non-mesodermal Spemann organizer markers such as chordin and goosecoid were unaffected. Although these findings revealed an important role for 14-3-3 in the formation of developmental tissues, it is important

to interpret this finding with respect to the location and degree of inhibition. This is apparent in embryos subjected to chemical perturbation of the H^+-ATPase and 14-3-3 complex, increases in 14-3-3 ε expression, or mislocalization of 14-3-3 ε expression (Bunney et al. 2003) These interventions result in the emergence of organ heterotaxia in late stages, identifying a role for 14-3-3 proteins in specification of tissue asymmetry (Bunney at al. 2003).

In a more comprehensive examination of the roles of separate 14-3-3 isoforms across development, the expression, localization, and effect of perturbing each isoform was described in *Xenopus* embryos (Lau et al. 2006). RNA transcripts for 14-3-3 isoforms were detected in early embryonic stages through late tailbud, demonstrating that 14-3-3 β, ε, τ/θ, ζ, and γ are present and abundant throughout development with only isoform η showing limitation of expression to rarely late stages. 14-3-3 γ and ε expression localizes across the early tailbud body surface in a widespread manner in contrast to isoforms τ/θ, ζ, η, and β that do not demonstrate observable patterns at this stage. Late tailbud embryos express γ, ε, and τ/θ in a variety of tissues including head structures, tissues of the nervous system, muscle, trunk, and tail tissue. Isoform γ shows a comparatively more dense localization in the head comparted to that of other isoforms, while ε and τ/θ localize most clearly to muscle, trunk, and tail structures. 14-3-3 ζ appears to mainly localize to the tailfin of late tailbud embryos, while isoforms η and β appear are expressed in the trunk, tail, and head.

The different localization of these isoforms appears to affect their functional significance in development, as partial knockdown of each 14-3-3 protein via

antisense RNA morpholino oligonucleotides results in different phenotypes. Knockdown of ε and τ/θ each result in failure of the blastopore to close and exogastrulation, with just over 30% of ε reduced embryos dying and nearly 90% of τ/θ depleted embryos dying. Reduction of isoform γ causes loss of the eye, while knockdown of β results in a bending of the embryo. Depletion of ζ and η does not produce an obvious phenotype. Failure of FGF treatment to induce animal cap differentiation to mesoderm was observed after τ/θ knockdown and rescued by reintroduction of τ/θ. Mesendodermal marker Xbra is reduced by loss of ε and τ/θ, and the embryonic death that occurs due to knockdown of these isoforms involves induction of apoptosis. Rescue by restoration of either isoform τ/θ or ε reduces exogastrulation caused by knockdown of τ/θ. Co-expression of either τ/θ or another isoform such as ζ demonstrates a rescue effect by preventing the increase in apoptosis.

While these results provide encouraging evidence of some discrete roles for 14-3-3 proteins in development, they must be interpreted with caution. The morpholino knockdown approach results in inhibition of both maternal and zygotic transcripts widely throughout the embryo, limiting control of both time and location of inhibition. Another caveat to this approach is that it cannot reduce maternal protein derived from the oocyte, where 14-3-3 proteins have been demonstrated to be abundant. Thus, this perturbation relies on turnover mechanisms to deplete existing protein. Nonetheless, there is descriptive evidence of requirement of 14-3-3 proteins during development, though the roles evidenced have yet to be described with regard to cellular or molecular mechanisms. Further examination of

the cellular functions of these proteins in the context of developing tissues is required to understand the nature of their contribution to important embryonic processes.

The relationship between 14-3-3 and intermediate filaments: IFs modulate 14-3-3

14-3-3 has been discovered to have a relationship with intermediate filament family proteins that both modulates filaments and IF networks directly and allows IF proteins to influence cellular signaling. A key functional characterization of the interaction between 14-3-3 proteins and IFs was described in the context of keratin networks during mitosis (Liao and Omary 1996). 14-3-3 was found to interact with K8/K18 filaments in a phosphorylation dependant manner, resulting in increased solubility of the bound keratins. This interaction was shown to specifically involve type I K18, to be disrupted by addition of phosphatase, and to result in establishment of comparatively 'loose' filament networks *in vitro* (Liao and Omary 1996). Follow-up work clearly demonstrated that the interaction between K18 and 14-3-3 is mediated by phosphorylation of Serine 33, which occurs within an atypical motif in regard to 14-3-3 binding (Ku et al. 1998). Mutation of Ser33 to alanine or aspartic acid results in failed binding to 14-3-3 and collapse of the cellular keratin network of fibroblasts from a widespread network into a comparatively thin peri-nuclear ring (Ku et al. 1998). One interpretation of these findings is that 14-3-3 promotes keratin network solubility during mitosis that could potentially allow for reorganization events during cellular division (Liao and Omary 1996).

Demonstration that interaction between phosphorylated keratin and 14-3-3 proteins is a feature of mitosis raises an important consideration; while 14-3-3 binding has an affect on filament properties, IFs may also be able to exert an effect on 14-3-3 in turn. Evidence of keratin IFs influencing 14-3-3 was described in the context of mouse K8 knockout *in vivo* (Toivola et al. 2001). K8 deplete liver hepatocyte cells that are unable to form IFs with K18/K19 evidenced mitotic arrest, indicated by increased proportions of S-phase cells, increased nuclear size, and the presence of abnormal multi-nucleated cells (Toivola et al. 2001). Interestingly, K8 deletion resulted in relocalization of 14-3-3 ζ from the cytoplasmic compartment to the nucleus of these cells (Toivola et al. 2001). Knock-in of K18 S33A in the mouse also induced a shift in 14-3-3 ζ distribution from the cytoplasm to the nucleus (Ku et al. 2002). Such findings demonstrated a role for the interaction between intermediate filaments and 14-3-3 proteins that allows the IF network to dictate compartmentalization of 14-3-3.

Furthermore, additional work illustrated the role of IF networks in 14-3-3 mediated regulation of mitosis. Study of 14-3-3 binding by vimentin illustrated that phosphorylation of vimentin is sufficient to sequester 14-3-3 and prevent interaction with known targets, such as Raf1 (Tzivion et al. 2000). This mechanism was demonstrated to be a key feature of 14-3-3 mediated mitotic checkpoint control, as a combination of 14-3-3 phosphorylation and subsequent binding to keratin liberates Cdc25 phosphatase from 14-3-3, allowing nuclear entry and progression of mitosis (Margolis et al. 2006). Keratins and other IF proteins therefore demonstrate the ability to influence 14-3-3 mediated cell signaling by

functioning as a sequestering ‘sink’, impacting both its interaction with other targets and cellular distribution (Margolis et al. 2006). This function of IF networks with regard to cellular signaling is particularly noteworthy, as regulation of 14-3-3 in this manner is not limited to mitosis-specific roles. In a similar fashion to that demonstrated in mitosis, deletion of mouse K17 has been shown to have ramifications for mTOR signaling and induction of autophagy (Kim et al. 2006). Loss of K17 results in keratinocyte size decrease as well as lower protein translation, concomitant with decreased activation of molecules of the mTOR pathway and increases in autophagy markers. Interestingly, K17-/- induces a nuclear distribution of 14-3-3 that is resistant to mTOR activation via serum introduction but rescued by expression of wild type K17 (Kim et al. 2006). These results imply that K17 is necessary and sufficient to bind and retain 14-3-3 in the cytosol as a requirement for its regulation of mTOR signaling. Moreover, this mechanism of 14-3-3 relocalization via IF binding identifies an interface through which IFs may influence a variety of cellular signaling events (Toivola et al. 2001; Kim et al. 2006; Deng et al. 2013).

The relationship between 14-3-3 and intermediate filaments: 14-3-3 regulates IFs

Study of the interaction between 14-3-3 proteins and intermediate filaments has elucidated regulatory roles for 14-3-3 that strongly influence the properties and activities of IF proteins and networks. Phosphorylation has been shown to mitigate disassembly of keratin networks, where extensive phosphorylation results in punctate IF protein patterns that match the distribution of 14-3-3 (Strnad et al.

2001; Strnad et al. 2002). Overexpression of 14-3-3 proteins yields a very similar effect, either resulting in IF network disassembly and diffusion or disassembly into punctate, non-filamentous granules (Li et al. 2006; Miao et al. 2013). Mechanical stretch and shear stress have been shown to activate kinases and shear stress leads to phosphorylation of K18 Ser33 (Ridge et al. 2005; Sivaramakrishnan et al. 2009; Flitney et al. 2009). This phosphorylation leads to increased dynamic exchange of filament precursors into filament networks that is dependent on 14-3-3 activity (Sivaramakrishnan et al. 2009). 14-3-3 proteins have been shown to affect the dynamic exchange rate of K18, GFAP, and NF-L intermediate filament proteins (Sivaramakrishnan 2009; Li et al. 2006; Miao et al. 2013). In addition, stretch and shear stress have both been demonstrated to result in broad reorganization of the filament network (Ridge et al. 2005; Sivaramakrishnan et al. 2009; Flitney et al. 2009). Mechanical stretch has been shown to induce keratin network reorganization that is characterized by thickened fibrils (Ridge et al. 2005). Shear stress resulted in reorganization of the network into a ‘wavy’ morphology that was also comprised of thickened filament bundles and dependent on 14-3-3 activity (Sivaramakrishnan et al. 2009).

Taken together, these findings illustrate the ability of 14-3-3 proteins to influence IF dynamics on a large scale, affecting both protein exchanges and network reorganization events. 14-3-3 induced changes in the solubility, organization, and activity of the IF network affect cellular aspects such as motility and invasiveness (Boudreau et al. 2013) and are likely to alter many others. These demonstrations also have particularly interesting implications for

compartmentalized IF phosphorylation events, such as those observed at the desmosomal adhesion (Fois et al. 2013). It remains to be seen whether 14-3-3 has a role in regulating dynamic network reorganization events at such subcellular locales (Weber et al. 2012).

Introduction to the thesis project

Cellular cytoskeleton serves as a structural framework for cells, much like the bones within our own bodies. The cytoskeleton is comprised of proteins that organize into filamentous arrays, of which three distinct networks exist. Intermediate filaments (IFs) comprise a diverse group of structurally conserved proteins that assemble into long fibrils that function as this 'cellular skeleton'. Found throughout many tissues of vertebrate animals, these cord-like proteins form intricate networks in cells. Keratins, a subtype of these IF proteins, are expressed in several cell types including epithelia. IFs have a well-established role in fortifying cells against the strains and stresses they encounter within the organismal microenvironment. This resistance to strain is critical for *Xenopus* mesendoderm, a collectively migrating cell group that experiences changes in force as it moves as a tissue. The IFs are linked to structures known as cell-cell adhesions, the molecular complexes that allow cells in tissues to remain joined to one another. IFs that are associated with the proteins of these cellular junctions provide resistance against the natural forces that a tissue in an organism encounters, as well as the forces that are generated when cells must migrate together.

Laboratory experiments that have examined the assembly of purified IF proteins alone have demonstrated that the formation of filament networks occurs autonomously. The filament networks that form in these in vitro experiments become dense, stable, and unchanging. However, examination of the IFs that exist in the cellular and organismal context demonstrates that these same networks

undergo constant change in the living environment. This ability to modify tension-bearing IFs represents a critical cellular process that is necessary for interaction with a changing cellular environment, but is also at present incompletely described. In conjunction with descriptions of ongoing filament modification, IF networks have been shown to undergo dramatic and large-scale reorganization in response to onset of mechanical stresses. Previous work by Weber and colleagues demonstrated a mechanically induced reorganization of the widespread keratin network to cell-cell adhesions. It is abundantly clear that the keratin network dynamics must be regulated to determine where and when such rearrangement events occur. These reorganization events highlight the strong likelihood that a molecule must exist to provide an interface between keratin filaments and signaling pathways that trigger changes in cells.

Phosphorylation is a cellular signaling mechanism that has been shown to affect IF networks. Filaments that undergo serine/threonine phosphorylation have been shown to have altered solubility, changes in location within cells, and abnormal morphology observed throughout the IF network. One molecule that requires phosphorylation in order to bind with and modify filament networks is 14-3-3. 14-3-3 proteins have been shown to exert control over target proteins by alternatively limiting or enhancing affinity of these molecules for other binding partners. In this fashion, 14-3-3 proteins directly modulate the activity of a variety of IFs, as well as other proteins that associate with and alter the activity of cytoskeleton including motors and scaffold molecules.

Although previous investigations have addressed the manner in which IFs are continually being formed and networks are subject to reorganization, little is known in regard to the processes that mediate specific subcellular keratin rearrangements, particular at interfaces that are typically exposed to strain. We provide here that 14-3-3 proteins target keratin intermediate filaments to mechanically sensitive cell-cell contacts.

Significance of the study

The study findings provide insight into an understudied area of cell biology that falls within a poorly described area – specifically, the role of accessory molecules in facilitating dynamic remodeling of intermediate filament (IF) cytoskeleton. The evidence that 14-3-3 has a role in targeting of IF proteins provides a foundation for future exploration of proteins in processes that facilitate broad IF rearrangement. Standout areas include mechanosensitivity and cellular signaling. Keratin interaction with 14-3-3 proteins, shown here in the context of migratory cells, may additionally influence 14-3-3 signaling in other processes or position cytoskeletal reorganization as a possible upstream/downstream event in a signaling pathway. We expect that the current work will provide insight into the mechanisms regulating active tissues ranging from collectively migrating cell groups to stationary tissues that absorb and withstand forces. Understanding how cells redirect keratins to fortify cellular junctions under stress will further inform our knowledge of significant cellular processes including barrier formation, embryonic tissue patterning, wound healing, and invasion of cancerous cells.

Specific aims

Specific Aim 1: To establish evidence of interaction between 14-3-3 proteins and keratins in *Xenopus laevis* embryos.

1-1: To examine the extent to which 14-3-3 proteins and keratins biochemically interact in *Xenopus* gastrula.

1-2: To characterize subcellular localization and association of 14-3-3 proteins and keratins in *Xenopus* embryos and migratory tissues.

1-3: To determine the expression of particular 14-3-3 isoforms in *Xenopus* embryos and mesendoderm.

Specific Aim 2: To characterize the role of 14-3-3 proteins in regulation of keratin filament reorganization dynamics in mesendoderm.

2-1: To determine the role of 14-3-3 in modulating intermediate filament protein dynamics of migratory mesendoderm.

2-2: To examine the extent to which 14-3-3 interaction with keratin regulates subcellular reorganization dynamics of the network.

Specific Aim 3: To determine the role of 14-3-3 proteins in cell-cell adhesion mediated recruit of keratin.

3-1: To examine the role of 14-3-3 in keratin recruit during establishment and maintenance of cell-cell adhesions.

3-2: To determine the extent to which 14-3-3 proteins mediate interaction between the keratin network and molecules of the cell-cell adhesion.

3-3: To determine the role of 14-3-3 in modulation of cell-cell adhesion molecules during establishment and maintenance of cell-cell adhesions.

CHAPTER 2

MATERIALS AND METHODS

Some information from this chapter is accepted for publication in Mariani *et al.* (2019) *MBoC.*

Xenopus embryo in vitro fertilization and staging

Embryos were obtained and cultured using standard methods and staged according to (Nieuwkoop and Faber, 1994). Embryos were dejellied in 2% cysteine and cultured at 15ºC in 0.1X Modified Barth's saline (MBS; 1X MBS: 88 mM NaCl, 1 mM KCl, 2.5 mM $NaHCO_3$, 0.35 mM $CaCl_2$, 0.5 mM $MgSO_4$, 5 mM HEPES pH 7.8).

Xenopus embryo protein lysate preparation and western blot

Xenopus whole embryos were solubilized in lysis buffer (50 mM Tris-HCl pH 7.5, 1 mM phenylmethylsulfonofluoride (PMSF), 1% mammalian protease inhibitor cocktail (Sigma-Aldrich, P2714), 0.2 mM H_2O_2, 3 mM sodium pyrophosphate, 1 mM sodium orthovanadate, 10 mM sodium fluoride, sodium β-glycerophosphate [10 mg/ml], 1% Triton X-100 (Sigma-Aldrich, T-9284) or 1% Tergitol type NP-40 (Spectrum Biosciences, T1279). Protein samples were prepared in 2x Laemmli buffer supplemented with 5% β-mercaptoethanol, incubated on a 95°C heat block for five minutes, and loaded onto 12% SDS-PAGE gels. Proteins were transferred onto nitrocellulose membrane prior to incubation with antibodies.

Antibodies

Several antibodies were used throughout this study: pan 14-3-3 pAb (Santa Cruz, K19 sc-629), Keratin 8 mAb (DSHB, 1h5), C-Cadherin mAb (DSHB, 6B6), pan Cadherin pAb (Santa Cruz, H-300 sc-10733), Vinculin mAb (Millipore, MAB3574), Keratin 19 mAb (Progen, 61010), pan keratin mAb (Sigma Aldrich, C2562), Actin-HRP (Sigma-Aldrich,A3854), GAPDH mAb (Abcam, mAbcam 9484), GFP mAb

(Invitrogen, A-11120), GFP mAb (Santa Cruz, B-2 sc-9996), mCherry pAb (BioVision, 5993-100), and FLAG mAb (Sigma-Aldrich, F1804). The 1h5 anti-XCK1(8) monoclonal antibody developed by Michael Klymkowsky and 6B6 anti-C-cadherin monoclonal antibody developed by Barry Gumbiner were obtained from the Developmental Studies Hybridoma Bank developed under the auspices of the NICHD and maintained by The University of Iowa, Department of Biology, Iowa City, IA 52242.

Plasmids

The following plasmids were used in this study: pCS2-mCherry-R18, pCS2-mCherry-R18M, pCS2-eGFP-K19, pCS2-mCherry-K19, pcDNA3-FLAG-HA-14-3-3β (Addgene plasmid # 8999), pCS2-FLAG-HA-14-3-3β, pCS2-eGFP-C-cadherin (B. Gumbiner, University of Washington), pCS2-eGFP-R18-K19, pCS2-eGFP-R18M-K19, pCS2-3xFLAG-R18-K19, pCS2-3xFLAG-R18M-K19, pCS2-mem-RFP, and pCS2-GFP-XCK8. Oligonucleotides that translate to the described R18 and R18M primary sequences (Wang *et al.* 1999) were commercial synthesized (Genewiz) and cloned into pCS2 vector backbone by the author. *Xenopus laevis* krt19.L (NP_001084992.1) was obtained as full length cDNA (GE Dharmacon MXL1736-202774753) and cloned into pCS2 vector backbone by the author. pCS2-FLAG-HA-14-3-3β was subcloned using 1478 pcDNA3 flag HA-14-3-3β, a gift from William Sellers (Addgene plasmid # 8999), as the origination source for the fusion construct. The mem-RFP construct was a kind gift from Megason and Fraser (Megason and Fraser, 2003).

RNA constructs and microinjection

RNA was prepared via *in vitro* transcription (Promega, P1420). DNA or RNA was diluted to microinject concentrations of 200-500 pg in 5 nl pulses for the following constructs: pCS2-eGFP-K19, pCS2-mCherry-K19, pCS2-mCherry-R18, pCS2-mCherry-R18M, pCS2-FLAG-HA-14-3-3β, pCS2-C-cadherin-eGFP, pCS2-mem-RFP, pCS2-3xFLAG/eGFP-R18-K19, and pCS2-3xFLAG/eGFP-R18M-K19. Embryos utilized for microscopy were injected dorsally into both blastomeres at two-cell stage to target mesendoderm. Embryos utilized for immunoprecipitation were twice injected at one-cell stage in the animal cap on both sides peripheral to the germinal vesicle.

Immunoprecipitation

Whole embryos or dissected mesendoderm for immunoprecipitation were processed in aforementioned lysis buffer with 1% Tergitol type NP-40 or 1% Triton X-100 as indicated in figure legends. Endogenous IP lysates (equivalent to 40 embryos) were initially incubated with 50 µl Protein-G agarose bead slurry (Roche Diagnostics, 11243233001) for an hour. Beads were pelleted by centrifugation at 3000 rpm for 5 minutes (4°C). The IP lysate was then removed and incubated with primary antibody (5 µg pan 14-3-3, Santa Cruz) for overnight immunoprecipitation. The Protein-G beads were washed three times in lysis buffer for ten minutes. Bead samples were stored in 2x Laemmli buffer with 5% β-mercaptoethanol at -80°C for subsequent gel electrophoresis. After overnight primary incubation, endogenous IP lysates were incubated with 50 µl Protein-G agarose bead slurry overnight. FLAG IP lysates (equivalent to 40 embryos) were incubated with 40 µl agarose

slurry covalently linked to anti-FLAG M2 mAb (Sigma-Aldrich, A2220) for overnight immunoprecipitation. IP samples were pelleted by centrifugation at 3000 rpm for 5 minutes (4°C), and lysates were removed for storage as supernatant samples. Beads were washed with three exchanges of lysis buffer (1% Tergitol type NP-40 or 1% Triton X-100 depending on IP detergent) for ten minutes. IP bead samples were dissociated in 25 µl of 2x Laemmli buffer with 5% β-mercaptoethanol, incubated on a 95°C heat block for five minutes, and loaded onto 12% SDS-PAGE polyacrylamide gels for electrophoresis. Gels were either stained using Sypro Red or transferred onto nitrocellulose membrane prior to incubation with antibodies. All incubation and wash steps were performed at 4°C using a vertical rotator. All centrifugation steps were performed at 4°C.

Urea precipitation

Detergent insoluble pellets were washed 3 times using aforementioned lysis buffer with 1% Tergitol type NP-40 or 1% Triton X-100 as indicated in figure legends. During each wash, the pellet was resuspended by pipetting and centrifuged for 10 minutes at 14,000xg at 4°C. After withdrawal of the final wash, pellets were incubated in a volume of syringe filter sterilized 10 mM Tris (pH 9), 9.5 M Urea, 1 mM DTT, and 2 mM EDTA. Solution volume varied depending on number of embryos and desired approximate protein concentrate per µl, but at a minimum was large enough to mix within microfuge tubes on a vertical rotator. Samples were rotated at room temperature for 3 hours. Urea precipitated samples were pipette mixed with an equal volume of 2x Laemmli buffer with 5% β-mercaptoethanol,

incubated on a 95°C heat block for five minutes, and loaded onto 12% SDS-PAGE polyacrylamide gels for electrophoresis.

LC/MS-MS proteomic analysis

All reagents used for proteomics were filtered and meticulous precautions were taken to avoid dust and other potential sources of keratin contamination. Prior to staining with Sypro Red dye (Invitrogen, S12000) SDS-PAGE gels were incubated twice in fixative solution consisting of 50% methanol and 7% glacial acetic acid for 30 minutes per incubation. After decanting the second fixative solution, the gel was placed in a fresh dish and incubated in 60 ml of Sypro Red dye overnight. The staining solution was decanted and the gel was incubated in a wash solution of 10% methanol and 7% glacial acetic acid for 30 minutes. Afterwards, the gel was washed three times in 100 ml of commercial ultrapure water before gel imaging and further preparation for LC/MS-MS. All incubations and washes were performed at room temperature on a flat rotator.

LC/MS-MS was performed by the Center for Advanced Proteomics Research (CAPR) at the Rutgers New Jersey Medical School. Sypro Red-labeled SDS-PAGE gel sections were excised at the facility and in-gel trypsin digestion was performed. The resulting peptides were C18 desalted and analyzed by LC/MS-MS on the Q Exactive instrument. The MS/MS spectra were searched against the NCBI *Xenopus laevis* database using MASCOT (v.2.3) search engines on the Proteome Discoverer (V1.4) platform. The protein false discovery rate is less than 1%. The mass spectrometry data were obtained from an Orbitrap instrument funded in part by NIH grant NS046593, for the support of the UMDNJ

Neuroproteomics Core Facility. Information in tables was derived utilizing Scaffold 4.7.3 with a protein and peptide false discovery rate of 1%.

Mesendoderm dissection and dissociation

Stage 10.5 embryos in 0.5x MBS were dissected at the animal cap surface to reveal the mesendodermal mantle. The dorsal side of the embryo was identified and the mesendoderm leading edge was excised from the rest of the tissue. These cells were pipette transferred into a solution of Ca^{2+}/Mg^{2+} free 1x MBS on 1% Ca^{2+}/Mg^{2+} free agarose and allowed to dissociate for 30 minutes at room temperature. Dissociated cells were transferred to fibronectin (Sigma-Aldrich, F4759) matrix (200 µl of 1:7.5 in water; incubated on MatTek glass bottom microwell dishes, P35G-1.5-14-C) and imaged. Fibronectin incubation was performed overnight at 4°C.

Dorsal marginal zone explant preparation

DMZ explants were excised and plated as described in (Davidson *et al.*, 2004). Stage 10.5 embryos in 0.5x MBS were carefully dissected at the animal cap surface to reveal the mesendodermal mantle. The embryo was then bisected and the dorsal side of the embryo was used. The remaining animal cap cells and endodermal cells were trimmed away, leaving the mesoderm, mesendoderm, and bottle cells of the embryo. The explant was flattened on fibronectin (Sigma-Aldrich, F4759) matrix (100 µl of 1:7.5 in water; incubated on MatTek glass bottom microwell dishes, P35G-1.5-14-C) and silicone grease was used to mount a coverslip. Fibronectin incubation was performed overnight at 4°C. Explants were slightly compressed and allowed to attach and migrate for 2 hours (live imaging

and dissociation experiments) or 5 hours (samples to be fixed). In order to fix explants, the coverslip was removed just prior to incubation in 100% methanol.

MDCK cell transfection and imaging

MDCK cells were seeded to approximately 30% confluence in a 35 mm MatTek glass bottom microwell dish (P35G-1.5-14-C). Media (DMEM with 10% FBS and 1x penstrep antibiotic) was removed and cells were washed with 4 mL of 1x PBS. PBS was removed and 2 mL media was introduced consisting of DMEM with no FBS or penstrep. Two microfuge tubes were prepared for each transfection reaction. One tube consisted of 125 µl of Optimem and 7.5 µl of Lipofectamine 3000. The second tube consisted of 125 µl of Optimem, 5 µl of P3000, and 1.25 µg of each DNA plasmid used. Reagents in each tube were pipette mixed and combined in a separate tube, followed by additional mixing. The transfection mix was incubated at room temperature for 20 minutes. Following incubation, mixes were introduced into 2 mL DMEM using a P1000 tip to slowly pipette the mixture into the media in drops. Afterward, dishes were gently pushed to provide additional mixing. Cells were incubated with transfection reagent for 4.5 to 6 hours at 37°C with 5% CO_2. Afterward, the transfection media was replaced with 2 mL of standard cell media and cells were incubated at 37°C with 5% CO_2 for 24 hours before live imaging using the SD Observer confocal microscope. During imaging, cells were kept at 37°C with 5% CO_2 for the duration of the imaging course.

Immunofluorescence

Embryos and dorsal marginal zone explants were fixed in ice-cold 100% methanol, Dent's fixative (80% methanol, 20% DMSO), or 4% PFA in 0.1x Modified Barth's

Saline (MBS) and incubated at either -20°C overnight (Methanol and Dent's fixation) or 4°C (4% PFA fixation). Embryos were rehydrated in partial changes of 0.1x Modified Barth's Saline (MBS). Embryos were either bisected using scalpels or prepared for sectioning using a cryostat. Embryos for sectioning were transferred into vinyl molds with dimensions of 15 mm x 15 mm x 5 mm (Electron Microscopy Sciences, 62534-15) containing tissue freezing medium (Electron Microscopy Sciences, 72592), and briefly immersed in liquid nitrogen to flash freeze. Frozen embryo blocks were stored at -80°C until sectioned (Leica 819, 14035838925; 40 µm per slice) at -20°C using a temperature controlled cryostat and mounted on slides (VWR, 48311-703). Prior to blocking, embryo sections and explants were rehydrated in 1x TBS. Samples were permeablized in 1x TBS with 0.25% Triton X-100 for 10 minutes before blocking in 5% goat serum for one hour at room temperature. Incubation in primary antibody (30 minutes at 37°C) was followed by three buffer exchanges with 1x TBS and incubation in Alexa Fluor 488 or 555 conjugated goat anti-mouse (Invitrogen, A11029; A21424) and/or goat anti-rabbit (Invitrogen, A11034; A21429) IgG (30 minutes at 37°C). Explants were imaged after three buffer exchanges with 1x TBS. Embryonic sections were serially dehydrated using 1x TBS with increasing percentages of methanol and cleared using benzyl benzoate/benzyl alcohol. Slides were coverslipped (Corning, 2980-245), sealed with multiple coats of nail polish, and left for drying overnight (4°C) before imaging. Bisected embryo halves were pipette transferred into 4 mL of 1x TBS in 35 mm MatTek glass bottom microwell dishes (P35G-1.5-14-C) and imaged.

Linescan analysis and quantification

Linescan measurements of fluorescence were conducted using the linescan tool in the profile tab of the Zen 2.3 lite software application. Two types of measurements were conducted to compare fluorescence of C-cadherin GFP and 14-3-3 across cellular compartments. The compartments measured included the approximate center of the cell (called ‘center’), the area nearby but not at the cell-cell adhesion (called ‘proximal’) and the cell-cell adhesion proper (called ‘adhesion’). To measure change in fluorescence at the proximal and adhesion compartments, lines were drawn from the center and extended to the area just prior to C-cadherin GFP signal (proximal compartment) or to the C-cadherin GFP signal (adhesion compartment).

Ratios were produced to analyze relative changes in fluorescence. These ratios were calculated using the average of the last five proximal or adhesion measurements versus the average of the first five center measurements. Five measurements in a linescan represented approximately 0.5 μm. This produced four ratios for each cell: proximal/center and adhesion/center for C-cadherin GFP, and proximal/center and adhesion/center for 14-3-3.

To compare the ratios of change in fluorescence across compartments, two statistical comparisons were conducted. These included a comparison of the proximal/center ratios of C-cadherin GFP and 14-3-3, as well a comparison of the adhesion/center ratios of C-cadherin and 14-3-3. Ratios paired as described were compared statistically using a paired sample t-test (one-way) to determine if statistically significant differences were present. Scatterplots were generated of

each cell's relative average C-cadherin intensity and corresponding 14-3-3 intensity at regions proximal to the cortex and at the adhesion. The bold horizontal line indicates the median relative C-cadherin intensity across both proximal and adhesion ROIs. The bold vertical line indicates the mean relative 14-3-3 intensity in ROIs proximal to the cortex.

This method was also utilized to compare change in fluorescence between C-cadherin GFP and mCherry-Keratin 19 across compartments in different cellular planes. The compartments measured included the center and adhesion zones. To measure fluorescence in compartments in different cellular planes, lines were drawn from the center and extended to the adhesion on an image corresponding to the basal plane of the cell (called 'basal plane') and on an image corresponding to the plane that includes the cell-cell adhesion junction (called 'junctional plane'). Using the aforementioned method, line measurements were utilized to produce ratios. Four ratios of adhesion/center intensities were derived: basal and junctional planes for both C-cadherin GFP and mCh-K19.

To compare the ratios of change in fluorescence across compartments in different cellular planes, two statistical comparisons were conducted. These included a comparison of the C-cadherin GFP adhesion/center ratios from the basal plane and the junction plane and a comparison of the mCh-K19 adhesion/center ratios from the basal plane and the junction plane. Ratios paired as described were compared statistically using a paired sample t-test (one-way) to determine if statistically significant differences were present. Scatterplots were generated of each cell's relative average C-cadherin intensity and corresponding mCh-K19

intensity at the adhesion in the imaged basal plane and the higher junctional plane. The bold horizontal line indicates the mean relative C-cadherin intensity in the basal plane. The bold vertical line indicates the mean relative mCh-K19 intensity in the basal plane.

FRAP experiments

Filaments chosen for photobleaching were imaged every fifteen seconds over the course of one minute to capture intensity of fluorescence prior to bleaching. The filament was then bleached using 100% power on the 488 channel for a duration of two minutes. The area of photobleaching was determined by a capture of the photobleaching mask acquired at the end of the two-minute bleach, along with the capture of the filament segment with reduced fluorescence at the start of the recovery period. Images of recovery of fluorescence within the bleach zone were captured in ten second intervals beginning after the conclusion of the bleach period.

Recovery of fluorescence was measured using the Zen 2.3 lite application. A region of interest (ROI) was aligned to the bleached segment of the filament in each of the post-bleach time points to determine the mean value of fluorescent intensity (mFI). This ROI was also used to measure the intensity of the bleach zone before photobleaching. An ROI was similarly used to measure a non-bleached control area of the filament proximal to the bleach zone. Using the method described by (Zheng et al., 2011) with minor alterations, the rate of photobleaching (rate r) was first established by determining the ratio of the control ROI mFI in each post-bleach time point to the average mFI across pre-bleach control ROIs [$r =$

$mFI_c \div mFI_{c0}$]. The normalized fluorescent intensity (NFI) was established by determining the ratio of the difference between the mFI of the initial experimental post-bleach time point and each subsequent experimental post-bleach time point to the rate established for that time point [$NFI = (mFI_{b\#} - mFI_{b1}) \div r$]. The recovery percentage (rec) of each time point was established by determining the ratio of the NFI in each experimental post-bleach time point to the average mFI across experimental pre-bleach ROIs and multiplying that ratio by 100 [$rec_{\#} = NFI_{\#} \div (mFI_{b0}) \times 100$]. Time point series to be measured for recovery of fluorescence in this way were first scrutinized for clarity of measurement. Exclusion criteria for recovery of fluorescence experiments included unclear bleach zones, measurement zones that were obstructed during the series by crossing or merging filaments, gross reorganization of filaments that resulted in loss of the measurement zone, and readily apparent movement of the measurement zone and proximal regions such that they did not remain in the plane of focus.

Analysis of fluorescent recovery was conducted by plotting the percentage of recovery for each post-bleach time point for a given series against time increments (seconds) and fitting a trendline to the data. Variation in time was controlled for by using the same time duration for each analysis (20 seconds to 330 seconds). The slope of the trendline was determined for each analysis and the mean slope was compared across R18 and R18M groups using a one-way t-test in which the sample variances were shown to be equal via an F-test.

Gap quantification

Z-stacks of eGFP-K19 expressing mesendoderm cells after collision were observed for the presence of a filament depleted zone proximal to a cell-cell contact. These gaps were counted and a proportion of total gaps to total cells was calculated for cells expressing mCh-R18 and cells expressing mCh-R18M. In order to detect if a statistical difference in these ratios was present, a z-test for proportions from two samples was utilized. 99.9% confidence interval for each sample proportion was calculated assuming a normal distribution. The length of gaps from the adhesion to the first visible filaments was measured using the linescan tool in the profile tab of the Zen 2.3 lite software application.

Image acquisition

Images for live and fixed samples were taken using a Zeiss Observer spinning disk confocal microscope using a 40x 1.3 NA or 63x 1.4 NA Apochromat objective, unless specified otherwise.

CHAPTER 3

CELLULAR-LOCALIZATION PROFILES AND TISSUE EXPRESSION PATTERNS OF 14-3-3 PROTEINS IMPLY A FUNCTIONAL INTERACTION WITH KERATIN 19 IN MIGRATORY TISSUES OF GASTRULATING EMBRYOS

Some information from this chapter is accepted for publication in Mariani *et al.* (2019) *MBoC.*

14-3-3 proteins have been shown to interact with and modulate the activity of a wide variety of intermediate filaments (Ku et al. 1998; Tzivion et al. 2000; Li et al. 2006; Miao et al. 2013). Demonstrated to be highly expressed in *Xenopus* as early as the oocyte, transcripts for 14-3-3 isoforms are largely plentiful throughout early stages of development (Wu and Muslin 2002; Lau et al. 2006). While some evidence exists regarding the distribution of 14-3-3 proteins in post-differentiation developmental stages such as tailbud, the expression and localization patterns of these proteins during early stages are largely undescribed (Lau et al. 2006). Moreover, little is known about the subcellular distributions of these molecules across early embryonic cell and tissue types.

Simple epithelial keratins have been shown to be expressed as the first intermediate filament types in *Xenopus* embryos (Franz et al. 1983; Klymkowsky et al. 1987; Klymkowsky et al. 1992). These IFs are present throughout the cell types of gastrulating embryos and demonstrate contact-mediated reorganization to cell junctions in mixed mesoderm and endoderm populations (Weber et al. 2012). Simple epithelial type II K8 is part of the recruited filament network, a keratin that forms filaments as an obligate heteropolymer with type I keratins (Steinert 1990; Hatzfeld and Weber 1990). Of these, at least K18 has been shown to bind 14-3-3 in cells and to be regulated by the interaction (Ku et al. 1998). Given the high conservation across eukaryotes that is characteristic of both 14-3-3 proteins and keratins, potential exists for a similar mechanism during morphogenetic movements of development. To determine whether 14-3-3 proteins could influence

keratin networks in mesendoderm, we investigated the interaction and subcellular association between these molecules.

Results

14-3-3 protein expression is ubiquitous throughout early embryonic stages

Our previous work demonstrated reorganization of the keratin network in mesendoderm of the *Xenopus* frog embryo (Weber et al., 2012). If 14-3-3 is to be a potential regulator of keratin intermediate filaments in the collectively migrating mesendoderm, 14-3-3 must be present in this tissue during the particular period of development in which this tissue differentiates and migrates, namely gastrulation. Previous work by Lau, Wu and Muslin examined mRNA expression levels and patterns of six different 14-3-3 isoforms during stages 2-38 of *Xenopus* embryonic development (Lau et al., 2006). While mRNA expression was found to be abundant for 14-3-3 β, ε, and τ during stages 2-14, mRNA is not necessarily indicative of protein expression in the embryo, which could be translationally regulated and/or maternally derived. We first confirmed whether 14-3-3 protein expression in developmental stages leading up to late gastrulation paralleled previously published mRNA expression data. Lysates were collected at time points beginning at one-cell stage through late gastrula (NF Stage 12.5), and immunoblot was performed using an antibody reactive with all isoforms of 14-3-3 (Figure 1 A-C). While some variability was evident across clutches, expression of 14-3-3 was consistently detected throughout these early embryonic stages. Although 14-3-3 protein levels increase slightly following mid-blastula transition (stage 7-9) when zygotic mRNA is transcriptionally upregulated (Figure 1 A and C), we saw relatively

high and persistent levels of 14-3-3 proteins present throughout early development.

14-3-3 proteins are differentially expressed in different tissue types

To further examine the extent to which 14-3-3 was present in various embryonic tissues, gastrulating embryos were dissected into several regions (Figure 2 B), and protein lysates were prepared. We examined the expression of 14-3-3 proteins in the animal cap, marginal zone, vegetal hemisphere, and mesendoderm tissues compared to that of whole embryos (Figure 2 A). 14-3-3 was found to be present in all tissues of *Xenopus* gastrula with varying expression levels. 14-3-3 expression was neither exclusive to nor absent from any one particular region, suggesting broadly ubiquitous functions for 14-3-3 across different tissue types. Expression levels of 14-3-3 were greater relative to actin in some tissues, including mesendoderm (Figure 2 A).

Keratin filaments co-localize with 14-3-3 at cell boundaries

Because 14-3-3 found to be expressed abundantly throughout the early embryo, we next sought to determine the subcellular localization of 14-3-3 in embryonic tissues. In order to assess the distribution of 14-3-3 proteins we performed immunofluorescence on fixed and bisected embryos. We found that several tissues showed compartmentalization of 14-3-3 rather than diffuse cytoplasmic distribution. Subcellular expression of 14-3-3 was confirmed in animal cap cells (Figure 3 A), in cells of the marginal zone (Figure 3 B), in vegetal hemisphere cells (Figure 3 C), and in mesendoderm (Figure 3 D). Interestingly, 14-3-3 appeared to be distributed to cell borders in mesendoderm (Figure 3 D-D’’).

Given that bisected embryos include whole cells that are arranged in different angular orientations, we next sought to determine the extent to which the mesendoderm localization of 14-3-3 shown in Figure 3 was a result of protein distribution or alternatively cell orientation. Fixed and cryosectioned gastrulating embryos demonstrate clear and distinct localization of 14-3-3 proteins to the cell periphery in mesendoderm at lower magnifications (Figure 4 C, red arrows). At higher magnifications, we were able to more precisely assess the subcellular distribution of 14-3-3, especially in relation to keratin filaments.

Due to the detected subcellular distribution of 14-3-3 proteins and known localization of keratin filament networks to peripheral cell contacts (Weber et al. 2012), we investigated the localization of 14-3-3 proteins with respect to keratin filaments. Keratin filaments in the early *Xenopus* gastrula are comprised of obligate heterodimers of Keratin 8 (K8) with either K18 and/or K19 (Franz et al., 1983; Suzuki et al., 2017; Briggs et al., 2018). As seen previously (Weber et al., 2012), keratin filaments, as visualized using antibody to K8, were found localized to the posterior of migratory mesendoderm cells in bisected embryos, where they link to cell-cell contacts (Figure 5 A and D). In leading edge mesendoderm cells, 14-3-3 immunofluorescence showed co-labeling of peripheral keratin densities at lower magnifications (Figure 5 C and F, white arrows). To determine whether 14-3-3 signal simply overlapped with the area of keratin localization at the cell periphery or if 14-3-3 proteins associated with junctional keratin filaments, embryos were cryosectioned and imaged at higher magnification. 14-3-3 was found to show strong co-localization with densities of keratins present at points of cell-cell

adhesion (Figure 6 A-C, white and red arrows). Moreover, 14-3-3 immunolabels filamentous patterns that align with those of junctional keratin filaments, providing convincing evidence of subcellular association of these molecules in living embryos.

The distribution, interaction, and activity of molecules in migrating mesendoderm can be studied *ex vivo* by preparing dorsal marginal zone (DMZ) explants (Davidson et al., 2004). Utilizing this strategy provides a different perspective of mesendoderm but might presumably induce changes in filament networks during explant preparation. To determine whether the association between 14-3-3 and keratin filaments could be observed and was not altered in DMZ explants, cells were fixed and immunolabeled using a pan-keratin antibody and pan-14-3-3. Explanted leader mesendoderm cells show co-localization of subsets of the keratin network and 14-3-3 proteins (Figure 7 A-C and F-H, white arrowheads) within the cellular keratin network at large (Figure 7 D-E and I-J). Close examination of the cell-cell contact between leader edge cells demonstrates decoration of keratin filament densities in this compartment by 14-3-3 (Figure 8). Furthermore, regions of signal overlap show filamentous immunolabeling of 14-3-3 that aligns with the keratin filament shape (Figure 8 C, A'-C'). Rather than extending across the entire filament density, the co-labeling occurs specifically at the area proximal to the cell-cell adhesion. 14-3-3 also appears to exhibit concentrated intensity in lamellipodia of mesendoderm cells, where keratin filaments are notably absent. Interestingly, 14-3-3 labeling in lamellipodia lacks the filamentous pattern observed in the posterior of cells.

K19 associates with 14-3-3 in whole embryos and collectively migrating tissues

We next sought to identify specifically which 14-3-3 protein isoforms were present in gastrula and examine whether association with keratin intermediate filament proteins could be detected. Rather than rely on antibody specificity for 14-3-3 isoforms in *Xenopus*, we took a proteomics approach to determine which 14-3-3 isoforms were expressed in the frog embryo and with which proteins 14-3-3 associated. Co-immunoprecipitation was performed using pan-14-3-3 antibody with NP-40 solubilized protein lysates from whole embryos. Samples were then separated by gel electrophoresis and stained to visualize protein band pattern (Figure 9A). Several distinct protein bands were visible in 14-3-3 immunoprecipitated lysates at the expected molecular weight for 14-3-3 proteins, between 28-30 kD. This molecular weight range for 14-3-3 is due to both the difference in amino acid sequences and post-translational modifications. In addition to the isolated 14-3-3 isoforms, an especially prominent band was detected at approximately 48 kD. These bands were selected for proteomic screening using LC/MS-MS.

Analysis of peptides identified by mass spectrometry confirmed the presence of multiple 14-3-3 protein isoforms (Figure 9 C). Several unique peptides as well as substantial total protein sequence coverage were found for 14-3-3 isoforms ζ, β, and θ (Figure 9 C). Isoform 14-3-3ε was detected with lower unique peptide and coverage spectra than other isoforms. Interestingly in the analysis of the 48 kD band, Keratin 19 (K19) was detected with many unique peptides and

substantial coverage in 14-3-3 co-immunoprecipitates from both *Xenopus* whole embryo lysates and mesendoderm (Figure 9 B and C). Only a single peptide was isolated that has identical conserved sequence with human K19, and the majority of peptide sequences correspond specifically to protein product of the *Xenopus laevis* krt19.L gene, not krt19.S. To our knowledge, this is the first time K19 has been shown to associate with 14-3-3. In order to determine whether the association between 14-3-3 and Keratin 19 occurs in mesendoderm, cells of this tissue were isolated and NP-40 solubilized protein lysates were prepared. Protein separation by gel electrophoresis was followed by band extraction and proteomic screening via LC/MS-MS. Keratin 19 was detected in mesendoderm specifically with multiple unique peptides (Figure 10 B and C). Several 14-3-3 isoforms were detected in mesendoderm, including isoforms ζ, β, and θ and lacking ε (Figure 10 C). This evidence demonstrates that K19 and 14-3-3 proteins associate in gastrulating embryos and that this interaction also occurs in mesendoderm.

14-3-3 is known to bind protein substrates containing particular primary amino acid sequences. Notably the motif sequence RXXS/TP is a preferred target, but other variations do exist (Muslin et al., 1996; Yaffe et al., 1997; Johnson et al., 2010). Several keratins, including Keratin 18 (K18), have been identified as phosphoserine-modified to become 14-3-3 substrates (Ku et al., 1998). Using three different bioinformatics analyses, we examined whether K19 might also contain similar binding phosphorylated sites and motifs that could provide 14-3-3 docking sites (Figure 11). *Xenopus* K19 contains three putative phosphorylated sites, S10, S33 and S52, which are highly conserved across phyla (Figure 9 and

10 B and Figure 11). S33 is of particular interest because it has previously been shown to be the primary phosphorylation site of K19 in several signaling and IF remodeling events (Zhou et al., 1999; Ju et al., 2015). We confirmed the association between 14-3-3 and K19 by immunoprecipitating 14-3-3 from whole embryo lysates and immunoblotting for K19 (Figure 12). Indeed, K19 was present in 14-3-3 immunoprecipitated samples by immunoblot analysis as well.

The keratin intermediate filament network has been shown to be reorganized proximal to cell-cell adhesions in mesendoderm cells (Weber et al., 2012). This reorganization of the keratin network occurs as a consequence of tugging forces on cell-cell interactions (Weber et al., 2012). In *Xenopus* gastrula, the classical cadherin protein C-cadherin provides the primary means of cell-cell adhesion (Heasman et al., 1994). Since keratin intermediate filaments are recruited to C-cadherin in mesendoderm cells as a function of applied force on the adhesions, we next investigated whether 14-3-3 was also associated with C-cadherin. 14-3-3 co-immunoprecipitated lysates were positive when immunoblotted for C-cadherin (Figure 12). Interestingly, although vinculin has been implicated in mechanosensation in both cadherin cell-cell adhesions and focal adhesions by several reports (Riveline et al., 2001; le Duc et al., 2010), we did not find vinculin to be associated with 14-3-3 (Figure 12).

Discussion

Prior to our study few and limited observations regarding the expression and distribution patterns of 14-3-3 proteins in *Xenopus laevis* embryos had been made. Identification of 14-3-3 had been accomplished through detection of mRNA for various 14-3-3 isoforms. These observations include the presence of transcripts for multiple 14-3-3 isoforms in *Xenopus* whole embryos across a variety of developmental stages (Lau et al. 2006). In addition, *in situ* hybridization assays demonstrated labeling of mRNA limited to 14-3-3 ε, ζ, and τ/θ in embryos across a variety of early stages (Bunney et al. 2003). Our findings demonstrate the presence of 14-3-3 proteins across a greater range of early developmental stages, focusing on the time points prior to and throughout *Xenopus* gastrulation. Furthermore, we demonstrate the expression of 14-3-3 proteins in all of the major tissues of embryos at gastrula relative to that of actin. We provide the subcellular distribution of 14-3-3 proteins in each of these tissues and devote particular attention to mesendoderm, demonstrating 14-3-3 localization in these cells across a variety of embryonic and tissue contexts. Our work shows a clear and consistent peripheral localization of 14-3-3 proteins of mesendoderm during *in vivo* and *ex vivo* migration. We speculate that this mesendoderm localization pattern implies a function for 14-3-3 proteins at this subcellular compartment during these migratory movements of gastrulation.

Observations by Weber and colleagues have demonstrated the presence of a junctional keratin network in *Xenopus* mesendoderm that is required for normal collective cell migration (Weber et al. 2012). In the current study, we show

that 14-3-3 proteins in mesendoderm are distributed to the same compartments as these keratin densities. We demonstrate that 14-3-3 proteins co-localize in filamentous spatial patterns that align with those of keratin filaments that are present at rearward and lateral cell-cell contacts in these cells during migration in the embryo. In addition, we show that the mesendoderm of DMZ explants that continues to collectively migrate outside of the embryo also displays association between 14-3-3 proteins and the keratin network that is specific to the junctions of cells. Through demonstrating that this association is readily apparent and consistent at cell-cell adhesions, we provide evidence that highlights the possibility for regulation of keratin activity at these sites through interaction with 14-3-3 proteins.

Despite previous descriptions of 14-3-3 isoform expression in *Xenopus* embryos (Lau et al. 2006), the role of dynamic keratin activity in cell migration (Weber et al. 2012), and demonstration of association between keratins and 14-3-3 proteins (Ku et al. 1998), the relationship between 14-3-3 and keratin intermediate filaments during mesendoderm migration has not been explored. In this study we utilized LC/MS-MS and detected 14-3-3 isoforms β, ζ, and τ/θ both in the whole embryo and specifically in mesendoderm. We find that 14-3-3 proteins associate with Keratin 19 in these analyses and biochemically confirm this interaction. Interestingly, K19 is a novel type I acidic keratin target of 14-3-3 proteins, as characterized interactions between acidic keratins and 14-3-3 have previously included K18 (Ku et al. 1998) and K17 (Kim et al. 2006). Though the relationship between 14-3-3 and K19 has not been studied as a consequence, our

analyses show that *Xenopus* and human K19 share conservation of the key serine in human K18 that has been shown to be a functionally important 14-3-3 binding site. Indeed, when this serine was charge mutated in human K19, the filament network demonstrated a dramatic collapse (Zhou et al. 1999). We speculate that 14-3-3 interaction with K19 in mesendoderm may be critically important for dynamic activity of keratin networks in these cells, particularly in regard to cell-cell proximal keratin filaments.

The evidence that 14-3-3 interacts with mesendodermal keratins and associates with filaments at the cell-cell junction is particularly interesting with regard to our identification of association between cadherin proteins and 14-3-3 in these cells. This identifies at least two possibilities for 14-3-3 regulation of keratin dynamics: firstly, that 14-3-3 modulates keratins directly through the demonstrated interaction, and/or that interactions between 14-3-3 bound keratins and molecules of the junctional adhesion complex augment keratin dynamics. In order to evaluate these hypotheses, we employ perturbation studies to interrogate the functional nature of the 14-3-3 relationship with K19 (shown in Chapter 5).

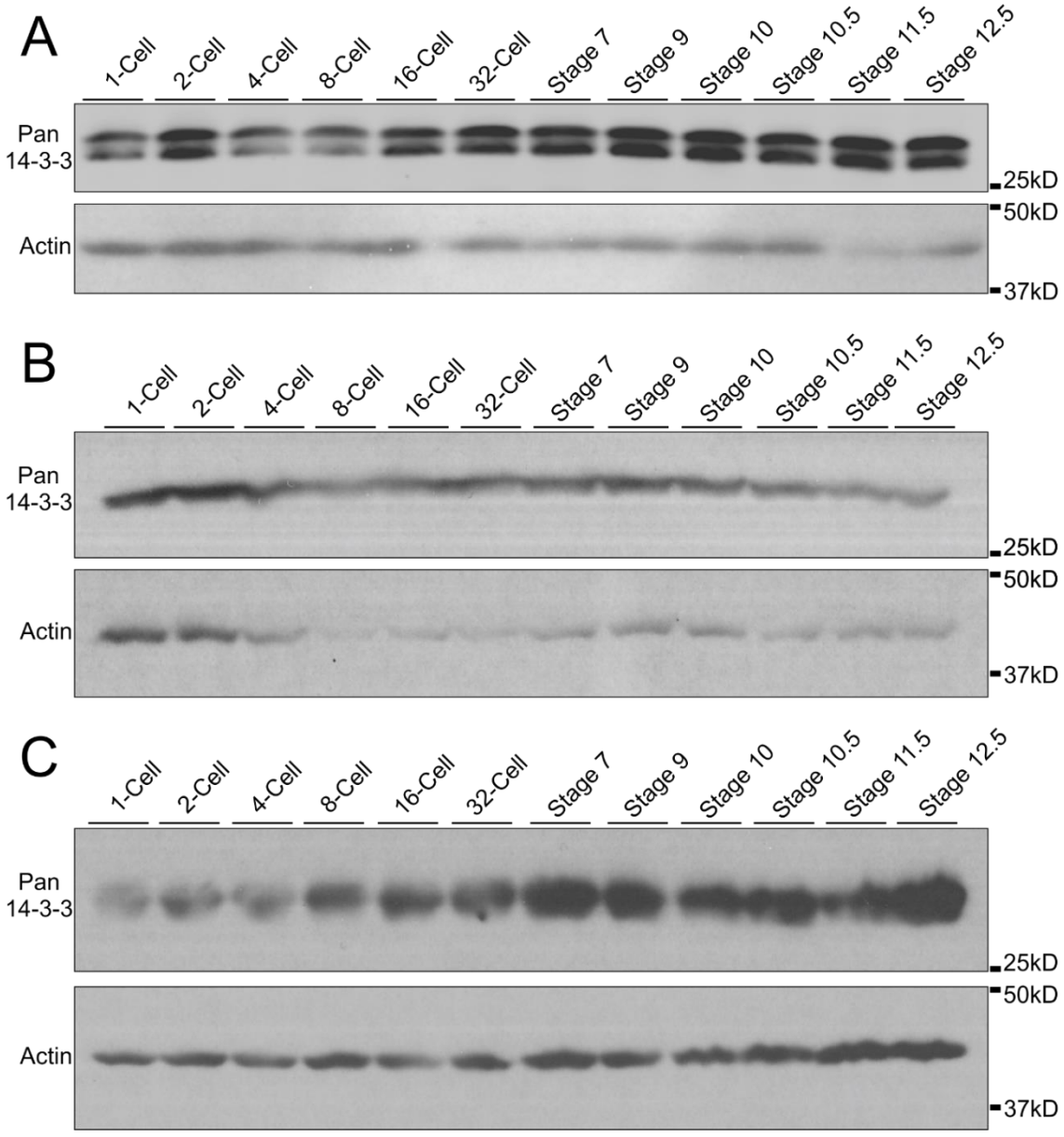
A
1-Cell
2-Cell
4-Cell
8-Cell
16-Cell
32-Cell
Stage 7
Stage 9
Stage 10
Stage 10.5
Stage 11.5
Stage 12.5
Pan
14-3-3
Actin
25kD
50kD
37kD
B
1-Cell
2-Cell
4-Cell
8-Cell
16-Cell
32-Cell
Stage 7
Stage 9
Stage 10
Stage 10.5
Stage 11.5
Stage 12.5
Pan
14-3-3
Actin
25kD
50kD
37kD
C
1-Cell
2-Cell
4-Cell
8-Cell
16-Cell
32-Cell
Stage 7
Stage 9
Stage 10
Stage 10.5
Stage 11.5
Stage 12.5
Pan
14-3-3
Actin
25kD
50kD
37kD

Figure 1. 14-3-3 proteins are expressed across early developmental stages.

A-C) *Xenopus laevis* embryo lysates harvested across post-fertilization early embryonic stages were probed for presence of 14-3-3 molecules. Three repetitions derived from different embryonic clutches (A-C) are provided. Whole embryo lysates (1% Triton X-100) were immunoblotted for 14-3-3 using a pan antibody that detects multiple isoforms. Actin was immunoblotted as a loading control. Each lane represents approximately 50 µg or 1 embryo worth of protein.

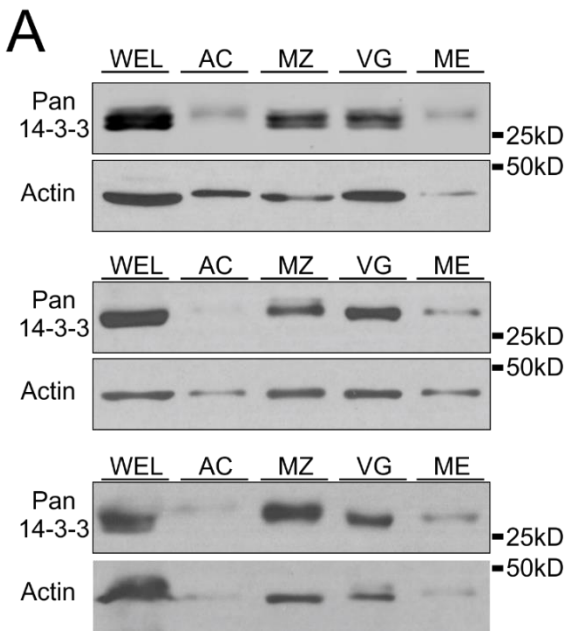
A
WEL
AC
MZ
VG
ME
Pan
14-3-3
25kD
50kD
Actin
WEL
AC
MZ
VG
ME
Pan
14-3-3
25kD
50kD
Actin
WEL
AC
MZ
VG
ME
Pan
14-3-3
25kD
50kD
Actin

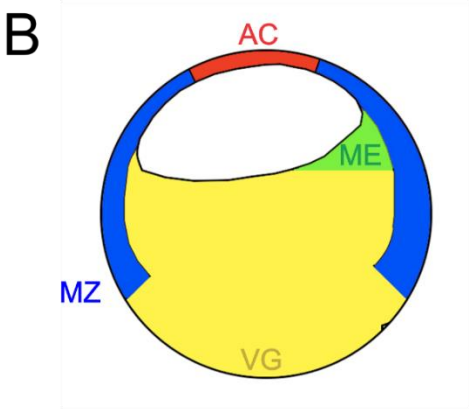
B
AC
ME
MZ
VG

Figure 2. 14-3-3 proteins are ubiquitously expressed across embryonic tissues.

A) Embryos were dissected into separate tissues and corresponding lysates (1% Triton X-100) were immunoblotted using pan 14-3-3 antibody to examine expression across the gastrulating embryo. Each lane represents a portion of protein equivalent to approximately 1 embryo. Three repetitions are included to demonstrate consistency of expression. **B**) Colored schematic of a bisected *Xenopus* embryo at gastrula depicting major tissue divisions. The tissues include the animal cap (AC), mesendoderm (ME), marginal zone (MZ), vegetal hemisphere (VG), and whole embryo lysate (WEL).

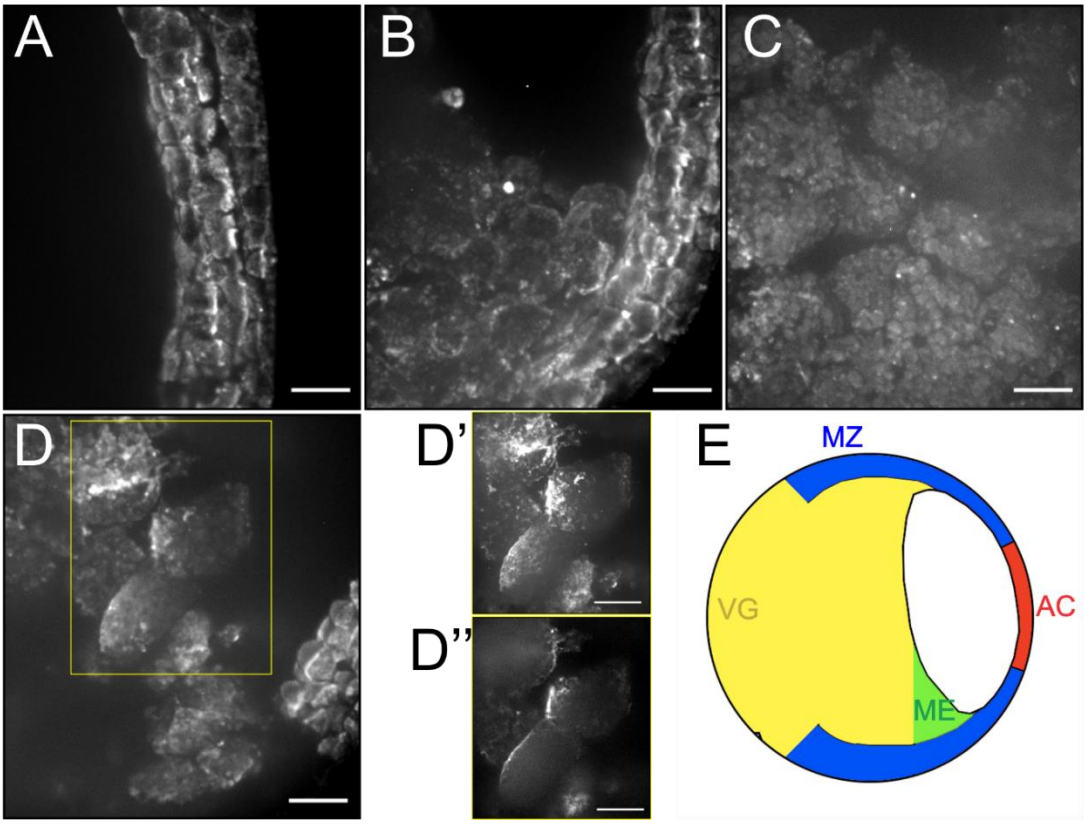
A
B
C
D
D'
D''
E
MZ
VG
AC
ME

Figure 3. Subcellular localization of 14-3-3 proteins differs across embryonic tissue types.

Immunofluorescent labeling of 14-3-3 proteins in bisected stage 10.5 gastrulating embryo halves fixed in 80% Methanol and 20% DMSO. **A**) Cells of the animal cap. **B**) Mesendoderm migrating edge with marginal zone and vegetal tissues. **C**) Vegetal tissue. **D**) Mesendoderm migrating edge cells demonstrating a rearward and peripheral localization of 14-3-3 proteins. **D'**) Higher magnification inset of cells that are highlighted by the yellow box in D. (**D''**) Single optical section of the cells in the yellow box. **E**) Embryo schematic rotated sideways to illustrate the relative positions of the tissues in the figure. Images are z-stacks (maximum intensity projection), except where stated otherwise. Images in A-D were taken using a 20x objective (0.8 NA) and 1.0 Tubelens. Images in D' and D'' were taken using a 20x objective (0.8 NA) and 1.6 Tubelens. Scalebars are 50 μm.

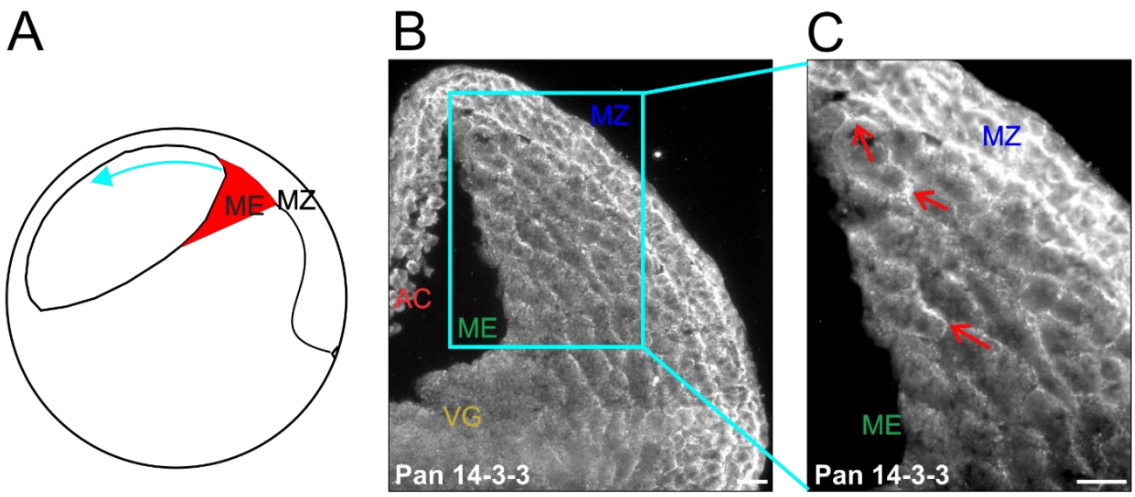
A
ME
MZ
B
MZ
AC
ME
VG
Pan 14-3-3
C
MZ
ME
Pan 14-3-3

Figure 4. 14-3-3 signal is enriched at the periphery of mesendoderm cells.

Low magnification of 14-3-3 immunofluorescence. **A**) Cartoon schematic depicting relative location of the mesendoderm tissue within the sagittally sectioned stage 11 embryo. **B**) Whole *Xenopus* embryos fixed in 4% PFA (0.1x MBS) were cryosectioned at stage 10.5 (40 µm thick slices) and immunolabeled using an antibody that detects multiple 14-3-3 isoforms. Labels refer to the animal cap (AC), mesendoderm (ME), marginal zone (MZ), and vegetal hemisphere (VG) of the embryo. Image taken using 10x objective (0.25 NA). **C**) Region labeled by the cyan box in panel A in increased magnification. Arrows indicate rear contacts of cells where 14-3-3 labeling is prominent. Image taken using 20x objective (0.75 NA). Scale bars are 50 µm.

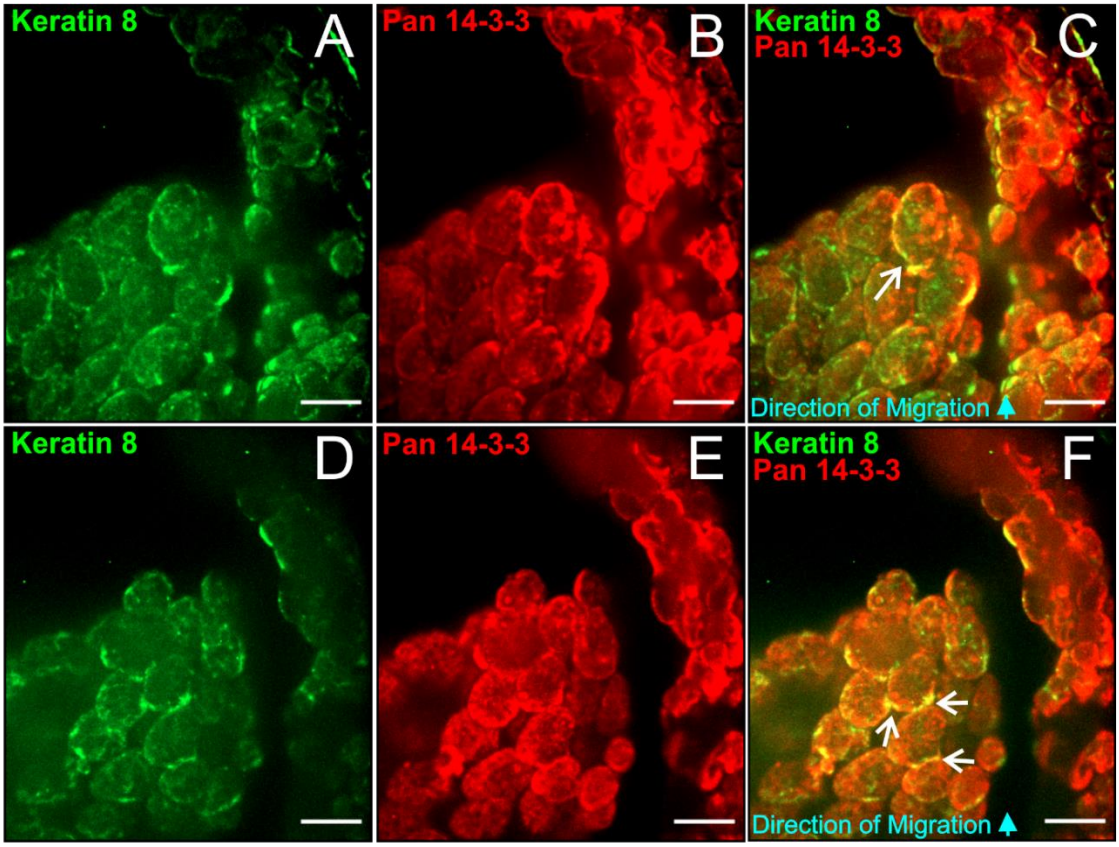
Keratin 8
A
Pan 14-3-3
B
Keratin 8
Pan 14-3-3
C
Direction of Migration
Keratin 8
D
Pan 14-3-3
E
Keratin 8
Pan 14-3-3
F
Direction of Migration

Figure 5. Gastrulating mesendoderm exhibits co-localization of 14-3-3 proteins and the keratin intermediate filament network.

Low magnification (20x) confocal images of stage 10.5 bisected embryos fixed in 80% methanol and 20% DMSO. **A-C**) Antibody immunolabeling of type II basic Keratin 8 (A) and multiple 14-3-3 isoforms (B) within a dorsal section that includes the leading mesendoderm migratory edge as well as portion of the marginal zone and animal cap tissues. Arrows in the channel merge image (C) highlight fluorophore co-localization at the lateral border and peripheral contact of the leading cell in the image. **D-F**) Similar perspective of the dorsal leading edge cells of embryonic mesendoderm migrating during gastrulation. Arrows in F denote signal co-localization at points of cell-cell contact between several cells of the leading edge. Blue arrow in merge images indicates direction of tissue migration. Images are z-stacks (maximum intensity projection). Images were taken using a 20x objective (0.8 NA) and 1.0 Tubelens. Scalebars are 50 μm.

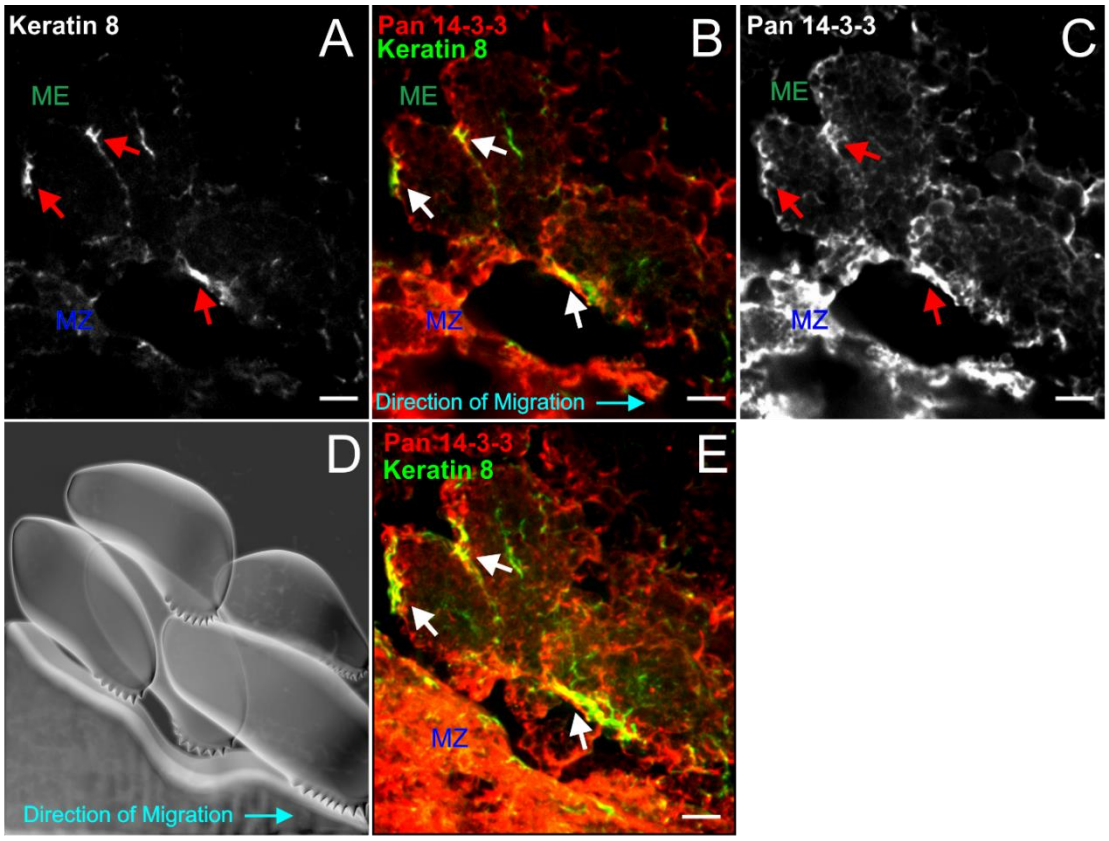
Keratin 8
A
ME
MZ
Pan 14-3-3
Keratin 8
B
ME
MZ
Direction of Migration
Pan 14-3-3
C
ME
MZ
D
Direction of Migration
Pan 14-3-3
Keratin 8
E
MZ

Figure 6. Filaments recruited to cell-cell adhesions in migrating mesendoderm associate with 14-3-3 in vivo.

A-C) Single plane confocal images showing a sagittal perspective of a cryosectioned gastrulating embryo (stage 10.5, 40 μm thick slices) labeled immunocytochemically for 14-3-3 proteins (red) and Keratin 8 (green). Areas where filamentous co-localization was detected in panel B are illustrated by arrows in all three panels. **D**) Cartoon schematic depicting three-dimensional orientation of cells in A-C relative to one another. Blue arrow in merge images indicates direction of tissue migration. **E**) Maximum intensity projection of confocal z-stack of cells shown in A-D to show more comprehensive filament distribution. Images were taken with a 63x objective (1.4 NA) and 1.0 Tubelens. Scale bars are 10 μm.

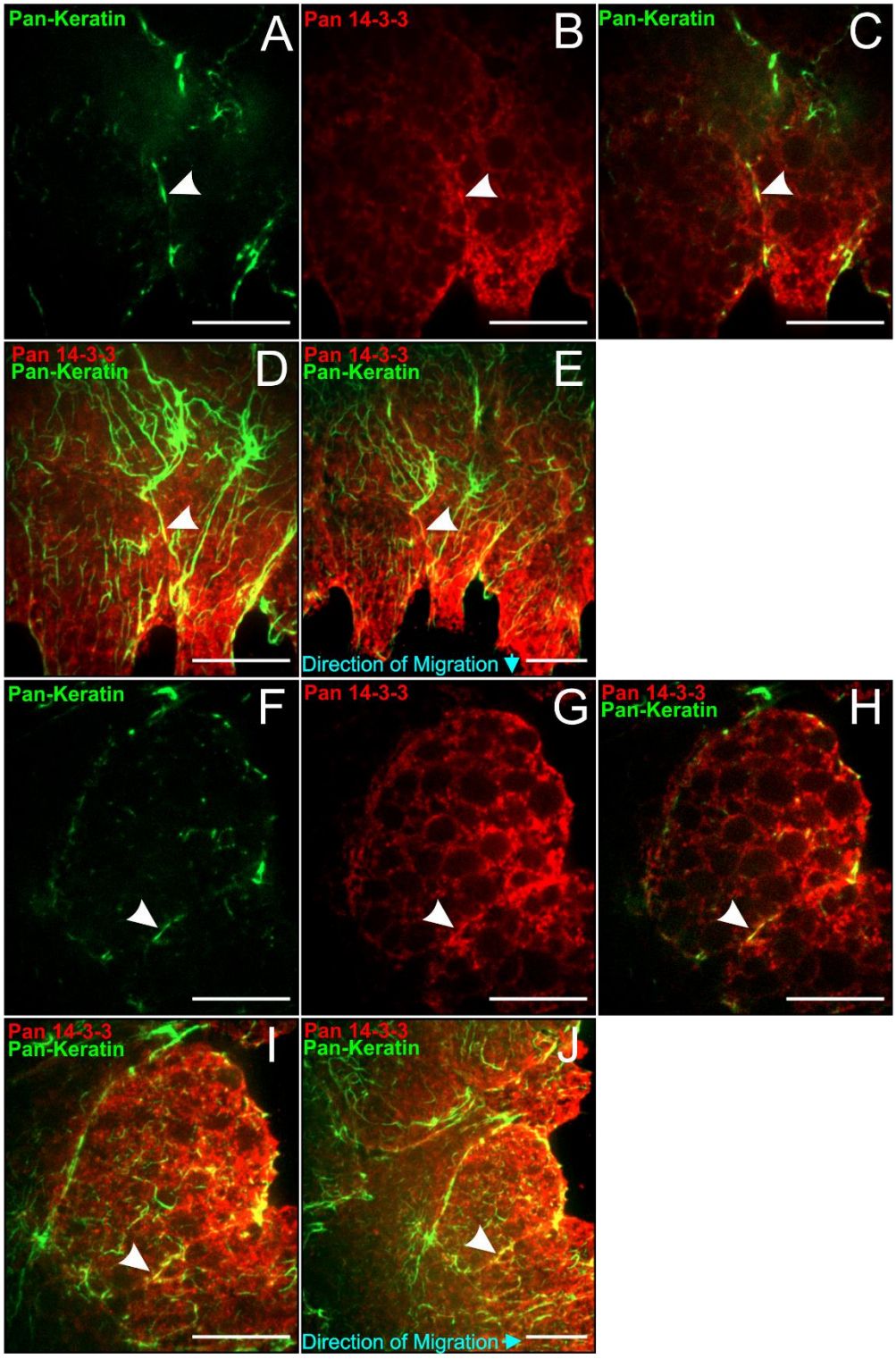
Pan-Keratin
A
Pan 14-3-3
B
Pan-Keratin
C
Pan 14-3-3
Pan-Keratin
D
Pan 14-3-3
Pan-Keratin
E
Direction of Migration
Pan-Keratin
F
Pan 14-3-3
G
Pan 14-3-3
Pan-Keratin
H
Pan 14-3-3
Pan-Keratin
I
Pan 14-3-3
Pan-Keratin
J
Direction of Migration

Figure 7. The mesendoderm leading edge of dorsal marginal zone explants demonstrates subcellular association of 14-3-3 and keratin filaments.

A-C) Single plane confocal images (63x, 1.6 Tubelens) of a dorsal marginal zone (DMZ) explant leading edge. Collectively migrating mesendoderm cells are immunolabeled for type I and type II keratins (A) and multiple 14-3-3 isoforms (B). The arrowhead in the merged image (C) indicates a subset of the keratin filament network that colocalizes with 14-3-3 at the lateral border of two leading cells. **D**) Maximum intensity projection of the confocal z-stack of cells shown in A-C to demonstrate the broader labeled keratin network and 14-3-3 localization. **E**) Lower magnification (63x, 1.0 Tubelens) of the maximum intensity projection shown in D. **F-H**) Single plane confocal images (63x, 1.6 Tubelens) depicting a different perspective of migratory leading edge mesendoderm. A portion of the keratin network (F) and peripherally distributed 14-3-3 (G) in this optical section demonstrate association at the rear lateral contact of leading cells (arrowhead in H). **I**) Maximum intensity projection of the confocal z-stack of cells shown in F-H. **J**) Lower magnification (63x, 1.0 Tubelens) of the maximum intensity projection shown in I. Blue arrow in merge images indicates direction of explant migration. The 63x objective referenced in this figure has a 1.4 NA. Scale bars are 20 μm.

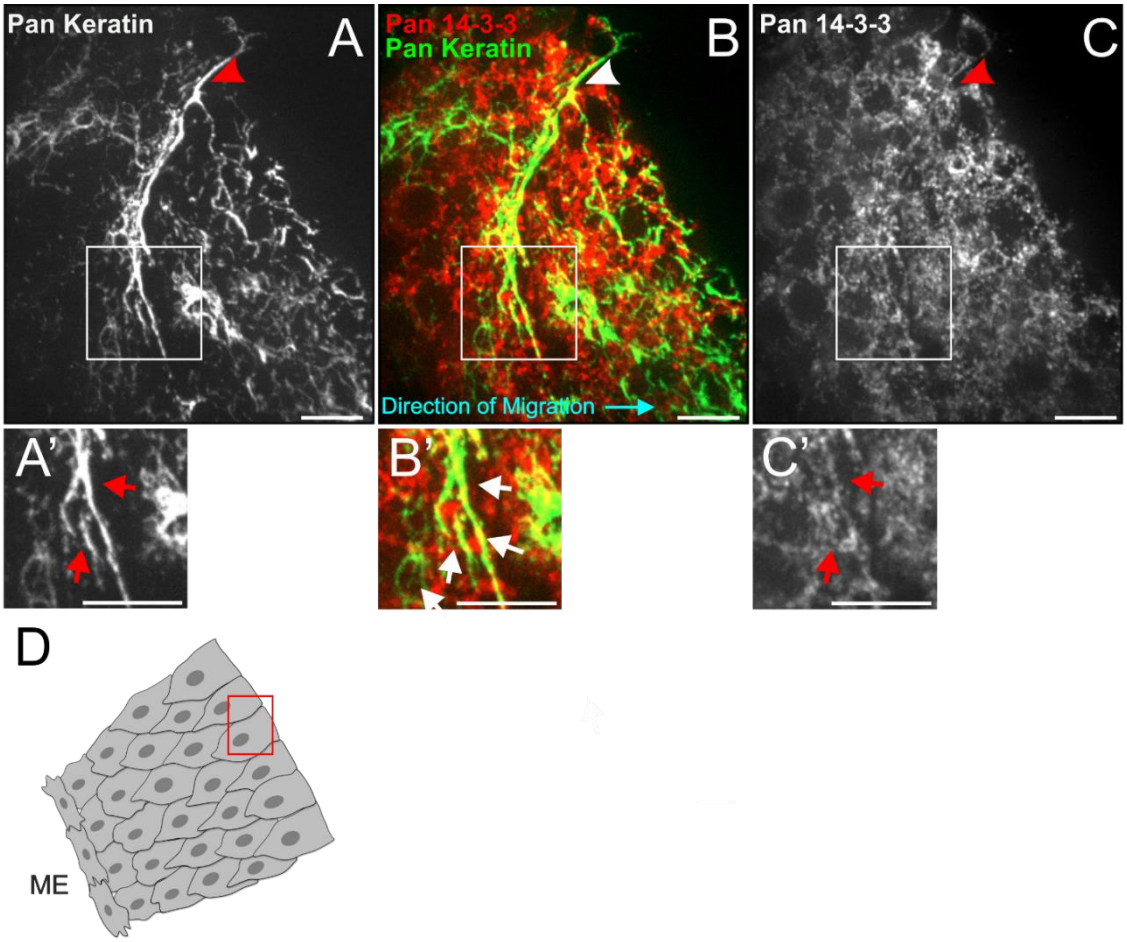
Pan Keratin
A
Pan 14-3-3
Pan Keratin
B
Pan 14-3-3
C
Direction of Migration
A'
B'
C'
D
ME

Figure 8. 14-3-3 proteins demonstrate filamentous immunolabeling of keratin densities at the cell-cell adhesion of *ex vivo* mesendoderm explants.

A-C) Leading edge of a mesendoderm explant demonstrating association between 14-3-3 and keratins. The keratin network is labeled with a pan-keratin antibody (A) and the distribution of multiple of 14-3-3 isoforms is depicted (C). The arrowheads in A-C highlight the cell-cell interface between two leading cells. **A'-C'**) Inset of a portion of the peripheral keratin network highlighted within the white box in A-C. Closer inspection of the keratin morphology at this area (red and white arrows) reveals filamentous 14-3-3 labeling. **D**) Cartoon explant schematic depicting the cell pair (A-C) relative to the rest of the tissue. Images are confocal z-stacks (maximum intensity projection). Images were taken using a 63x objective (1.4 NA) and 1.6 Tubelens. Scale bars are 10 μm.

A

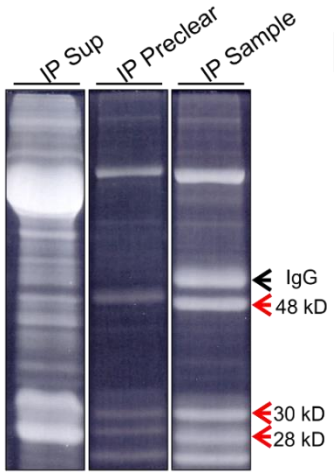

B

Xenopus laevis Keratin 19 Sequence

MTSYSIRQTSSGSYRGLGAPVGVGRVSYKAPSVHGGYGG
QGISVSSARLVSSGIGGGLGGGSYGGGSYGGGSYGSGFSS
GFGSGYGGGLSVNVSGDGLLSGNEKETMQNLNDRLASYL
DKVRTLETANSGLELKIREWYEKQGPSPSSDYSNYFKIIEDL
RGKILDATVDNSKIVLQIDNARLAADDFRTKYENELALRQSV
ECDINGLRKVLDELTLCRTDLELQIESLKEELAYLKKNHEEEM
NAMRGQVGGQISVEVDAAPTVDITKRLTEMRDQYELLAEKN
RRDAEEWFFAQSEELNKEVATHTEQIQTSKSEITDLRRTIQG
LEIELQSQLSMKAALENTLGETEARYGAQLSHIQNMISSLEA
QLADLRSDMERQNHEYKMLMDIKTRLEKEISTYRQLLEGHD

Peptide Hits Possible 14-3-3 Sites K18 14-3-3 Site

C

Approximate Molecular Weight (kD)	Molecule of Interest	% Peptide Coverage-WEL	Unique Hits Count-WEL	Exclusive Unique Spectra-WEL	Total Spectra-WEL	AA Coverage-WEL	Accession Number
48	Keratin 19	32.8	15	15	27	135/412	gi | 148232403
30	14-3-3 ε	12.2	1	1	1	31/255	gi | 148225538
	14-3-3 ζ (a)	38.8	8	8	9	95/245	gi | 147899826
	14-3-3 ζ (b)	38.5	2	2	2	95/245	gi | 1360640
	14-3-3 θ	11.8	1	1	1	26/246	gi | 147906019
	14-3-3 β (a)	22.1	3	4	4	52/244	gi | 285026416
28	14-3-3 β (b)	32.4	4	5	5	79/244	gi | 147901574
	14-3-3 ζ (a)	38.8	8	11	14	95/245	gi | 147899826
	14-3-3 ζ (b)	38.5	2	3	3	95/247	gi | 1360640
	14-3-3 θ	42.7	6	8	8	105/246	gi | 147906019

Figure 9. *Xenopus* Type I Keratin 19 associates with 14-3-3 proteins in whole embryos.

A) Pan 14-3-3 immunoprecipitates (1% Tergitol type NP-40) from whole embryo lysates prior to band extraction and processing using LC/MS-MS. Prominent bands at 48, 30, and 28 kD (red arrows) were processed. Heavy chain IgG from the antibody used for IP was not excised. Immunoprecipitation was performed using approximately 2000 µg of protein lysate. **B**) Summary schematic of Keratin 19 peptides (red) detected in the 48 kD sample. Peptides are depicted within the context of the Keratin 19 primary structure and alongside described (green) and predicted (blue) possible 14-3-3 interaction sites. **C**) Table summary of relevant proteins detected in gel extracts processed using LC/MS-MS. Experiments were conducted using 14-3-3 immunoprecipitates from whole embryo lysates (WEL). Analysis was performed using Scaffold 4.7.3

A

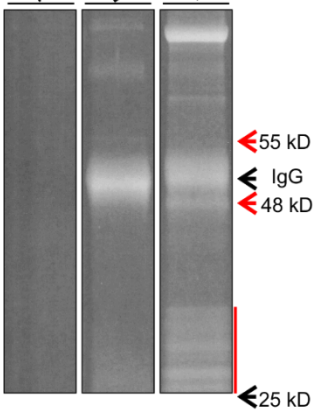

B

Xenopus laevis Keratin 19 Sequence (DME)

MTSYSIRQTSSGSYRGLGAPVGVGRVSYKAPSVHGGYGG
QGISVSSARLVSSGIGGGLGGGSYGGGSYGGGSYGSGFSS
GFGSGYGGGLSVNVSGDGLLSGNEKETMQNLNDRLASYL
DKVRTLETANSGLELKIREWYEKQGPSPSSDYSNYFKIIEDL
RGKILDATVDNSKIVLQIDNARLAADDFRTKYENELALRQSV
ECDINGLRKVLDELTLCRTDLELQIESLKEELAYLKKNHEEEM
NAMRGQVGGQISVEVDAAPTVDITKRLTEMRDQYELLAEKN
RRDAEEWFFAQSEELNKEVATHTEQIQTSKSEITDLRRTIQG
LEIELQSQLSMKAALENTLGETEARYGAQLSHIQNMISSLEA
QLADLRSDMERQNHEYKMLMDIKTRLEKEISTYRQLLEGHD

Peptide Hits Possible 14-3-3 Sites K18 14-3-3 Site

C

Approximate Molecular Weight (kD)	Molecule of Interest	% Peptide Coverage-ME	Unique Hits Count-ME	Exclusive Unique Spectra-ME	Total Spectra-ME	AA Coverage-ME	Accession Number
48	Keratin 19	14.8	7	8	19	61/412	gi | 148232403
30-25	14-3-3 ε	0	0	0	0	0	gi | 148225538
	14-3-3 ζ (a)	38.8	2	2	4	95/245	gi | 147899826
	14-3-3 ζ (b)	38.5	6	7	16	95/247	gi | 1360640
	14-3-3 θ	36.2	6	7	12	89/246	gi | 147906019
	14-3-3 β (a)	41.8	1	2	4	102/244	gi | 285026416
	14-3-3 β (b)	46.3	10	12	23	113/244	gi | 147901574
55	Keratin 8	17.9	10	12	32	92/508	gi | 125112

Figure 10. Mesendoderm *Xenopus* Type I Keratin 19 associates with 14-3-3 proteins.

A) Mesendoderm tissue was isolated and processed into lysates (1% Tergitol type NP-40) for immunoprecipitation using Pan 14-3-3 antibody prior to gel electrophoresis, band extraction, and processing via LC/MS-MS. A 14-3-3 immunoprecipitated sample from whole embryo lysates was utilized as a proxy for band separation to assist in extraction of less prominent bands in the mesendoderm only sample. Prominent bands at 55 and 48 kD (red arrows) were processed, as well as a range of bands from 25-30 kD (red line). Immunoprecipitation was performed using approximately 2000 µg of protein lysate. **B**) Summary schematic of mesendoderm Keratin 19 peptides (red) detected in the 48 kD sample. Peptides are depicted within the context of the Keratin 19 primary structure and alongside described (green) and predicted (blue) possible 14-3-3 interaction sites. **C**) Table summary of relevant proteins detected in gel extracts processed using LC/MS-MS. Experiments were conducted using 14-3-3 immunoprecipitates from mesendoderm (ME) tissue lysates. Analysis was performed using Scaffold 4.7.3

A

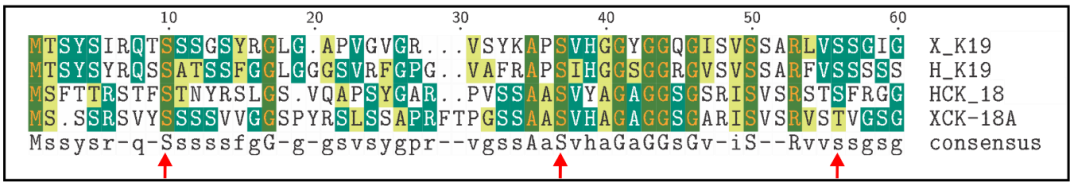

B

K19 Serine Site	Adjacent Sequence	Phosphorylation Prediction (Proportion)	Mode 1 14-3-3 Site Prediction (Percentile)
10	SYSIRQT**S**SSGSYRG	0.992	3.157%
33	RVSYKAP**S**VHGGYGG	0.983	13.882%
52	VSSARLV**S**SGIGGGL	0.488	3.629%

C

Predicted Kinase	Site Prediction [NetPhos 3.1] (Proportion)	K19 Serine Site	Site Prediction [Scansite 4.0] (Percentile)
Calmodulin dependent Kinase 2	0.489	10	0.973%
Akt Kinase	0.167	10	4.014%
GSK3	0.467	10	9.335%
Protein Kinase A	0.3	10	12.468%
Casein Kinase 1	0.375	33	5.621%
Protein Kinase A	0.202	33	7.926%
PKC delta	0.25	33	11.396%
PKC zeta	0.25	33	12.618%
PKC alpha/beta/gamma	0.25	33	13.649%
Akt Kinase	0.228	52	6.286%

Figure 11. 14-3-3 and Keratin 19 informatics.

A) Sequence alignment of *Xenopus laevis* Keratin 18A and 19 with human Keratin 18 and 19. The arrows indicate serine sites referenced in B and C. The sequence alignment was created using the San Diego Supercomputer (SDSC) Biology Workbench. **B**) Table reporting the likelihood that a given site is phosphorylated (NetPhos 3.1) (Blom et al., 1999) and is a 14-3-3 site (Scansite 4.0) (Obenauer et al., 2003). **C**) Table reporting the likelihood that a given site is a kinase site. Reported results were restricted to sites identified in both NetPhos3.1 (Blom et al., 2004) and Scansite 4.0 analyses. NetPhos 3.1 proportions display the likelihood that a given site is a true site relative to how close the score is to 1. Lower Scansite 4.0 percentiles (closer to 0%) represent greater likelihood that a given site is a true site. NetPhos 3.1 likelihoods in A are for unspecified kinases. Scansite 4.0 was utilized at the minimum stringency to report all predictions at the selected sites.

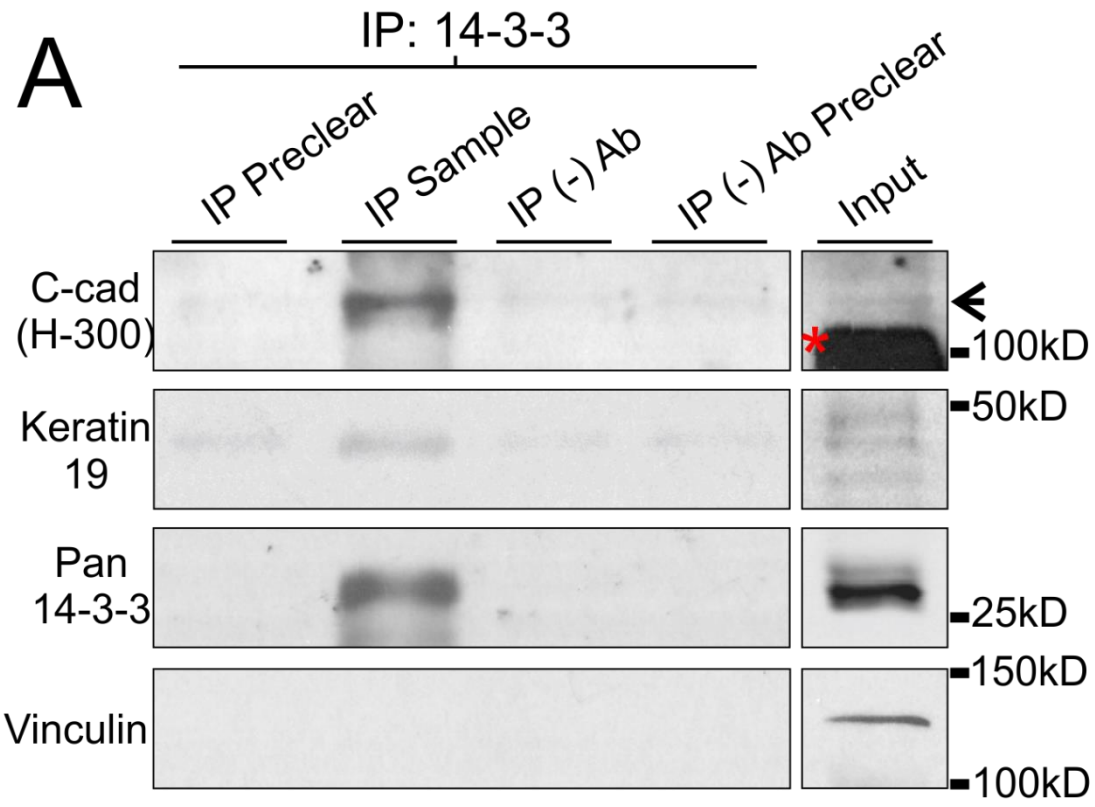
A
IP: 14-3-3
IP Preclear
IP Sample
IP (-) Ab
IP (-) Ab Preclear
Input
C-cad
(H-300)
Keratin
19
Pan
14-3-3
Vinculin
100kD
50kD
25kD
150kD
100kD

Figure 12. *Xenopus* Keratin 19 associates with 14-3-3 proteins and C-cadherin.

A) Co-IP of 14-3-3 proteins from whole embryo lysates immunoblotted for keratin network and cell-cell adhesion proteins. 5 µg of pan-14-3-3 antibody was preincubated with approximately 2000 µg of lysates (1% Tergitol type NP-40) from stage 10.5 gastrulating embryos and immunoprecipitated following incubation with protein-g conjugated agarose beads. Type I acidic Keratin 19 and cadherin proteins were immunolabeled using a monoclonal antibody and polyclonal pan-antibody respectively. Vinculin was detected using a monoclonal antibody. An arrow highlights the cadherin band in the input lane while an asterisk highlights the embryonic yolk protein that migrates at approximately 100 kD. Input lanes include approximately 1 embryo worth of protein.

CHAPTER 4

DEVELOPMENT OF GENETICALLY ENCODED PEPTIDE FUSION PROTEINS TO SEPARATELY INHIBIT 14-3-3 INTERACTIONS AND INDUCE BINDING OF 14-3-3 PROTEINS

Some information from this chapter is accepted for publication in Mariani *et al.* (2019) *MBoC.*

14-3-3 proteins are a family of adapter proteins comprised of several isoforms that bind target molecules in a phosphorylation dependent manner and augment their activity (Obsil and Obsilova 2011). The vast interactome of 14-3-3 proteins (>200 known molecular substrates) demonstrates the importance of these proteins but also highlights the challenge inherent in attempting to deduce specific roles for these proteins through knockdown or deletion (Pozuelo Rubio et al. 2004).

The identification of roles for 14-3-3 proteins in many signaling pathways has led to the discovery and development of a variety of tools designed to investigate the function of these proteins. Among these are a variety of naturally occurring and synthetic chemical inhibitors that target the 14-3-3 binding groove as well as chemical stabilizers of interactions between 14-3-3 and other proteins (Bartel et al. 2014). In addition to chemical substrates, one of the most well-described high affinity molecules that interacts with 14-3-3 is a 20-mer peptide named ‘R18’ (Wang et al. 1999). The ability to encode this sequence in DNA and RNA for targeted expression in specific cell populations of embryos has proven to be a useful method for studying 14-3-3 in *Xenopus* development (Wu and Muslin 2002; Lau et al. 2006).

The R18 peptide was a viral phage derived peptide product identified via binding to immobilized 14-3-3 τ/θ protein (Wang et al. 1999). This peptide sequence, PHCVPRDLSWLDLEANMCLP, was converted into a corresponding DNA sequence to design a GST-R18 fusion protein for purification and biochemical study (Wang et al. 1999). The peptide demonstrated several qualities *in vitro* that confirmed its usefulness in the study of 14-3-3 protein-protein interactions; firstly,

it was shown to specifically bind and precipitate 14-3-3 proteins from NIH 3T3 fibroblast lysates (Wang et al. 1999). Additionally, though the peptide was identified by binding assay with the τ isoform, GST-R18 demonstrated similar binding affinity for multiple 14-3-3 isoforms including β and ζ (Wang et al. 1999).

The interaction between GST-R18 and 14-3-3 was shown to be inhibitory via the effect demonstrated with regard to other 14-3-3 substrates. Incubation of 14-3-3 τ with both GST-R18 and R18 alone before Raf1 prevented the interaction between these proteins (Wang et al. 1999). Furthermore, R18 was demonstrated to disrupt the ability of 14-3-3 proteins to prevent Raf1 activation by phosphatase addition (Wang et al. 1999). While addition of more 14-3-3 τ was able to rescue this inhibitory effect, pre-incubation of the additional 14-3-3 with R18 prevented the rescue effect (Wang et al. 1999). Taken together, these data demonstrate that the R18 peptide sequence inhibits 14-3-3 proteins via a specific binding interaction that prevents 14-3-3 binding with other substrates and related functions of those interactions (Wang et al. 1999).

Co-crystal structures of 14-3-3 and R18 along with biochemical experiments have demonstrated that this peptide induces inhibition of 14-3-3 protein-protein interactions by associating with the 14-3-3 binding groove in an amphipathic manner (Wang et al. 1999; Petosa et al. 1998). Charge mutation of lysine 49 of the 14-3-3 ‘basic pocket’ to glutamic acid prevented biochemical interaction between R18 and 14-3-3, while mutation of valine 176 of the ‘hydrophobic roof’ to aspartic acid greatly reduced the interaction (Wang et al. 1999). Predictions based on co-crystal structure identify the WLDLE motif of the R18 peptide as the central

determinant for binding to 14-3-3 proteins (Petosa et al. 1998). The aspartic acid is predicted to be in proximity with lysine 49, while the glutamic acid is thought to be in proximity to the arginines of the site (Petosa et al. 1998). The two leucines of the WLDLE motif are predicted to be in proximity to a variety of hydrophobic residues of the 14-3-3 binding groove roof (Petosa et al. 1998).

Since the discovery and characterization of the R18 peptide, several studies have adapted it for the study of 14-3-3 in cellular contexts. The peptide was utilized as a GST-R18 fusion protein inhibitor in *Xenopus laevis* embryos, microinjected as RNA that translates into the fusion protein (Wu and Muslin 2002). Given that the WLDLE motif was identified as the R18 binding determinant, the authors designed a control ALALE mutant named 'R18M' that demonstrates inability to bind 14-3-3 proteins (Wu and Muslin 2002). Utilizing this method, it was shown that at least when the RNA for GST-R18 was injected in relatively high amounts, developmental abnormalities emerged (Wu and Muslin 2002). Moreover, developmental roles for 14-3-3 proteins that were shown to be both tissue and isoform specific could be disrupted by targeted injection of this peptide (Lau et al. 2006). This work demonstrates that expression of R18 can be spatially controlled, allowing for inhibition of specific tissue populations. Research has been conducted with fluorophore-fused trackable versions of R18 and R18M peptides, further demonstrating spatial control of these tools (Jin et al. 2004).

We sought to determine whether the R18 peptide sequence could be applied to specifically interrogate the nature of the relationship between 14-3-3 proteins and keratin filaments in distinct cell populations. In this study, we

developed 14-3-3-keratin binding loss-of-function and gain-of-function trackable R18 fusion proteins and examined their effect on keratin properties and networks.

Results

Design of a fluorophore and epitope fusion with a phage-derived 'R18' 14-3-3 inhibitory peptide

Given that work by Muslin had demonstrated specific inhibition of 14-3-3 proteins in *Xenopus laevis* (Wu and Muslin 2002; Lau et al. 2006), we utilized DNA sequences published by the authors to derive R18 and R18M sequences. Nucleotides encoding the R18 and R18M peptides were flanked by sequences for a number of restriction sites and binding epitopes in preparation for the design several possible fusion proteins (Figure 13). The sequences were synthesized by the company Genewiz and cloned into pUC57 vectors. The pUC57-R18 and R18M plasmids were digested using the BamHI and XhoI restriction enzymes to clone the sequences into the pCS2+ plasmid vector. The pCS2+ contains an SP6 polymerase binding site that is utilized during *in vitro* transcription of RNA for cellular microinjection. In order to produce R18 and R18M fusion proteins that were trackable by light microscopy, the restriction enzymes AgeI and BglII were utilized to clone the sequence of mCherry in frame with the peptides (Figure 13). Further minor cloning was performed to remove an upstream out of frame kozak sequence and to introduce a second linker type. The protein sequences of the pCS2-mCherry-R18/M plasmids are included for reference (Figure 14).

mCherry-R18 fusion proteins specifically bind 14-3-3 in Xenopus embryos

Although 14-3-3 proteins had been demonstrated to specifically bind to GST-R18 (Wang et al. 1999; Wu and Muslin 2002), we sought to determine whether mCherry-R18 was able to bind 14-3-3 proteins. RNA encoding either mCherry-R18 or R18M was co-injected into *Xenopus* embryos alongside RNA encoding FLAG-14-3-3 β (Figure 15). Immunoprecipitation of FLAG-14-3-3 β demonstrated interaction between 14-3-3 and mCherry-R18, but not between 14-3-3 and mCherry-R18M (Figure 15 A). Given that mCherry-R18 retained the binding specificity characteristic of both R18 and GST-R18, we decided to investigate functional utilization of this peptide. Our tools and method for microinjection of *Xenopus laevis* embryos did not permit injection of more than approximately 2 ng of DNA or RNA, preventing ability to follow-up published experiments to broadly inhibit 14-3-3 in *Xenopus* via R18 (Wu and Muslin 2002). Instead, we opted to broadly investigate the effect of 14-3-3 inhibition via mCherry-R18 in regard to establishment of keratin networks in cells.

Expression of mCherry-R18 in subconfluent MDCK epithelial cells results in collapse of Xenopus cytokeratin networks

Previous work has demonstrated that mutation of serine 33 to alanine in K18 results in collapse of the network to a peri-nuclear ring (Ku et al. 1998). In order to determine whether 14-3-3 inhibition could induce a similar effect on *Xenopus* keratin containing filament networks, mCherry-R18 was co-transfected into subconfluent MDCK epithelial cells alongside GFP-XCK8, the type I *Xenopus* analog of Keratin 8 (Figure 16 and Figure 17). Time lapse imaging over a 12 hour

period demonstrated a disruption of the GFP-XCK8 keratin network that is detectable approximately 4 hours after the onset of fluorescent signal (Figure 16). Inspection of MDCK cells co-expressing mCherry-R18M with GFP-XCK8 after the 12 hour course demonstrated that these cells are able to produce a normal cytoplasmic and junctional GFP-XCK8 network (Figure 17 C and D). In contrast, mCherry-R18 expression results in formation of an abnormal and retracted GFP-XCK8 network (Figure 17 A and B).

Given that high GFP-XCK8 expression could potentially contribute to the abnormality of networks in the presence of 14-3-3 inhibition, mCherry-R18 and mCherry-R18M were transfected alone into MDCK cell stable expressors of GFP-XCK8 (Figure 18 and Figure 19). Time lapse imaging demonstrated an obvious retraction of the keratin network to a thin ring shape that was concomitant with a cell morphological change to a circular shape (Figure 18). Investigation of MDCK cells expressing mCherry-R18M after the 12 hour time lapse demonstrated cells that were able to engage in contacts with cell clusters and express a normal GFP-XCK8 network across cellular compartments, showing a normal morphology similar to that within MDCK cells expressing GFP-XCK8 alone (Figure 19 D-F). Cells that were 14-3-3 inhibited via mCherry-R18 expression showed a collapsed peri-nuclear network reminiscent of that formed by K18 S33A (Ku et al. 1998) and remained as single cells that appeared rounded and longer in height relative to mCherry R18M expressors (Figure 19 A-C). These findings present evidence that 14-3-3 inhibition results in collapse of *Xenopus* cytokeratin 8 containing networks in subconfluent epithelia.

Design of a novel R18 peptide fusion with Keratin 19 to induce synthetic-coupling in-vivo

Implementation of mCherry-R18 via DNA or RNA microinjection allows for tissue specific subcellular study of the roles of 14-3-3 in *Xenopus* embryos, but with a caveat; R18 peptide broadly inhibits 14-3-3 protein-protein interactions. This presents an issue when trying to study a particular interaction in a cellular context, such as the role of 14-3-3 and keratin interaction in regard to keratin network dynamics in mesendoderm. In addition, because prevention of 14-3-3 interaction via mutation of 14-3-3 sites in intermediate filaments has widespread consequences for the network, these methods do not easily allow us to interrogate how 14-3-3 proteins modulate filament activity. With these experimental limitations in mind, we designed a gain-of-function keratin protein utilizing the R18 sequence to induce binding of 14-3-3 proteins. This GFP-R18-K19 design represents a fusion protein where the R18 sequence becomes an additional high-affinity binding site for 14-3-3 proteins in frame with Keratin 19 (Figure 20). A series of cloning experiments were required to place R18 and R18M sequences in frame with both the sequence of K19 as well as with trackable epitopes. The plasmids produced included pCS2-GFP-R18-K19 and pCS2-GFP-R18M-K19 as well as pCS2-3xFLAG-R18-K19 and pCS2-3xFLAG-R18-K19. The protein sequences for these fusions are provided (Figure 20).

R18-K19 demonstrates robust high affinity for 14-3-3 proteins

In order to determine the extent to which inclusion of the R18 sequence in frame with K19 increases binding to 14-3-3 proteins, RNA encoding either GFP-

R18-K19 or GFP-R18M-K19 was co-injected into *Xenopus* embryos alongside RNA encoding FLAG-14-3-3 β (Figure 21). Immunoprecipitation of FLAG-14-3-3 β demonstrated that 14-3-3 proteins interacted with GFP-R18-K19 in a highly increased manner when compared to the interaction between 14-3-3 and GFP-R18M-K19 (Figure 21 C). This interaction proved to be robust and reliable, showing that fusion of the R18 sequence increased the affinity of the keratin with regard to 14-3-3 proteins (Figure 21 A-C). In addition, injection of RNA encoding 3xFLAG-R18-K19 and 3xFLAG-R18M-K19 followed by FLAG immunoprecipitation demonstrated increased interaction between 3xFLAG-R18-K19 and endogenous 14-3-3 proteins compared to that of 3xFLAG-R18M-K19 (Figure 22). Taken together, these results illustrate that fusion of the R18 sequence with keratin specifically increases binding of 14-3-3 to these proteins. This binding enhancement allows these constructs suitability in regard to experiments aimed at investigating the relationship between 14-3-3 and keratins in mesendoderm (Shown in Chapter 5).

Discussion

Our data demonstrate that the phage derived R18 sequence (Wang et al. 1999) is phosphorylation independent 14-3-3 inhibitor that effectively binds 14-3-3 proteins across a variety of fusion protein types. With the addition of a fluorophore, the R18 peptide sequence functions as trackable 14-3-3 inhibitor that allows for identification of inhibited cells and study in a multitude of contexts. When expressed mosaically in either cell culture by transfection or embryos via microinjection, this becomes an especially powerful tool for studying the function of 14-3-3 in both single cells and during adhesion with either non-inhibited or inhibited cells.

Utilization of the mCherry-R18 fusion protein demonstrated that 14-3-3 inhibition in subconfluent MDCK cell epithelia results in abnormal contraction of the widespread GFP-XCK8 containing keratin network to a peri-nuclear restricted ‘cage-like’ morphology. These results closely resemble those that result from mutation of the serine 33 site in Keratin 18 (Ku et al. 1998), providing evidence that both direct perturbation of 14-3-3 proteins and disruption of the inability of these proteins to bind are similarly important for formation of keratin networks. It is interesting to note that mutation of this conserved serine in Keratin 19 (shown in Chapter 3) also results in a similar peri-nuclear collapse of the keratin network (Zhou et al. 1999). Taken together, these data mark the possibility that *Xenopus* K19 may require 14-3-3 interaction for filament network integrity or activity dynamics.

Although R18 protein fusions provide outstanding utility due to their ability to inhibit 14-3-3 proteins and disrupt interactions both *in vitro* and *in vivo* (Wang et al. 1999, Wu and Muslin 2002), the large interactome of 14-3-3 proteins creates difficulty in determining the specific effect of 14-3-3 disruption that is causal in any phenotype. While knockdown or deletion of particular isoforms allows specificity in the particular 14-3-3 protein that is perturbed, evidence that different isoforms can compensate for these deletions and even rescue phenotypes demonstrates that these methods do not abrogate the specificity issue. Another alternative strategy is to interrogate the function of a specific 14-3-3 interaction via gain-of-function. In this study we demonstrate that fusing the R18 peptide sequence to full length K19 results in a mutant that binds a strongly increased amount of 14-3-3 proteins, both exogenous and endogenous. By employing this fusion within a trackable GFP-K19 (GFP-R18-K19), we are able to study the effect of increasing association with 14-3-3 on keratin network activity (shown in Chapter 5). Thus, we provide that utilization of R18 as a high-affinity site for 14-3-3 proteins via fusion with a trackable protein of interest provides a method to deduce the effect of 14-3-3 binding with regard to the molecule of choice, specifically.

A

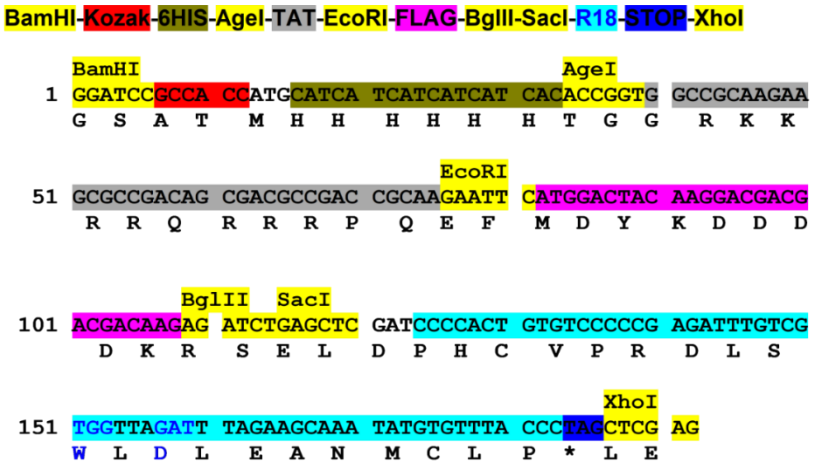
BamHI-Kozak-6HIS-AgeI-TAT-EcoRI-FLAG-BglII-SacI-R18-STOP-XhoI
BamHI
AgeI
1 GGATCCGCCA CCATGCATCA TCATCATCAT CACACCGGTG GCCGCAAGAA
G S A T M H H H H H H T G G R K K
EcoRI
51 GCGCCGACAG CGACGCCGAC CGCAAGAATT CATGGACTAC AAGGACGACG
R R Q R R R P Q E F M D Y K D D D
BglII SacI
101 ACGACAAGAG ATCTGAGCTC GATCCCCACT GTGTCCCCCG AGATTTGTCG
D K R S E L D P H C V P R D L S
XhoI
151 TGGTTAGATT TAGAAGCAAA TATGTGTTTA CCCTAGCTCG AG
W L D L E A N M C L P * L E

B

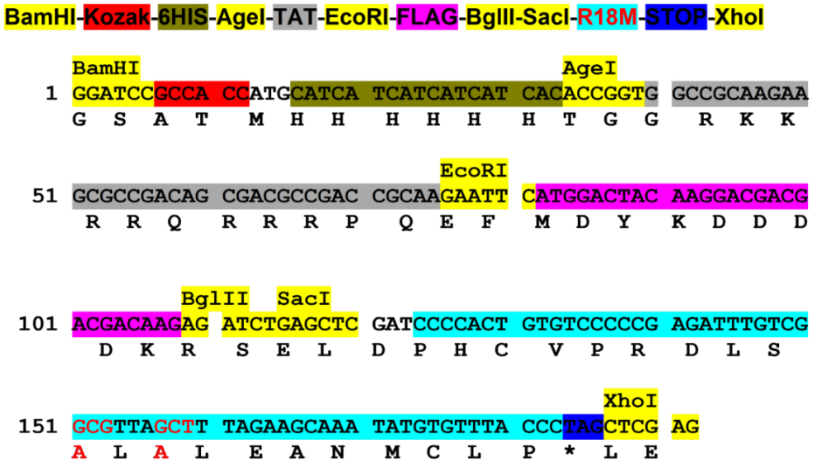
BamHI-Kozak-6HIS-AgeI-TAT-EcoRI-FLAG-BglII-SacI-R18M-STOP-XhoI
BamHI
AgeI
1 GGATCCGCCA CCATGCATCA TCATCATCAT CACACCGGTG GCCGCAAGAA
G S A T M H H H H H H T G G R K K
EcoRI
51 GCGCCGACAG CGACGCCGAC CGCAAGAATT CATGGACTAC AAGGACGACG
R R Q R R R P Q E F M D Y K D D D
BglII SacI
101 ACGACAAGAG ATCTGAGCTC GATCCCCACT GTGTCCCCCG AGATTTGTCG
D K R S E L D P H C V P R D L S
XhoI
151 GCGTTAGCTT TAGAAGCAAA TATGTGTTTA CCCTAGCTCG AG
A L A L E A N M C L P * L E

Figure 13. DNA and amino acid sequences for R18 and R18M peptides.

A) Nucleotide sequence designed to encode R18 peptide. Various binding epitopes, transcription elements, and restriction digest sequences are included to enable multiple cloning options. The restriction sites are highlighted in yellow and the epitopes are marked in purple, bronze and silver. The kozak sequence is highlighted in red. Key nucleotides particular to the R18 peptide sequence are included in blue text. **B**) Similar design sequence encoding R18M peptide. The nucleotides particular to the R18M sequence are included in red text. Sequences were prepared using the pDRAW32 program.

A

Kozak-Linker1-mCherry-R18/R18M

ATMVSKGEEDNMAIIKEFMRFKVHMEGSVNGHEFEIEGEGEGRPYEGTQTAKLKVTKGGPLPFAWDILSPQFMYGSK
AYVKHPADIPDYLKLSFPEGFKWERVMNFEDGGVVTVTQDSSLQDGEFIYKVKLRGTNFPSDGPVMQKKTMGWEASS
ERMYPEDGALKGEIKQRLKLKDGGHYDAEVKTTYKAKKPVQLPGAYNVNIKLDITSHNEDYTIVEQYERAEGRHSTG
GMDELYKSGLRSELDPHCVPRDLS[W/A]L[D/A]LEANMCLP*

B

Kozak-Linker2-mCherry-R18/R18M

ATMVSKGEEDNMAIIKEFMRFKVHMEGSVNGHEFEIEGEGEGRPYEGTQTAKLKVTKGGPLPFAWDILSPQFMYGSK
AYVKHPADIPDYLKLSFPEGFKWERVMNFEDGGVVTVTQDSSLQDGEFIYKVKLRGTNFPSDGPVMQKKTMGWEASS
ERMYPEDGALKGEIKQRLKLKDGGHYDAEVKTTYKAKKPVQLPGAYNVNIKLDITSHNEDYTIVEQYERAEGRHSTG
GMDELYKSGLRSRAQALDPHCVPRDLS[W/A]L[D/A]LEANMCLP*

Figure 14. Design of mCherry-R18/R18M fusion peptides.

A) Full sequence of mCherry-R18 and mCherry-R18M fusion proteins including the mCherry fluorophore, linker sequence, peptide sequence, and stop. The pre-methionine kozak site is included for positional demonstration. Sequence for mCherry is highlighted in red, the linker sequence is highlighted in gray, and the R18/R18M peptide is highlighted in teal. The key amino acids for the R18 peptide are included in blue text and the key R18M amino acids are included in red text. **B**) mCherry-R18 and mCherry R18 protein sequences including an alternative linker.

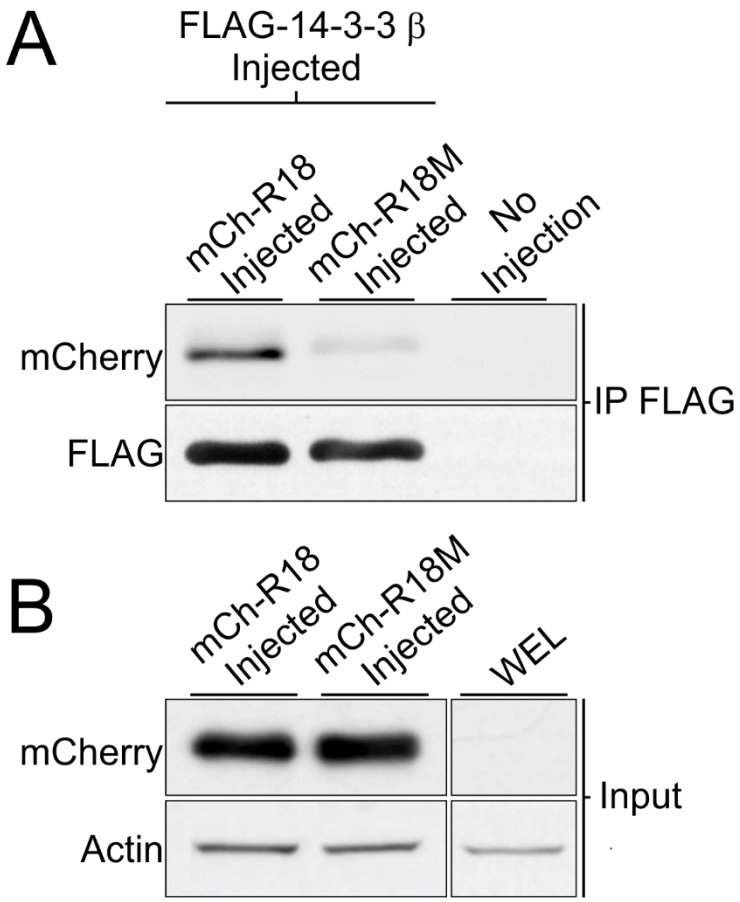
A
FLAG-14-3-3 β
Injected
mCh-R18
Injected
mCh-R18M
Injected
No
Injection
mCherry
FLAG
IP FLAG
B
mCh-R18
Injected
mCh-R18M
Injected
WEL
mCherry
Actin
Input

Figure 15. mCherry-R18 specifically binds 14-3-3 expressed in *Xenopus* embryos.

A) Immunoblot of FLAG-14-3-3 β immunoprecipitated embryonic lysates (1% Triton X-100) co-expressing mCherry R18 or mCherry R18M peptide. One-cell embryos were injected with RNA encoding mCherry-R18 or mCherry-R18M alongside RNA encoding FLAG-14-3-3 β. Lysates were prepared at embryonic stage 10.5 and immunoprecipitation for FLAG proteins was performed. FLAG immunoprecipitates were blotted for mCherry and FLAG. Non-injected lysate incubated with FLAG antibody conjugated agarose beads was immunoblotted as a negative control. **B**) Input lanes for non-injected whole embryo lysates (WEL) and lysates injected with mCherry-R18 and mCherry-R18M.

A

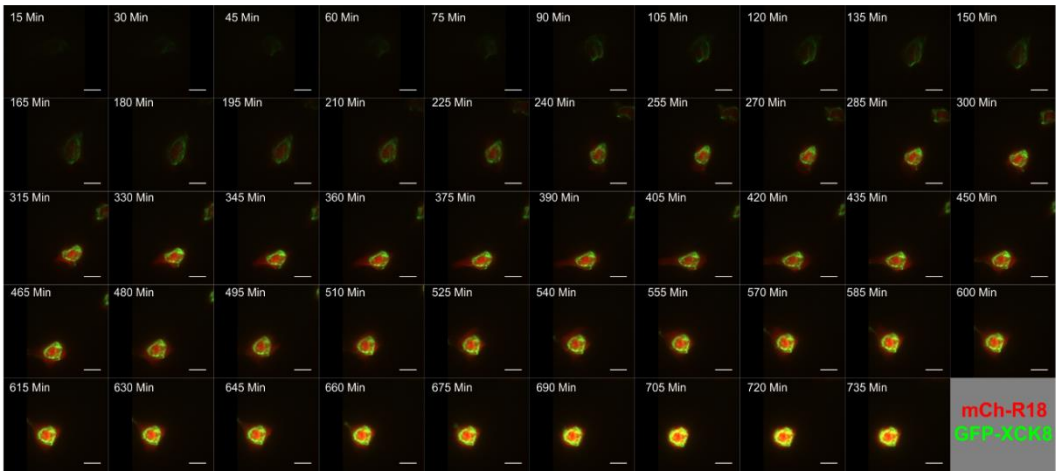
15 Min
30 Min
45 Min
60 Min
75 Min
90 Min
105 Min
120 Min
135 Min
150 Min
165 Min
180 Min
195 Min
210 Min
225 Min
240 Min
255 Min
270 Min
285 Min
300 Min
315 Min
330 Min
345 Min
360 Min
375 Min
390 Min
405 Min
420 Min
435 Min
450 Min
465 Min
480 Min
495 Min
510 Min
525 Min
540 Min
555 Min
570 Min
585 Min
600 Min
615 Min
630 Min
645 Min
660 Min
675 Min
690 Min
705 Min
720 Min
735 Min
mCh-R18
GFP-XCK8

Figure 16. mCherry-R18 disrupts expressed *Xenopus* keratin.

A) Live imaging time lapse of a single MDCK cell expressing GFP-XCK8 (*Xenopus* Keratin 8) and mCherry-R18. MDCK cells seeded to subconfluency on 35mm glass cover slipped dishes were double transfected with pCS2-GFP-XCK8 and either pCS2-mCherry R18 or pCS2-mCherry R18M. Single plane confocal optical sections were taken in 15-minute intervals over 12 hours to image GFP and mCherry signal. Images are single plane confocal optical sections. Images were taken using a 63x objective (1.4 NA) and 1.0 Tubelens. Scale bars are 20 μm.

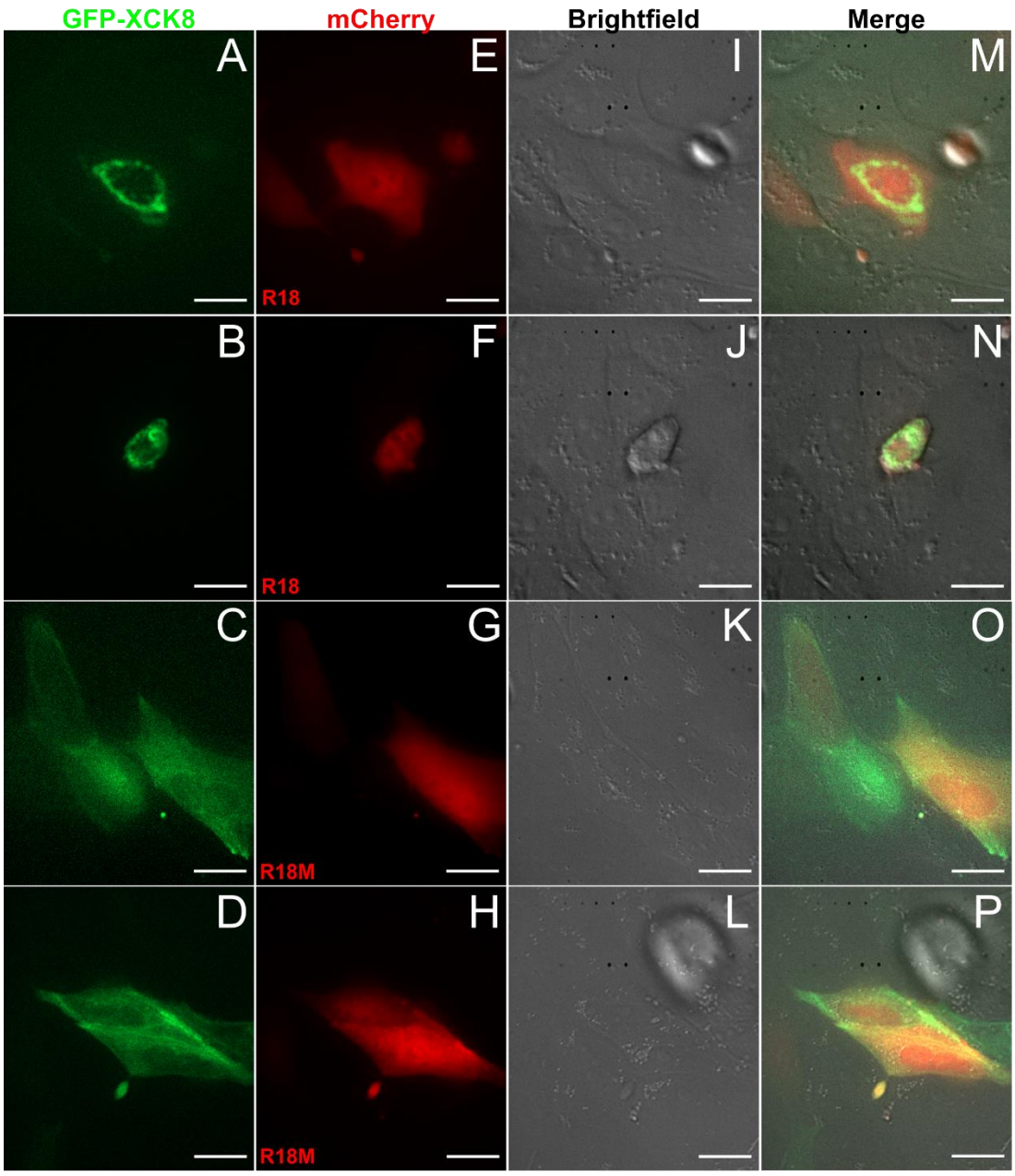
GFP-XCK8
mCherry
Brightfield
Merge
A
E
I
M
R18
B
F
J
N
R18
C
G
K
O
R18M
D
H
L
P
R18M

Figure 17. 14-3-3 inhibition via mCherry-R18 expression perturbs *Xenopus* keratin containing filaments.

Live images acquired after 12-hour time lapse. **A-D**) GFP-XCK8 filaments co-expressed with either mCherry-R18 (A and B) or mCherry-R18M (C and D) in MDCK cells after 12 hour time course. **E-H**) Cellular expression of mCherry-R18 (E and F) and mCherry-R18M (G and H). **I-L**) Brightfield images were taken to provide cellular context. **M-P**) Merge images of fluorescent channels with brightfield images. Images are single plane confocal optical sections. Images were taken using a 63x objective (1.4 NA) with a 1.0 Tubelens. Scale bars are 20 μm.

A

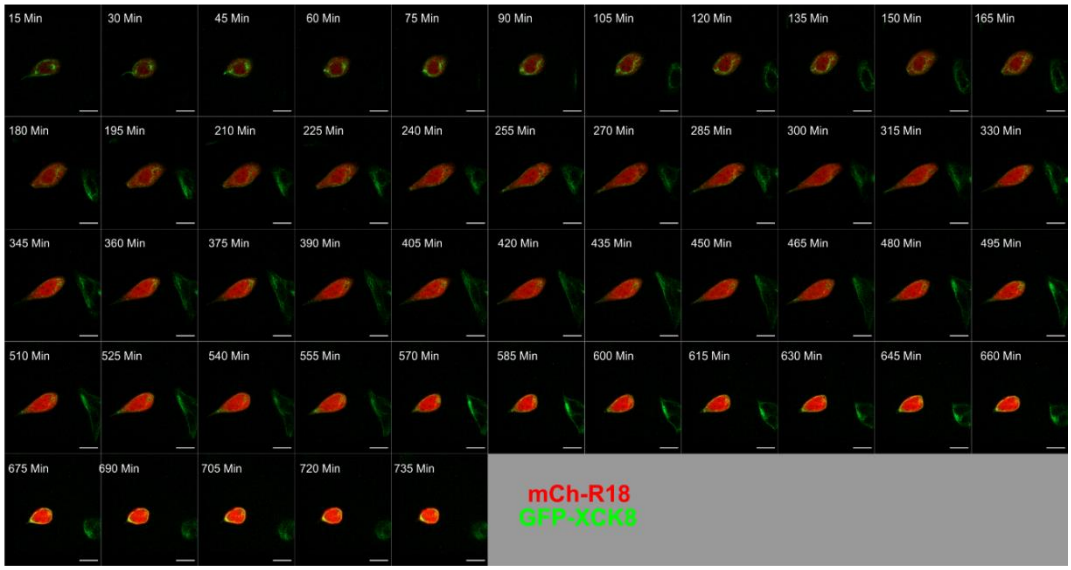
15 Min
30 Min
45 Min
60 Min
75 Min
90 Min
105 Min
120 Min
135 Min
150 Min
165 Min
180 Min
195 Min
210 Min
225 Min
240 Min
255 Min
270 Min
285 Min
300 Min
315 Min
330 Min
345 Min
360 Min
375 Min
390 Min
405 Min
420 Min
435 Min
450 Min
465 Min
480 Min
495 Min
510 Min
525 Min
540 Min
555 Min
570 Min
585 Min
600 Min
615 Min
630 Min
645 Min
660 Min
675 Min
690 Min
705 Min
720 Min
735 Min
mCh-R18
GFP-XCK8

Figure 18. mCherry-R18 disrupts stably expressed *Xenopus* keratin.

A) Live imaging time lapse of a single MDCK cell expressing GFP-XCK8 (*Xenopus* Keratin 8) and transfected to express mCherry-R18. MDCK cells stably expressing GFP-XCK8 were seeded to subconfluency on 35mm glass cover slipped dishes and transfected with either pCS2-mCherry R18 or pCS2-mCherry R18M. Single plane confocal optical sections were taken in 15-minute intervals over 12 hours to image GFP and mCherry signal. Images are single plane confocal optical sections taken using a 63x objective (1.4 NA) with a 1.0 Tubelens. Scale bars are 20 μm. MDCK cells stably expressing GFP-XCK8 were produced and provided by R.S. Shah.

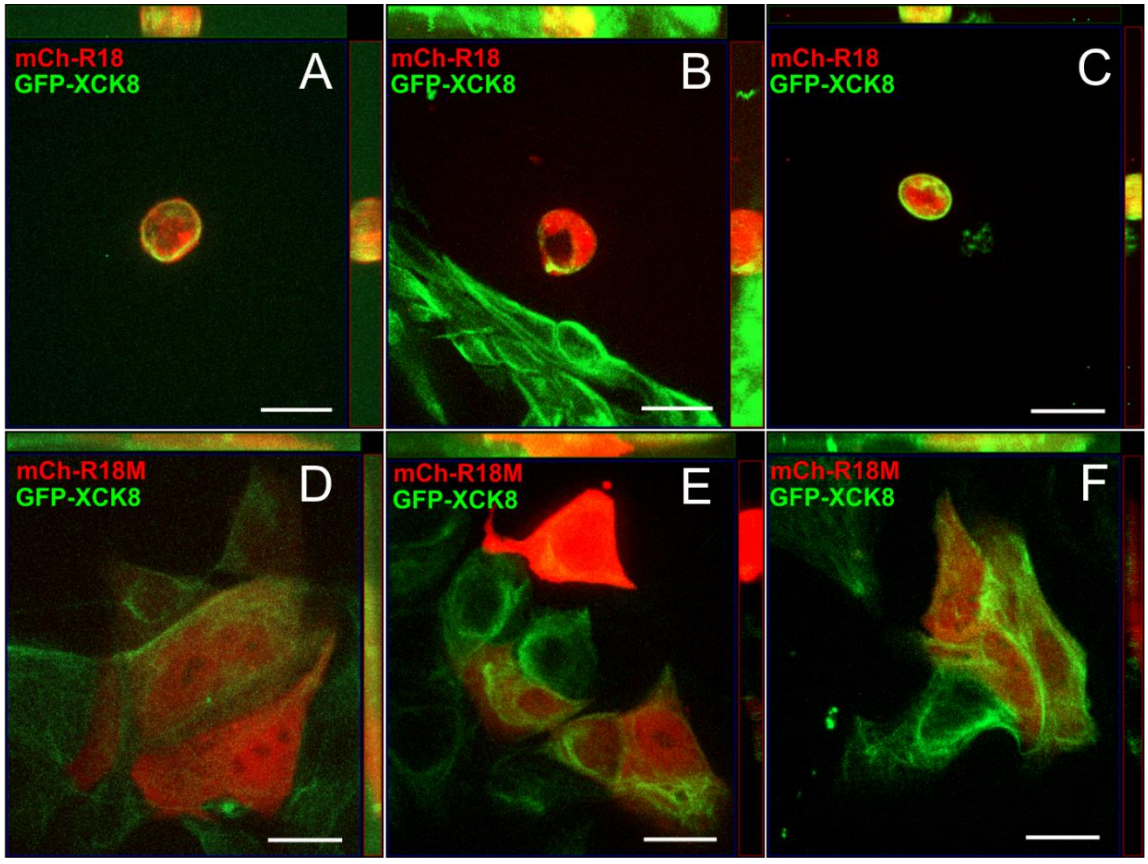
mCh-R18
GFP-XCK8
A
mCh-R18
GFP-XCK8
B
mCh-R18
GFP-XCK8
C
mCh-R18M
GFP-XCK8
D
mCh-R18M
GFP-XCK8
E
mCh-R18M
GFP-XCK8
F

Figure 19. Inhibition of 14-3-3 results in collapse of *Xenopus* keratin filament networks and abnormal MDCK cell morphology.

Z stacks (maximum intensity projection) of live cells acquired after 12-hour time lapse. **A-C**) GFP-XCK8 filaments in cells co-expressing mCherry-R18 after 12 hour time lapse. **D-F**) GFP-XCK8 networks co-expressed with mCherry-R18M after 12 hour time lapse. Orthogonal views for each Z-stack are included to provide cellular context. Images were taken using a 63x objective (1.4 NA) and 1.0 Tubelens. Scale bars are 20 μm. MDCK cells stably expressing GFP-XCK8 were produced and provided by R.S. Shah.

A

Kozak-GFP-R18/R18M-K19

ATMVSKGEELFTGVVPILVELDGDVNGHKFSVSGEGEGDATYGKLTLKFICTTGKLPVPWPTLVTTLTYGVQCFSRY
PDHMKQHDFFKSAMPEGYVQERTIFFKDDGNYKTRAEVKFEGDTLVNRIELKGIDFKEDGNILGHKLEYNYNSHNVY
IMADKQKNGIKVNFKIRHNIEDGSVQLADHYQQNTPIGDGPVLLPDNHYLSTQSALSKDPNEKRDHMVLLEFVTAAG
ITLGMDELYKSGLRSELDPHCVPRDLS[W/A]L[D/A]LEANMCLPSRAQASNSAVDPRVRNSKPDTATMTSYSIRQ
TSSSGSYRGLGAPVGVGRVSYKAPSVHGGYGGQGISVSSARLVSSGIGGGLGGGSYGGGSYGGGSYGSGFSSGFGSG
YGGGLSVNVSGDGLLSGNEKETMQNLNDRLASYLDKVRTLETANSGLELKIREWYEKQGPSPSSDYSNYFKIIEDLR
GKILDATVDNSKIVLQIDNARLAADDFRTKYENELALRQSVECDINGLRKVLDELTLCRTDLELQIESLKEELAYLK
KNHEEEMNAMRGQVGGQISVEVDAAPTVDITKRLTEMRDQYELLAEKNRRDAEEWFFAQSEEFLVASICLFPEECLG
LLNKEVATHTEQIQTSKSEITDLRRTIQGLEIELQSQLSMKAALENTLGETEARYGAQLSHIQNMISSLEAQLADLR
SDMERQNHEYKMLMDIKTRLEKEISTYRQLLEGHD*

B

Kozak-6HIS-TAT-3xFLAG-R18/R18M-K19

ATMHHHHHHTGGRKKRRQRRRPQEFMDYKDDDDKDYKDDDDKDYKDDDDKRSELDPHCVPRDLS[W/A]L[D/A]LE
ANMCLPSRAQASNSAVDPRVRNSKPDTATMTSYSIRQTSSSGSYRGLGAPVGVGRVSYKAPSVHGGYGGQGISVSSA
RLVSSGIGGGLGGGSYGGGSYGGGSYGSGFSSGFGSGYGGGLSVNVSGDGLLSGNEKETMQNLNDRLASYLDKVRTL
ETANSGLELKIREWYEKQGPSPSSDYSNYFKIIEDLRGKILDATVDNSKIVLQIDNARLAADDFRTKYENELALRQS
VECDINGLRKVLDELTLCRTDLELQIESLKEELAYLKKNHEEEMNAMRGQVGGQISVEVDAAPTVDITKRLTEMRDQ
YELLAEKNRRDAEEWFFAQSEEFLVASICLFPEECLGLLNKEVATHTEQIQTSKSEITDLRRTIQGLEIELQSQLSM
KAALENTLGETEARYGAQLSHIQNMISSLEAQLADLRSDMERQNHEYKMLMDIKTRLEKEISTYRQLLEGHD*

Figure 20. Design of R18-K19 and R18M-K19 fusion peptides.

A) Full sequence of GFP-R18-K19 and GFP-R18M-K19 fusion proteins including the GFP fluorophore, linker sequences, peptide sequence, K19 protein, and stop. The pre-methionine kozak site is included for positional demonstration. Sequence for GFP is highlighted in light green, the linker sequences are highlighted in gray, the R18/R18M peptide is highlighted in teal, and the K19 sequence is highlighted in dark green. The key amino acids for the R18 peptide are included in blue text and the key R18M amino acids are included in red text. **B**) Full sequence of 3xFLAG-R18-K19 and 3xFLAG-R18M-K19 fusion proteins. The additional epitopes including 6 histidine and the TAT motif are labeled in blue and bronze, respectively. The 3xFLAG sequence is highlighted in bright purple. Red highlight indicates residues encoded by nucleotides that function as key restriction sites. Additional highlights are as described in A.

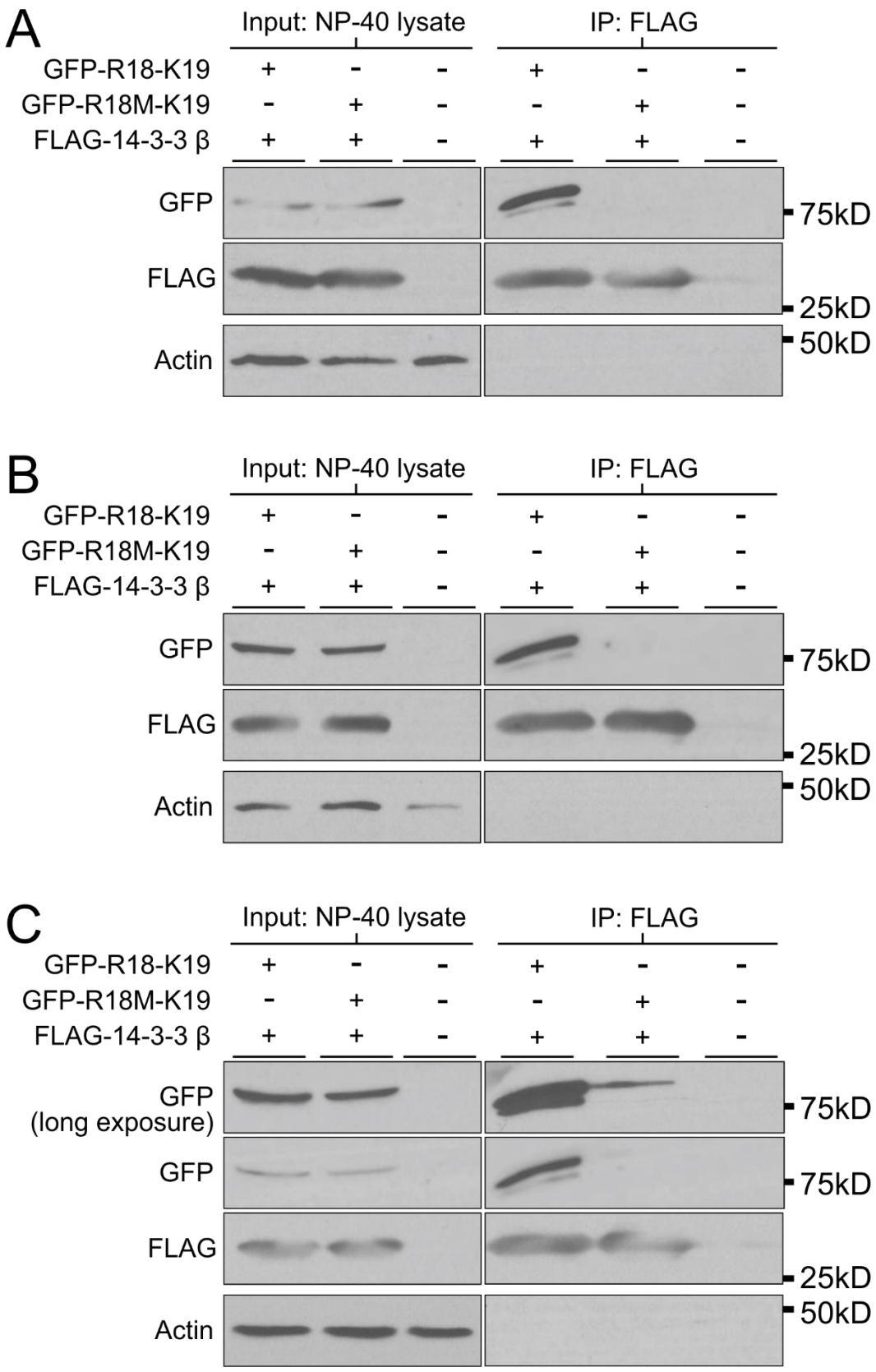
A
Input: NP-40 lysate
IP: FLAG
GFP-R18-K19 + - - + - -
GFP-R18M-K19 - + - - + -
FLAG-14-3-3 β + + - + + -
GFP
FLAG
Actin
75kD
25kD
50kD
B
Input: NP-40 lysate
IP: FLAG
GFP-R18-K19 + - - + - -
GFP-R18M-K19 - + - - + -
FLAG-14-3-3 β + + - + + -
GFP
FLAG
Actin
75kD
25kD
50kD
C
Input: NP-40 lysate
IP: FLAG
GFP-R18-K19 + - - + - -
GFP-R18M-K19 - + - - + -
FLAG-14-3-3 β + + - + + -
GFP
(long exposure)
GFP
FLAG
Actin
75kD
75kD
25kD
50kD

Figure 21. GFP-R18-K19 reliably and robustly binds 14-3-3 expressed in *Xenopus* embryos.

A-C) Immunoblots of FLAG-14-3-3 β immunoprecipitated embryonic lysates (1% Tergitol type NP-40) co-expressing GFP-R18-K19 or GFP-R18M-K19 fusion proteins. One-cell embryos were injected with RNA encoding GFP-R18-K19 or GFP-R18-K19 alongside RNA encoding FLAG-14-3-3 β. Lysates were prepared at embryonic stage 10.5 and immunoprecipitation for FLAG proteins was performed. FLAG immunoprecipitates were blotted for GFP, FLAG, and Actin. Non-injected lysate incubated with FLAG antibody conjugated agarose beads was immunoblotted as a negative control. High exposure in C is provided for relative comparison of R18-K19 and R18M-K19 binding of 14-3-3 proteins. Immunoprecipitation was performed using approximately 2000 µg of protein lysate. Input lanes include approximately 1 embryo worth of protein.

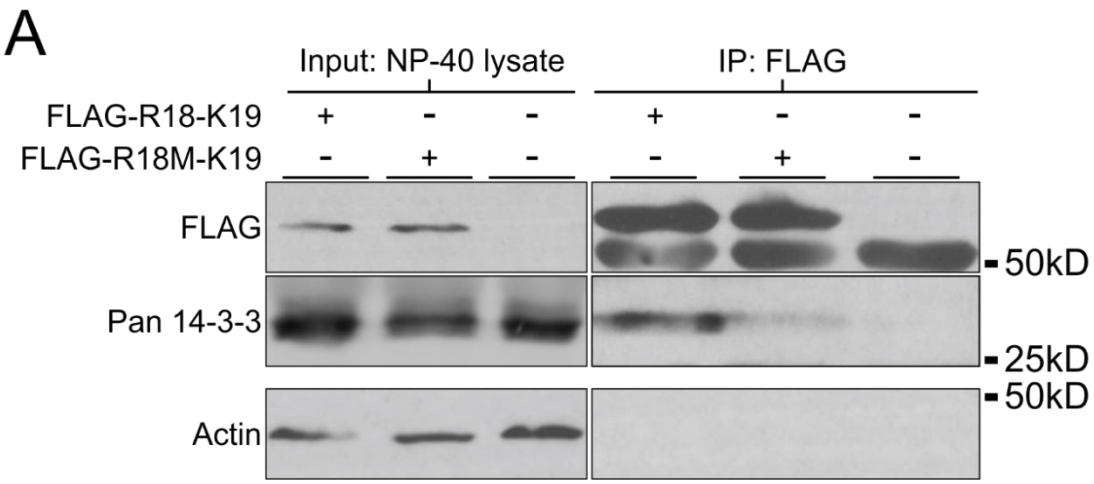
A
Input: NP-40 lysate
IP: FLAG
FLAG-R18-K19
+ - - + - -
FLAG-R18M-K19
- + - - + -
FLAG
Pan 14-3-3
Actin
50kD
25kD
50kD

Figure 22. R18-K19 binds endogenous *Xenopus* 14-3-3 proteins.

3xFLAG-R18-K19 and 3xFLAG-R18M-K19 immunoprecipitates blotted for interaction with 14-3-3 proteins in *Xenopus* embryos. **A**) Immunoblot of FLAG immunoprecipitated embryonic lysates (1% Tergitol type NP-40). One-cell embryos were injected with RNA encoding 3xFLAG-R18-K19 or 3xFLAG-R18M-K19. Lysates were prepared at embryonic stage 10.5 and immunoprecipitation for FLAG proteins was performed. FLAG immunoprecipitates were blotted utilizing GFP antibody and pan-14-3-3 antibody. Actin was also immunolabeled. Non-injected lysate incubated with FLAG antibody conjugated agarose beads was immunoblotted as a negative control. Immunoprecipitation was performed using approximately 2000 µg of protein lysate. Input lanes include approximately 1 embryo worth of protein.

.

CHAPTER 5

THE ROLE OF 14-3-3 IN TARGETING KERATIN 19 TO MECHANICALLY SENSITIVE CELL-CELL CONTACTS

Some information from this chapter is accepted for publication in Mariani *et al.* (2019) *MBoC.*

Owing largely to early descriptions as ‘cellular integrators’ (Lazarides 1980) and characterizations of the extreme mechanical fragility that arise from loss of epidermal keratins (Letai et al. 1993; Chan et al. 1994; Peters et al. 2001), intermediate filaments are broadly appreciated as cellular stabilizers. In contrast, the dynamic nature of IFs and the networks they comprise has only recently been explored and represents an area that requires much more study to uncover both the mechanisms and roles of IF activity (Windoffer et al. 2004; Kolsch et al. 2010; Schwarz et al. 2015). The inherent compromise cells must manage between withstanding strains and adapting to environmental change necessitates an IF network that must be amenable to modification, highlighting a critical role for regulatory mechanisms and molecules.

14-3-3 proteins have been shown to modulate the activity of multiple intermediate filaments in different cellular contexts. The interaction between IF proteins and 14-3-3 has been shown to affect the properties of filaments, such as dynamic exchange, as well as the localization and activity of 14-3-3 proteins themselves (Ku et al. 1998; Tzivion et al. 2000; Li et al. 2006; Miao et al. 2013; Toivola et al. 2001; Kim et al. 2006). While the known relationship between these molecules implies a potentially important role for 14-3-3 with regard to IF dynamics, little is known about how these proteins facilitate changes in IF networks. Cells that reorganize IF networks in response to stresses, especially those that re-localize networks as a result of force transduction, likely require molecular facilitators to enable such activity (Sivaramakrishnan et al. 2009; Weber et al. 2012). To determine whether 14-3-3 could influence reorganization of keratin networks in

mesendoderm, we investigated the role of these molecules in IF protein dynamics during collective cell migration and establishment of cell-cell adhesion.

Results

14-3-3 inhibition induces decreases in keratin dynamics in ex-vivo migratory tissues

The observation that 14-3-3 associates with keratins and co-localizes with filaments implies a shared functional relationship. Given that 14-3-3 proteins have been shown to have a role in disassembly of IFs (Li et al., 2006; Miao et al., 2013) and to associate with keratin filaments induced to remodel by okadaic acid treatment (Strnad et al., 2002), one possible function of this association is to facilitate modification of pre-existing filament networks. Modification of polymerized filaments involves addition or subtraction of IF proteins along the length of a filament polymer, known as lateral exchange or dynamic exchange (Vikstrom et al., 1992; Colakoğlu and Brown, 2009; Nöding et al., 2014). Keratin networks show filament remodeling and 14-3-3 dependent increases in dynamic exchange rate after exposure to shear stress (Sivaramakrishnan et al., 2009). Since changes in mechanical stress are continually transduced across junctions during collective cell migration and result in keratin reorganization (Weber et al., 2012), we examined whether 14-3-3 might have a role in the keratin filament organization in mesendoderm explants. To functionally inhibit 14-3-3, we expressed a short peptide sequence (R18) previously shown to bind 14-3-3 with high affinity and block its binding to endogenous substrates (Petosa et al., 1998; Wang et al., 1999). A negative control peptide (R18M) containing two point

mutations was used for comparison. We created mCherry-tagged R18 and R18M constructs so that we could readily identify living cells in which R18 or R18M was expressed (Described in Chapter 4). No change in overall protein expression of C-cadherin, acidic keratins, 14-3-3, or actin resulted from R18 expression (Figure 23). The ability of mCherry-R18, but not mCherry-R18M, to bind 14-3-3 was confirmed by co-immunoprecipitation analyses (Figure 24). As mCherry-R18 bound to 14-3-3, a corresponding decrease in the association of 14-3-3 with K19 was observed (Figure 24). Thus, R18 functions as a competitive inhibitor of 14-3-3 association with K19.

To examine the role of 14-3-3, we co-expressed mCherry-R18 or R18M with eGFP-K19. R18 expression did not initially result in any apparent changes to the keratin network detectable by fluorescent microscopy. Through early gastrulation and explant preparation, no gross morphological changes were observed in the overall keratin network or subcellular localization of filaments. We suspect that this may be because of a delayed onset of R18 expression until after mid-blastula transition. Nonetheless, subtler effects on the intermediate filament dynamics were observed in native mesendoderm explants. FRAP experiments of eGFP-K19 revealed that 14-3-3 inhibition results in attenuation of dynamic exchange rate when compared to that of explants expressing control peptide R18M (Figure 25). Despite inherent differences in the width and subcellular location of filaments bleached across trials, the lower recovery rate in 14-3-3 inhibited samples persisted (Figure 25 C and D). Though additional reports provide evidence of different times of lateral exchange onset that range from within an hour to eight

hours (Colakoğlu and Brown, 2009; Nöding et al., 2014), we detect more rapid differences in recovery after 14-3-3 inhibition that occurs within minutes (Figure 25). This finding demonstrates that the interaction between 14-3-3 and Keratin 19 is required for modification of filaments that occurs on an appreciably fine timescale in motile tissues.

14-3-3 is required for targeting of keratin to cell-cell adhesions

Force transmitted through mesendoderm cell-cell contacts induces both changes in the keratin network throughout the cell and recruits filaments to sites of transduced tension (Weber et al., 2012). We were surprised to find that expression of R18 did not dramatically alter the distribution of keratin intermediate filaments in the mesendoderm given its association with keratin and role in dynamic exchange. We reasoned that this could be because expression of R18 did not occur until after relatively stable cell-cell adhesions were formed. To determine whether 14-3-3 is required for localization of filaments to cell junctions, both DMZ explants and mesendoderm expressing mCherry-R18 or R18M and eGFP-K19 were dissociated into single cells via calcium switch (Ca^{2+} and Mg^{2+} for mesendoderm only) and imaged as cells collided and formed cell pairs. Mesendoderm cells co-expressing mCherry-R18M and GFP-K19 demonstrated localization of keratin filaments to the adhesion between the cell pair over the course of the time lapse (Figure 26 J-L). The GFP-K19 reorganization became more marked as the cells continued to protrude away from one another (Figure 26 L, white arrowhead). In contrast, 14-3-3 inhibition due to expression of mCherry-R18 perturbs reorganization of keratin filaments to the cell-cell adhesion between

cell pairs, resulting in failure of keratin localization to this compartment (Figure 26 A-I). This failure of keratin localization to the junctional compartment persists despite evidence of cells protruding away from one another and an extended time of contact relative to the time sufficient to junctionally localize keratins in mCherry-R18M post collision mesendoderm (Figure 26 A-F, white arrows in G-I).

Our work and others' have shown that many migratory cells polarize in opposite directions upon collision, resulting in substantial force at the cell-cell junction (Nelson and Chen, 2003; Maruthamuthu et al., 2011; Weber et al., 2012; Mertz et al., 2013). We additionally showed that keratin intermediate filaments are recruited to cell-cell adhesions between mesendoderm cells as a function of force on C-cadherin (Weber et al., 2012). This is also the case in mesendoderm cells expressing the control construct mCherry-R18M (Figure 27 A-C). When 14-3-3 was inhibited by expression of mCherry-R18, a distinct zone lacking fluorescent K19 filaments was observed at points of *de novo* cell-cell adhesion (Figure 27 D-F). This K19-deplete zone was observed at a significantly higher frequency in 14-3-3 inhibited cells after establishment of cell-cell contact relative to controls (Figure 27). These regions lacking K19 IFs had a size range of 2 μm to 17 μm with an average of 7 μm when measured from the cell-cell contact to the onset of visible filament fluorescence. The zone was surprisingly uniform along the width of the cell-cell contact in these cells and very few R18-positive cells were found to have K19 targeted to cell-cell contacts (Figure 27 G).

14-3-3 proteins are distributed proximal to cell-cell adhesions.

C-cadherin co-localizes with keratin filaments at points of cell-cell contact in mesendoderm and co-immunoprecipitates with keratin in lysates from *Xenopus* gastrula (Weber et al., 2012). Given that co-immunoprecipitation of 14-3-3 also shows association with C-cadherin, we examined how the subcellular localization of each relate to one another. Curiously, although 14-3-3 appears at the cell periphery at low magnification and resolution (Shown in Chapter 4), an appreciable separation between 14-3-3 and C-cadherin is observed at higher resolution (Figure 28). 14-3-3 is increasingly concentrated nearer to cell-cell contacts (Figure 29 C) as compared to more centrally located regions of the cytoplasm. However, at the more precise point of cell-cell contact, indicated by C-cadherin-eGFP labeling, we noted a decrease in 14-3-3 signal intensity (Figure 29 D). Average mean fluorescence intensities for C-cadherin were high in adhesion ROIs, but this did not correspond with high 14-3-3 intensities (Figure 29 E). In contrast, K19 colocalized with C-cadherin at the cell-cell contact (Figure 30 F-G) and coordinately increased in intensity at the cell-cell contact (Figure 30 H-I). Adhesion ROIs analyzed in the junctional plane exhibited high fluorescence intensity of both C-cadherin and K19 (Figure 30 J). This positioning of K19 mirrors the colocalization previously observed between C-cadherin, plakoglobin, and K8 in these cells (Weber et al., 2012). Taken together with evidence of biochemical association, these data suggest that the association between 14-3-3 and C-cadherin is likely indirect. 14-3-3 appears to localize with keratin intermediate

filaments and concentrate near cell-cell contacts, but not exactly at the cell-cell contact itself.

14-3-3 association with K19 is sufficient for cell-cell adhesion targeting.

Since inhibition of 14-3-3 prevented keratin localization to cell-cell contacts, we wanted to see whether forced association of K19 with 14-3-3 would be sufficient to drive targeting to cell junctions. 14-3-3 endogenously binds to phosphorylated serine and threonine residues contained in motifs within certain substrates (Yaffe et al., 1997; Johnson et al., 2010). Mutation of serine residues to non-phosphorylatable alanines (e.g. S33A of hK18) eliminates binding between keratins and 14-3-3; however, mutation of serine to phosphomimetic amino acids (e.g. S33D of hK18) is similarly dysfunctional at promoting association between 14-3-3 and keratins, presumably because of differences in the side chain compared to phosphate groups (Ku et al., 1998). In order to promote the association of K19 with 14-3-3, we created an eGFP-R18-K19 fusion protein (Shown in Chapter 4; Figure 31 A). Immunoprecipitation analyses showed robust association of R18-K19 fusion proteins with FLAG-14-3-3 (Figure 31 B). Note that FLAG-14-3-3 also associated with eGFP-R18M-K19 (Figure 31 B), albeit at a much reduced level, likely via the normal intrinsic phosphorylation sites within K19. Since R18 is a high affinity peptide for 14-3-3, this fusion protein results in a traceable K19 protein with a constitutive signaling site for 14-3-3 binding that is phosphorylation-independent.

Mosaic expression of these fusion constructs was established in mesendoderm tissue by injecting DNA, and the intermediate filament distribution

in live mesendoderm cells, ~4 rows back from the leading edge, was examined by confocal microscopy. Expressed eGFP-R18M-K19 in mesendoderm explants forms filaments spread throughout the cell body but absent from cell protrusions (Figure 32 A-C and G-I), typical of keratin networks described previously in unpolarized mesendoderm (Weber et al., 2012). In mesendoderm expressing eGFP-R18-K19, the fluorescence appeared as densities that preferentially localize to areas of cell-cell adhesion and lack widespread expression throughout the cytosol (Figure 32 D-F and J-L). In the most robust instances, eGFP-R18-K19 localized as an intense aggregate exclusively at the cell-cell boundary (Figure 32 F, red arrowhead). In other cases, distinct filaments could be seen and the population was limited to near the cell-cell adhesion (Figure 32 L, white arrowhead). The forced association of K19 with 14-3-3 through this fusion construct created a distribution that in many ways was the exact opposite of when 14-3-3 was inhibited (compare Figure 32 F with Figure 27 D).

14-3-3 does not induce K19-Cadherin coupling or junctional targeting of Plakoglobin in Xenopus mesendoderm.

Our findings have demonstrated that 14-3-3 specifically binds to K19 and also associates with C-cadherin, the classical cadherin that mediates cell-cell adhesion in mesendoderm. In addition, inhibition of 14-3-3 resulted in abnormal filament dynamics and failures of keratin localization to newly formed cell-cell junctions. Given that the R18-K19 fusion preferentially localizes to cell junctions, we investigated the role of 14-3-3 proteins in linking K19 to C-cadherin adhesions. To examine the extent to which filament compartmentalization of R18-K19 was

related to association with adhesion molecules, C-cadherin GFP association with 3xFLAG-R18-K19 was compared to that of 3xFLAG-R18M-K19 (Figure 33). Interestingly, the association of R18-K19 with C-cadherin GFP appeared to be roughly equivalent to that of R18M-K19. These data indicate that K19 association with 14-3-3 is important for targeting K19 populations to the cell-cell junctional region, but does not induce extended coupling of K19 with cadherins themselves.

A previous study published by our group has shown that plakoglobin, a molecule that binds to the c-terminal of cadherins, is part of the cadherin-keratin complex in mesendoderm (Weber et al. 2012). It has also been observed that 14-3-3 knockdown results in failures of plakoglobin to localize to cell-cell contacts and deficient cell-cell junction formation (Sehgal et al. 2014; Vishal et al. 2018). Because plakoglobin could potentially influence the association of K19 with the cell-cell adhesion, we sought to determine the affect of 14-3-3 inhibition on junctional recruit of plakoglobin. Dissociation of mesendoderm and subsequent cell collision demonstrated that mesendoderm cells expressing mCherry-R18 localize GFP-PG to adhesions in a comparable manner to that of mCherry-R18M expressing cells (Figure 34). The adhesions formed between GFP-PG/mCherry-R18 expressing cells and GFP-PG/mCherry-R18M expressing cells protruding away from one another also appear comparable (Figure 35, white arrowhead). Taken together, while 14-3-3 proteins are necessary and sufficient for targeting of K19 to the junctional compartment, these molecules do not appear to directly promote keratin linkage to cadherin or augment the junctional targeting of adhesion plaque protein plakoglobin in mesendoderm.

Discussion

The finding that mCherry-R18 mediated inhibition of 14-3-3 did not result in obvious mesendoderm keratin network abnormalities compared to that of subconfluent MDCK cells (shown in Chapter 4) was unexpected but not unprecedented. Similarly, charge mutation of serine 33 in Keratin 18 to prevent binding of 14-3-3 proteins resulted in peri-nuclear collapse in NIH 3T3 fibroblasts, but not in mouse liver hepatocytes that express K8/K18 networks (Ku et al. 1998; Ku et al. 2002). In both cases, the differences between the cultured cells and those of the embryo are potentially marked enough to invoke different mechanisms of filament regulation as well as 14-3-3 expression or activity. Our data demonstrate that 14-3-3 inhibition disrupts interactions between K19 and 14-3-3 that are normally present in uninhibited cells and that such changes are not the result of alterations in protein expression. Moreover, mCherry-R18 inhibition of 14-3-3 in the mesendoderm of migrating DMZ explants results in a decrease in dynamic exchange within filaments, providing evidence of a role for 14-3-3 in mediating this activity. These findings suggest that 14-3-3 proteins in mesendoderm are involved in modulating the dynamic properties of the filament network rather than broadly ensuring its stability.

Given that the endogenous keratin network is able to form in the absence of 14-3-3 inhibition prior to the blastula stage in mCherry-R18 microinjected embryos, it is possible that stable cell-cell adhesion allows the formation of GFP-K19 incorporating or containing networks despite onset of mCherry-R18 expression. We demonstrate that employing calcium switch to dissociate 14-3-3

inhibited mesendoderm and subsequently allow for cellular collision and *de novo* adhesion formation results in failed localization of GFP-K19 to the junction. This failure is stark in contrast to the rapid junctional filament localization that is observed in mCherry-R18M expressing cells. Remarkably, the loss of ability to junctionally localize K19 in mCherry-R18 expressing mesendoderm persists over the course of cell-cell contact despite obvious opposing protrusion and pulling activity of the cells within the pairs.

We observe increases in the signal of immunolabeled 14-3-3 close to the junctions of mesendoderm, implying a role for 14-3-3 within this compartment. It is interesting that the 14-3-3 signal appears to peak just before the onset of C-cadherin-GFP fluorescence at high magnification (63x with 1.6 Tubelens) and that no apparent co-localization between these two molecules is detected. In contrast, a subset of the keratin network co-localizes with C-cadherin proteins at the cell-cell junction, with the fluorescent signal of both of these molecules concomitantly increasing at the adhesion site in the junctional plane. Presumably, this keratin portion is connected to the wider network that characterizes the basal plane. Evidence that 14-3-3 proteins convincingly label keratin populations at the junctions of mesendoderm and that these proteins immunoprecipitate with cadherins suggests that the 14-3-3 and cadherin relationship is mediated by indirect association.

Fusion of the R18 sequence to full length K19 (GFP-R18-K19) to include a high affinity phosphorylation independent 14-3-3 binding site resulted in dramatic localization of keratin densities to the cellular periphery. This inclusion of the R18

sequence, which increased binding of exogenous and endogenous 14-3-3 proteins, induced a rearrangement of keratin that was the inverse of that observed during inhibition and disruption of the K19 and 14-3-3 interaction via mCherry-R18. Expression of mem-RFP to demonstrate the broad morphology of explanted mesendoderm showed that GFP-R18-K19 densities preferentially localize at the contacts opposite to cellular protrusions, reminiscent of junctional recruit of keratin networks induced by mechanical force (Weber et al. 2012).

Because the rapid reorganization of keratin filaments to cell-cell adhesions transducing stress is characteristic of mesendoderm keratin network dynamics, we were surprised that FLAG-R18-K19 did not result in increased biochemical interaction with C-cadherin-GFP. Previous evidence has demonstrated that cell-cell adhesion plakoglobin is associated with keratin and C-cadherin in mesendoderm. In addition, 14-3-3 proteins have been shown to be required for transport of plakoglobin to desmosomal cell-cell adhesions in epithelial cell lines (Sehgal et al. 2014; Vishal et al. 2018). Plakoglobin localizes to cell-cell adhesions of mesendoderm pairs after calcium switch equally well in mCherry-R18 and mCherry-R18M expressing cells. This evidence supports a role for 14-3-3 in increasing solubility of K19 proteins and targeting these keratins to the mesendoderm junctional compartment through direct interaction with these proteins and independent of direct linkage to molecules of the cell-cell adhesion.

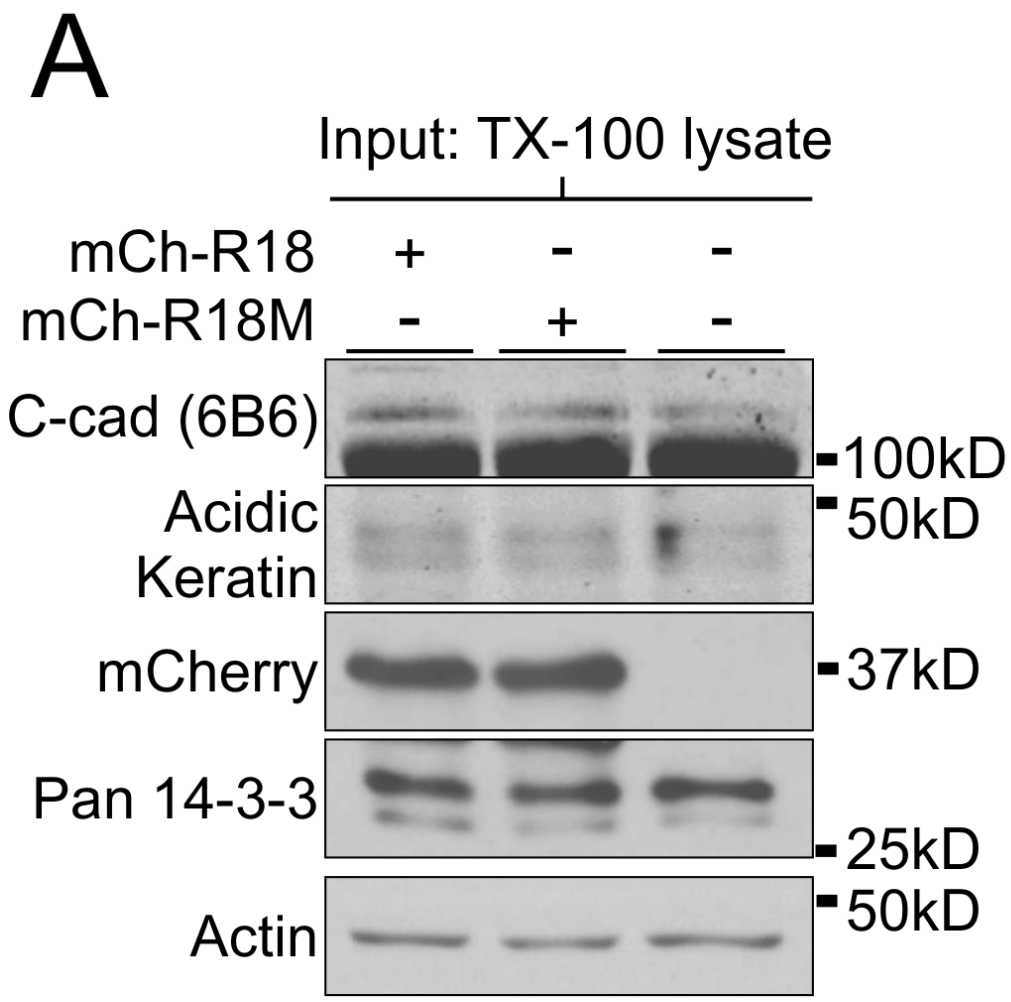
A
Input: TX-100 lysate
mCh-R18
mCh-R18M
+
-
-
-
+
-
C-cad (6B6)
Acidic Keratin
mCherry
Pan 14-3-3
Actin
100kD
50kD
37kD
25kD
50kD

Figure 23. R18 and R18M peptides do not alter expression of molecules of the *Xenopus* mechanically sensitive cell-cell junction.

A) Immunoblot analyses of protein extracts (1% Triton X-100) of stage 10.5 *Xenopus* embryos expressing mCh-R18 or mCh-R18M. One-cell embryos were injected with RNA encoding either mCherry-R18 or mCherry-R18M. Whole embryo lysates were blotted for C-cadherin (6B6 ab), pan-acidic keratin (AE1 ab), multiple 14-3-3 isoforms (pan 14-3-3 ab), mCherry, and actin. Non-injected whole embryo lysate was immunoblotted as a control comparison for expression of mCherry-R18 and mCherry-R18M. Lanes include approximately 1 embryo worth of protein.

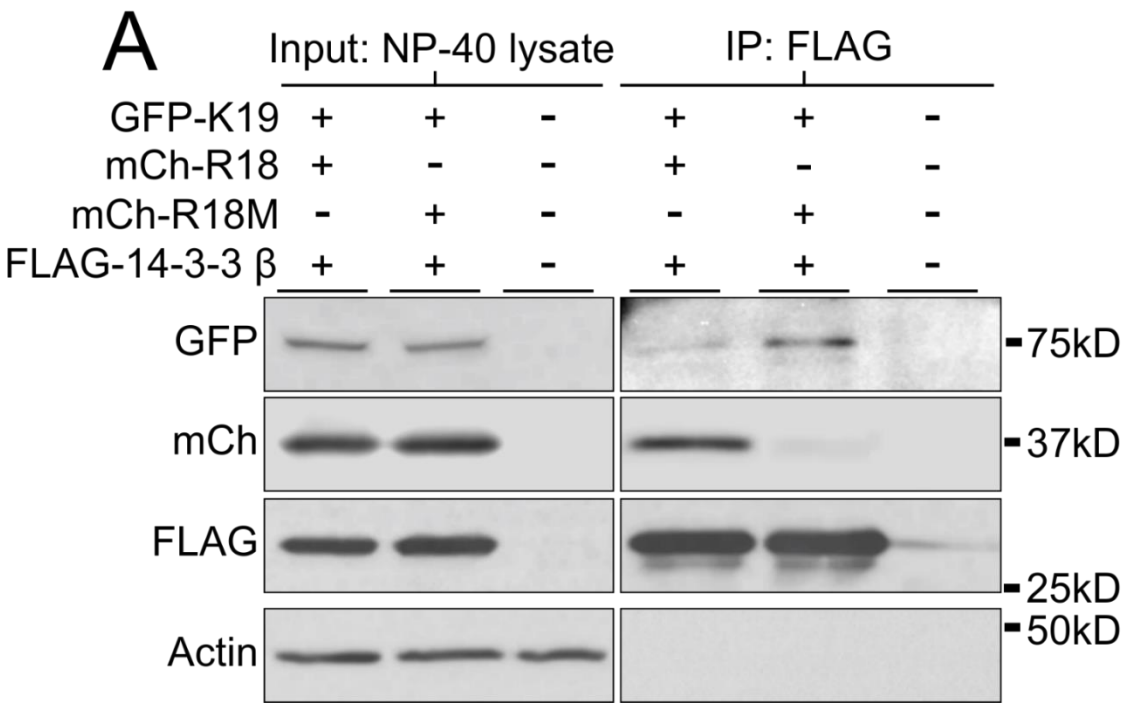
A
Input: NP-40 lysate
IP: FLAG
GFP-K19 + + - + + -
mCh-R18 + - - + - -
mCh-R18M - + - - + -
FLAG-14-3-3 β + + - + + -
GFP
mCh
FLAG
Actin
75kD
37kD
25kD
50kD

Figure 24. 14-3-3 inhibition disrupts binding of K19 to 14-3-3 proteins.

A) Immunoblot of FLAG-14-3-3 β immunoprecipitated embryonic lysates (1% Tergitol type NP-40) co-expressing GFP-K19 and either mCherry R18 or mCherry R18M peptide. One-cell embryos were injected with RNA encoding mCherry-R18 or mCherry-R18M alongside RNA encoding FLAG-14-3-3 β and GFP-K19. Lysates were prepared at embryonic stage 10.5 and immunoprecipitation for FLAG proteins was performed. FLAG immunoprecipitates were blotted for FLAG, mCherry, GFP, and actin. Non-injected lysate incubated with FLAG antibody conjugated agarose beads was immunoblotted as a negative control. Immunoprecipitation was performed using approximately 2000 µg of protein lysate. Input lanes include approximately 1 embryo worth of protein.

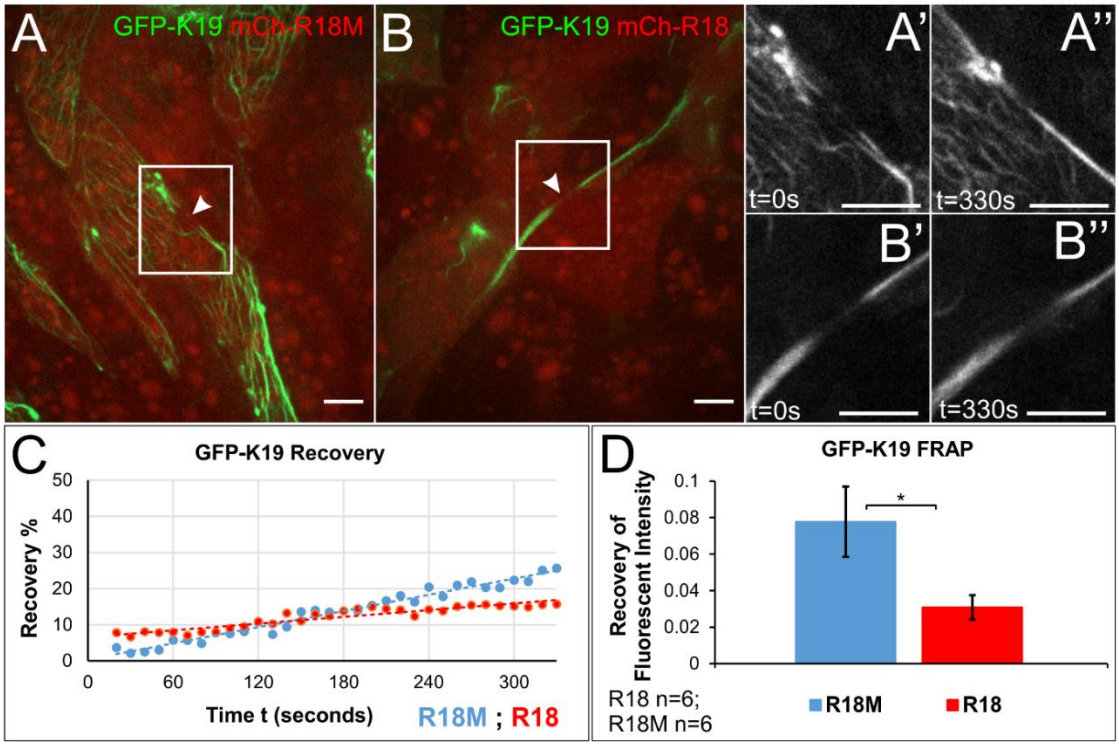
A
GFP-K19 mCh-R18M
B
GFP-K19 mCh-R18
A'
A''
t=0s
t=330s
B'
B''
t=0s
t=330s
C
GFP-K19 Recovery
Recovery %
50
40
30
20
10
0
0
60
120
180
240
300
Time t (seconds)
R18M ; R18
D
GFP-K19 FRAP
Recovery of Fluorescent Intensity
0.1
0.08
0.06
0.04
0.02
0
*
R18 n=6;
R18M n=6
R18M
R18

Figure 25. Mesendoderm keratin filament dynamic exchange is decreased by 14-3-3 inhibition.

A-B) Still images from photobleach and recovery time lapse movies. Mesendoderm explants expressing either 14-3-3 inhibitor peptide mCherry-R18 or control peptide mCherry-R18M (red) with eGFP-K19 (green) were exposed to GFP photobleaching and fluorescent recovery at the site was measured. **A'-B''**) Enlarged view of the region of filament bleaching (white boxes) during recovery measurements. The time annotations in seconds refer to start of capture (t=0s) and end of capture (t=330s). **C**) Representative analysis plotting fluorescent recovery against time of image capture. **D**) Comparison of mean eGFP-K19 recovery rate in explants expressing either mCherry-R18 or mCherry-R18M. Analysis was performed using a one tailed t-test, * = $p<0.05$. Error Bars are ± SEM. Photobleaching and imaging was performed using a 63x objective (1.4 NA) and 1.0 Tubelens. Scale bars are 10 μm.

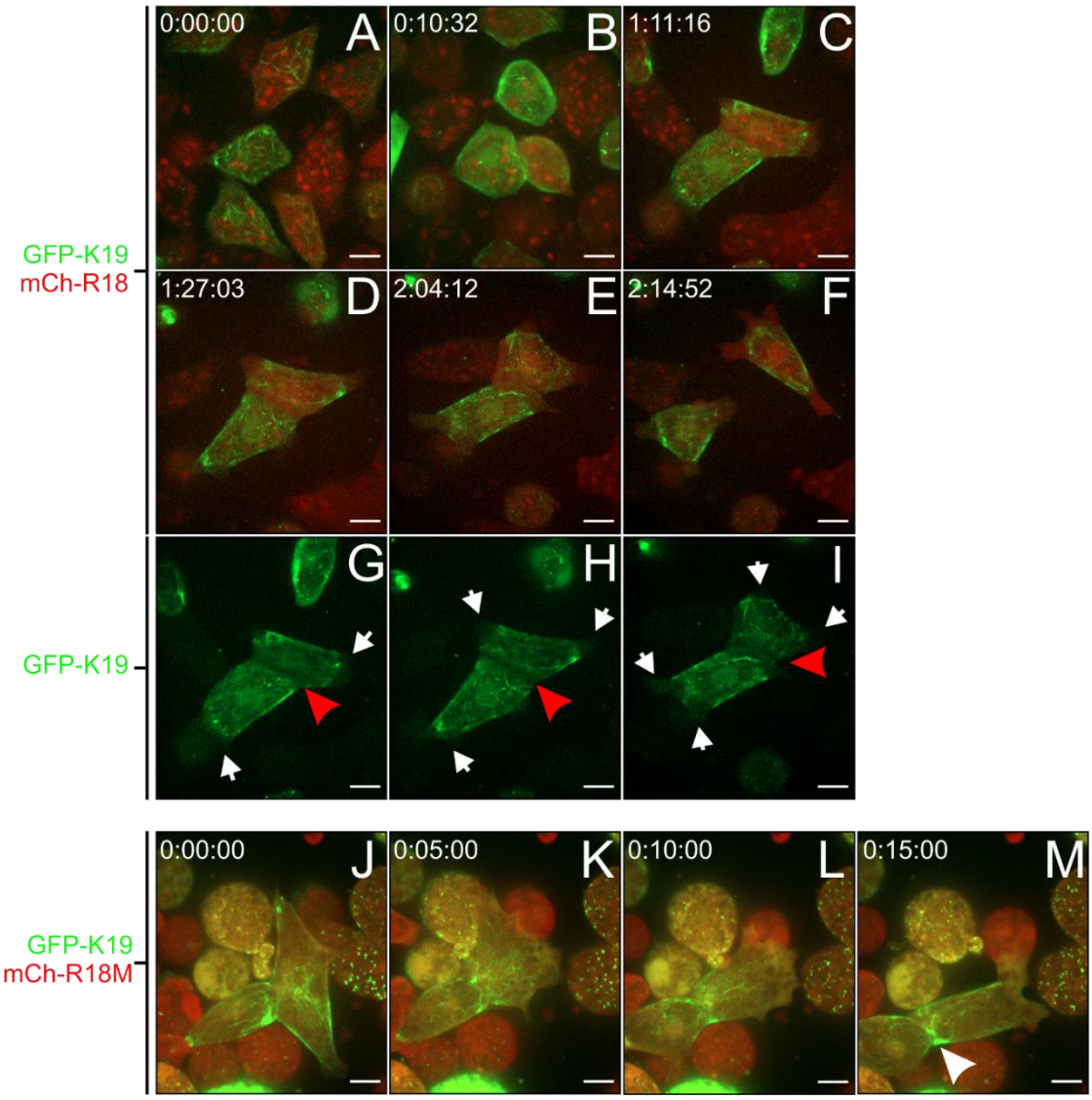
GFP-K19
mCh-R18
0:00:00
A
0:10:32
B
1:11:16
C
1:27:03
D
2:04:12
E
2:14:52
F
GFP-K19
G
H
I
GFP-K19
mCh-R18M
0:00:00
J
0:05:00
K
0:10:00
L
0:15:00
M

Figure 26. Inhibition of 14-3-3 perturbs keratin recruit during formation of *de novo* cell-cell adhesions.

Migratory DMZ explants expressing GFP-K19 and either mCherry-R18 or mCherry-R18M were dissociated by introduction of Ca^{2+} deplete media to allow cadherins to disengage. After an hour, media with Ca^{2+} was reintroduced and mesendoderm cells were imaged after collision. **A-F**) Mesendoderm expressing GFP-K19 and mCherry-R18 was imaged from dissociation (A) to cell-cell contact (B) and through adhesion formation (C-E). **G-I**) GFP channel only perspective of images in C-E. Red arrowheads indicate the presence of a keratin lacking gap. White arrows highlight protrusions formed in the cells of the opposing pair. **J-M**) Mesendoderm expressing GFP-K19 and mCherry-R18M after dissociation and cell-cell contact establishment. The white arrowhead in M highlights localization of GFP-K19 at the cell-cell interface. Images were taken using a 40x objective (1.3 NA) with a 1.0 Tubelens and are z-stacks (maximum intensity projection). Scale bars are 20 μm.

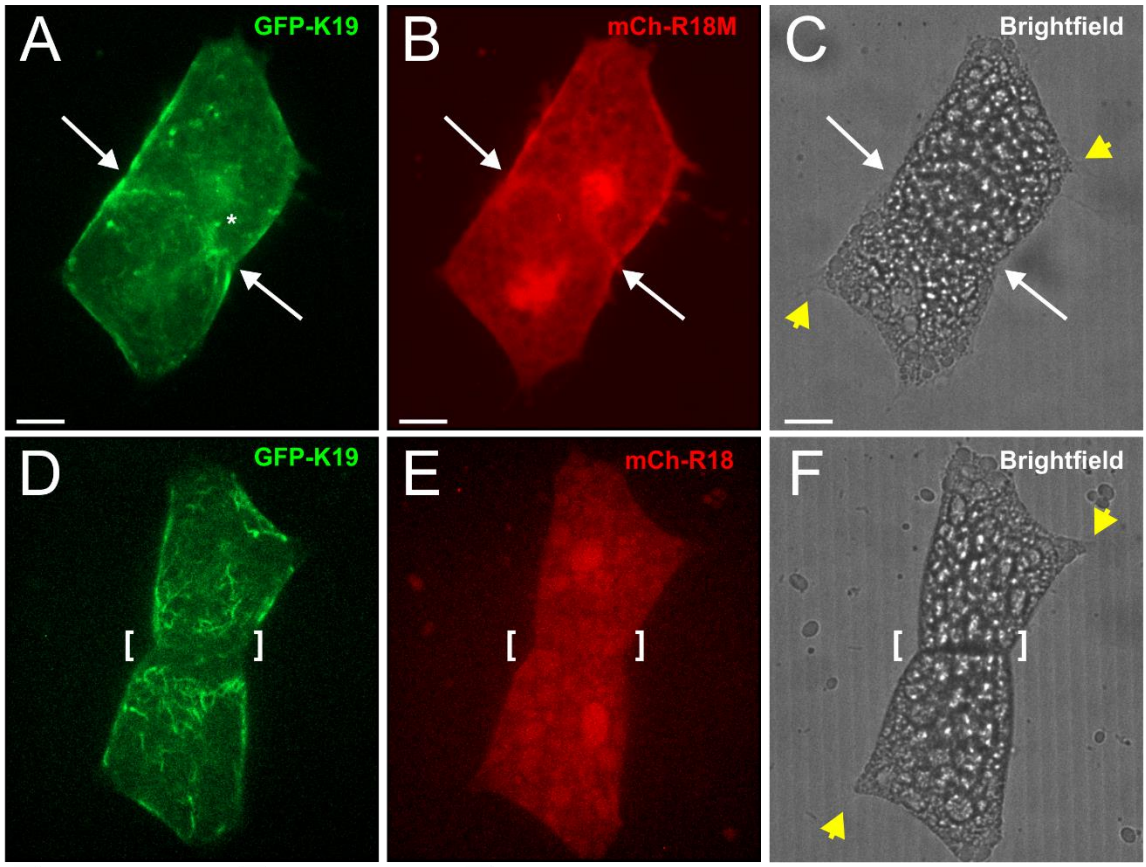
A
GFP-K19
B
mCh-R18M
C
Brightfield
D
GFP-K19
E
mCh-R18
F
Brightfield

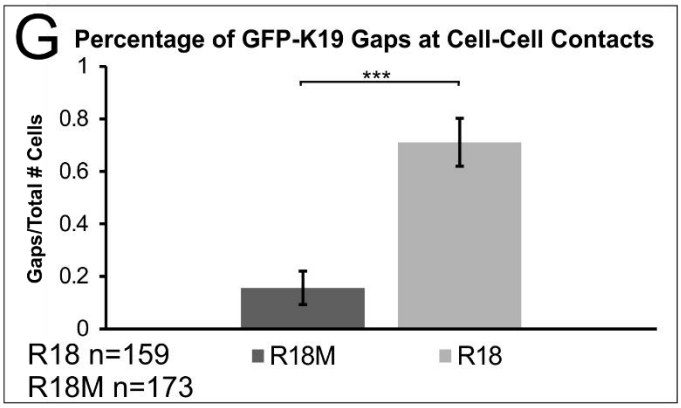
G
Percentage of GFP-K19 Gaps at Cell-Cell Contacts
Gaps/Total # Cells
1
0.8
0.6
0.4
0.2
0
***
R18 n=159
R18M n=173
R18M
R18

Figure 27. 14-3-3 is necessary for targeting of keratin to cell-cell contacts.

A-C) Mesendoderm cell pair establishing *de novo* cell-cell contact after collision. Cells are expressing mCherry-R18M and eGFP-K19. The white arrows depict the cell-cell adhesion where keratin densities (asterisk) have localized. The yellow arrows highlight apparent protrusions. Image stack is 35 slices (10.54 μm). **D-F**) Post collision mesendoderm cell pair expressing mCherry-R18 and eGFP-K19. The bracket depicts the cell-cell adhesion that demonstrates a gap where keratin filaments have failed to reorganize. The yellow arrows mark apparent protrusions. Image stack is 40 slices (10.92 μm). **G**) Comparison of the number of keratin gaps at cell-cell adhesions in post collision pairs expressing either mCherry-R18M or mCherry-R18. Analysis was performed using a z-test for proportions from two samples, *** = $p<0.001$. Error bars represent the 99.9% CI for each sample proportion. Fluorescent images are z-stacks (maximum intensity projection). Brightfield images are single planes. Images were taken using a 40x objective (1.3 NA) and 1.0 Tubelens. Scale bars are 20 μm.

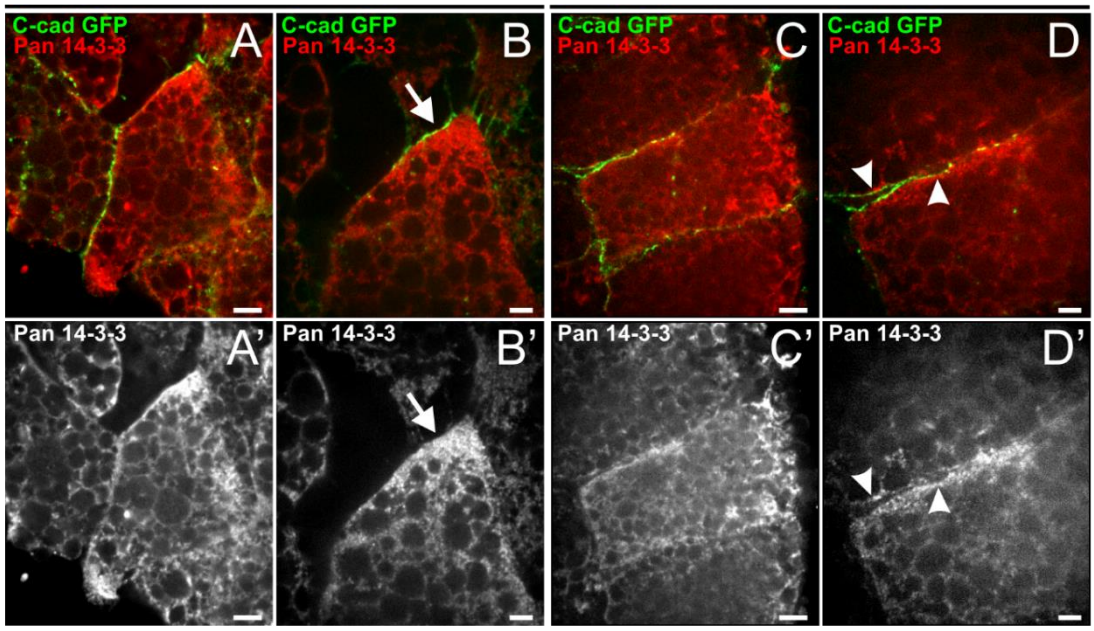
C-cad GFP
Pan 14-3-3
A
C-cad GFP
Pan 14-3-3
B
C-cad GFP
Pan 14-3-3
C
C-cad GFP
Pan 14-3-3
D
Pan 14-3-3
A'
Pan 14-3-3
B'
Pan 14-3-3
C'
Pan 14-3-3
D'

Figure 28. 14-3-3 proteins are distributed proximally to cell-cell adhesions.

DMZ explants expressing C-cadherin-GFP were fixed in 100% methanol and immunolabeled for GFP and multiple 14-3-3 proteins. **A-B'**) Immunofluorescent image of a leading edge mesendoderm cell labeled for 14-3-3 and expressing C-cadherin (GFP label). Increased magnification was utilized to capture the rear contact of the cell (arrow, **B** and **B'**). The direction of migration in A-B' is down. **C-D'**) Image of a leading edge mesendoderm cell highlighting a rear-lateral contact (arrowheads), with D and D' at higher magnification. The direction of migration in C-D' is right. Images were taken using a 63x objective (1.4 NA) with a 1.0 Tubelens (A,A',C,C') and a 1.6 Tubelens (B,B',D,D'). Scale bars are 10 μm (A,A',C,C') and 5 μm (B,B',D,D').

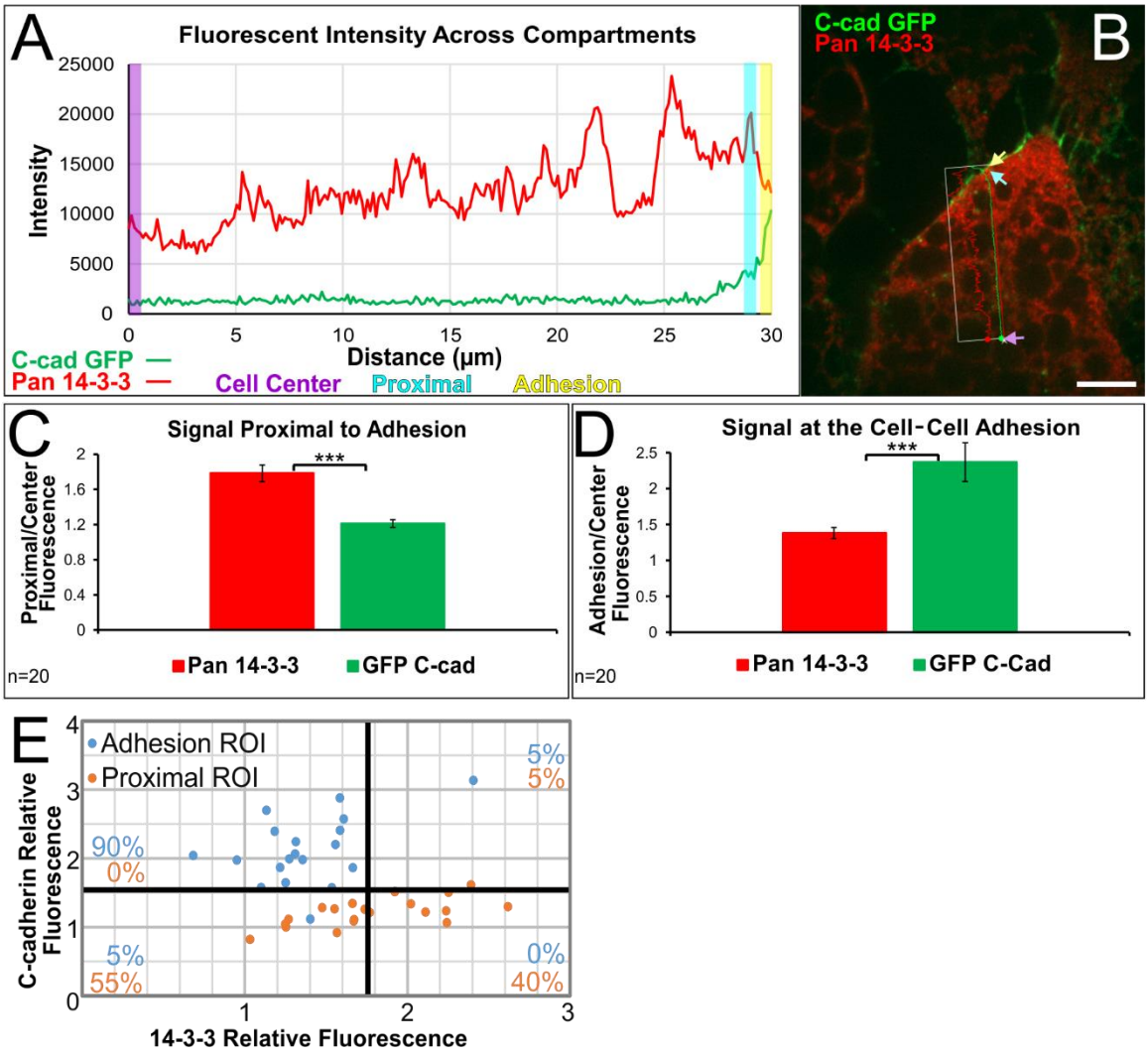
A
Fluorescent Intensity Across Compartments
Intensity
25000
20000
15000
10000
5000
0
0
5
10
15
20
25
30
Distance (µm)
C-cad GFP
Pan 14-3-3
Cell Center
Proximal
Adhesion
B
C-cad GFP
Pan 14-3-3
C
Signal Proximal to Adhesion
Proximal/Center Fluorescence
***
n=20
Pan 14-3-3
GFP C-cad
D
Signal at the Cell-Cell Adhesion
Adhesion/Center Fluorescence
***
n=20
Pan 14-3-3
GFP C-Cad
E
Adhesion ROI
Proximal ROI
90%
0%
5%
55%
5%
5%
0%
40%
C-cadherin Relative Fluorescence
14-3-3 Relative Fluorescence

Figure 29. 14-3-3 proteins increase in localization close to but not at cadherin mediated cell-cell adhesions.

A) Representative linescan analysis of fluorescence across cellular compartments indicated in panel B. Lines extended from the approximate middle of the cell to the area just prior to C-cadherin signal and to the onset of C-cadherin signal. Measurements were taken from the cell center (purple rectangle), proximal to the adhesion (teal rectangle), and at the adhesion (yellow rectangle). Each rectangle represents 0.5 μm in length. **B**) Immunofluorescent image of a leading edge mesendoderm cell labeled for 14-3-3 and expressing C-cadherin (eGFP label). Colored arrows indicate regions represented by rectangles in A. **C and D**) Comparison of the mean increase in 14-3-3 signal and C-cadherin signal from the cell center to the area proximal to the cell-cell adhesion (in panel C) and at the cell-cell adhesion (in panel D). Analysis was performed using paired sample t-tests, *** = $p<0.001$. Error Bars are ± SEM. **E**) Scatterplot of the mean relative fluorescence intensities of C-cadherin and 14-3-3 in 20 cells near and at the cell-cell contact zone. Percentages indicate the proportion of corresponding mean intensities in each quadrant. Images were taken using a 63x objective (1.4 NA) and 1.6 Tubelens. Scale bars are 10 μm.

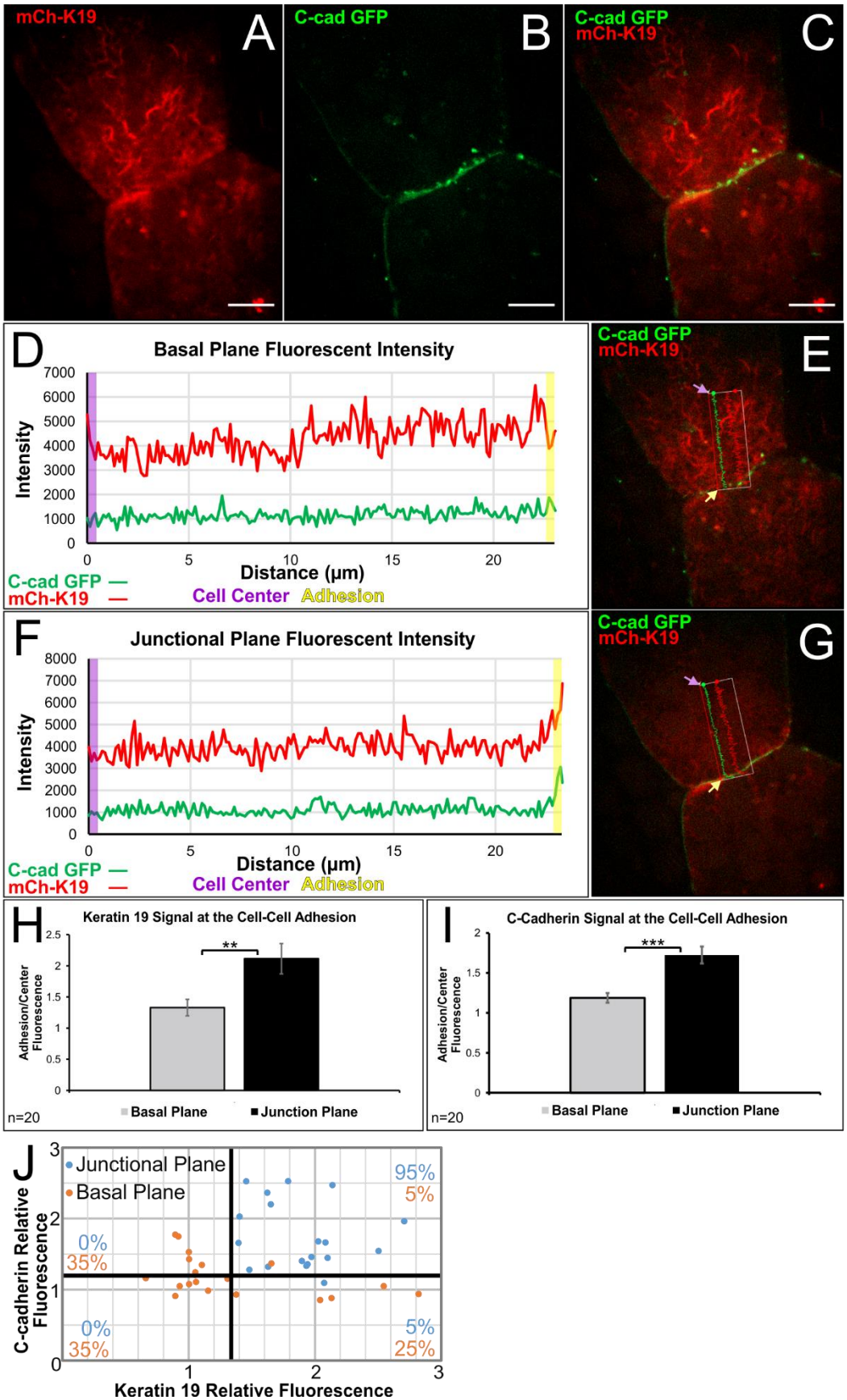
mCh-K19
A
C-cad GFP
B
C-cad GFP
mCh-K19
C
D
Basal Plane Fluorescent Intensity
Intensity
7000
6000
5000
4000
3000
2000
1000
0
0
5
10
15
20
Distance (μm)
C-cad GFP
mCh-K19
Cell Center
Adhesion
C-cad GFP
mCh-K19
E
F
Junctional Plane Fluorescent Intensity
Intensity
8000
7000
6000
5000
4000
3000
2000
1000
0
0
5
10
15
20
Distance (μm)
C-cad GFP
mCh-K19
Cell Center
Adhesion
C-cad GFP
mCh-K19
G
H
Keratin 19 Signal at the Cell-Cell Adhesion
Adhesion/Center Fluorescence
2.5
2
1.5
1
0.5
0
**
n=20
Basal Plane
Junction Plane
I
C-Cadherin Signal at the Cell-Cell Adhesion
Adhesion/Center Fluorescence
2
1.5
1
0.5
0
***
n=20
Basal Plane
Junction Plane
J
Junctional Plane
Basal Plane
95%
5%
0%
35%
0%
35%
5%
25%
C-cadherin Relative Fluorescence
3
2
1
0
1
2
3
Keratin 19 Relative Fluorescence

Figure 30. A subset of filaments in Keratin 19 networks interacts with cell-cell adhesions.

A-C) Immunofluorescent image of a cell-cell junction between cells within a DMZ explant. Provided images are maximum intensity projections. **D**) Representative linescan analysis of fluorescence across cellular compartments at the basal plane. **E**) Source image for linescan data provided in panel D. **F**) Representative linescan analysis of flourescence across cellular compartments at the junction plane. **G**) Source image for linescan data provided in panel F. Lines depicted in D-G extended from the approximate middle of the cell to the onset of C-cadherin signal. Measurements in D-G were taken from the cell center (purple rectangle) and the adhesion (yellow rectangle). Each rectangle represents 0.5 μm in length. Colored arrows in E and G indicate region represented by rectangles in D and F, respectively. **H**) Comparison of the mean increase in mCherry-Keratin 19 signal from the cell center to the cell-cell adhesion in the basal plane and the junction plane. **I**) Comparison of the mean increase in C-cadherin signal from the cell center to the cell-cell adhesion in the basal plane and the junction plane. Analysis was performed using paired sample t-tests, **p = 0.005 ; ***p = 0.0005. Error Bars are ± SEM. Scale bars are 10 μm. **J**) Scatterplot of the mean relative fluorescence intensities of C-cadherin and Keratin 19 in 20 cells imaged by confocal in the basal plane and a higher junctional plane. Percentages indicate the proportion of corresponding mean intensities in each quadrant. Images were taken using a 63x objective (1.4 NA) with 1.6 Tubelens. Scale bars are 10 μm.

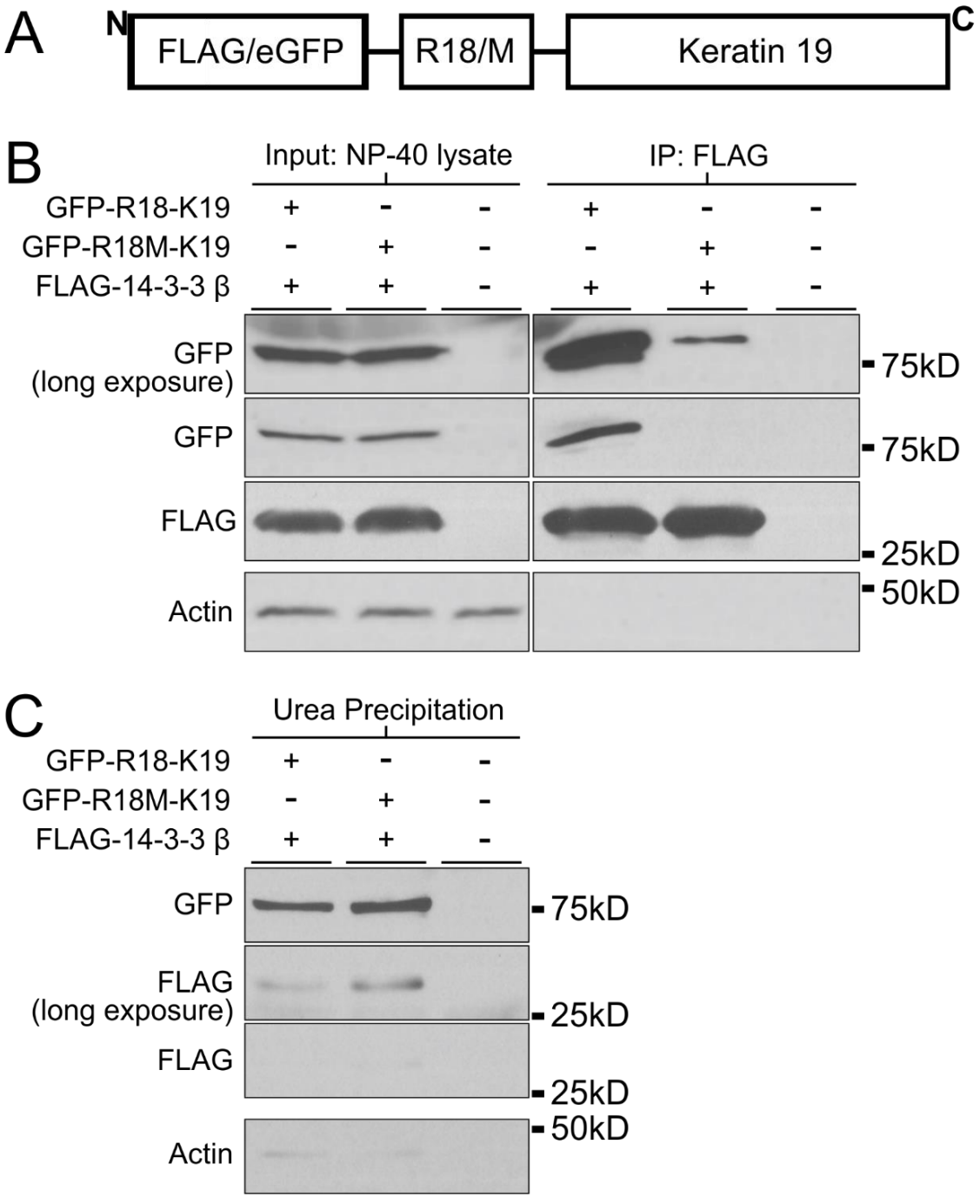
A
N
FLAG/eGFP
R18/M
Keratin 19
C
B
Input: NP-40 lysate
IP: FLAG
GFP-R18-K19 + - - + - -
GFP-R18M-K19 - + - - + -
FLAG-14-3-3 β + + - + + -
GFP (long exposure)
GFP
FLAG
Actin
75kD
75kD
25kD
50kD
C
Urea Precipitation
GFP-R18-K19 + - -
GFP-R18M-K19 - + -
FLAG-14-3-3 β + + -
GFP
FLAG (long exposure)
FLAG
Actin
75kD
25kD
25kD
50kD

Figure 31. 14-3-3 binds R18-K19 fusion proteins.

A) Schematic of fusion peptides created by the insertion of R18 or R18M (R18/M) into FLAG/eGFP-K19. **B**) Nonionic detergent soluble protein lysates (1% Tergitol type NP-40) from stage 10.5 *Xenopus* embryos expressing FLAG-14-3-3 β and either eGFP-R18-K19 or eGFP-R18M-K19 were immunoprecipitated for FLAG proteins. One-cell embryos were injected with RNA encoding GFP-R18-K19 or GFP-R18-K19 alongside RNA encoding FLAG-14-3-3 β. Lysates were prepared and FLAG immunoprecipitation was performed. FLAG immunoprecipitates were blotted for GFP, FLAG, and Actin. Non-injected lysate incubated with FLAG antibody conjugated agarose beads was immunoblotted as a negative control. Immunoprecipitation was performed using approximately 2000 µg of protein lysate. Input lanes include approximately 1 embryo worth of protein. **C**) Immunoblot of Urea solubilized 1% Tergitol type NP-40 insoluble protein lysates from stage 10.5 embryos expressing FLAG-14-3-3 β and either eGFP-R18-K19 or eGFP-R18M-K19. Urea soluble lysates were immunolabeled for FLAG, GFP, and actin. Lanes include approximately 6 embryos worth of 1% Tergitol type NP-40 detergent insoluble protein.

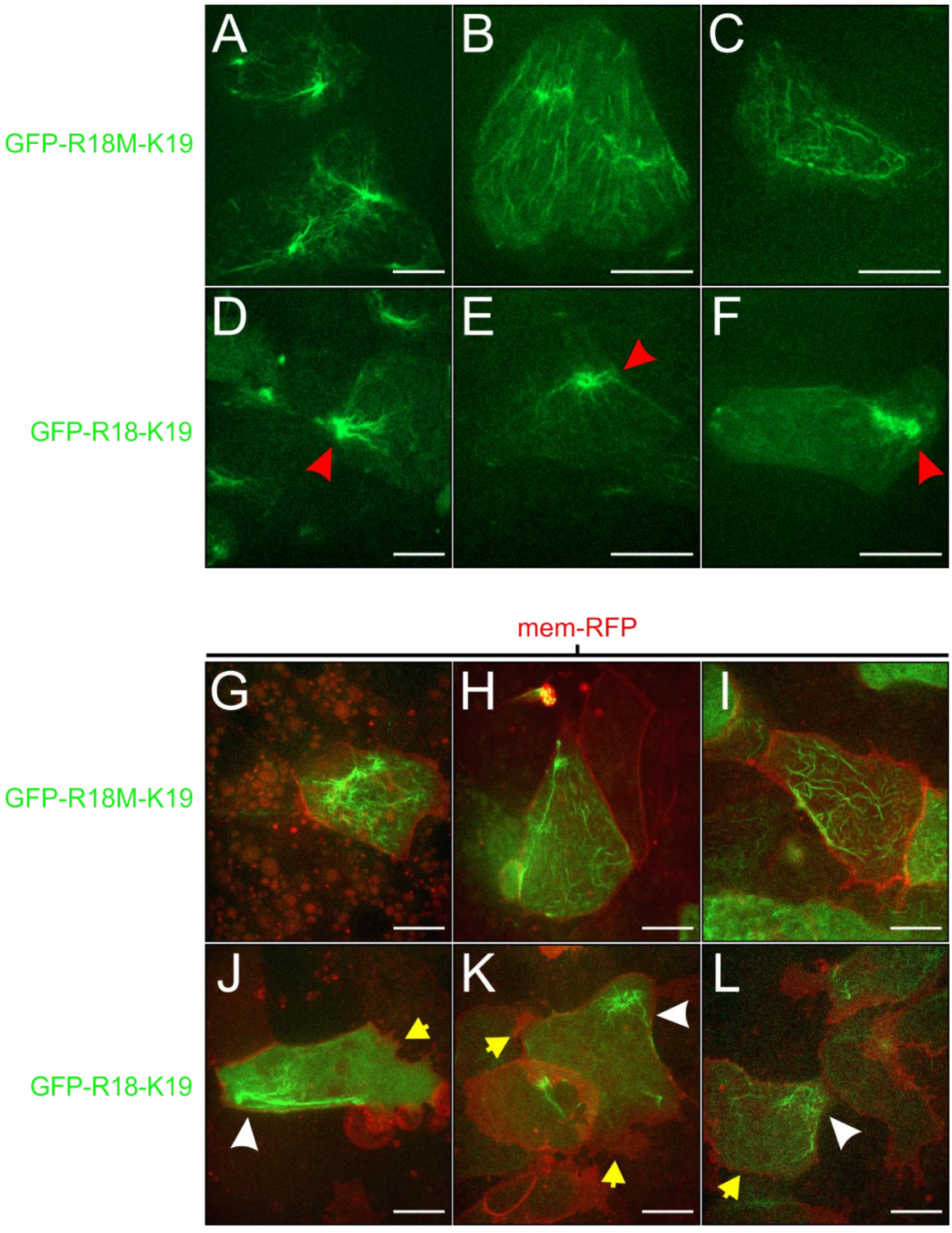
A
B
C
GFP-R18M-K19
D
E
F
GFP-R18-K19
mem-RFP
G
H
I
GFP-R18M-K19
J
K
L
GFP-R18-K19

Figure 32. 14-3-3 proteins target keratins to cell-cell adhesions.

Live imaging of DMZ explants mosaically expressing GFP-R18-K19 or GFP-R18M-K19 with or without mem-RFP. **A-C**) Mesendoderm cells expressing GFP-R18M-K19 filament networks. **D-F**) Mesendoderm expressing GFP-R18-K19. Red arrowheads indicate areas where filament densities have localized. **G-I**) GFP-R18M-K19 co-expressed with mem-RFP in mesendoderm cells. **J-L**) GFP-R18-K19 co-expressed with mem-RFP. White arrowheads indicate areas where filament densities have localized. Yellow arrows highlight apparent cellular protrusions. Images are z-stacks (maximum intensity projection) taken using a 63x objective (1.4 NA) with a 1.0 Tubelens (A, D, G-L) and a 1.6 Tubelens (B, C, E, F). Scale bars are 20 μm.

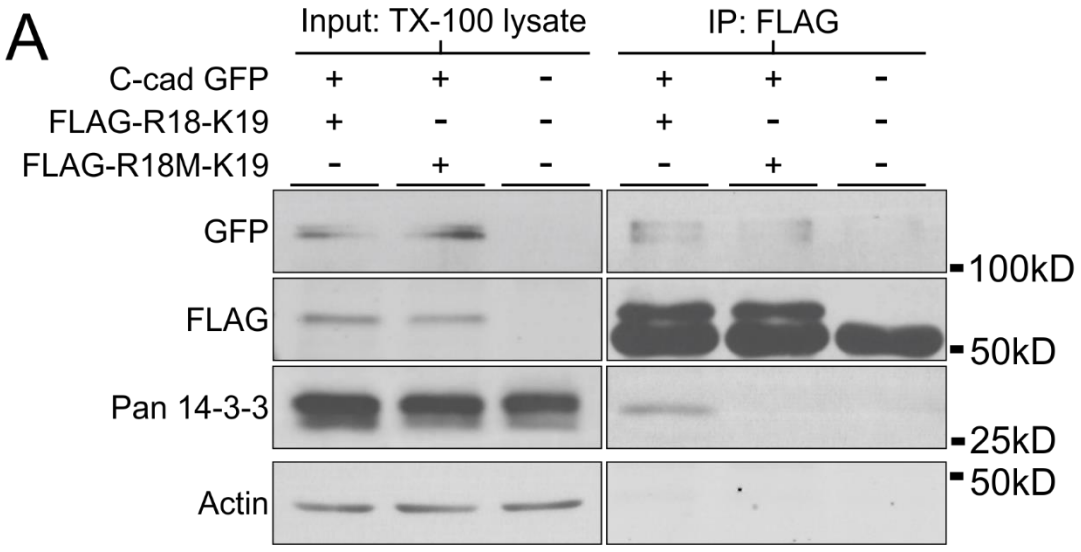
A
Input: TX-100 lysate
IP: FLAG
C-cad GFP + + - + + -
FLAG-R18-K19 + - - + - -
FLAG-R18M-K19 - + - - + -
GFP
FLAG
Pan 14-3-3
Actin
100kD
50kD
25kD
50kD

Figure 33. 14-3-3 binding to R18-K19 does not increase interaction with C-cadherin.

3xFLAG-R18-K19 and 3xFLAG-R18M-K19 immunoprecipitates blotted for interaction with 14-3-3 proteins and C-cadherin GFP. **A**) Immunoblot of FLAG immunoprecipitated embryonic lysates (1% Triton X-100). One-cell embryos were injected with RNA encoding C-cadherin GFP with either 3xFLAG-R18-K19 or 3xFLAG-R18M-K19. Lysates were prepared at embryonic stage 10.5 and immunoprecipitation for FLAG proteins was performed. FLAG immunoprecipitates were immunoblotted for GFP, FLAG, pan 14-3-3, and actin. Non-injected lysate incubated with FLAG antibody conjugated agarose beads was immunoblotted as a negative control. Immunoprecipitation was performed using approximately 2000 µg of protein lysate. Input lanes include approximately 1 embryo worth of protein.

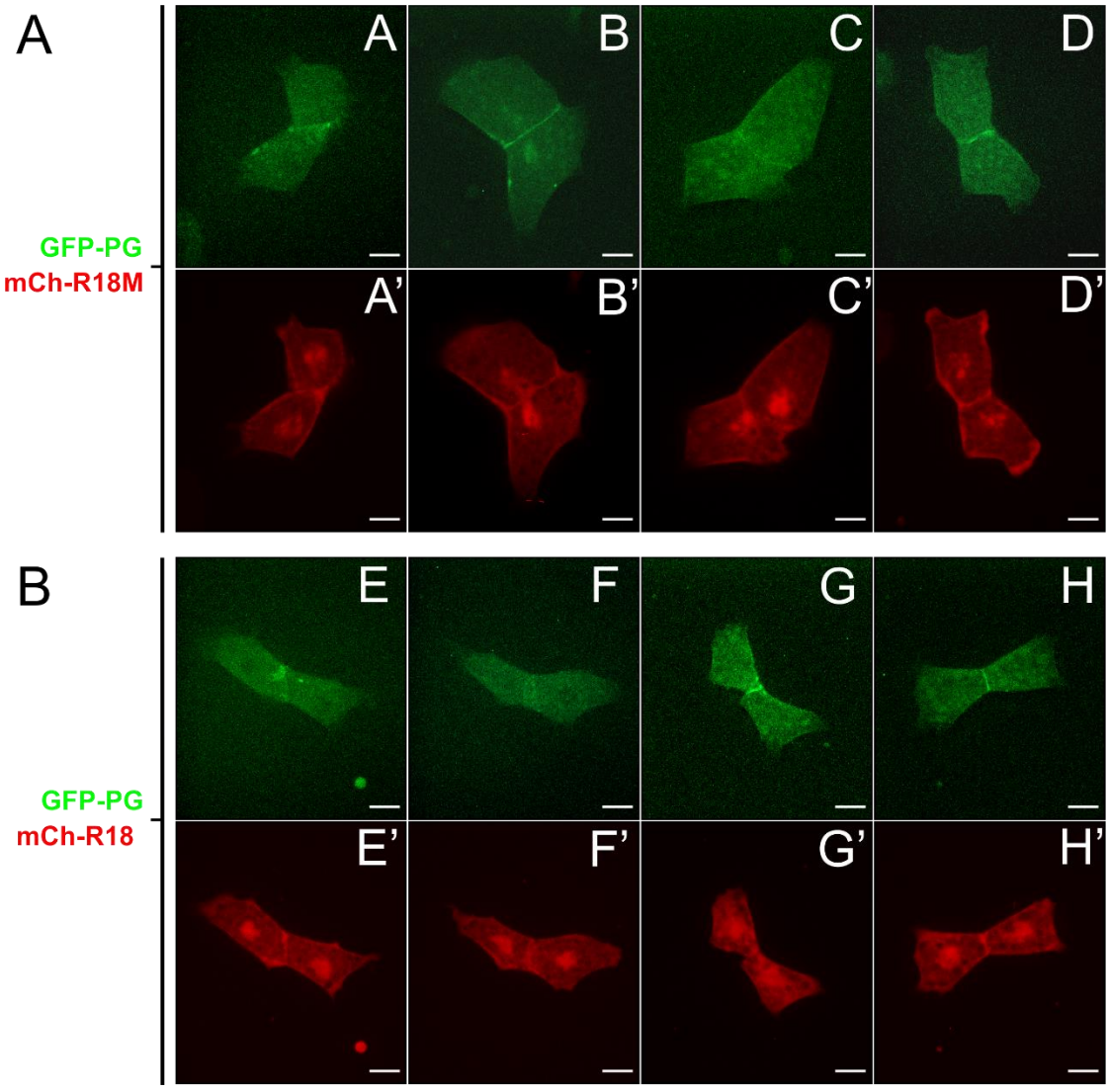
A
A
B
C
D
GFP-PG
mCh-R18M
A'
B'
C'
D'
B
E
F
G
H
GFP-PG
mCh-R18
E'
F'
G'
H'

Figure 34. 14-3-3 inhibition does not perturb junctional localization of Plakoglobin in *Xenopus* mesendoderm.

Live imaging of mesendoderm cell pairs. Mesendoderm was dissected from stage 10.5 embryos expressing GFP-PG with either mCherry-R18 or mCherry-R18M and incubated in Ca^{2+} and Mg^{2+} deplete media to allow cadherins to disengage. After 25 minutes, Ca^{2+} and Mg^{2+} were reintroduced and mesendoderm cells were imaged after collision. **A-D**) GFP-PG distribution in post collision mesendoderm cell pairs expressing GFP-PG and mCherry-R18M. **A'-D'**) mCherry-R18M signal in pairs depicted in A-D. **E-H**) GFP-PG distribution in post collision cell pairs expressing mCherry-R18 alongside GFP-PG. **E-H'**) mCherry-R18 signal in pairs depicted in E-H. Images were taken using a 40x objective (1.3 NA) with a 1.0 Tubelens. Images are confocal single plane optical sections. Scale bars are 20 μm.

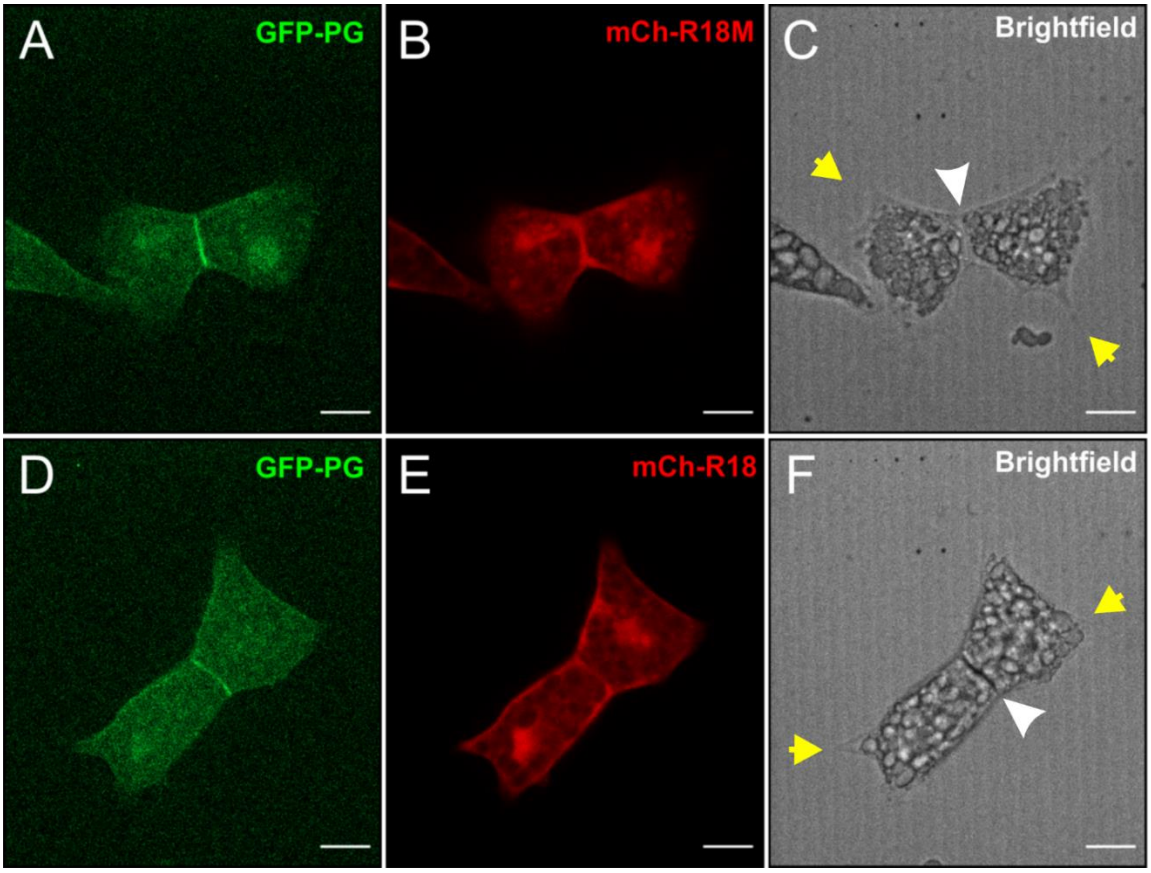
A
GFP-PG
B
mCh-R18M
C
Brightfield
D
GFP-PG
E
mCh-R18
F
Brightfield

Figure 35. 14-3-3 is not required for Plakoglobin targeting to mesendoderm cell-cell contacts.

Live imaging of stage 10.5 mesendoderm cell pairs expressing GFP-PG with either mCherry-R18 or mCherry R18M after dissociation and collision. **A-C**) Mesendoderm pair expressing GFP-PG with mCherry-R18M. The white arrowhead in C highlights the cell-cell adhesion, while the yellow arrows mark apparent cellular protrusions. **D-F**) Mesendoderm pair expressing mCherry-R18 with GFP-PG. The white arrowhead in F denotes the cell-cell adhesion, while the yellow arrows mark apparent cellular protrusions. Images were taken using a 40x objective (1.3 NA) with a 1.0 Tubelens. Images are confocal single plane optical sections. Scale bars are 20 μm.

CHAPTER 6

DISCUSSION AND FUTURE DIRECTIONS

Some information from this chapter is accepted for publication in Mariani *et al.* (2019) *MBoC.*

Our findings in the current study lead us to propose that 14-3-3 proteins are responsible for targeting keratin intermediate filaments to sites of cell-cell adhesion that are transmitting tension. Expression of a fluorescent keratin fused to a high affinity 14-3-3 binding domain causes filaments assembled from these keratins to mobilize to cell-cell junctions. In reciprocal support, inhibition of 14-3-3 through expression of a peptide inhibitor results in the failed targeting of keratin filament to sites of *de novo* cell-cell adhesion. These observations provide evidence for the first time that 14-3-3 functions as a critical spatial determinant of the intermediate filament network in response to mechanical loading at cell contacts (Figure 36).

Cytoskeletal structures must be able to efficiently sense tension and undergo remodeling in order to fortify cells against changes in the direction, magnitude, and nature of tension transmitted. Rapid changes in force application require concomitant responses by cytoskeletal proteins, necessitating mechanistic filament assembly strategies that are effective within a short time scale. Cellular mechanisms that induce changes within a shorter time-scale than that required for biosynthesis include pathways that make post-translational modifications to pre-existing proteins. Intermediate filament proteins, which have no known intrinsic catalytic activity, are modified by other molecules that respond to changes in cellular tension, such as kinases (Loschke et al., 2015). It follows that accessory proteins recognize and bind these post-translational modifications and accordingly alter the filament dynamics and spatial localization of intermediate filament proteins. These interactions can reorganize filament populations to particular locales within the cell and change polymerization-depolymerization characteristics.

Our data support a functional role for 14-3-3 in mediating keratin intermediate filament dynamic exchange and reorganization in cells that are actively migrating and encountering changes in the direction and magnitude of loading forces.

We show here an interaction between 14-3-3 and keratin proteins. Indeed, 14-3-3 proteins have been demonstrated to interact with a variety of intermediate filaments (Tzivion et al., 2000; Li et al., 2006; Miao et al., 2013), including some keratin types (Ku et al., 1998; Kim et al., 2006; Margolis et al., 2006; Sivaramakrishnan et al., 2009; Boudreau et al., 2013). We show for the first time an interaction between K19 and 14-3-3. We do not yet know the specific 14-3-3 isoform that binds endogenously. Our finding of particularly high expression of 14-3-3 β and ζ is in agreement with recent independent data from (Peshkin et al., 2019). Previous work has shown that K18 directly binds to 14-3-3 when phosphorylated on serine 33, but an association between K19 and 14-3-3 was not observed (Ku et al., 1998). Nonetheless, this serine residue is conserved between K18 and K19, conserved across species, and is a putative phosphorylation target in K19 (Ku et al., 1998; Zhou et al., 1999; Ju et al., 2015). 14-3-3 associates with a number of Type I acidic keratins aside from K18 (Kim et al., 2006; Boudreau et al., 2013). Serine residues 10, 33 (S35 in human) and 52 (S54 in human) of K19 are predicted to be phosphorylated by several kinases including protein kinase C and to be 14-3-3 binding sites by our bioinformatics analyses (Figure 11). Regardless of which specific phosphorylation site provides for interaction with 14-3-3, an association is evident by our experimental observations and supported by numerous predictive computational analyses. While one might contend that K19

could be associating with 14-3-3 indirectly through other keratins, K19 was uniquely abundant in our 14-3-3 immunoprecipitation samples.

Several separate points of evidence support the observation that K19 is target of 14-3-3 proteins and that this interaction modulates the activity of these proteins. While initial descriptions of interactions between simple epithelial keratins and 14-3-3 did not identify K19 as a binding partner of 14-3-3 (Ku et al. 1998), subsequent investigation demonstrated that mutation of the conserved serine in K19 that is essential for 14-3-3 binding to K18 (Ku et al. 1998) disrupts the K19 filament network (Zhou et al. 1999). Moreover, phosphorylation of this site has been shown to reorganize the keratin network and induce peripheral membrane proximal localization of K19 proteins (Ju et al. 2015). This phosphorylation and subsequent localization is necessary to stabilize receptor HER2 in breast cancer cells and protect it from degradation (Ju et al. 2015). While this particular finding was not explored with regard to 14-3-3 activity, the above described protein translocation, stabilization, and protection from ubiquitylation are all well characterized functions of 14-3-3 proteins (Obsil and Obsilova 2011). The finding in the current study that synthetic coupling of K19 to 14-3-3 proteins induces a cell-cell adhesion proximal targeting of this proteins both potentially illuminates and is illuminated by these previous studies of K19 activity.

What is the interaction of 14-3-3 with K19 actually doing to the intermediate filaments? Generally, the binding of 14-3-3 proteins to keratins is known to induce IF solubility in detergent buffers (Liao and Omary 1996), an effect that we also demonstrate here. At a whole-cell level, association of keratins with 14-3-3 is

necessary for keratin network disassembly during mitosis (Liao and Omary, 1996). Knockdown of 14-3-3 has been shown to result in abnormal increases in keratin filament abundance and decreases in soluble filament precursors (Boudreau et al., 2013). Fluid flow shear stress of alveolar cells results in phosphorylation of known 14-3-3 sites in K18 along with increases in dynamic exchange that are 14-3-3 dependent (Sivaramakrishnan et al., 2009). Similarly, we see decreased FRAP recovery when 14-3-3 is inhibited in eGFP-K19 expressing mesendoderm tissue, which is known to endure intrinsic mechanical stresses through the cell-cell contacts (Weber et al., 2012; Sonavane et al., 2017). We expect that expression of R18 peptide results in inhibition of 14-3-3 in multiple contexts throughout the cell rather than perturbation of the subset of 14-3-3 molecules that associate with the keratin-cadherin complex. Nonetheless, we find it remarkable that 14-3-3 inhibition still resulted in a distinct change in keratin subcellular distribution as a consequence of cell-cell adhesion signals.

Though several functions of 14-3-3 proteins have been deduced via study of its interaction with many binding partners, we still lack direct evidence to demonstrate how 14-3-3 binding increases the rate of processes such as dynamic exchange. The same can be said of the targeting of GFP-R18-K19 filament densities to cell junctions, described in our report. A range of speculations may be worth consideration here (Figure 37). It is possible that 14-3-3 proteins behave as a molecular ‘anvil’, as proposed by Yaffe and colleagues, here functioning to disassemble K19 from filaments and change their conformation so they cannot reassemble until 14-3-3 dissociates (Yaffe et al. 2002). Likewise, 14-3-3 may

‘precapture’ filament subunits prior to assembly, allowing them to exist as a soluble pool that can resist assembly until removed from 14-3-3 (Windoffer et al. 2011). Neither of these propositions prevent the possibility that 14-3-3 proteins may localize bound K19 by transport via interactions with molecular motors (Ichimura et al. 2002; Sehgal et al. 2014). Future studies that continue to explore both the range of filament activities coordinated by 14-3-3 binding as well as the complex mechanisms that allow this regulatory activity will provide valuable information with regard to the dynamic activities of the IF network across cellular compartments.

We find that 14-3-3 provides for targeting of K19 toward cadherin-mediated cell-cell contacts. While 14-3-3 inhibition resulted in the establishment of a keratin deplete zone proximal to the contact, forced association of K19 with 14-3-3 conversely localized the filament population to the cell-cell contact compartment. 14-3-3 is observed decorating the filamentous keratin population proximal to these adhesions. Despite finding biochemical association between 14-3-3 and C-cadherin, we note that at high resolution these molecules do not precisely co-localize. This suggests that there are additional components that may facilitate interaction between 14-3-3/keratin protein complexes and other molecules of the cell-cell junction, and which may play a role in the reorganization event. 14-3-3 has been demonstrated to associate with a number of molecules important for establishment of cytoskeletal networks at the cell-cell adhesion (Acehan et al., 2008) including plakoglobin (Sehgal et al., 2014; Vishal et al., 2018) and plakophilin (Jin et al., 2004; Roberts et al., 2013). The association and function of 14-3-3 in relation to keratin intermediate filaments may provide an interface

between cytoskeletal networks and a host of scaffolding proteins and signal transduction pathways (Margolis et al., 2006; Loschke et al., 2016; Sonavane et al., 2017). In turn, the targeting of keratin to sites of tension due to local signaling/phosphorylation events could promote a positive feedback loop for keratin filament assembly dynamics (Ridge et al., 2005; Woll et al., 2007; Ju et al., 2015; Sonavane et al., 2017). The enriched presence of 14-3-3 near both the cell-cell adhesion and in the lamellipodia suggest either non-intermediate filament related functions in the latter region or a possible function in intermediate filament transport or formation (Windoffer et al., 2004, 2011). Further elucidation of these macromolecular complexes in polarized migratory cells will be the subject of ongoing studies.

Our findings demonstrate distinct localization of 14-3-3 proteins to the peripheral and cell-junction proximal compartment of *Xenopus* mesendoderm cells. The nature of functional roles for molecules often correlates with their spatial distribution in cells, and we propose such is the case for 14-3-3 proteins in mesendoderm. Many observations of 14-3-3 distribution demonstrate presence of these proteins in the cytoplasmic and nuclear compartments of cells, two broad areas of cells where 14-3-3 proteins can interact with a large variety of targets (Sehnke et al. 2002; Cutler et al. 2000). Indeed, the interaction between 14-3-3 and keratins has been shown to mediate between these two distributions. Both K8 and K17 containing filaments bind and retain 14-3-3 proteins in the cytoplasm that localize to the nucleus in the absence of these keratins (Toivola et al. 2001; Kim et al. 2006). Studies directly focused on examining protein distribution have

demonstrated that 14-3-3 proteins can also localize to peripheral cell borders (Sehnke et al. 2002; Cutler et al. 2000). While the capacity for 14-3-3 proteins to localize to this compartment is not especially surprising given known interactions between 14-3-3 proteins and membrane associated proteins (Ottmann et al. 2007) as well as junctional adhesion proteins (Sehgal et al. 2014; Vishal et al. 2018; Roberts et al. 2013; Amaya et al. 2019), it is important to consider in the context of 14-3-3 activity. Evidence of 14-3-3 distribution in several cellular compartments including the cell periphery presents the likelihood that 14-3-3 is well positioned to influence relocalization of target proteins from one compartment to another. We observe this function in action when K19 is fused to the sequence of the R18 peptide, which increases binding of these K19 fusions to 14-3-3 proteins.

The functional importance of K19 is generally unexplored, with known roles in the mammal limited to spatial coordination of contractile structures in mouse muscle and protection against liver damage (Stone et al. 2007; Chen et al. 2015). Given the lack of knowledge regarding cell specific roles for K19 containing networks, evidence from which to draw insight about its function is mainly limited to examination of its structural features. It is notable that *Xenopus* K19 has only a single amino acid in the tail domain and human K19 has only 13 amino acids, making this keratin structurally deviant from other IF proteins (Herrmann et al., 1996; Kirmse et al., 2007; Lee et al., 2012). The function of the IF tail region is a subject of ongoing debate, especially in regard to keratins. Studies have demonstrated that tailless keratins, including K19 and tail deleted K18, are able to form heteropolymers with tail deleted K8 (Hatzfeld and Weber, 1990; Bader et al.

1991). Similarly, desmin mutated to be tailless assembles into normal networks in assembly assays (Bar et al. 2010). When such networks are studied during application of forces, however, they demonstrate inability to stiffen (Bar et al. 2010). This mechanical difference has been observed in networks comprised of tailless desmin, vimentin, and keratins 8 and 18 (Bar et al. 2010; Lin et al. 2010b; Pawelzyk et al. 2014). It has proposed that these changes in the properties of the IF network result from loss of tail domain residues thought to be important for crosslinking between filaments within networks (Lin et al. 2010a; Pawelyzk et al. 2014). However, whether such features are at play with regard to K19 containing networks or how they may influence/impart function to keratin networks mechanically recruited to cell-cell adhesions is completely unknown. Thus, study of the role of K8/K19 networks compared to K8/18 networks with regard to mechanical and cellular features is an open and important area of investigation that will further inform knowledge of IF function. Lack of the K19 tail region has been speculated to result in keratin networks with greater dynamic potential (Hofmann and Franke, 1997; Fradette et al., 1998) which may afford these proteins particular suitability to a dynamic tissue such as collectively migrating mesendoderm.

Our data describe a relationship between 14-3-3 activity and keratin localization that is apparently complex when considered in terms of mechanical recruit of keratin networks and formation of cell-cell adhesions. Evidence that 14-3-3 binding of K19 is necessary and sufficient for targeting of K19 to the junctional compartment is especially interesting in light of the demonstration that it does not

additionally result in increases in K19 coupling to the adhesion complex. Furthermore, while we know that mechanical stimulation of cadherin proteins in mesendoderm results in recruit of keratin filaments to the site of force transduction, we are still unaware of the components of the adhesion complex that directly link to keratins in these cells (Weber et al. 2012). At least in the case of desmosomal adhesion formation the junctional complex can form in the absence of keratin filaments, with the consequence of the keratin loss (K5 and K14) manifesting in tissue fragility (Letai et al. 1993; Chan et al. 1994; Peters et al. 2001). Of the two adhesion scaffold proteins that are known to be junctionally localized via interaction with 14-3-3 proteins, plakophilin proteins were not detected as part of the mesendoderm c-cadherin complex, while plakoglobin only partially diminished junctional recruit of keratin (Weber et al. 2012). Additionally, plakoglobin localization to newly formed cell-cell adhesions appeared unaffected by inhibition of 14-3-3 in mesendoderm. We speculate that the binding between 14-3-3 and K19 targets these proteins to the junction independent of direct coupling with the adhesion and believe that this this model of activity is substantiated by very recent research describing targeting of the tight junction protein ZO-2 to the cell-cell periphery (Amaya et al. 2019). Upon dissociation of cell-cell contacts during calcium switch, ZO-2 is demonstrated to interact with 14-3-3 proteins and co-localize with 14-3-3 in the cytosol (Amaya et al. 2019). When Ca^{2+} is restored and adhesions are established, ZO-2 shows brief co-localization with 14-3-3 at the cell-cell contact followed by distinct junctional localization of ZO-2 and concomitant with a decrease in interaction with 14-3-3 proteins (Amaya et al. 2019). The

authors suggest that ZO-2 is localized to the junction by 14-3-3 proteins that then must dissociate from these proteins prior to their association with the junctions (Amaya et al. 2019). Given our own distinct evidence of 14-3-3 binding of K19 and regulation of targeting to the cell-cell borders but not direct association with cadherin proteins, we believe it is a likely that a similar mechanism may be invoked with regard to junctional keratin recruit in mesendoderm.

Although the findings of this study add to our understanding of the molecular consequences of the association between 14-3-3 proteins and intermediate filaments, the insights that can be gathered from the work are not limited to the study of IFs. 14-3-3 proteins both affect and are affected by IFs as a result of the association between these molecules. While the influence that each of these molecules exert on the compartmental localization of the other has direct implications for each of their respective functions, this information has broader application beyond these particular interactions. Indeed, even the junctional compartment targeting of Keratin 19 as a result of interaction with 14-3-3 that is described in this work shares similarity with reports describing junctional localization of non-IF proteins via 14-3-3 (Sehgal et al. 2014; Vishal et al. 2018; Amaya et al. 2019).

The results of this study, when considered alongside many other pivotal contributions, offer a window into the bigger picture of 14-3-3 function within the cellular environment. Throughout this work 14-3-3 has been referred to as a ‘regulator’. In this particular case, that description is based upon the change in Keratin 19 activity that can be observed as a consequence of both peptide

inhibition of 14-3-3 as well as induced interaction between Keratin 19 and 14-3-3. More stands to be considered with regard to the meaning of the term ‘regulator’ along with ramifications for general protein function.

For any given protein, our current understanding of fundamental molecular biology lends the assumption that its properties endow it with a limited number of functions. These molecular properties include and stem from the primary sequence, as this feature influences secondary through quaternary structure. All interactions between a particular protein and any number of partners are a result of these features; additionally, interactions with other molecules can also further influence secondary through quaternary structure. It follows that a ‘regulator’ of any protein target that induces an effect via binding must both be able to interact with its target through these features and augment these features through the interaction. In doing so, the interacting regulator would then be able to prohibit functions of its target and/or permit new functions, as the properties of the molecule have been changed.

This definition applies to 14-3-3 proteins as binding regulators that typically depend upon phosphorylation to exert an effect on targets. The specific effect that 14-3-3 binding induces with regard to any particular protein target depends on the primary through quaternary features that the binding alters, the nature of these alterations, and the functional implications of such changes. Due to the great diversity of 14-3-3 targets and binding locations within targets, ‘regulation’ by 14-3-3 binding can have a dramatically different effect in different contexts despite the simplicity of the mechanism through which this effect is achieved. Given this

complex picture of 14-3-3 activity, what can we understand about the essential functional nature of this protein?

As stated in the preface of this document, had we complete knowledge of every molecule, ascribing a comprehensive definition of function to 14-3-3 proteins would likely be a simpler endeavor. Despite lacking such knowledge, we can gain a broad perspective of 14-3-3 function in light of cellular signaling from aspects of the current study that resound with a plethora of others. Taken together, our current knowledge allows us to widely appreciate 14-3-3 proteins as ‘inducers of complexity’ in cellular systems.

While the array of functions that proteins can host are otherwise limited to intrinsic properties, interacting partners, and modifications, changes induced by 14-3-3 binding alter function and thus serve to generally enhance the range of activities of a given molecule. As a result, interaction with 14-3-3 can serve as the mechanism to add complexity in the form of a ‘checkpoint’ step, a feedback loop, or a permissive signal in a signaling pathway, for example. In this manner 14-3-3 proteins largely allow for additional change in the cellular environment, extending that which is present due to instrinsic features of proteins and further endowing a malleable and dynamic nature outside of that dictated solely by the structural properties of molecules. It is quite clear to this author that such functions of 14-3-3 proteins provide a benefit to cells at large. Through providing a mechanism to enhance change, 14-3-3 proteins certainly confer advantages to cells that must adapt to any variety of challenges encountered in complex and constantly changing living environments.

The significance of K19 association with 14-3-3 to development of the early embryo remains uncertain. Previous work has shown important roles for 14-3-3 in *Xenopus* development through the targeted knockdown of different isoforms by morpholino oligonucleotides (Lau et al., 2006). Knockdown of certain 14-3-3 isoforms caused severe gastrulation defects including exogastrulation and failed mesodermal patterning (Lau et al., 2006). Knockdown or inhibition of K8, the lone Type II keratin in early embryogenesis, similarly induces exogastrulation (Klymkowsky et al., 1992; Torpey et al., 1992). The specific functions of K18 and K19 in early embryonic development have yet to be determined, but it is likely that there exists some functional redundancy as evidenced by murine knockouts (Magin et al., 1998). Our finding of K19 in the mesendoderm is in agreement with two recent –omics reports broadly examining mRNA and protein expression patterns in the *Xenopus* embryo (Briggs et al., 2018; Peshkin et al., 2019). Further investigation is required to examine the developmental roles for K19 proteins in both different cell types and stages.

Molecular control of reorganization of filaments is a process that is as critical to cellular migration as it is to cellular and junctional integrity. The results of the current study lend insights into the mechanisms of active tissues ranging from cellular sheets in migration to three dimensional tissues that balance changes in loading (Winklbauer et al., 1992; Weber et al., 2012). These observations can also inform cancer models that detect roles for 14-3-3 proteins and keratins in promoting invasiveness of cells (Boudreau et al., 2013; Cheung et al., 2013; Deng et al., 2013; Ju et al., 2015). Decrease in the ability of IFs to form the networks that

fortify sealed junctions across cells, enable cells to form resistant tissues, and coordinate the activity of tissues has implications for essential processes including barrier function, embryonic tissue patterning, would healing, and cancer progression.

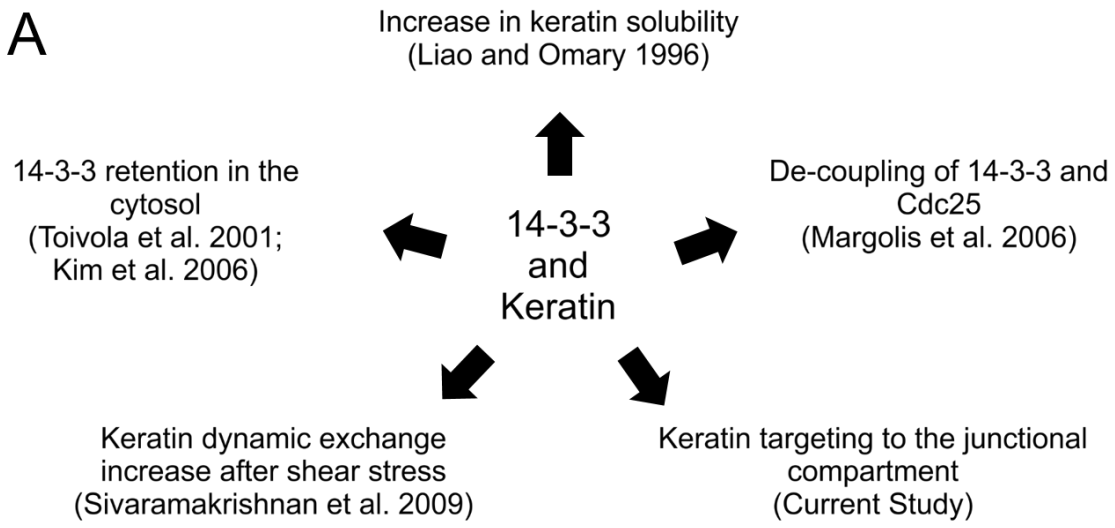
A
Increase in keratin solubility
(Liao and Omary 1996)
14-3-3 retention in the cytosol
(Toivola et al. 2001; Kim et al. 2006)
14-3-3 and Keratin
De-coupling of 14-3-3 and Cdc25
(Margolis et al. 2006)
Keratin dynamic exchange increase after shear stress
(Sivaramakrishnan et al. 2009)
Keratin targeting to the junctional compartment
(Current Study)

Figure 36. Reported effects of the interaction between 14-3-3 proteins and keratin.

A) The interaction between 14-3-3 and keratin has been described to result in increases in solubility during phases of mitosis, and has been reported to be required to release Cdc25 from 14-3-3 and allow progression of mitosis. Multiple reports have demonstrated that keratin filaments are required to retain 14-3-3 in the cellular cytosol, as depletion of keratin filaments results in abnormal 14-3-3 translocation to the nucleus. 14-3-3 is required for the increase in the rate of dynamic exchange that is stimulated via shear stress mediated keratin phosphorylation. In the current study, 14-3-3 has been shown to be necessary and sufficient to target keratin to the cellular junctional compartment.

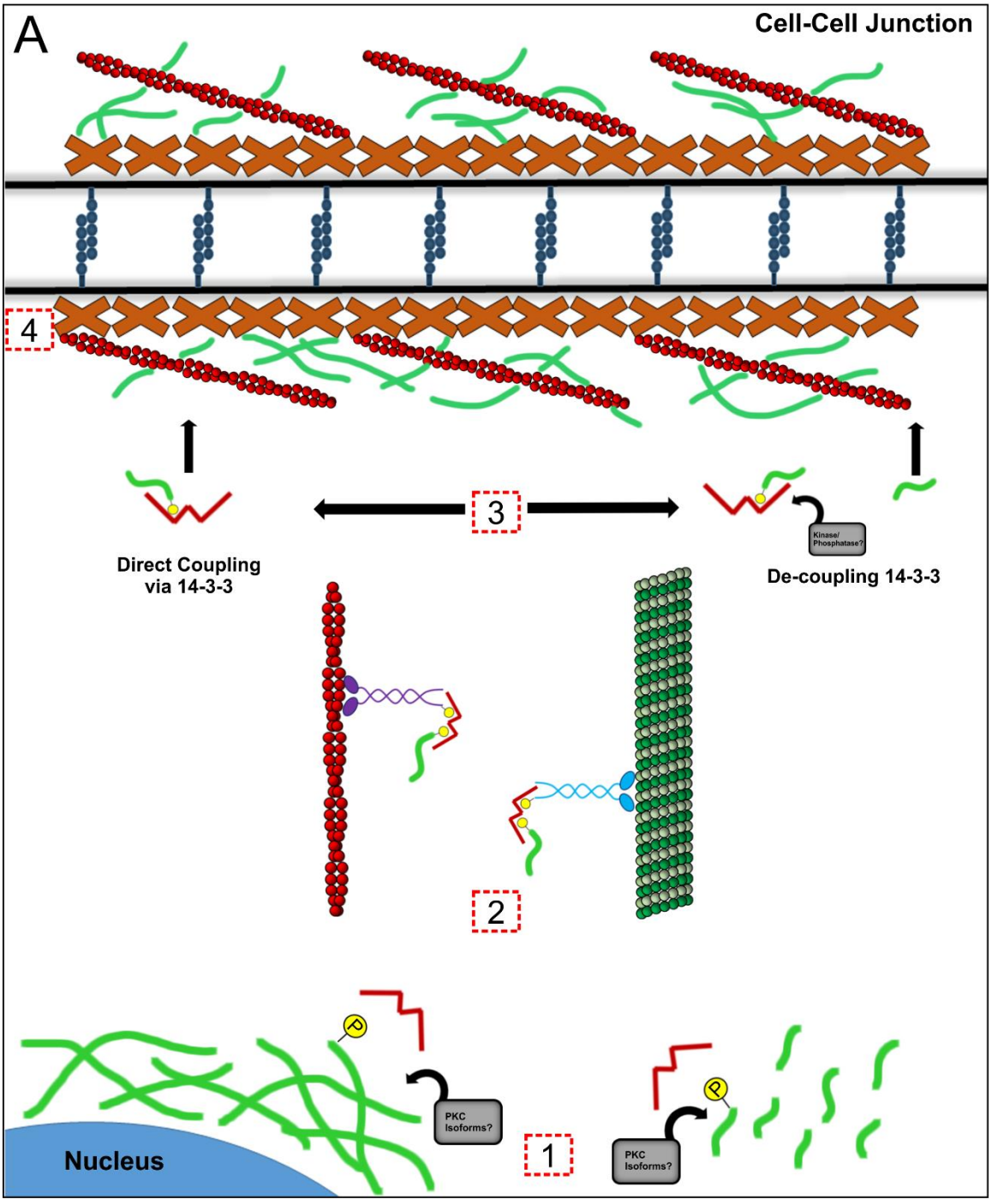
A
Cell-Cell Junction
4
3
Direct Coupling
via 14-3-3
Kinase/
Phosphatase?
De-coupling 14-3-3
2
P
PKC
Isoforms?
Nucleus
1
P
PKC
Isoforms?

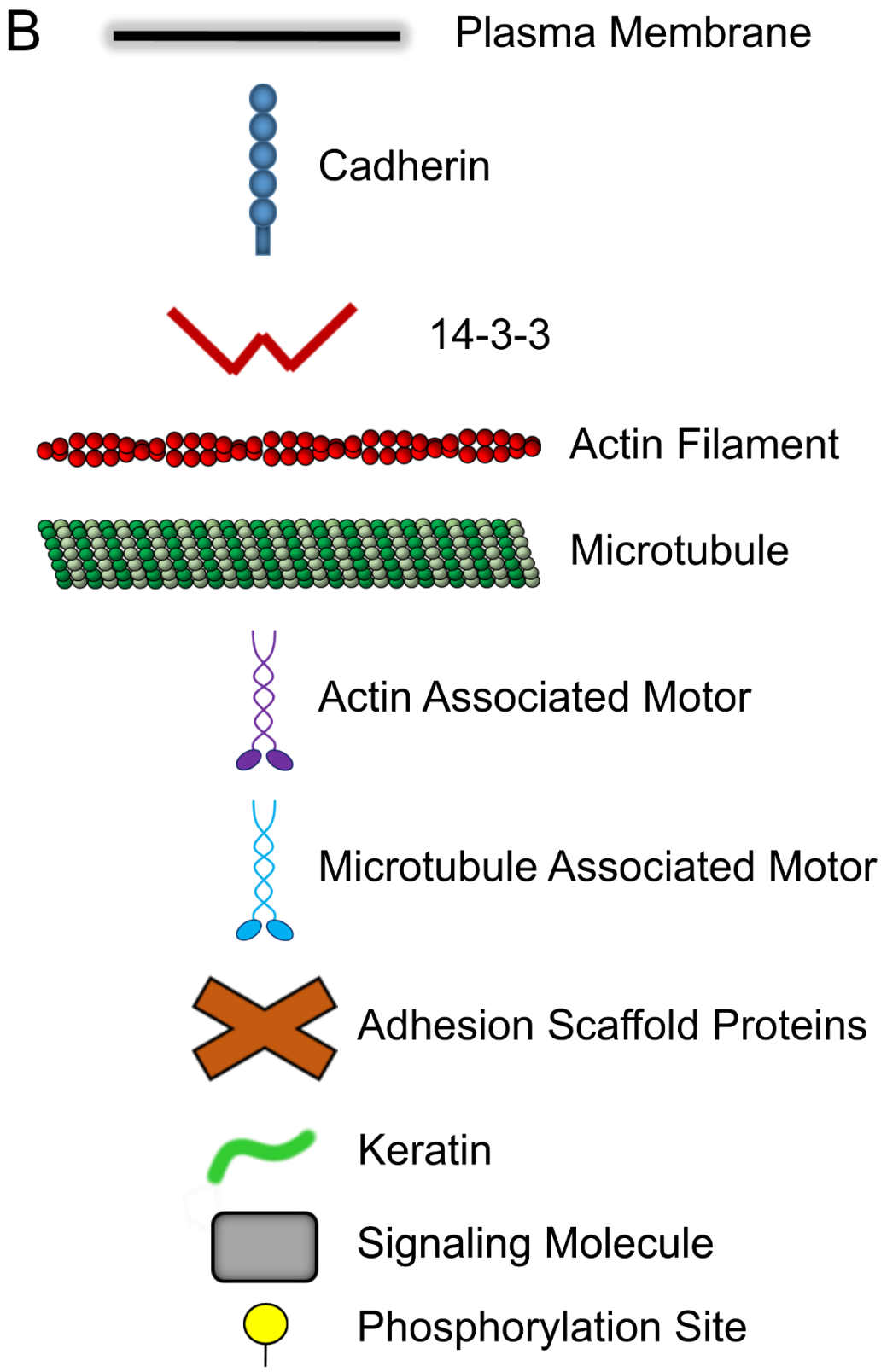
B
Plasma Membrane
Cadherin
14-3-3
Actin Filament
Microtubule
Actin Associated Motor
Microtubule Associated Motor
Adhesion Scaffold Proteins
Keratin
Signaling Molecule
Phosphorylation Site

Figure 37. Potential mechanism for 14-3-3 mediated junctional recruitment of Keratin 19.

A) Junctional targeting of Keratin 19 is mediated by the binding of 14-3-3, either proximal to the cell-cell interface or at another cytosolic compartment. A number of basophilic kinases have been shown to act on 14-3-3 sites, and members of the PKC family have been shown to phosphorylate Keratin 18 within its known 14-3-3 binding motif (Johnson et al. 2010; Sivaramakrishnan et al. 2009; Figure 11). The potential Keratin 19 binding pool may include keratins removed from filamentous networks or precursors that have yet to assemble into networks (1). K19 that is bound by 14-3-3 in a compartment distal to the adhesion could potentially be translocated to the junction through association with actin or microtubule associated motors, mediated either by 14-3-3 or through another method of interaction (2). 14-3-3 bound K19 that is proximal to the junction may associate with the adhesion complex either directly through 14-3-3 interaction with another intermediate, or after release from 14-3-3 through the activity of kinases or phosphatases that weaken the association of 14-3-3 with K19 (3). Keratins that associate with the junctional complex could potentially engage in interaction through association with filamentous actin and actin binding proteins, scaffold molecules of the adhesion complex, or both (4). **B**) Key defining descriptors used to depict the model of activity in A.

Conclusion

14-3-3 proteins show extensive subcellular association with keratin filaments *in vivo* and *ex vivo* at the cell-cell contacts of *Xenopus* mesendoderm. In *Xenopus* embryos, these proteins interact with K19, a novel type I keratin target, and cadherin proteins. Disruption of 14-3-3 binding of K19 decreases dynamic exchange within filaments of migrating mesendoderm mesendoderm. 14-3-3 is required for junctional recruit of K19 containing filament networks upon formation of cell-cell adhesion. Synthetic coupling of 14-3-3 proteins to K19 preferentially localizes these filaments to the cell-cell contact in a manner that does not involve increased linkage to the cell-cell contact. We believe that these results demonstrate an important novel role for regulation of keratin filament dynamics via 14-3-3 binding; specifically, 14-3-3 dependent subcellular localization of keratins to mechanically sensitive cell-cell contacts. Our findings reveal an important component of junctional keratin recruit that has importance concerning both cell-cohesiveness and migratory activity during collective cell migration of embryonic gastrula.

Appendix 1

Xenopus Embryo Extraction Protocol

1. Combine the following for 5ml of “extraction buffer with phosphatase inhibitors”:

1) 4.1 ml diH2O
2) 100ul 5M NaCl ([final]=100mM)
3) 250ul 1M Tris-HCl, pH 7.5 ([final]=50mM)
4) 50ul Triton X-100 (Sigma #T-9284) or Tergitol type NP-40 (Spectrum Biosciences, T1279) ([final]=1%)
5) 50ul 0.1M Phenylmethylsulfonofluoride (PMSF) ([final]=1mM)
6) 50ul Sigma mammalian protease inhibitor cocktail (#P2714)
7) 50mg sodium □-glycerophosphate (10mg/ml)
8) 50ul 1M sodium fluoride ([final]=10mM)
9) 50ul 100mM sodium orthovanadate ([final]=1mM)
10) 50ul 20mM H2O2 (dilute 30%/9.79M stock immediately before use 20.5ul into 10ml H2O), ([final]=0.2mM)
11) 250ul 60mM sodium pyrophosphate ([final]=3mM)

Combine the following for 5ml of “extraction buffer without phosphatase inhibitors”:

1) 4.5 ml diH2O
2) 100ul 5M NaCl ([final]=100mM)
3) 250ul 1M Tris-HCl, pH 7.5 ([final]=50mM)

4) 50ul Triton X-100, Sigma #T-9284 ([final]=1%)
5) 50ul 0.1M Phenylmethylsulfonofluoride (PMSF) ([final]=1mM)
6) 50ul Sigma mammalian protease inhibitor cocktail (#P2714)

2. Vortex solution and chill extraction buffer on ice prior to use. Pre-chill on ice microcentrifuge tubes that will receive protein extracts.

3. Transfer embryos to fresh microfuge tube.

4. Using a P200, remove as much 0.1x MBS from embryos as possible without lysing embryos.

5. Add extraction buffer (10 ul per embryo). Pipette embryos and extraction buffer to lyse and homogenize samples.

6. Incubate “extraction with inhibitors” on ice for 15’. OPTIONAL: Add 1ul Antarctic phosphatase (5000U/ul) to “extraction without inhibitors” and incubate at 37^{o}C for 15’.

7. Pre-chill microfuge tubes on ice for final protein lysates.

8. Centrifuge protein extracts for 10’ at 14000xg at 4^{o}C.

9. Aspirate yolk from upper layer. Transfer supernatants to fresh pre-chilled microfuge tubes. Be careful to avoid pipetting the pelleted insoluble material. If necessary, centrifuge supernatant again to further purify fraction.

10. Wash pellet with Extraction Buffer (above) 3 times, resuspending pellet and centrifuging 10’ at 14000xg at 4^{o}C each time.

11. OPTIONAL: Resuspend pellet in syringe filter sterilized 10mM Tris pH9, 9.5M Urea, 1mM DTT, 2mM EDTA (10 ul per 1-3 embryos). Incubate on rocker for 3 hours.

12. OPTIONAL: Centrifuge 10’ at 20000xg at room temperature. Transfer supernatant to fresh tube labeled as Urea fraction.

13. Samples may be frozen at -80^{o}C, assayed for protein concentration, aliquoted for SDS/PAGE, and/or immunoprecipitated.

Appendix 2

Making mRNA for *Xenopus* Embryo Injection

Preparation of Template

1. **Linearize Plasmid DNA Template.**

   Do not use enzymes that generate a 3' overhang. (Not I is the enzyme most commonly used with the pCS2 vector)

   6ug plasmid

   5ul 10x CutSmart Buffer

   2ul restriction enzyme

   H_2O to 50 ul

   Digest at 37^oC for 1 hour.

   Run 2ul of digest on 0.8-1.0% agarose gel to check for complete linearization of DNA template. Gel purify template if digestion is incomplete or multiple fragments are expected.

2. **Extract and precipitate linearized DNA template.**

   Add 50ul H_2O to digest.

   Add 100ul phenol:chloroform:IAA. Vortex vigorously. Centrifuge 5min at 14 000xg.

   Remove upper aqueous phase (~100ul) to fresh tube.

Add 100ul chloroform. Vortex vigorously. Centrifuge 5min at 14000xg.

Remove upper aqueous phase (~100ul) to fresh tube.

Add 10ul 3M NaAcetate. Vortex. Add 275ul 100% EtOH.

Precipitate on dry ice for 30min or overnight at -20^{o}C.

Centrifuge at 14000xg for 10 min at 4^{o}C. Remove EtOH (to new tube if you do not see a pellet).

Add 100ul 70% EtOH to pellet. Centrifuge 5 min, 14000xg at 4^{o}C.

Remove EtOH and let pellet dry, ~5min @37^{o}C heat block.

***In Vitro* Transcription**

3. **Transcription Reaction**

Resuspend pellet in 6.5 ul nuclease-free H_2O.

Add the following reagents at room temperature in order:

5ul 5x transcription reaction buffer

5ul 10mM rATP

5ul 10mM rCTP

5ul 10mM rUTP

5ul **1mM rGTP**

5ul 10mM RNA Cap

1ul RNase Inhibitor

2.5ul SP6 RNA polymerase

Incubate at 40^{o}C for 30 minutes.

Add 1.25ul **10mM rGTP**. Incubate for addition 1 hour at 40^{o}C.

Add 0.5ul RNase Inhibitor and 2.5ul RQDNase1. Incubate 15 minutes at 37^{o}C.

4. **Remove free nucleotides (and digested DNA).**

Resuspend resin in column by vortexing.

Snap bottom off column.

Turn cap ¼ of turn. Place in capture tube.

Centrifuge at 700xg for 1 minute.

Transfer column to fresh microfuge tube.

Transfer transcription reaction mix directly to resin column. (Do not apply to sides of tube.)

Centrifuge at 700xg for 2 minutes.

RNA sample is now in microfuge tube.

5. **Extract and precipitate RNA.**

Add 50ul H_2O to RNA.

Add 100ul phenol:chloroform:IAA. Vortex vigorously. Centrifuge 5min at 14000xg.

Remove upper aqueous phase (~100ul) to fresh tube.

Add 100ul chloroform. Vortex vigorously. Centrifuge 5min at 14000xg.

Remove upper aqueous phase (~100ul) to fresh tube.

Add 10ul 3M NaAcetate. Vortex. Add 275ul 100% EtOH.

Precipitate on dry ice for 30min or overnight at -20^{o}C.

Centrifuge at 14000xg for 10 min at 4^{o}C. Remove EtOH (to new tube if you do not see a pellet).

Add 100ul 70% EtOH to pellet. Centrifuge 5 min, 14000xg at 4^{o}C.

Remove EtOH and let pellet air dry.

Resuspend pellet in 28ul nuclease-free H_2O.

6. Analysis

Dilute 1ul in 99ul H2O. Read OD260.

1 OD = 40ug/ml

OD260 x 100 x 40ug/ml = [RNA]

Future dilutions will be easier if you dilute the RNA to a concentration that is easily divisible, such as 1ug/ml or 0.5ug/ml.

Mix 2ul of RNA with 6ul H2O, 1ul 10% SDS, 1ul 10x DNA loading buffer. Run on 1% agarose gel to confirm quality of transcript. It should appear as a single band, not a smear.

Freeze RNA in small aliquots (2ul/tube) at -80^{o}C.

Appendix 3

Co-IP Protocol for Optimizing IP Efficiency

Keep all lysates on ice or at 4ºC for the duration of the experiment! Be careful not to warm lysates at any point. Make fresh lysis buffer daily. This method requires **3 days**. The following IP is based on an antibody that contains 5ug of IgG in 25ul; you must vary the amount of lysis buffer in the incubations to account for the volume of antibody you will need to include 5ug.

DAY 1- ANTIBODY-ANTIGEN PRECAPTURE

1. Create lysate for Co-IP using the standard lysis buffer (1% detergent of choice). The lysate should be derived using **at least 60 embryos** to ensure you will have enough protein.
2. Remove vial of Roche-G agarose beads from 4ºC and vortex well for 30 seconds. After vortexing, pipette mix the bead slurry in the vial using a p200 tip. This step is important to make sure that the beads mix into solution instead of clustering.
3. Immediately after pipette mixing, remove **50ul of agarose beads** and pipette into an autoclaved 1.5ml tube. Repeat this two more times for a total of three tubes (50ul beads in each). **Avoid bead settling** in the vial to pipette the same amount of beads consistently.

4. Centrifuge tubes at 3000g for 5 minutes (4ºC). Withdraw solution above the bead pellet carefully, either with a 1ml syringe or 200ul pipette tip. Discard solution. Be careful not to disturb the pellet.
5. Add 1ml of sterile MilliQ water to each tube. Centrifuge tubes at 3000g for 5 minutes (4ºC).
6. Withdraw solution above the bead pellet carefully with either a 1ml syringe or p200 tip without disturbing the bead pellet. Discard solution. **Make up each of the following solutions** in the separate bead tubes:

    I. 500ug Co-IP: 100ul Lysate (10 Embryos), 325ul fresh extraction buffer, 50ul beads.

    II. 2000ug Co-IP: 400ul Lysate (40 Embryos), 25ul fresh extraction buffer, 50ul beads.

    III. Lysis Buffer Only: 425ul fresh extraction buffer, 50ul beads.

7. Store remaining lysate at -80ºC.
8. Parafilm seal the tube lids. Rotate each of these tubes on an end-over-end rotator for **1 hour at 4ºC**.
9. Centrifuge tubes at 3000g for 5 minutes (4ºC). Withdraw solution above the bead pellet carefully, either with a 1ml syringe or 200ul pipette tip. **Keep each withdrawn solution on ice** in preparation for antibody incubation. Be careful not to disturb the pellet during supernatant removal.
10. Add 500ul fresh extraction buffer to each bead sample to **wash beads**. Rotate each of these tubes on an end-over-end rotator for **10 minutes at 4ºC**.

11. Centrifuge tubes at 3000g for 5 minutes (4ºC). Withdraw solution above the bead pellet carefully, either with a 1ml syringe or 200ul pipette tip. Discard solution. Be careful not to disturb the pellet during solution removal.
12. Repeat steps 9 and 10 two more times.
13. Add 25ul 2x sample buffer with BME to each bead sample. Vortex briefly and incubate samples at 100ºC for 5 minutes. Quickly vortex samples, spin briefly to pellet, and store the tubes at -80ºC as your **pre-clear samples**.
14. Add **5ug** of your primary antibody for immunoprecipitation to the tubes on ice containing solutions I, II, and III.
15. Parafilm seal the tube lids. Rotate each of these tubes on an end-over-end rotator overnight at 4ºC to **perform antibody-antigen capture** in the lysate.

DAY 2- SAMPLE Co-IP

16. Repeat steps 2-5 to prepare three more fresh 50ul bead tubes for Co-IP.
17. Withdraw the wash solution above the bead pellets carefully with either a 1ml syringe or p200 tip without disturbing the bead pellet. Discard wash solution.
18. Remove solutions 1, II, and III from the rotator at 4ºC. Spin solutions I, II, and III briefly to draw lysate off the tube lids and place them on ice. **Add solutions I, II, and III to the fresh bead tubes to make up each of the following Co-IP solutions**:

    I. 500ug Co-IP: 100ul Lysate (10 Embryos), 325ul fresh extraction buffer, 5ug antibody (25ul), 50ul fresh beads.

II. 2000ug Co-IP: 400ul Lysate (40 Embryos), 25ul fresh extraction buffer, 5ug antibody (25ul), 50ul fresh beads.

III. Lysis Buffer Only: 425ul fresh extraction buffer, 5ug antibody (25ul), 50ul fresh beads.

19. Parafilm seal the tube lids. Rotate each of these tubes on an end-over-end rotator overnight at 4^{o}C to **perform Co-IP**.

DAY 3- SAMPLE PREPARATION AND GEL RUNNING

20. Remove Co-IP solutions 1, II, and III from the rotator at 4^{o}C. Centrifuge solutions at 3000g for 5 minutes (4^{o}C).
21. Withdraw solution above the bead pellet carefully, either with a 1ml syringe or 200ul pipette tip. **Keep each withdrawn solution on ice** in preparation for creation of **supernatant samples**. Be careful not to disturb the pellet during supernatant removal.
22. Add 500ul fresh extraction buffer to each bead sample to **wash beads**. Rotate each of these tubes on an end-over-end rotator for **10 minutes at 4^{o}C**.
23. Centrifuge tubes at 3000g for 5 minutes (4^{o}C). Withdraw solution above the bead pellet carefully, either with a 1ml syringe or 200ul pipette tip. Discard solution. Be careful not to disturb the pellet during solution removal.
24. Repeat steps 22 and 23 two more times.
25. Add 25ul 2x sample buffer with BME to each bead sample. For your 500ug Co-IP supernatant sample, add 10ul of supernatant to 10ul 2x sample buffer with

BME. For your 2000ug Co-IP supernatant sample, add 2.5ul of supernatant to 2.5ul 2x sample buffer with BME. For your Lysate and Antibody only Co-IP supernatant sample, add 10ul of supernatant to 10ul 2x sample buffer with BME.

26. Remove pre-clear samples from -80^{o}C, thaw, and include with the rest of your samples. Vortex all samples briefly and incubate at 100^{o}C for 5 minutes. Quickly vortex samples, spin briefly to pellet, and run on a gel or store the tubes at -80^{o}C to run at a later time.
27. Use the following gel loading order:

Ladder - 500ug IP Preclear - 2000ug IP Preclear - Lysate Buffer Only IP Preclear - 500ug IP - 2000ug IP - Lysate

Buffer with Antibody IP - Supernatant 500ug IP - Supernatant 2000ug IP - Supernatant Lysate Buffer with Antibody IP

Bibliography

Acehan, D., Petzold, C., Gumper, I., Sabatini, D.D., Mueller, E.J., Cowin, P., and Stokes, D.L. (2008). Plakoglobin Is Required for Effective Intermediate Filament Anchorage to Desmosomes. J Invest Dermatol *128*, 2665-2675.

Aebi, U., Cohn, J., Buhle, L., and Gerace, L. (1986). The nuclear lamina is a meshwork of intermediate-type filaments. Nature *323*, 560-564.

Aitken, A. (2002). Functional specificity in 14-3-3 isoform interactions through dimer formation and phosphorylation. Chromosome location of mammalian isoforms and variants. Plant molecular biology *50*, 993-1010.

Aitken, A. (2011). Post-translational modification of 14-3-3 isoforms and regulation of cellular function. Semin Cell Dev Biol *22*, 673-680.

Aitken, A., Howell, S., Jones, D., Madrazo, J., and Patel, Y. (1995). 14-3-3 alpha and delta are the phosphorylated forms of raf-activating 14-3-3 beta and zeta. In vivo stoichiometric phosphorylation in brain at a Ser-Pro-Glu-Lys MOTIF. The Journal of biological chemistry *270*, 5706-5709.

Alam, H., Gangadaran, P., Bhate, A.V., Chaukar, D.A., Sawant, S.S., Tiwari, R., Bobade, J., Kannan, S., D'Cruz A, K., Kane, S.*, et al.* (2011). Loss of keratin 8 phosphorylation leads to increased tumor progression and correlates with clinico-pathological parameters of OSCC patients. PLoS One *6*, e27767.

Amaya, E., Alarcon, L., Martin-Tapia, D., Cuellar-Perez, F., Cano-Cortina, M., Ortega-Olvera, J.M., Cisneros, B., Rodriguez, A.J., Gamba, G., and Gonzalez-Mariscal, L. (2019). Activation of the Ca(2+) sensing receptor and the PKC/WNK4 downstream signaling cascade induces incorporation of ZO-2 to tight junctions and its separation from 14-3-3. Mol Biol Cell, mbcE18090591.

Ameen, N.A., Figueroa, Y., and Salas, P.J. (2001). Anomalous apical plasma membrane phenotype in CK8-deficient mice indicates a novel role for intermediate filaments in the polarization of simple epithelia. J Cell Sci *114*, 563-575.

Astbury William, T., Woods, H.J., and Bragg William, L. (1933). X-Ray studies of the structure of hair, wool, and related fibres. II.- the molecular structure and elastic properties of hair keratin. Philosophical Transactions of the Royal Society of London Series A, Containing Papers of a Mathematical or Physical Character *232*, 333-394.

Ausmees, N., Kuhn, J.R., and Jacobs-Wagner, C. (2003). The bacterial cytoskeleton: an intermediate filament-like function in cell shape. Cell *115*, 705-713.

Bader, B.L., Magin, T.M., Freudenmann, M., Stumpp, S., and Franke, W.W. (1991). Intermediate filaments formed de novo from tail-less cytokeratins in the cytoplasm and in the nucleus. The Journal of cell biology *115*, 1293-1307.

Balin, B.J., and Lee, V.M. (1991). Individual neurofilament subunits reassembled in vitro exhibit unique biochemical, morphological and immunological properties. Brain research *556*, 196-208.

Bar, H., Schopferer, M., Sharma, S., Hochstein, B., Mucke, N., Herrmann, H., and Willenbacher, N. (2010). Mutations in desmin's carboxy-terminal "tail" domain severely modify filament and network mechanics. J Mol Biol *397*, 1188-1198.

Bar, J., Kumar, V., Roth, W., Schwarz, N., Richter, M., Leube, R.E., and Magin, T.M. (2014). Skin fragility and impaired desmosomal adhesion in mice lacking all keratins. The Journal of investigative dermatology *134*, 1012-1022.

Baribault, H., Penner, J., Iozzo, R.V., and Wilson-Heiner, M. (1994). Colorectal hyperplasia and inflammation in keratin 8-deficient FVB/N mice. Genes Dev *8*, 2964-2973.

Baribault, H., Price, J., Miyai, K., and Oshima, R.G. (1993). Mid-gestational lethality in mice lacking keratin 8. Genes Dev *7*, 1191-1202.

Bartel, M., Schafer, A., Stevers, L.M., and Ottmann, C. (2014). Small molecules, peptides and natural products: getting a grip on 14-3-3 protein-protein modulation. Future medicinal chemistry *6*, 903-921.

Basu, S., Totty, N.F., Irwin, M.S., Sudol, M., and Downward, J. (2003). Akt phosphorylates the Yes-associated protein, YAP, to induce interaction with 14-3-3 and attenuation of p73-mediated apoptosis. Molecular cell *11*, 11-23.

Bendit, E.G. (1960). A Quantitative X-Ray Diffraction Study of the Alpha-Beta Transformation in Wool Keratin. Textile Research Journal *30*, 547-555.

Benzinger, A., Popowicz, G.M., Joy, J.K., Majumdar, S., Holak, T.A., and Hermeking, H. (2005). The crystal structure of the non-liganded 14-3-3sigma protein: insights into determinants of isoform specific ligand binding and dimerization. Cell research *15*, 219-227.

Blom, N., Gammeltoft, S., and Brunak, S. (1999). Sequence and structure-based prediction of eukaryotic protein phosphorylation sites. J Mol Biol *294*, 1351-1362.

Blom, N., Sicheritz-Ponten, T., Gupta, R., Gammeltoft, S., and Brunak, S. (2004). Prediction of post-translational glycosylation and phosphorylation of proteins from the amino acid sequence. Proteomics *4*, 1633-1649.

Bornslaeger, E.A., Corcoran, C.M., Stappenbeck, T.S., and Green, K.J. (1996). Breaking the connection: displacement of the desmosomal plaque protein desmoplakin from cell-cell interfaces disrupts anchorage of intermediate filament bundles and alters intercellular junction assembly. The Journal of cell biology *134*, 985-1001.

Boudreau, A., Tanner, K., Wang, D., Geyer, F.C., Reis-Filho, J.S., and Bissell, M.J. (2013). 14-3-3sigma stabilizes a complex of soluble actin and intermediate filament to enable breast tumor invasion. Proceedings of the National Academy of Sciences of the United States of America *110*, E3937-3944.

Braselmann, S., and McCormick, F. (1995). Bcr and Raf form a complex in vivo via 14-3-3 proteins. The EMBO journal *14*, 4839-4848.

Briggs, J.A., Weinreb, C., Wagner, D.E., Megason, S., Peshkin, L., Kirschner, M.W., and Klein, A.M. (2018). The dynamics of gene expression in vertebrate embryogenesis at single-cell resolution. Science *360*, eaar5780.

Brulet, P., Babinet, C., Kemler, R., and Jacob, F. (1980). Monoclonal antibodies against trophectoderm-specific markers during mouse blastocyst formation. Proceedings of the National Academy of Sciences of the United States of America *77*, 4113-4117.

Bunney, T.D., De Boer, A.H., and Levin, M. (2003). Fusicoccin signaling reveals 14-3-3 protein function as a novel step in left-right patterning during amphibian embryogenesis. Development *130*, 4847-4858.

Burkhard, P., Stetefeld, J., and Strelkov, S.V. (2001). Coiled coils: a highly versatile protein folding motif. Trends Cell Biol *11*, 82-88.

Busch, T., Armacki, M., Eiseler, T., Joodi, G., Temme, C., Jansen, J., von Wichert, G., Omary, M.B., Spatz, J., and Seufferlein, T. (2012). Keratin 8 phosphorylation regulates keratin reorganization and migration of epithelial tumor cells. J Cell Sci *125*, 2148-2159.

Celis, J.E., Gesser, B., Rasmussen, H.H., Madsen, P., Leffers, H., Dejgaard, K., Honore, B., Olsen, E., Ratz, G., Lauridsen, J.B., *et al.* (1990). Comprehensive two-dimensional gel protein databases offer a global approach to the analysis of human cells: the transformed amnion cells (AMA) master database and its link to genome DNA sequence data. Electrophoresis *11*, 989-1071.

Chan, Y., Anton-Lamprecht, I., Yu, Q.C., Jackel, A., Zabel, B., Ernst, J.P., and Fuchs, E. (1994). A human keratin 14 "knockout": the absence of K14 leads to severe epidermolysis bullosa simplex and a function for an intermediate filament protein. Genes Dev *8*, 2574-2587.

Chang, H.C., and Rubin, G.M. (1997). 14-3-3 epsilon positively regulates Ras-mediated signaling in Drosophila. Genes Dev *11*, 1132-1139.

Chang, L., and Goldman, R.D. (2004). Intermediate filaments mediate cytoskeletal crosstalk. Nat Rev Mol Cell Biol *5*, 601-613.

Chen, Y., Guldiken, N., Spurny, M., Mohammed, H.H., Haybaeck, J., Pollheimer, M.J., Fickert, P., Gassler, N., Jeon, M.K., Trautwein, C.*, et al.* (2015). Loss of keratin 19 favours the development of cholestatic liver disease through decreased ductular reaction. The Journal of pathology *237*, 343-354.

Chernyatina, A.A., Nicolet, S., Aebi, U., Herrmann, H., and Strelkov, S.V. (2012). Atomic structure of the vimentin central alpha-helical domain and its implications for intermediate filament assembly. Proceedings of the National Academy of Sciences of the United States of America *109*, 13620-13625.

Cheung, K.J., Gabrielson, E., Werb, Z., and Ewald, A.J. (2013). Collective invasion in breast cancer requires a conserved basal epithelial program. Cell *155*, 1639-1651.

Colakoglu, G., and Brown, A. (2009). Intermediate filaments exchange subunits along their length and elongate by end-to-end annealing. The Journal of cell biology *185*, 769-777.

Conway, D.E., Breckenridge, M.T., Hinde, E., Gratton, E., Chen, C.S., and Schwartz, M.A. (2013). Fluid shear stress on endothelial cells modulates mechanical tension across VE-cadherin and PECAM-1. Current biology : CB *23*, 1024-1030.

Conway, J.F., and Parry, D.A.D. (1988). Intermediate filament structure: 3. Analysis of sequence homologies. International Journal of Biological Macromolecules *10*, 79-98.

Cornell, B., and Toyo-Oka, K. (2017). 14-3-3 Proteins in Brain Development: Neurogenesis, Neuronal Migration and Neuromorphogenesis. Frontiers in molecular neuroscience *10*, 318.

Coulombe, P.A., and Fuchs, E. (1990). Elucidating the early stages of keratin filament assembly. The Journal of cell biology *111*, 153-169.

Crewther, W.G., Dowling, L.M., Steinert, P.M., and Parry, D.A.D. (1983). Structure of intermediate filaments. International Journal of Biological Macromolecules *5*, 267-274.

Crick, F.H. (1952). Is alpha-keratin a coiled coil? Nature *170*, 882-883.

Crick, F. H.(1953). The packing of α-helices: simple coiled-coils. *Acta Cryst, 6,* 689-697.

Culkins, C.C., and Setzer, S.V. (2007). Spotting desmosomes: the first 100 years. The Journal of investigative dermatology *127*, E2-3.

Cutler, S.R., Ehrhardt, D.W., Griffitts, J.S., and Somerville, C.R. (2000). Random GFP::cDNA fusions enable visualization of subcellular structures in cells of Arabidopsis at a high frequency. Proceedings of the National Academy of Sciences of the United States of America *97*, 3718-3723.

Darling, D.L., Yingling, J., and Wynshaw-Boris, A. (2005). Role of 14-3-3 proteins in eukaryotic signaling and development. Current topics in developmental biology *68*, 281-315.

Davidson, L.A., Hoffstrom, B.G., Keller, R., and DeSimone, D.W. (2002). Mesendoderm extension and mantle closure in Xenopus laevis gastrulation: combined roles for integrin alpha(5)beta(1), fibronectin, and tissue geometry. Developmental biology *242*, 109-129.

Davidson, L.A., Keller, R., and DeSimone, D. (2004). Patterning and tissue movements in a novel explant preparation of the marginal zone of Xenopus laevis. Gene expression patterns : GEP *4*, 457-466.

Deng, M., Zhang, W., Tang, H., Ye, Q., Liao, Q., Zhou, Y., Wu, M., Xiong, W., Zheng, Y., Guo, X.*, et al.* (2013). Lactotransferrin acts as a tumor suppressor in nasopharyngeal carcinoma by repressing AKT through multiple mechanisms. Oncogene *32*, 4273-4283.

Dobson, M., Ramakrishnan, G., Ma, S., Kaplun, L., Balan, V., Fridman, R., and Tzivion, G. (2011). Bimodal regulation of FoxO3 by AKT and 14-3-3. Biochimica et biophysica acta *1813*, 1453-1464.

Dowling, L.M., Crewther, W.G., and Parry, D.A. (1986). Secondary structure of component 8c-1 of alpha-keratin. An analysis of the amino acid sequence. The Biochemical journal *236*, 705-712.

Duckworth, B.C., Weaver, J.S., and Ruderman, J.V. (2002). G2 arrest in Xenopus oocytes depends on phosphorylation of cdc25 by protein kinase A. Proceedings of the National Academy of Sciences of the United States of America *99*, 16794-16799.

Dumaz, N., and Marais, R. (2003). Protein kinase A blocks Raf-1 activity by stimulating 14-3-3 binding and blocking Raf-1 interaction with Ras. The Journal of biological chemistry *278*, 29819-29823.

Erber, A., Riemer, D., Bovenschulte, M., and Weber, K. (1998). Molecular phylogeny of metazoan intermediate filament proteins. J Mol Evol *47*, 751-762.

Fedoroff, S., White, R., Neal, J., Subrahmanyan, L., and Kalnins, V.I. (1983). Astrocyte cell lineage. II. Mouse fibrous astrocytes and reactive astrocytes in cultures have vimentin- and GFP-containing intermediate filaments. Brain research *283*, 303-315.

Feick, P., Foisner, R., and Wiche, G. (1991). Immunolocalization and molecular properties of a high molecular weight microtubule-bundling protein (syncolin) from chicken erythrocytes. The Journal of cell biology *112*, 689-699.

Ferrera, D., Canale, C., Marotta, R., Mazzaro, N., Gritti, M., Mazzanti, M., Capellari, S., Cortelli, P., and Gasparini, L. (2014). Lamin B1 overexpression increases nuclear rigidity in autosomal dominant leukodystrophy fibroblasts. FASEB journal : official publication of the Federation of American Societies for Experimental Biology *28*, 3906-3918.

Fisher, D.Z., Chaudhary, N., and Blobel, G. (1986). cDNA sequencing of nuclear lamins A and C reveals primary and secondary structural homology to intermediate filament proteins. Proceedings of the National Academy of Sciences of the United States of America *83*, 6450-6454.

Fliegner, K.H., Ching, G.Y., and Liem, R.K. (1990). The predicted amino acid sequence of alpha-internexin is that of a novel neuronal intermediate filament protein. The EMBO journal *9*, 749-755.

Flitney, E.W., Kuczmarski, E.R., Adam, S.A., and Goldman, R.D. (2009). Insights into the mechanical properties of epithelial cells: the effects of shear stress on the assembly and remodeling of keratin intermediate filaments. FASEB journal : official publication of the Federation of American Societies for Experimental Biology *23*, 2110-2119.

Fois, G., Weimer, M., Busch, T., Felder, E.T., Oswald, F., von Wichert, G., Seufferlein, T., Dietl, P., and Felder, E. (2013). Effects of keratin phosphorylation on the mechanical properties of keratin filaments in living cells. FASEB journal : official publication of the Federation of American Societies for Experimental Biology *27*, 1322-1329.

Fradette, J., Germain, L., Seshaiah, P., and Coulombe, P.A. (1998). The type I keratin 19 possesses distinct and context-dependent assembly properties. The Journal of biological chemistry *273*, 35176-35184.

Franke, W.W. (2009). Discovering the molecular components of intercellular junctions--a historical view. Cold Spring Harb Perspect Biol *1*, a003061.

Franke, W.W., Goldschmidt, M.D., Zimbelmann, R., Mueller, H.M., Schiller, D.L., and Cowin, P. (1989). Molecular cloning and amino acid sequence of human plakoglobin, the common junctional plaque protein. Proceedings of the National Academy of Sciences of the United States of America *86*, 4027-4031.

Franke, W.W., Schmid, E., Grund, C., MÜLler, H., Engelbrecht, I., Moll, R., Stadler, J., and Jarasch, E.-D. (1981). Antibodies to High Molecular Weight Polypeptides of Desmosomes: Specific Localization of a Class of Junctional Proteins in Cells and Tissues. Differentiation *20*, 217-241.

Franke, W.W., Schmid, E., Osborn, M., and Weber, K. (1978). Different intermediate-sized filaments distinguished by immunofluorescence microscopy. Proceedings of the National Academy of Sciences of the United States of America *75*, 5034-5038.

Franz, J.K., Gall, L., Williams, M.A., Picheral, B., and Franke, W.W. (1983). Intermediate-size filaments in a germ cell: Expression of cytokeratins in oocytes and eggs of the frog Xenopus. Proceedings of the National Academy of Sciences of the United States of America *80*, 6254-6258.

Ganguly, S., Weller, J.L., Ho, A., Chemineau, P., Malpaux, B., and Klein, D.C. (2005). Melatonin synthesis: 14-3-3-dependent activation and inhibition of arylalkylamine N-acetyltransferase mediated by phosphoserine-205. Proceedings of the National Academy of Sciences of the United States of America *102*, 1222-1227.

Geerts, D., Fontao, L., Nievers, M.G., Schaapveld, R.Q., Purkis, P.E., Wheeler, G.N., Lane, E.B., Leigh, I.M., and Sonnenberg, A. (1999). Binding of integrin alpha6beta4 to plectin prevents plectin association with F-actin but does not interfere with intermediate filament binding. The Journal of cell biology *147*, 417-434.

Geisler, N., Kaufmann, E., and Weber, K. (1982a). Proteinchemical characterization of three structurally distinct domains along the protofilament unit of desmin 10 nm filaments. Cell *30*, 277-286.

Geisler, N., Plessmann, U., and Weber, K. (1982b). Related amino acid sequences in neurofilaments and non-neural intermediate filaments. Nature *296*, 448-450.

Geisler, N., Plessmann, U., and Weber, K. (1985). The complete amino acid sequence of the major mammalian neurofilament protein (NF-L). FEBS letters *182*, 475-478.

Geisler, N., Schunemann, J., and Weber, K. (1992). Chemical cross-linking indicates a staggered and antiparallel protofilament of desmin intermediate filaments and characterizes one higher-level complex between protofilaments. European journal of biochemistry *206*, 841-852.

Geisler, N., and Weber, K. (1981). Comparison of the proteins of two immunologically distinct intermediate-sized filaments by amino acid sequence analysis: desmin and vimentin. Proceedings of the National Academy of Sciences of the United States of America *78*, 4120-4123.

Geisler, N., and Weber, K. (1982). The amino acid sequence of chicken muscle desmin provides a common structural model for intermediate filament proteins. The EMBO journal *1*, 1649-1656.

Gerace, L. (1986). Nuclear lamina and organization of nuclear architecture. Trends BiochemSci *11*, 443-446.

Gerace, L., and Blobel, G. (1980). The nuclear envelope lamina is reversibly depolymerized during mitosis. Cell *19*, 277-287.

Goldberg, M.W., Huttenlauch, I., Hutchison, C.J., and Stick, R. (2008). Filaments made from A- and B-type lamins differ in structure and organization. J Cell Sci *121*, 215-225.

Goldman, R.D., Khuon, S., Chou, Y.H., Opal, P., and Steinert, P.M. (1996). The function of intermediate filaments in cell shape and cytoskeletal integrity. The Journal of cell biology *134*, 971-983.

Gorbsky, G., Cohen, S.M., Shida, H., Giudice, G.J., and Steinberg, M.S. (1985). Isolation of the non-glycosylated proteins of desmosomes and immunolocalization of a third plaque protein: desmoplakin III. Proceedings of the National Academy of Sciences of the United States of America *82*, 810-814.

Gounari, F., Merdes, A., Quinlan, R., Hess, J., FitzGerald, P.G., Ouzounis, C.A., and Georgatos, S.D. (1993). Bovine filensin possesses primary and secondary structure similarity to intermediate filament proteins. The Journal of cell biology *121*, 847-853.

Granger, B.L., Repasky, E.A., and Lazarides, E. (1982). Synemin and vimentin are components of intermediate filaments in avian erythrocytes. The Journal of cell biology *92*, 299-312.

Green, K.J., Parry, D.A., Steinert, P.M., Virata, M.L., Wagner, R.M., Angst, B.D., and Nilles, L.A. (1990). Structure of the human desmoplakins. Implications for function in the desmosomal plaque. The Journal of biological chemistry *265*, 2603-2612.

Green, K.J., Stappenbeck, T.S., Parry, D.A., and Virata, M.L. (1992). Structure of desmoplakin and its association with intermediate filaments. The Journal of dermatology *19*, 765-769.

Guo, L., Degenstein, L., Dowling, J., Yu, Q.C., Wollmann, R., Perman, B., and Fuchs, E. (1995). Gene targeting of BPAG1: abnormalities in mechanical strength and cell migration in stratified epithelia and neurologic degeneration. Cell *81*, 233-243.

Guzman, C., Jeney, S., Kreplak, L., Kasas, S., Kulik, A.J., Aebi, U., and Forro, L. (2006). Exploring the mechanical properties of single vimentin intermediate filaments by atomic force microscopy. J Mol Biol *360*, 623-630.

Hanada, S., Harada, M., Kumemura, H., Omary, M.B., Kawaguchi, T., Taniguchi, E., Koga, H., Yoshida, T., Maeyama, M., Baba, S.*, et al.* (2005). Keratin-containing inclusions affect cell morphology and distribution of cytosolic cellular components. Exp Cell Res *304*, 471-482.

Hanukoglu, I., and Fuchs, E. (1982). The cDNA sequence of a human epidermal keratin: divergence of sequence but conservation of structure among intermediate filament proteins. Cell *31*, 243-252.

Hanukoglu, I., and Fuchs, E. (1983). The cDNA sequence of a Type II cytoskeletal keratin reveals constant and variable structural domains among keratins. Cell *33*, 915-924.

Hatzfeld, M., and Burba, M. (1994). Function of type I and type II keratin head domains: their role in dimer, tetramer and filament formation. J Cell Sci *107 (Pt 7)*, 1959-1972.

Hatzfeld, M., Kristjansson, G.I., Plessmann, U., and Weber, K. (1994). Band 6 protein, a major constituent of desmosomes from stratified epithelia, is a

novel member of the armadillo multigene family. J Cell Sci *107 (Pt 8)*, 2259-2270.

Hatzfeld, M., and Weber, K. (1990a). The coiled coil of in vitro assembled keratin filaments is a heterodimer of type I and II keratins: use of site-specific mutagenesis and recombinant protein expression. The Journal of cell biology *110*, 1199-1210.

Hatzfeld, M., and Weber, K. (1990b). Tailless keratins assemble into regular intermediate filaments in vitro. J Cell Sci *97 (Pt 2)*, 317-324.

Hatzfeld, M., and Weber, K. (1992). A synthetic peptide representing the consensus sequence motif at the carboxy-terminal end of the rod domain inhibits intermediate filament assembly and disassembles preformed filaments. The Journal of cell biology *116*, 157-166.

Heasman, J., Ginsberg, D., Geiger, B., Goldstone, K., Pratt, T., Yoshida-Noro, C., and Wylie, C. (1994). A functional test for maternally inherited cadherin in Xenopus shows its importance in cell adhesion at the blastula stage. Development *120*, 49-57.

Heasman, J., Torpey, N., and Wylie, C. (1992). The role of intermediate filaments in early Xenopus development studied by antisense depletion of maternal mRNA. Development (Cambridge, England) Supplement, 119-125.

Heins, S., Wong, P.C., Müller, S., Goldie, K., Cleveland, D.W., and Aebi, U. (1993). The rod domain of NF-L determines neurofilament architecture, whereas the end domains specify filament assembly and network formation. The Journal of cell biology *123*, 1517.

Heitlinger, E., Peter, M., Haner, M., Lustig, A., Aebi, U., and Nigg, E.A. (1991). Expression of chicken lamin B2 in Escherichia coli: characterization of its structure, assembly, and molecular interactions. The Journal of cell biology *113*, 485-495.

Helfand, B.T., Chang, L., and Goldman, R.D. (2003). The dynamic and motile properties of intermediate filaments. Annu Rev Cell Dev Biol *19*, 445-467.

Helfand, B.T., Mikami, A., Vallee, R.B., and Goldman, R.D. (2002). A requirement for cytoplasmic dynein and dynactin in intermediate filament network assembly and organization. The Journal of cell biology *157*, 795-806.

Helmke, B.P., Goldman, R.D., and Davies, P.F. (2000). Rapid displacement of vimentin intermediate filaments in living endothelial cells exposed to flow. Circulation research *86*, 745-752.

Herrmann, H., and Aebi, U. (1998). Intermediate filament assembly: fibrillogenesis is driven by decisive dimer-dimer interactions. Current opinion in structural biology *8*, 177-185.

Herrmann, H., and Aebi, U. (2004). Intermediate filaments: molecular structure, assembly mechanism, and integration into functionally distinct intracellular Scaffolds. Annu Rev Biochem *73*, 749-789.

Herrmann, H., Haner, M., Brettel, M., Ku, N.O., and Aebi, U. (1999). Characterization of distinct early assembly units of different intermediate filament proteins. J Mol Biol *286*, 1403-1420.

Herrmann, H., Haner, M., Brettel, M., Muller, S.A., Goldie, K.N., Fedtke, B., Lustig, A., Franke, W.W., and Aebi, U. (1996). Structure and assembly properties of the intermediate filament protein vimentin: The role of its head, rod and tail domains. J Mol Biol *264*, 933-953.

Herrmann, H., Hesse, M., Reichenzeller, M., Aebi, U., and Magin, T.M. (2003). Functional complexity of intermediate filament cytoskeletons: from structure to assembly to gene ablation. International review of cytology *223*, 83-175.

Herrmann, H., Strelkov, S.V., Burkhard, P., and Aebi, U. (2009). Intermediate filaments: primary determinants of cell architecture and plasticity. J Clin Invest *119*, 1772-1783.

Herrmann, H., Strelkov, S.V., Feja, B., Rogers, K.R., Brettel, M., Lustig, A., Haner, M., Parry, D.A., Steinert, P.M., Burkhard, P.*, et al.* (2000). The intermediate filament protein consensus motif of helix 2B: its atomic structure and contribution to assembly. J Mol Biol *298*, 817-832.

Hesse, M., Franz, T., Tamai, Y., Taketo, M.M., and Magin, T.M. (2000). Targeted deletion of keratins 18 and 19 leads to trophoblast fragility and early embryonic lethality. The EMBO journal *19*, 5060-5070.

Hesse, M., Magin, T.M., and Weber, K. (2001). Genes for intermediate filament proteins and the draft sequence of the human genome: novel keratin genes and a surprisingly high number of pseudogenes related to keratin genes 8 and 18. J Cell Sci *114*, 2569-2575.

Hirokawa, N., Glicksman, M.A., and Willard, M.B. (1984). Organization of mammalian neurofilament polypeptides within the neuronal cytoskeleton. The Journal of cell biology *98*, 1523-1536.

Hisanaga, S.-i., and Hirokawa, N. (1988). Structure of the peripheral domains of neurofilaments revealed by low angle rotary shadowing. J Mol Biol *202*, 297-305.

Hoffman, P.N., and Lasek, R.J. (1975). The slow component of axonal transport. Identification of major structural polypeptides of the axon and their generality among mammalian neurons. The Journal of cell biology *66*, 351-366.

Hofmann, I., and Franke, W.W. (1997). Heterotypic interactions and filament assembly of type I and type II cytokeratins in vitro: viscometry and determinations of relative affinities. Eur J Cell Biol *72*, 122-132.

Hogervorst, F., Admiraal, L.G., Niessen, C., Kuikman, I., Janssen, H., Daams, H., and Sonnenberg, A. (1993). Biochemical characterization and tissue distribution of the A and B variants of the integrin alpha 6 subunit. The Journal of cell biology *121*, 179-191.

Hookway, C., Ding, L., Davidson, M.W., Rappoport, J.Z., Danuser, G., and Gelfand, V.I. (2015). Microtubule-dependent transport and dynamics of vimentin intermediate filaments. Mol Biol Cell *26*, 1675-1686.

Hopkinson, S.B., and Jones, J.C. (2000). The N terminus of the transmembrane protein BP180 interacts with the N-terminal domain of BP230, thereby

mediating keratin cytoskeleton anchorage to the cell surface at the site of the hemidesmosome. Mol Biol Cell *11*, 277-286.

Ichimura, T., Isobe, T., Okuyama, T., Takahashi, N., Araki, K., Kuwano, R., and Takahashi, Y. (1988). Molecular cloning of cDNA coding for brain-specific 14-3-3 protein, a protein kinase-dependent activator of tyrosine and tryptophan hydroxylases. Proceedings of the National Academy of Sciences of the United States of America *85*, 7084-7088.

Ichimura, T., Isobe, T., Okuyama, T., Yamauchi, T., and Fujisawa, H. (1987). Brain 14-3-3 protein is an activator protein that activates tryptophan 5-monooxygenase and tyrosine 3-monooxygenase in the presence of Ca2+,calmodulin-dependent protein kinase II. FEBS letters *219*, 79-82.

Ichimura, T., Wakamiya-Tsuruta, A., Itagaki, C., Taoka, M., Hayano, T., Natsume, T., and Isobe, T. (2002). Phosphorylation-dependent interaction of kinesin light chain 2 and the 14-3-3 protein. Biochemistry *41*, 5566-5572.

Ishikawa, H., Bischoff, R., and Holtzer, H. (1968). MITOSIS AND INTERMEDIATE-SIZED FILAMENTS IN DEVELOPING SKELETAL MUSCLE. The Journal of cell biology *38*, 538.

Jackson, B.W., Grund, C., Schmid, E., BÜRki, K., Franke, W.W., and Illmensee, K. (1980). Formation of Cytoskeletal Elements During Mouse Embryogenesis: Intermediate Filaments of the Cytokeratin Type and Desmosomes in Preimplantation Embryos. Differentiation *17*, 161-179.

Janmey, P.A., Euteneuer, U., Traub, P., and Schliwa, M. (1991). Viscoelastic properties of vimentin compared with other filamentous biopolymer networks. The Journal of cell biology *113*, 155-160.

Jin, J., Smith, F.D., Stark, C., Wells, C.D., Fawcett, J.P., Kulkarni, S., Metalnikov, P., O'Donnell, P., Taylor, P., Taylor, L.*, et al.* (2004). Proteomic, functional, and domain-based analysis of in vivo 14-3-3 binding proteins involved in cytoskeletal regulation and cellular organization. Current biology : CB *14*, 1436-1450.

Johnson, C., Crowther, S., Stafford, M.J., Campbell, D.G., Toth, R., and MacKintosh, C. (2010). Bioinformatic and experimental survey of 14-3-3-binding sites. Biochem J *427*, 69-78.

Jones, D.H., Ley, S., and Aitken, A. (1995). Isoforms of 14-3-3 protein can form homo- and heterodimers in vivo and in vitro: implications for function as adapter proteins. FEBS letters *368*, 55-58.

Ju, J.H., Oh, S., Lee, K.M., Yang, W., Nam, K.S., Moon, H.G., Noh, D.Y., Kim, C.G., Park, G., Park, J.B.*, et al.* (2015). Cytokeratin19 induced by HER2/ERK binds and stabilizes HER2 on cell membranes. Cell death and differentiation *22*, 665-676.

Karantza, V. (2011). Keratins in health and cancer: more than mere epithelial cell markers. Oncogene *30*, 127-138.

Kasahara, K., Kartasova, T., Ren, X.Q., Ikuta, T., Chida, K., and Kuroki, T. (1993). Hyperphosphorylation of keratins by treatment with okadaic acid of BALB/MK-2 mouse keratinocytes. The Journal of biological chemistry *268*, 23531-23537.

Keller, R., Davidson, L., Edlund, A., Elul, T., Ezin, M., Shook, D., and Skoglund, P. (2000). Mechanisms of convergence and extension by cell intercalation. Philosophical transactions of the Royal Society of London Series B, Biological sciences *355*, 897-922.

Kelly, D.E. (1966). Fine structure of desmosomes. , hemidesmosomes, and an adepidermal globular layer in developing newt epidermis. The Journal of cell biology *28*, 51-72.

Kim, S., and Coulombe, P.A. (2007). Intermediate filament scaffolds fulfill mechanical, organizational, and signaling functions in the cytoplasm. Genes Dev *21*, 1581-1597.

Kim, S., Wong, P., and Coulombe, P.A. (2006). A keratin cytoskeletal protein regulates protein synthesis and epithelial cell growth. Nature *441*, 362-365.

Kirmse, R., Portet, S., Mucke, N., Aebi, U., Herrmann, H., and Langowski, J. (2007). A quantitative kinetic model for the in vitro assembly of intermediate filaments from tetrameric vimentin. J Biol Chem *282*, 18563-18572.

Klymkowsky, M.W., Maynell, L.A., and Polson, A.G. (1987). Polar asymmetry in the organization of the cortical cytokeratin system of Xenopus laevis oocytes and embryos. Development *100*, 543-557.

Klymkowsky, M.W., Shook, D.R., and Maynell, L.A. (1992). Evidence that the deep keratin filament systems of the Xenopus embryo act to ensure normal gastrulation. Proceedings of the National Academy of Sciences of the United States of America *89*, 8736-8740.

Koch, P.J., Goldschmidt, M.D., Walsh, M.J., Zimbelmann, R., Schmelz, M., and Franke, W.W. (1991). Amino acid sequence of bovine muzzle epithelial desmocollin derived from cloned cDNA: A novel subtype of desmosomal cadherins. Differentiation *47*, 29-36.

Koch, P.J., Walsh, M.J., Schmelz, M., Goldschmidt, M.D., Zimbelmann, R., and Franke, W.W. (1990). Identification of desmoglein, a constitutive desmosomal glycoprotein, as a member of the cadherin family of cell adhesion molecules. Eur J Cell Biol *53*, 1-12.

Kockel, L., Vorbruggen, G., Jackle, H., Mlodzik, M., and Bohmann, D. (1997). Requirement for Drosophila 14-3-3 zeta in Raf-dependent photoreceptor development. Genes Dev *11*, 1140-1147.

Kolb, T., Maass, K., Hergt, M., Aebi, U., and Herrmann, H. (2011). Lamin A and lamin C form homodimers and coexist in higher complex forms both in the nucleoplasmic fraction and in the lamina of cultured human cells. Nucleus (Austin, Tex) *2*, 425-433.

Kolsch, A., Windoffer, R., and Leube, R.E. (2009). Actin-dependent dynamics of keratin filament precursors. Cell motility and the cytoskeleton *66*, 976-985.

Kolsch, A., Windoffer, R., Wurflinger, T., Aach, T., and Leube, R.E. (2010). The keratin-filament cycle of assembly and disassembly. J Cell Sci *123*, 2266-2272.

Kreplak, L., Bar, H., Leterrier, J.F., Herrmann, H., and Aebi, U. (2005). Exploring the mechanical behavior of single intermediate filaments. J Mol Biol *354*, 569-577.

Kreplak, L., Doucet, J., Dumas, P., and Briki, F. (2004). New Aspects of the α-Helix to β-Sheet Transition in Stretched Hard α-Keratin Fibers. Biophysical Journal *87*, 640-647.

Kreplak, L., Herrmann, H., and Aebi, U. (2008). Tensile properties of single desmin intermediate filaments. Biophys J *94*, 2790-2799.

Kroger, C., Loschke, F., Schwarz, N., Windoffer, R., Leube, R.E., and Magin, T.M. (2013). Keratins control intercellular adhesion involving PKC-alpha-mediated desmoplakin phosphorylation. The Journal of cell biology *201*, 681-692.

Ku, N.O., Gish, R., Wright, T.L., and Omary, M.B. (2001). Keratin 8 mutations in patients with cryptogenic liver disease. The New England journal of medicine *344*, 1580-1587.

Ku, N.O., Liao, J., and Omary, M.B. (1998). Phosphorylation of human keratin 18 serine 33 regulates binding to 14-3-3 proteins. Embo J *17*, 1892-1906.

Ku, N.O., Michie, S., Resurreccion, E.Z., Broome, R.L., and Omary, M.B. (2002). Keratin binding to 14-3-3 proteins modulates keratin filaments and hepatocyte mitotic progression. Proceedings of the National Academy of Sciences of the United States of America *99*, 4373-4378.

Ku, N.O., and Omary, M.B. (2000). Keratins turn over by ubiquitination in a phosphorylation-modulated fashion. The Journal of cell biology *149*, 547-552.

Ku, N.O., and Omary, M.B. (2006). A disease- and phosphorylation-related nonmechanical function for keratin 8. The Journal of cell biology *174*, 115-125.

Ku, N.O., Toivola, D.M., Strnad, P., and Omary, M.B. (2010). Cytoskeletal keratin glycosylation protects epithelial tissue from injury. Nature cell biology *12*, 876-885.

Ku, N.O., Wright, T.L., Terrault, N.A., Gish, R., and Omary, M.B. (1997). Mutation of human keratin 18 in association with cryptogenic cirrhosis. The Journal of clinical investigation *99*, 19-23.

Kumemura, H., Harada, M., Omary, M.B., Sakisaka, S., Suganuma, T., Namba, M., and Sata, M. (2004). Aggregation and loss of cytokeratin filament networks inhibit golgi organization in liver-derived epithelial cell lines. Cell motility and the cytoskeleton *57*, 37-52.

Kusakabe, M., and Nishida, E. (2004). The polarity-inducing kinase Par-1 controls Xenopus gastrulation in cooperation with 14-3-3 and aPKC. The EMBO journal *23*, 4190-4201.

Lammerding, J., Schulze, P.C., Takahashi, T., Kozlov, S., Sullivan, T., Kamm, R.D., Stewart, C.L., and Lee, R.T. (2004). Lamin A/C deficiency causes defective nuclear mechanics and mechanotransduction. The Journal of clinical investigation *113*, 370-378.

Lau, J.M.C., Wu, C.L., and Muslin, A.J. (2006). Differential role of 14-3-3 family members in Xenopus development. Dev Dyn *235*, 1761-1776.

Lazarides, E. (1980). Intermediate filaments as mechanical integrators of cellular space. Nature *283*, 249-256.

Lazarides, E., Granger, B.L., Gard, D.L., O'Connor, C.M., Breckler, J., Price, M., and Danto, S.I. (1982). Desmin- and vimentin-containing filaments and their role inthe assembly of the Z disk in muscle cells. Cold Spring Harbor symposia on quantitative biology *46 Pt 1*, 351-378.

le Duc, Q., Shi, Q.M., Blonk, I., Sonnenberg, A., Wang, N., Leckband, D., and de Rooij, J. (2010). Vinculin potentiates E-cadherin mechanosensing and is recruited to actin-anchored sites within adherens junctions in a myosin II-dependent manner. J Cell Biol *189*, 1107-1115.

Lee, C.H., Kim, M.S., Chung, B.M., Leahy, D.J., and Coulombe, P.A. (2012). Structural basis for heteromeric assembly and perinuclear organization of keratin filaments. Nat Struct Mol Biol *19*, 707-+.

Lee, M.K., Xu, Z., Wong, P.C., and Cleveland, D.W. (1993). Neurofilaments are obligate heteropolymers in vivo. The Journal of cell biology *122*, 1337-1350.

Lees, J.F., Shneidman, P.S., Skuntz, S.F., Carden, M.J., and Lazzarini, R.A. (1988). The structure and organization of the human heavy neurofilament subunit (NF-H) and the gene encoding it. The EMBO journal *7*, 1947-1955.

Leffers, H., Madsen, P., Rasmussen, H.H., Honore, B., Andersen, A.H., Walbum, E., Vandekerckhove, J., and Celis, J.E. (1993). Molecular Cloning and Expression of the Transformation Sensitive Epithelial Marker Stratifin: A Member of a Protein Family that has been Involved in the Protein Kinase C Signalling Pathway. J Mol Biol *231*, 982-998.

Lendahl, U., Zimmerman, L.B., and McKay, R.D.G. (1990). CNS stem cells express a new class of intermediate filament protein. Cell *60*, 585-595.

Leonard, M., Chan, Y., and Menko, A.S. (2008). Identification of a novel intermediate filament-linked N-cadherin/gamma-catenin complex involved in the establishment of the cytoarchitecture of differentiated lens fiber cells. Developmental biology *319*, 298-308.

Letai, A., Coulombe, P.A., McCormick, M.B., Yu, Q.C., Hutton, E., and Fuchs, E. (1993). Disease severity correlates with position of keratin point mutations in patients with epidermolysis bullosa simplex. Proceedings of the National Academy of Sciences of the United States of America *90*, 3197-3201.

Leube, R.E., Moch, M., and Windoffer, R. (2015). Intermediate filaments and the regulation of focal adhesion. Current opinion in cell biology *32*, 13-20.

Levy, E., Liem, R.K., D'Eustachio, P., and Cowan, N.J. (1987). Structure and evolutionary origin of the gene encoding mouse NF-M, the middle-molecular-mass neurofilament protein. European journal of biochemistry *166*, 71-77.

Li, H.H., Guo, Y., Teng, J.L., Ding, M.X., Yu, A.C.H., and Chen, J.G. (2006). 14-3-3 gamma affects dynamics and integrity of glial filaments by binding to phosphorylated GFAP. J Cell Sci *119*, 4452-4461.

Li, W., Skoulakis, E.M., Davis, R.L., and Perrimon, N. (1997). The Drosophila 14-3-3 protein Leonardo enhances Torso signaling through D-Raf in a Ras 1-dependent manner. Development *124*, 4163-4171.

Liao, J., and Omary, M.B. (1996). 14-3-3 proteins associate with phosphorylated simple epithelial keratins during cell cycle progression and act as a solubility cofactor. J Cell Biol *133*, 345-357.

Lichtenstern, T., Mücke, N., Aebi, U., Mauermann, M., and Herrmann, H. (2012). Complex formation and kinetics of filament assembly exhibited by the simple epithelial keratins K8 and K18. Journal of Structural Biology *177*, 54-62.

Lin, Y.C., Broedersz, C.P., Rowat, A.C., Wedig, T., Herrmann, H., Mackintosh, F.C., and Weitz, D.A. (2010a). Divalent cations crosslink vimentin intermediate filament tail domains to regulate network mechanics. J Mol Biol *399*, 637-644.

Lin, Y.C., Yao, N.Y., Broedersz, C.P., Herrmann, H., Mackintosh, F.C., and Weitz, D.A. (2010b). Origins of elasticity in intermediate filament networks. Physical review letters *104*, 058101.

Liu, D., Bienkowska, J., Petosa, C., Collier, R.J., Fu, H., and Liddington, R. (1995). Crystal structure of the zeta isoform of the 14-3-3 protein. Nature *376*, 191-194.

Loffek, S., Woll, S., Hohfeld, J., Leube, R.E., Has, C., Bruckner-Tuderman, L., and Magin, T.M. (2010). The ubiquitin ligase CHIP/STUB1 targets mutant keratins for degradation. Human mutation *31*, 466-476.

Lombardi, M.L., Jaalouk, D.E., Shanahan, C.M., Burke, B., Roux, K.J., and Lammerding, J. (2011). The interaction between nesprins and sun proteins at the nuclear envelope is critical for force transmission between the

nucleus and cytoskeleton. The Journal of biological chemistry *286*, 26743-26753.

Longo, D., Peirce, S.M., Skalak, T.C., Davidson, L., Marsden, M., Dzamba, B., and DeSimone, D.W. (2004). Multicellular computer simulation of morphogenesis: blastocoel roof thinning and matrix assembly in Xenopus laevis. Developmental biology *271*, 210-222.

Loschke, F., Homberg, M., and Magin, T.M. (2016). Keratin Isotypes Control Desmosome Stability and Dynamics through PKCalpha. The Journal of investigative dermatology *136*, 202-213.

Loschke, F., Seltmann, K., Bouameur, J.E., and Magin, T.M. (2015). Regulation of keratin network organization. Current opinion in cell biology *32*, 56-64.

Lu, M.S., and Prehoda, K.E. (2013). A NudE/14-3-3 pathway coordinates dynein and the kinesin Khc73 to position the mitotic spindle. Dev Cell *26*, 369-380.

Lupas, A. (1996). Coiled coils: new structures and new functions. Trends Biochem Sci *21*, 375-382.

Magin, T.M., Schroder, R., Leitgeb, S., Wanninger, F., Zatloukal, K., Grund, C., and Melton, D.W. (1998). Lessons from keratin 18 knockout mice: formation of novel keratin filaments, secondary loss of keratin 7 and accumulation of liver-specific keratin 8-positive aggregates. The Journal of cell biology *140*, 1441-1451.

Margolis, S.S., Perry, J.A., Forester, C.M., Nutt, L.K., Guo, Y., Jardim, M.J., Thomenius, M.J., Freel, C.D., Darbandi, R., Ahn, J.H.*, et al.* (2006). Role for the PP2A/B56delta phosphatase in regulating 14-3-3 release from Cdc25 to control mitosis. Cell *127*, 759-773.

Margolis, S.S., Walsh, S., Weiser, D.C., Yoshida, M., Shenolikar, S., and Kornbluth, S. (2003). PP1 control of M phase entry exerted through 14-3-3-regulated Cdc25 dephosphorylation. The EMBO journal *22*, 5734-5745.

Maruthamuthu, V., Sabass, B., Schwarz, U.S., and Gardel, M.L. (2011). Cell-ECM traction force modulates endogenous tension at cell–cell contacts. Proceedings of the National Academy of Sciences *108*, 4708.

Masters, S.C., Pederson, K.J., Zhang, L., Barbieri, J.T., and Fu, H. (1999). Interaction of 14-3-3 with a Nonphosphorylated Protein Ligand, Exoenzyme S of Pseudomonas aeruginosa. Biochemistry *38*, 5216-5221.

Mayordomo, I., and Sanz, P. (2002). The Saccharomyces cerevisiae 14-3-3 protein Bmh2 is required for regulation of the phosphorylation status of Fin1, a novel intermediate filament protein. The Biochemical journal *365*, 51-56.

McKeon, F.D., Kirschner, M.W., and Caput, D. (1986). Homologies in both primary and secondary structure between nuclear envelope and intermediate filament proteins. Nature *319*, 463-468.

Megason, S.G., and Fraser, S.E. (2003). Digitizing life at the level of the cell: high-performance laser-scanning microscopy and image analysis for in toto imaging of development. Mech Dev *120*, 1407-1420.

Mencarelli, C., Ciolfi, S., Caroti, D., Lupetti, P., and Dallai, R. (2011). Isomin: a novel cytoplasmic intermediate filament protein from an arthropod species. BMC biology *9*, 17.

Mendez, M.G., Kojima, S., and Goldman, R.D. (2010). Vimentin induces changes in cell shape, motility, and adhesion during the epithelial to mesenchymal transition. FASEB journal : official publication of the Federation of American Societies for Experimental Biology *24*, 1838-1851.

Merdes, A., Brunkener, M., Horstmann, H., and Georgatos, S.D. (1991). Filensin: a new vimentin-binding, polymerization-competent, and membrane-associated protein of the lens fiber cell. The Journal of cell biology *115*, 397-410.

Merdes, A., Gounari, F., and Georgatos, S.D. (1993). The 47-kD lens-specific protein phakinin is a tailless intermediate filament protein and an assembly partner of filensin. The Journal of cell biology *123*, 1507-1516.

Mertens, C., Kuhn, C., and Franke, W.W. (1996). Plakophilins 2a and 2b: constitutive proteins of dual location in the karyoplasm and the desmosomal plaque. The Journal of cell biology *135*, 1009-1025.

Mertz, A.F., Che, Y., Banerjee, S., Goldstein, J.M., Rosowski, K.A., Revilla, S.F., Niessen, C.M., Marchetti, M.C., Dufresne, E.R., and Horsley, V. (2013). Cadherin-based intercellular adhesions organize epithelial cell–matrix traction forces. Proceedings of the National Academy of Sciences *110*, 842.

Miao, L.Q., Teng, J.L., Lin, J.Q., Liao, X.Z., and Chen, J.G. (2013). 14-3-3 proteins interact with neurofilament protein-L and regulate dynamic assembly of neurofilaments. J Cell Sci *126*, 427-436.

Moch, M., Schwarz, N., Windoffer, R., and Leube, R.E. (2019). The keratin-desmosome scaffold: pivotal role of desmosomes for keratin network morphogenesis. Cellular and molecular life sciences : CMLS.

Moch, M., Windoffer, R., Schwarz, N., Pohl, R., Omenzetter, A., Schnakenberg, U., Herb, F., Chaisaowong, K., Merhof, D., Ramms, L.*, et al.* (2016). Effects of Plectin Depletion on Keratin Network Dynamics and Organization. PLoS One *11*, e0149106.

Moll, R., Franke, W.W., Schiller, D.L., Geiger, B., and Krepler, R. (1982). The catalog of human cytokeratins: patterns of expression in normal epithelia, tumors and cultured cells. Cell *31*, 11-24.

Moore, B. W. and Perez, V. J. (1967). Specific acidic proteins of the nervous system in Physiological and Biochemical Aspects of Nervous Integration (Carlson, FD, ed.) pp. 343-359.

Moorhead, G., Douglas, P., Morrice, N., Scarabel, M., Aitken, A., and MacKintosh, C. (1996). Phosphorylated nitrate reductase from spinach leaves is inhibited by 14-3-3 proteins and activated by fusicoccin. Current biology : CB *6*, 1104-1113.

Morgan, J.T., Pfeiffer, E.R., Thirkill, T.L., Kumar, P., Peng, G., Fridolfsson, H.N., Douglas, G.C., Starr, D.A., and Barakat, A.I. (2011). Nesprin-3 regulates

endothelial cell morphology, perinuclear cytoskeletal architecture, and flow-induced polarization. Mol Biol Cell *22*, 4324-4334.

Muslin, A.J., Tanner, J.W., Allen, P.M., and Shaw, A.S. (1996). Interaction of 14-3-3 with signaling proteins is mediated by the recognition of phosphoserine. Cell *84*, 889-897.

Nakamura, Y., Takeda, M., Aimoto, S., Hariguchi, S., Kitajima, S., and Nishimura, T. (1993). Acceleration of bovine neurofilament L assembly by deprivation of acidic tail domain. European journal of biochemistry *212*, 565-571.

Nelson, C.M., and Chen, C.S. (2003). VE-cadherin simultaneously stimulates and inhibits cell proliferation by altering cytoskeletal structure and tension. J Cell Sci *116*, 3571.

Nieuwkoop, P.D., and Faber J. (1994). Normal table of Xenopus laevis (Daudin): a systematical and chronological survey of the development from the fertilized egg till the end of metamorphosis, Garland Pub.

Nishida, K., Honma, Y., Dota, A., Kawasaki, S., Adachi, W., Nakamura, T., Quantock, A.J., Hosotani, H., Yamamoto, S., Okada, M.*, et al.* (1997). Isolation and chromosomal localization of a cornea-specific human keratin 12 gene and detection of four mutations in Meesmann corneal epithelial dystrophy. American journal of human genetics *61*, 1268-1275.

Noding, B., Herrmann, H., and Koster, S. (2014). Direct observation of subunit exchange along mature vimentin intermediate filaments. Biophys J *107*, 2923-2931.

Nolting, J.F., Mobius, W., and Koster, S. (2014). Mechanics of individual keratin bundles in living cells. Biophys J *107*, 2693-2699.

Obenauer, J.C., Cantley, L.C., and Yaffe, M.B. (2003). Scansite 2.0: proteome-wide prediction of cell signaling interactions using short sequence motifs. Nucleic acids research *31*, 3635-3641.

Obsil, T., Ghirlando, R., Klein, D.C., Ganguly, S., and Dyda, F. (2001). Crystal structure of the 14-3-3zeta:serotonin N-acetyltransferase complex. a role for scaffolding in enzyme regulation. Cell *105*, 257-267.

Obsil, T., and Obsilova, V. (2011). Structural basis of 14-3-3 protein functions. Seminars in Cell & Developmental Biology *22*, 663-672.

Obsilova, V., Herman, P., Vecer, J., Sulc, M., Teisinger, J., and Obsil, T. (2004). 14-3-3zeta C-terminal stretch changes its conformation upon ligand binding and phosphorylation at Thr232. The Journal of biological chemistry *279*, 4531-4540.

Okabe, S., Miyasaka, H., and Hirokawa, N. (1993). Dynamics of the neuronal intermediate filaments. The Journal of cell biology *121*, 375.

Omary, M.B., Ku, N.O., Tao, G.Z., Toivola, D.M., and Liao, J. (2006). 'Heads and tails' of intermediate filament phosphorylation: multiple sites and functional insights. Trends BiochemSci *31*, 383-394.

Oshima, R.G., Howe, W.E., Klier, F.G., Adamson, E.D., and Shevinsky, L.H. (1983). Intermediate filament protein synthesis in preimplantation murine embryos. Developmental biology *99*, 447-455.

Ottmann, C., Marco, S., Jaspert, N., Marcon, C., Schauer, N., Weyand, M., Vandermeeren, C., Duby, G., Boutry, M., Wittinghofer, A.*, et al.* (2007). Structure of a 14-3-3 coordinated hexamer of the plant plasma membrane H+ -ATPase by combining X-ray crystallography and electron cryomicroscopy. Molecular cell *25*, 427-440.

Parry, D.A. (1982). Coiled-coils in alpha-helix-containing proteins: analysis of the residue types within the heptad repeat and the use of these data in the prediction of coiled-coils in other proteins. Bioscience reports *2*, 1017-1024.

Parry, D.A. (2005). Microdissection of the sequence and structure of intermediate filament chains. Advances in protein chemistry *70*, 113-142.

Paulin, D., Babinet, C., Weber, K., and Osborn, M. (1980). Antibodies as probes of cellular differentiation and cytoskeletal organization in the mouse blastocyst. Experimental Cell Research *130*, 297-304.

Pauling, L., Corey, R.B., and Branson, H.R. (1951). The structure of proteins; two hydrogen-bonded helical configurations of the polypeptide chain. Proceedings of the National Academy of Sciences of the United States of America *37*, 205-211.

Pawelzyk, P., Mucke, N., Herrmann, H., and Willenbacher, N. (2014). Attractive interactions among intermediate filaments determine network mechanics in vitro. PLoS One *9*, e93194.

Pearson, R.W. (1962). Studies on the pathogenesis of epidermolysis bullosa. The Journal of investigative dermatology *39*, 551-575.

Pekny, M., and Lane, E.B. (2007). Intermediate filaments and stress. Exp Cell Res *313*, 2244-2254.

Peng, C.Y., Graves, P.R., Thoma, R.S., Wu, Z., Shaw, A.S., and Piwnica-Worms, H. (1997). Mitotic and G2 checkpoint control: regulation of 14-3-3 protein binding by phosphorylation of Cdc25C on serine-216. Science *277*, 1501-1505.

Peshkin, L., Lukyanov, A., Kalocsay, M., Gage, R.M., Wang, D., Pells, T.J., Karimi, K., Vize, P.D., Wühr, M., and Kirschner, M.W. (2019). The protein repertoire in early vertebrate embryogenesis. bioRxiv, 571174.

Peter, A., and Stick, R. (2015). Evolutionary aspects in intermediate filament proteins. Current opinion in cell biology *32*, 48-55.

Peters, B., Kirfel, J., Bussow, H., Vidal, M., and Magin, T.M. (2001). Complete cytolysis and neonatal lethality in keratin 5 knockout mice reveal its fundamental role in skin integrity and in epidermolysis bullosa simplex. Mol Biol Cell *12*, 1775-1789.

Petosa, C., Masters, S.C., Bankston, L.A., Pohl, J., Wang, B.C., Fu, H.I., and Liddington, R.C. (1998). 14-3-3 zeta binds a phosphorylated Raf peptide and an unphosphorylated peptide via its conserved amphipathic groove. J Biol Chem *273*, 16305-16310.

Portier, M.M., de Nechaud, B., and Gros, F. (1983). Peripherin, a new member of the intermediate filament protein family. Developmental neuroscience *6*, 335-344.

Pozuelo Rubio, M., Geraghty, K.M., Wong, B.H., Wood, N.T., Campbell, D.G., Morrice, N., and Mackintosh, C. (2004). 14-3-3-affinity purification of over 200 human phosphoproteins reveals new links to regulation of cellular metabolism, proliferation and trafficking. The Biochemical journal *379*, 395-408.

Prahlad, V., Yoon, M., Moir, R.D., Vale, R.D., and Goldman, R.D. (1998). Rapid movements of vimentin on microtubule tracks: kinesin-dependent assembly of intermediate filament networks. The Journal of cell biology *143*, 159-170.

Preisner, H., Habicht, J., Garg, S.G., and Gould, S.B. (2018). Intermediate filament protein evolution and protists. *75*, 231-243.

Quinlan, R.A., and Franke, W.W. (1982). Heteropolymer filaments of vimentin and desmin in vascular smooth muscle tissue and cultured baby hamster kidney cells demonstrated by chemical crosslinking. Proceedings of the National Academy of Sciences of the United States of America *79*, 3452-3456.

Quinlan, R.A., Hatzfeld, M., Franke, W.W., Lustig, A., Schulthess, T., and Engel, J. (1986). Characterization of dimer subunits of intermediate filament proteins. J Mol Biol *192*, 337-349.

Ramms, L., Fabris, G., Windoffer, R., Schwarz, N., Springer, R., Zhou, C., Lazar, J., Stiefel, S., Hersch, N., Schnakenberg, U*., et al.* (2013). Keratins as the main component for the mechanical integrity of keratinocytes. Proceedings of the National Academy of Sciences of the United States of America *110*, 18513-18518.

Reeves, S.A., Helman, L.J., Allison, A., and Israel, M.A. (1989). Molecular cloning and primary structure of human glial fibrillary acidic protein. Proceedings of

the National Academy of Sciences of the United States of America *86*, 5178-5182.

Ridge, K.M., Linz, L., Flitney, F.W., Kuczmarski, E.R., Chou, Y.H., Omary, M.B., Sznajder, J.I., and Goldman, R.D. (2005). Keratin 8 phosphorylation by protein kinase C delta regulates shear stress-mediated disassembly of keratin intermediate filaments in alveolar epithelial cells. J Biol Chem *280*, 30400-30405.

Rittinger, K., Budman, J., Xu, J., Volinia, S., Cantley, L.C., Smerdon, S.J., Gamblin, S.J., and Yaffe, M.B. (1999). Structural analysis of 14-3-3 phosphopeptide complexes identifies a dual role for the nuclear export signal of 14-3-3 in ligand binding. Molecular cell *4*, 153-166.

Riveline, D., Zamir, E., Balaban, N.Q., Schwarz, U.S., Ishizaki, T., Narumiya, S., Kam, Z., Geiger, B., and Bershadsky, A.D. (2001). Focal contacts as mechanosensors: Externally applied local mechanical force induces growth of focal contacts by an mDia1-dependent and ROCK-independent mechanism. J Cell Biol *153*, 1175-1185.

Roberts, B.J., Reddy, R., and Wahl, J.K. (2013). Stratifin (14-3-3 sigma) Limits Plakophilin-3 Exchange with the Desmosomal Plaque. PLoS One *8*, 14.

Roczniak-Ferguson, A., Petit, C.S., Froehlich, F., Qian, S., Ky, J., Angarola, B., Walther, T.C., and Ferguson, S.M. (2012). The transcription factor TFEB links mTORC1 signaling to transcriptional control of lysosome homeostasis. Sci Signal *5*, ra42.

Roy, S., McPherson, R.A., Apolloni, A., Yan, J., Lane, A., Clyde-Smith, J., and Hancock, J.F. (1998). 14-3-3 facilitates Ras-dependent Raf-1 activation in vitro and in vivo. Mol Cell Biol *18*, 3947-3955.

Salas, P.J., Rodriguez, M.L., Viciana, A.L., Vega-Salas, D.E., and Hauri, H.P. (1997). The apical submembrane cytoskeleton participates in the organization of the apical pole in epithelial cells. The Journal of cell biology *137*, 359-375.

Satoh, M.I., Hovington, H., and Cadrin, M. (1999). Reduction of cytochemical ecto-ATPase activities in keratin 8-deficient FVB/N mouse livers. Medical electron microscopy : official journal of the Clinical Electron Microscopy Society of Japan *32*, 209-212.

Schmidt, A., Langbein, L., Pratzel, S., Rode, M., Rackwitz, H.R., and Franke, W.W. (1999). Plakophilin 3--a novel cell-type-specific desmosomal plaque protein. Differentiation *64*, 291-306.

Schopferer, M., Bar, H., Hochstein, B., Sharma, S., Mucke, N., Herrmann, H., and Willenbacher, N. (2009). Desmin and vimentin intermediate filament networks: their viscoelastic properties investigated by mechanical rheometry. J Mol Biol *388*, 133-143.

Schwarz, N., Windoffer, R., Magin, T.M., and Leube, R.E. (2015). Dissection of keratin network formation, turnover and reorganization in living murine embryos. Sci Rep *5*, 8.

Schweizer, J., Bowden, P.E., Coulombe, P.A., Langbein, L., Lane, E.B., Magin, T.M., Maltais, L., Omary, M.B., Parry, D.A., Rogers, M.A.*, et al.* (2006). New consensus nomenclature for mammalian keratins. The Journal of cell biology *174*, 169-174.

Sehgal, L., Mukhopadhyay, A., Rajan, A., Khapare, N., Sawant, M., Vishal, S.S., Bhatt, K., Ambatipudi, S., Antao, N., Alam, H.*, et al.* (2014). 14-3-3 gamma-mediated transport of plakoglobin to the cell border is required for the initiation of desmosome assembly in vitro and in vivo. J Cell Sci *127*, 2174-2188.

Sehnke, P.C., DeLille, J.M., and Ferl, R.J. (2002). Consummating signal transduction: the role of 14-3-3 proteins in the completion of signal-induced transitions in protein activity. The Plant cell *14 Suppl*, S339-354.

Seltmann, K., Fritsch, A.W., Kas, J.A., and Magin, T.M. (2013). Keratins significantly contribute to cell stiffness and impact invasive behavior. Proceedings of the National Academy of Sciences of the United States of America *110*, 18507-18512.

Shen, W., Clark, A.C., and Huber, S.C. (2003). The C-terminal tail of Arabidopsis 14-3-3omega functions as an autoinhibitor and may contain a tenth alpha-helix. The Plant journal : for cell and molecular biology *34*, 473-484.

Shoeman, R.L., and Traub, P. (1993). Assembly of intermediate filaments. BioEssays : news and reviews in molecular, cellular and developmental biology *15*, 605-611.

Silhan, J., Obsilova, V., Vecer, J., Herman, P., Sulc, M., Teisinger, J., and Obsil, T. (2004). 14-3-3 protein C-terminal stretch occupies ligand binding groove and is displaced by phosphopeptide binding. The Journal of biological chemistry *279*, 49113-49119.

Sivaramakrishnan, S., Schneider, J.L., Sitikov, A., Goldman, R.D., and Ridge, K.M. (2009). Shear Stress Induced Reorganization of the Keratin Intermediate Filament Network Requires Phosphorylation by Protein Kinase C zeta. Mol Biol Cell *20*, 2755-2765.

Sluchanko, N.N., and Gusev, N.B. (2017). Moonlighting chaperone-like activity of the universal regulatory 14-3-3 proteins. The FEBS journal *284*, 1279-1295.

Snider, N.T., and Omary, M.B. (2014). Post-translational modifications of intermediate filament proteins: mechanisms and functions. Nat Rev Mol Cell Biol *15*, 163-177.

Snider, N.T., Weerasinghe, S.V., Iniguez-Lluhi, J.A., Herrmann, H., and Omary, M.B. (2011). Keratin hypersumoylation alters filament dynamics and is a marker for human liver disease and keratin mutation. The Journal of biological chemistry *286*, 2273-2284.

Sonavane, P.R., Wang, C., Dzamba, B., Weber, G.F., Periasamy, A., and DeSimone, D.W. (2017). Mechanical and signaling roles for keratin intermediate filaments in the assembly and morphogenesis of Xenopus mesendoderm tissue at gastrulation. *144*, 4363-4376.

Sonnenberg, A., Calafat, J., Janssen, H., Daams, H., van der Raaij-Helmer, L.M., Falcioni, R., Kennel, S.J., Aplin, J.D., Baker, J., Loizidou, M*., et al.* (1991). Integrin alpha 6/beta 4 complex is located in hemidesmosomes, suggesting

a major role in epidermal cell-basement membrane adhesion. The Journal of cell biology *113*, 907-917.

Stappenbeck, T.S., and Green, K.J. (1992). The desmoplakin carboxyl terminus coaligns with and specifically disrupts intermediate filament networks when expressed in cultured cells. The Journal of cell biology *116*, 1197-1209.

Steinert, P.M. (1990). The two-chain coiled-coil molecule of native epidermal keratin intermediate filaments is a type I-type II heterodimer. The Journal of biological chemistry *265*, 8766-8774.

Steinert, P.M., Chou, Y.H., Prahlad, V., Parry, D.A., Marekov, L.N., Wu, K.C., Jang, S.I., and Goldman, R.D. (1999). A high molecular weight intermediate filament-associated protein in BHK-21 cells is nestin, a type VI intermediate filament protein. Limited co-assembly in vitro to form heteropolymers with type III vimentin and type IV alpha-internexin. The Journal of biological chemistry *274*, 9881-9890.

Steinert, P.M., Idler, W.W., and Goldman, R.D. (1980). Intermediate filaments of baby hamster kidney (BHK-21) cells and bovine epidermal keratinocytes have similar ultrastructures and subunit domain structures. Proceedings of the National Academy of Sciences of the United States of America *77*, 4534-4538.

Steinert, P.M., and Parry, D.A. (1985). Intermediate filaments: conformity and diversity of expression and structure. Annual review of cell biology *1*, 41-65.

Steinert, P.M., and Parry, D.A. (1993). The conserved H1 domain of the type II keratin 1 chain plays an essential role in the alignment of nearest neighbor molecules in mouse and human keratin 1/keratin 10 intermediate filaments at the two- to four-molecule level of structure. The Journal of biological chemistry *268*, 2878-2887.

Steinert, P.M., Rice, R.H., Roop, D.R., Trus, B.L., and Steven, A.C. (1983). Complete amino acid sequence of a mouse epidermal keratin subunit and implications for the structure of intermediate filaments. Nature *302*, 794-800.

Stone, M.R., O'Neill, A., Lovering, R.M., Strong, J., Resneck, W.G., Reed, P.W., Toivola, D.M., Ursitti, J.A., Omary, M.B., and Bloch, R.J. (2007). Absence of keratin 19 in mice causes skeletal myopathy with mitochondrial and sarcolemmal reorganization. J Cell Sci *120*, 3999-4008.

Strelkov, S.V., Herrmann, H., Geisler, N., Lustig, A., Ivaninskii, S., Zimbelmann, R., Burkhard, P., and Aebi, U. (2001). Divide-and-conquer crystallographic approach towards an atomic structure of intermediate filaments. J Mol Biol *306*, 773-781.

Strelkov, S.V., Herrmann, H., Geisler, N., Wedig, T., Zimbelmann, R., Aebi, U., and Burkhard, P. (2002). Conserved segments 1A and 2B of the intermediate filament dimer: their atomic structures and role in filament assembly. The EMBO journal *21*, 1255-1266.

Strnad, P., Harada, M., Siegel, M., Terkeltaub, R.A., Graham, R.M., Khosla, C., and Omary, M.B. (2007). Transglutaminase 2 regulates mallory body inclusion formation and injury-associated liver enlargement. Gastroenterology *132*, 1515-1526.

Strnad, P., Windoffer, R., and Leube, R.E. (2001). In vivo detection of cytokeratin filament network breakdown in cells treated with the phosphatase inhibitor okadaic acid. Cell and tissue research *306*, 277-293.

Strnad, P., Windoffer, R., and Leube, R.E. (2002). Induction of rapid and reversible cytokeratin filament network remodeling by inhibition of tyrosine phosphatases. J Cell Sci *115*, 4133-4148.

Sun, T.T., Tseng, S.C., Huang, A.J., Cooper, D., Schermer, A., Lynch, M.H., Weiss, R., and Eichner, R. (1985). Monoclonal antibody studies of mammalian epithelial keratins: a review. Annals of the New York Academy of Sciences *455*, 307-329.

Suzuki, K.T., Suzuki, M., Shigeta, M., Fortriede, J.D., Takahashi, S., Mawaribuchi, S., Yamamoto, T., Taira, M., and Fukui, A. (2017). Clustered Xenopus keratin genes: A genomic, transcriptomic, and proteomic analysis. Developmental biology *426*, 384-392.

Svitkina, T.M., Verkhovsky, A.B., and Borisy, G.G. (1996). Plectin sidearms mediate interaction of intermediate filaments with microtubules and other components of the cytoskeleton. The Journal of cell biology *135*, 991-1007.

Tamai, Y., Ishikawa, T., Bosl, M.R., Mori, M., Nozaki, M., Baribault, H., Oshima, R.G., and Taketo, M.M. (2000). Cytokeratins 8 and 19 in the mouse placental development. The Journal of cell biology *151*, 563-572.

Tao, G.Z., Looi, K.S., Toivola, D.M., Strnad, P., Zhou, Q., Liao, J., Wei, Y., Habtezion, A., and Omary, M.B. (2009). Keratins modulate the shape and function of hepatocyte mitochondria: a mechanism for protection from apoptosis. J Cell Sci *122*, 3851-3855.

Terrinoni, A., Rugg, E.L., Lane, E.B., Melino, G., Felix, D.H., Munro, C.S., and McLean, W.H. (2001). A novel mutation in the keratin 13 gene causing oral white sponge nevus. Journal of dental research *80*, 919-923.

Toivola, D.M., Goldman, R.D., Garrod, D.R., and Eriksson, J.E. (1997). Protein phosphatases maintain the organization and structural interactions of hepatic keratin intermediate filaments. J Cell Sci *110 (Pt 1)*, 23-33.

Toivola, D.M., Nieminen, M.I., Hesse, M., He, T., Baribault, H., Magin, T.M., Omary, M.B., and Eriksson, J.E. (2001). Disturbances in hepatic cell-cycle regulation in mice with assembly-deficient keratins 8/18. Hepatology (Baltimore, Md) *34*, 1174-1183.

Toivola, D.M., Tao, G.Z., Habtezion, A., Liao, J., and Omary, M.B. (2005). Cellular integrity plus: organelle-related and protein-targeting functions of intermediate filaments. Trends Cell Biol *15*, 608-617.

Toivola, D.M., Zhou, Q., English, L.S., and Omary, M.B. (2002). Type II keratins are phosphorylated on a unique motif during stress and mitosis in tissues and cultured cells. Mol Biol Cell *13*, 1857-1870.

Tommerup, N., and Leffers, H. (1996). Assignment of the Human Genes Encoding 14-3-3 Eta (YWHAH) to 22q12, 14-3-3 Zeta (YWHAZ) to 2p25.1–p25.2, and 14-3-3 Beta (YWHAB) to 20q13.1 byin SituHybridization. Genomics *33*, 149-150.

Torpey, N.P., Heasman, J., and Wylie, C.C. (1992). Distinct distribution of vimentin and cytokeratin in Xenopus oocytes and early embryos. J Cell Sci *101 (Pt 1)*, 151-160.

Traub, P., Scherbarth, A., Wiegers, W., and Shoeman, R.L. (1992). Salt-stable interaction of the amino-terminal head region of vimentin with the alpha-helical rod domain of cytoplasmic intermediate filament proteins and its relevance to protofilament structure and filament formation and stability. J Cell Sci *101 (Pt 2)*, 363-381.

Truong, A.B., Masters, S.C., Yang, H., and Fu, H. (2002). Role of the 14-3-3 C-terminal loop in ligand interaction. Proteins *49*, 321-325.

Tzivion, G., Luo, Z.J., and Avruch, J. (2000). Calyculin A-induced vimentin phosphorylation sequesters 14-3-3 and displaces other 14-3-3 partners in vivo. J Biol Chem *275*, 29772-29778.

Verdoodt, B., Benzinger, A., Popowicz, G.M., Holak, T.A., and Hermeking, H. (2006). Characterization of 14-3-3sigma dimerization determinants: requirement of homodimerization for inhibition of cell proliferation. Cell cycle (Georgetown, Tex) *5*, 2920-2926.

Vikstrom, K.L., Lim, S.S., Goldman, R.D., and Borisy, G.G. (1992). STEADY-STATE DYNAMICS OF INTERMEDIATE FILAMENT NETWORKS. J Cell Biol *118*, 121-129.

Vishal, S.S., Tilwani, S., and Dalal, S.N. (2018). Plakoglobin localization to the cell border restores desmosome function in cells lacking 14-3-3gamma. Biochemical and biophysical research communications *495*, 1998-2003.

Wang, B.C., Yang, H.Z., Liu, Y.C., Jelinek, T., Zhang, L.X., Ruoslahti, E., and Fu, H. (1999). Isolation of high-affinity peptide antagonists of 14-3-3 proteins by phage display. Biochemistry *38*, 12499-12504.

Wang, E., Cairncross, J.G., and Liem, R.K. (1984). Identification of glial filament protein and vimentin in the same intermediate filament system in human glioma cells. Proceedings of the National Academy of Sciences of the United States of America *81*, 2102-2106.

Wang, H., Zhang, L., Liddington, R., and Fu, H. (1998). Mutations in the hydrophobic surface of an amphipathic groove of 14-3-3zeta disrupt its interaction with Raf-1 kinase. The Journal of biological chemistry *273*, 16297-16304.

Weber, G.F., Bjerke, M.A., and DeSimone, D.W. (2012). A Mechanoresponsive Cadherin-Keratin Complex Directs Polarized Protrusive Behavior and Collective Cell Migration. Dev Cell *22*, 104-115.

Wiche, G., Gromov, D., Donovan, A., Castanon, M.J., and Fuchs, E. (1993). Expression of plectin mutant cDNA in cultured cells indicates a role of COOH-terminal domain in intermediate filament association. The Journal of cell biology *121*, 607-619.

Wilker, E.W., Grant, R.A., Artim, S.C., and Yaffe, M.B. (2005). A structural basis for 14-3-3sigma functional specificity. The Journal of biological chemistry *280*, 18891-18898.

Windoffer, R., Beil, M., Magin, T.M., and Leube, R.E. (2011). Cytoskeleton in motion: the dynamics of keratin intermediate filaments in epithelia. J Cell Biol *194*, 669-678.

Windoffer, R., Kolsch, A., Woll, S., and Leube, R.E. (2006). Focal adhesions are hotspots for keratin filament precursor formation. The Journal of cell biology *173*, 341-348.

Windoffer, R., Woll, S., Strnad, P., and Leube, R.E. (2004). Identification of novel principles of keratin filament network turnover in living cells. Mol Biol Cell *15*, 2436-2448.

Winklbauer, R., Selchow, A., Nagel, M., and Angres, B. (1992). Cell interaction and its role in mesoderm cell migration during Xenopus gastrulation. Developmental dynamics : an official publication of the American Association of Anatomists *195*, 290-302.

Woll, S., Windoffer, R., and Leube, R.E. (2005). Dissection of keratin dynamics: different contributions of the actin and microtubule systems. Eur J Cell Biol *84*, 311-328.

Woll, S., Windoffer, R., and Leube, R.E. (2007). p38 MAPK-dependent shaping of the keratin cytoskeleton in cultured cells. J Cell Biol *177*, 795-807.

Wu, C.L., and Muslin, A.J. (2002). Role of 14-3-3 proteins in early Xenopus development. Mech Dev *119*, 45-54.

Wylie, C.C., Brown, D., Godsave, S.F., Quarmby, J., and Heasman, J. (1985). The cytoskeleton of Xenopus oocytes and its role in development. Journal of embryology and experimental morphology *89 Suppl*, 1-15.

Xiao, B., Smerdon, S.J., Jones, D.H., Dodson, G.G., Soneji, Y., Aitken, A., and Gamblin, S.J. (1995). Structure of a 14-3-3 protein and implications for coordination of multiple signalling pathways. Nature *376*, 188-191.

Xing, H., Kornfeld, K., and Muslin, A.J. (1997). The protein kinase KSR interacts with 14-3-3 protein and Raf. Current biology : CB *7*, 294-300.

Yaffe, M.B. (2002). How do 14-3-3 proteins work?-- Gatekeeper phosphorylation and the molecular anvil hypothesis. FEBS letters *513*, 53-57.

Yaffe, M.B., Rittinger, K., Volinia, S., Caron, P.R., Aitken, A., Leffers, H., Gamblin, S.J., Smerdon, S.J., and Cantley, L.C. (1997). The structural basis for 14-3-3 : phosphopeptide binding specificity. Cell *91*, 961-971.

Yang, X., Lee, W.H., Sobott, F., Papagrigoriou, E., Robinson, C.V., Grossmann, J.G., Sundstrom, M., Doyle, D.A., and Elkins, J.M. (2006). Structural basis for protein-protein interactions in the 14-3-3 protein family. Proceedings of the National Academy of Sciences of the United States of America *103*, 17237-17242.

Yoon, K.H., Yoon, M., Moir, R.D., Khuon, S., Flitney, F.W., and Goldman, R.D. (2001). Insights into the dynamic properties of keratin intermediate filaments in living epithelial cells. The Journal of cell biology *153*, 503-516.

Zeng, Y., and Piwnica-Worms, H. (1999). DNA damage and replication checkpoints in fission yeast require nuclear exclusion of the Cdc25 phosphatase via 14-3-3 binding. Mol Cell Biol *19*, 7410-7419.

Zha, J., Harada, H., Yang, E., Jockel, J., and Korsmeyer, S.J. (1996). Serine phosphorylation of death agonist BAD in response to survival factor results in binding to 14-3-3 not BCL-X(L). Cell *87*, 619-628.

Zhang, L., Wang, H., Liu, D., Liddington, R., and Fu, H. (1997). Raf-1 kinase and exoenzyme S interact with 14-3-3zeta through a common site involving lysine 49. The Journal of biological chemistry *272*, 13717-13724.

Zheng, C.Y., Petralia, R.S., Wang, Y.X., and Kachar, B. (2011). Fluorescence recovery after photobleaching (FRAP) of fluorescence tagged proteins in dendritic spines of cultured hippocampal neurons. Journal of visualized experiments : JoVE.

Zhong, B., Strnad, P., Selmi, C., Invernizzi, P., Tao, G.Z., Caleffi, A., Chen, M., Bianchi, I., Podda, M., Pietrangelo, A.*, et al.* (2009). Keratin variants are overrepresented in primary biliary cirrhosis and associate with disease severity. Hepatology (Baltimore, Md) *50*, 546-554.

Zhou, Q., Cadrin, M., Herrmann, H., Chen, C.H., Chalkley, R.J., Burlingame, A.L., and Omary, M.B. (2006). Keratin 20 serine 13 phosphorylation is a stress and intestinal goblet cell marker. The Journal of biological chemistry *281*, 16453-16461.

Zhou, X., Liao, J., Hu, L., Feng, L., and Omary, M.B. (1999). Characterization of the major physiologic phosphorylation site of human keratin 19 and its role in filament organization. The Journal of biological chemistry *274*, 12861-12866.